

**Improving Durability of Asphalt Mixes Produced With Reclaimed Asphalt  
Pavement (Rap) by Enhancing Binder Blending**

by

Hawraa Kadhim

A thesis

presented to the University of Waterloo

in fulfillment of the

thesis requirement for the degree of

Doctor of Philosophy

in

Civil Engineering

Waterloo, Ontario, Canada, 2019

© Hawraa Kadhim 2019

## **Examining Committee Membership**

The following served on the Examining Committee for this thesis. The decision of the Examining Committee is by majority vote.

**External Examiner**

**Dr. Elie Y. Hajj**

Civil & Environmental Engineering, University of Nevada

**Supervisor**

**Dr. Hassan Baaj**

Civil and Environmental Engineering, University of Waterloo

**Internal Member**

**Dr. Susan Tighe**

Civil and Environmental Engineering, University of Waterloo

**Internal Member**

**Dr. Giovanni Cascante**

Civil and Environmental Engineering, University of Waterloo

**Internal Member**

**Dr. Christine Moresoli**

Chemical Engineering, University of Waterloo

## **Author's Declaration**

I hereby declare that I am the sole author of this thesis. This is a true copy of the thesis, including any required final revisions, as accepted by my examiners.

I understand that my thesis may be made electronically available to the public.

## Abstract

Reclaimed Asphalt Pavement (RAP) has been favoured over virgin materials in the light of the unstable cost of virgin asphalt binders, shortage of quality aggregates, and compelling need to preserve the environment and natural resources. Mixes containing up to 20% RAP are commonly considered to have similar behaviour to virgin mixes. However, during the production process of HMA with RAP, the blending between aged and virgin binders would be partial, which would create heterogeneity in distribution of the aged recycled binder and the soft virgin binder in the HMA-RAP mixes. Hence, it is important to control the blending process between old and new binders to obtain more homogenous mix. Therefore, the main objectives of this research are to examine the kinematics of blending of aged and virgin binders by considering the time-temperature effect during mixing and silo-storage, and assess the thermo-mechanical behaviour of Hot Mix Asphalt (HMA) containing RAP at different blending states.

The asphalt mixes used in this research were produced and collected at two plants (Plant 1) and (Plant 2) located in Ontario, Canada. Two Marshall mixes were produced and collected from Plant 1 including a surface course HL-3 containing 15 percent RAP and a base course HL-8 containing 30 percent RAP. These mixes were labelled as 1HL-3 and 1HL-8 respectively. In addition, two Marshall mixes were produced and collected from Plant 2 including a surface course HL-3 containing 20 percent RAP and a base course HL-8 containing 40 percent RAP. These mixes were labelled as 2HL-3 and 2HL-8 respectively. To investigate the impact of storage time on the blending progress and achieving a cohesive final binder, the mix samples were collected as a function of storage time in the silo. The first sampling was done immediately after production ( $t = 0$ -hour), and then at several time intervals of silo-storage; i.e., at 1, 4, 8, and 12 hours. In case of Plant 2, the samples were additionally collected after 24-hour of storage time. All samples were then kept in a storage room at  $7^{\circ}\text{C}$  until the day of compaction to minimize any further blending between aged and virgin binder.

To understand the blending phenomena and its effect on the performance of the pavement, a multi-scale investigation is carried out. The blending was examined in terms of micro-mechanical and rheological properties. The microstructure of the blending zones were examined under The Environmental Scanning Electron Microscope (ESEM). In addition the effect of the silo-storage time on the rheology of the binders was investigated. The results indicate that

increasing the interaction time and temperature between the aged and virgin binder significantly results in a better blending.

The performance of RAP-HMA with respect to the silo-storage time was examined using Dynamic Modules Test, Thermal Stress Restrained Specimen Test (TSRST), Rutting Test, and Flexural Beam Fatigue Test. The experimental data indicates that samples collected after 12-hour of silo storage exhibited a reduction in the stiffness due to better blending of aged and virgin binder. In addition, the 12-hour samples showed enhancement in their fracture temperature, rutting depth, and fatigue life, accompanied with a better blending between their aged and virgin binder. On the other hand, the samples that collected after 24-hour silo-storage had a higher stiffness in comparison with the 8 and 12-hour samples.

Moreover, the AASHTOWare Pavement Mechanistic-Empirical Design was utilized to examine the effect of the 12-hour silo-storage time on the long term performance of the pavements. Four pavement structures have been designed for this purpose. These pavements have the same structure of their granular A, granular B, and the subgrade. Yet, the first layer (surface course and base course) is a silo-storage time-dependent. The long-term field performance prediction indicates a slight improvement with the 12-hour pavements (Plant1 12hrs and Plant2 12hrs). However, it should be noted that AASHTOWare Pavement Mechanistic-Empirical Design does not appear to properly capture the effect of blending in the pavement performance.

The collected experimental evidences unveils correlations between time-temperature effects and mixture performance. Based on these findings, the research provides practical recommendations to the professionals of the Canadian asphalt industry for a better use of RAP. Ultimately, this research recommends a 12-hour silo-storage time for the RAP-HMA for better performance and durability of the mixes.

## Acknowledgement

This research project would not be achievable without the excellent guidance, caring, and useful comments from Prof. Hassan Baaj. Deepest thanks for you for being such a great and helpful mentor and supervisor. I would like to thank my thesis committee members, Professor Elie Y. Hajj, Professor Christine Moresoli, Professor Giovanni Cascante, and Professor Susan Tighe.

My gratitude also goes to the following supporting partners of this research:

- The Centre for Pavement and Transportation Technology (CPATT), Norman W. McLeod Chair, University of Waterloo,
- Imperial Oil Limited -Imperial Oil University Research Award for funding this project for funding this research and for the scientific contribution of its experts and researchers in this study. Especial thanks goes to Pavel Kriz, Payman Pirzadeh, and Daniel L. Grant for their great support,
- The Miller Group Asphalt Plant for supplying the HL-3 and HL-8 mixes at the required time intervals. Great appreciation goes to the technical team including Trever Moore, Justin Baxter, and Tim Ouellette,
- Steed and Evans Asphalt Plant for supplying the HL-3 and HL-8 mixes at the required time intervals. Great appreciation goes to the technical team including Jim Karageorgos and Richard Marco,
- The Natural Sciences and Engineering Research Council of Canada (NSERC) Collaborative Research and Development Program,
- The Civil and Environmental Engineering Department's technical staff: Richard Morrison, Doug Hirst, Terry Ridgway, and Peter Volcic.

I would like to thank Kate Robertson for her endless support throughout the last years. Also, I would like to express my deepest gratitude to Peter Mikhailenko for his collective assistance. I sincerely thank Wei Yu for his valuable suggestions and help. A big thank you to Pezhouhan Tavassoti-Kheiry for his valuable feedback. I thank all my colleagues at CPATT and the co-op students. A big thank you to Haya Almutari, Eskedil Abebaw Melese, Seyedata Nahidi, Hanaa Al-Bayati, Taha Youns, Abdulrahman Hamid, Jessica Achebe, Yang Liu (Frank#2), Taher Baghaee Moghaddam, Yashar Azimi Alamdary, Ali Qabur, Roberto Aurilio, Dandi Zhao, and Edward Abreu for their countless hours of assistance in various capacities throughout my study. I am also so grateful for all of the fun memories that we share.

Last but not least, I would like to thank my parents and my beloved sisters for their encouragement, moral support, and endless love.

To my wisest mentor, grandmother.

Rest in Peace

## Table of Contents

1	Introduction .....	1
1.1	Background .....	1
1.2	Research Hypothesis .....	3
1.3	Scope and Objectives .....	4
1.4	Novelty of the Work.....	4
1.5	Research Methodology.....	5
1.6	Organization of the thesis.....	5
2	Literature Review .....	7
2.1	The Basic Theory of Diffusion.....	7
2.2	Properties of the materials.....	10
2.2.1	Elasticity, Viscosity, and Plasticity.....	10
2.2.2	Viscoelastic Materials .....	11
2.3	SuperPave Performance Grade Binder System (PG) .....	13
2.4	Recycled Asphalt Pavement.....	14
2.4.1	Current Studies on Blending.....	15
2.4.2	Microstructure of virgin and aged binder .....	23
2.5	HMA performance Tests .....	26
2.5.1	Dynamic Modulus Test.....	26
2.5.2	Thermal Cracking Test .....	27
2.5.3	Rutting Test.....	29
2.5.4	Fatigue Testing.....	30
2.6	Asphalt Plants and Silo-Storage.....	31
2.7	Summary of the Literature Review .....	32



3	Research Methodology .....	33
3.1	Literature Review and state of the current practice.....	34
3.2	Sample collection .....	34
3.3	Asphalt Binder Testing.....	37
3.3.1	Microstructure investigation of Asphalt Binder using ESEM .....	37
3.3.1.1	Material .....	37
3.3.1.2	Sample Holder.....	37
3.3.1.3	Sample Preparation .....	39
3.3.1.4	ESEM Observation.....	39
3.3.2	Asphalt Binder Recovery .....	40
3.3.3	Binder rheology .....	40
3.3.4	SAR-AD analysis.....	40
3.4	HMA Testing.....	41
3.4.1	Volumetric Properties of the HMA.....	41
3.4.1.1	Voids in Mineral Aggregate (VMA).....	42
3.4.1.2	Voids Filled with Asphalt (VFA).....	43
3.4.2	Asphalt Mixture Characterization.....	43
3.4.2.1	Specimen Compaction.....	43
3.4.2.2	HMA Performance Tests.....	45
3.5	ANOVA Statistical Analysis.....	50
4	Asphalt Binder Testing Analysis and Discussion.....	52
4.1	Environmental Scanning Electron Microscope (ESEM) .....	52
4.1.1	ESEM Sample Preparation .....	52
4.1.1.1	Virgin and Oxidized Samples .....	52
4.1.1.2	Blended Samples .....	52

4.1.1.3	Blending Zone at the Interface of the Aged and Virgin Binder .....	52
4.1.2	Image processing .....	54
4.1.3	ESEM Results .....	55
4.1.3.1	Virgin Asphalt Binder .....	55
4.1.3.2	Asphalt Binder Oxidation.....	56
4.1.3.3	Blended Samples .....	57
4.1.3.4	Blending Zone at the Interface of the Aged and Virgin Binder .....	59
4.2	Binder Characterization.....	64
4.3	Summary of the Results .....	69
5	HMA Performance Testing Analysis and Discussion .....	71
5.1	Volumetric Properties .....	71
5.2	Dynamic Modulus Test Results .....	76
5.3	Thermal Cracking Test Results .....	81
5.4	Rutting Test Results .....	90
5.5	Flexural Beam Fatigue Test Results .....	97
5.6	Summary of the Results .....	106
6	Long-Term Field Performance Prediction.....	109
6.1	Inputs.....	110
6.1.1	Traffic Input .....	113
6.1.2	Climate input.....	114
6.2	Performance Prediction and Analysis .....	114
7	Conclusions, Outcome, and Future Research .....	118
7.1	Summary of Findings and Conclusions .....	118
7.2	Scientific Contribution .....	120
7.3	Future Research Opportunities.....	121

Publications.....	123
References.....	124
Appendix (A) – HMA Test Results .....	135
Appendix (B) –Specimen Preparation and Testing .....	154

## Table of Figures

Figure 1-1 Basic flexible pavement structure .....	1
Figure 1-2 Estimated asphalt production cost categories (Copeland 2011) .....	2
Figure 1-3 MTO asphalt binder price index (OHMPA, 2019) .....	3
Figure 2-1 Schematic representations of (a) vacancy diffusion and (b) interstitial (William and Callister 2007).....	8
Figure 2-2 Stress-strain curve A) an elastic material B) an Elastic-Plastic material C) a Plastic material D) a viscoelastic material (Chawla, 1999).....	12
Figure 2-3 Asphalt behavior at different temperatures (McGennis et al., 1994).....	12
Figure 2-4 Prediction of PG grades for different crude oil blends (Pavement Interactive, 2010) 13	
Figure 2-5 Statistical results of interaction between aged and virgin binders evaluated in NCHRP 9-12 study.....	16
Figure 2-6 RAP binder and virgin binder blending scenarios (Moghaddam and Baaj, 2016b) ...	17
Figure 2-7 RAP preheat time before mixing comparing the unconfined compression and indirect tension.....	18
Figure 2-8 Schematic representation of procedure of blending study (Poulikakos et al., 2014)..	21
Figure 2-9 Diffusion at varying temperature. (Kriz et al, 2014).....	22
Figure 2-10 ESEM image showing the crack formation at the border between RAP and virgin materials (Rinaldini et al., 2014).....	25
Figure 2-11 ESEM images, Left: fresh binder. Right: aged binder (Stangl et al., 2006) .....	26
Figure 2-12 Master curve of the complex modulus of asphalt mixes (Baaj et al., 2013).....	27
Figure 2-13 Typical results from the TSRST test (Baaj et al. 2013) .....	28
Figure 2-14 Schematic flexural fatigue test (Pavement Interactive, 2010) .....	30
Figure 3-1 Outline of the research methodology .....	33
Figure 3-2 Plant 1 (left), Plant 2 (right) .....	34
Figure 3-3 Monitoring the temperature of the collected mixes during sampling .....	36

Figure 3-4 Stainless steel sample moulds for ESEM test .....	38
Figure 3-5 Stainless steel sample mould with divider for ESEM test .....	38
Figure 3-6 ESEM device at WATLAB.....	39
Figure 3-7 Illustration of VMA in a compacted asphalt mix specimen.....	42
Figure 3-8 SuperPave Gyrotory Compactor (left) and ShearBox slab compactor (right) .....	44
Figure 3-9 (a) coring machine, (b) saw-cutting machine, and (c) grinding machine .....	44
Figure 3-10 Bulk Relative Density (BRD) apparatus for the compacted HMA.....	45
Figure 3-11 MTS loading farm with dynamic modulus test setup .....	46
Figure 3-12 MTS loading farm with TSRST setup .....	47
Figure 3-13 CPATT Hamburg Wheel Tracking Device.....	48
Figure 3-14 CPATT Repeated Flexural Fatigue Bending Test Setup .....	49
Figure 3-15 WÖHLER (or fatigue) curve and determination of " $\epsilon_6$ " .....	50
Figure 4-1 Illustrates the preparation procedure for ESEM samples.....	53
Figure 4-2 The developed MATLAB code for fibril size measurement .....	54
Figure 4-3 ESEM Images of 58-28 binder with SE (left) and BSE (right) modes at 1000x magnification .....	55
Figure 4-4 ESEM Images of oxidized 58-28 binder with SE (left) and BSE (right) modes at 1000x magnification .....	56
Figure 4-5 B1 blending sample under ESEM.....	57
Figure 4-6 B2 blending sample under ESEM.....	58
Figure 4-7 B3 blending sample under ESEM.....	59
Figure 4-8 ESEM images of virgin binder (left) and oxidized binder (right).....	60
Figure 4-9 ESEM images of the blended zone for 8hrs sample at 60 °C .....	60
Figure 4-10 ESEM images of the blended zone for 12hrs sample 60 °C .....	61
Figure 4-11 ESEM images of the blended zone for 8hrs sample at 90 °C .....	62

Figure 4-12 ESEM images of the blended zone for 12hrs sample at 90 °C .....	62
Figure 4-13 ESEM images of the blended zone for 8 hrs sample at 120 °C .....	63
Figure 4-14 ESEM images of the blended zone for 12 hrs samples at 120 °C.....	63
Figure 4-15 High temperature PG of source and extracted binders for all HL-3 and HL-8.....	65
Figure 4-16 Low temperature PG of source and extracted binders for all HL-3 and HL-8 .....	66
Figure 4-17 SAR-AD analysis for all the tested asphalt binder.....	67
Figure 4-18 Comparison of virgin PG 52-34 of Plant 1 and Plant 2 .....	68
Figure 4-19 Asphaltenes content of the extracted binder from the silo-stored mixes .....	69
Figure 4-20 Asphalt binder components from SARA analysis .....	69
Figure 5-1 Effect of silo-storage time on VFA for (left) HL-3 and (right) HL-8 mixes .....	74
Figure 5-2 Effect of silo-storage time on VMA for (left) HL-3 and (right) HL-8 mixes.....	74
Figure 5-3 Effect of silo-storage time on the $V_{be}$ for HL-3 mixes .....	75
Figure 5-4 Effect of silo-storage time on the $V_{be}$ for HL-8 mixes .....	76
Figure 5-5 Master curve of HL-3 and HL-8 for all mixes .....	77
Figure 5-6 Modulus Ratio Values ( $E_0/E_{12}$ ) of 1HL-3 mixes.....	78
Figure 5-7 Modulus Ratio Values ( $E_0/E_{12}$ ) of 2HL-3 mixes.....	79
Figure 5-8 Modulus Ratio Values ( $E_0/E_{12}$ ) of 1HL-8 mixes.....	79
Figure 5-9 Modulus Ratio Values ( $E_0/E_{12}$ ) of 2HL-8 mixes.....	80
Figure 5-10 Modulus Ratio Values ( $E_0/24$ ) of 2HL-3 mixes.....	81
Figure 5-11 Modulus Ratio Values ( $E_0/24$ ) of 2HL-8 mixes.....	81
Figure 5-12 Average fracture temperature for all the tested mixes .....	84
Figure 5-13 Average fracture stress for all the tested mixes .....	85
Figure 5-14 Fracture curve behavior of the three replicates of 1HL-3 0hrs .....	86
Figure 5-15 Fracture curve behavior of the three replicates of 1HL-3 12hrs .....	86
Figure 5-16 Fracture curve behavior of the three replicates of 1HL-8 0hrs .....	87

Figure 5-17 Fracture curve behavior of the three replicates of 1HL-8 12hrs .....	87
Figure 5-18 Fracture curve behavior of the three replicates of 2HL-3 0hrs .....	88
Figure 5-19 Fracture curve behavior of the three replicates of 2HL-3 12hrs .....	88
Figure 5-20 Fracture curve behavior of the three replicates of 2HL-8 0hrs .....	89
Figure 5-21 Fracture curve behavior of the three replicates of 2HL-8 12hrs .....	89
Figure 5-22 Hamburg Wheel Track rutting results of 1HL-3.....	92
Figure 5-23 Hamburg Wheel Track rutting results of 1HL-8.....	93
Figure 5-24 Hamburg Wheel Track rutting results of 2HL-3.....	93
Figure 5-25 Hamburg Wheel Track rutting results of 2HL-8.....	94
Figure 5-26 Rut depth with the standard deviation error bar for all the tested mixes .....	96
Figure 5-27 Fatigue life at different strain levels for 1HL-3 .....	97
Figure 5-28 Fatigue life at different strain levels for 1HL-8 .....	98
Figure 5-29 Fatigue life at different strain levels for 2HL-3 .....	98
Figure 5-30 Fatigue life at different strain levels for 2HL-8 .....	99
Figure 5-31 WÖHLER curve for 1HL-3 0hrs.....	100
Figure 5-32 WÖHLER curve for 1HL-3 8hrs.....	100
Figure 5-33 WÖHLER curve for 1HL-3 12hrs.....	100
Figure 5-34 WÖHLER curve for 1HL-8 0hrs.....	101
Figure 5-35 WÖHLER curve for 1HL-8 8hrs.....	101
Figure 5-36 WÖHLER curve for 1HL-8 12hrs.....	101
Figure 5-37 WÖHLER curve for 2HL-3 0hrs.....	102
Figure 5-38 WÖHLER curve for 2HL-3 8hrs.....	102
Figure 5-39 WÖHLER curve for 2HL-3 12hrs.....	102
Figure 5-40 WÖHLER curve for 2HL-3 24hrs.....	103
Figure 5-41 WÖHLER curve for 2HL-8 0hrs.....	103

Figure 5-42 WÖHLER curve for 2HL-8 8hrs..... 103  
Figure 5-43 WÖHLER curve for 2HL-8 12hrs..... 104  
Figure 5-44 WÖHLER curve for 2HL-8 24hrs..... 104  
Figure 6-1 A systematic structure of all the designed pavements ..... 111  
Figure 6-2 Comparison of IRI value at 90% reliability for Plant1 0hrs with Plant1 12hrs ..... 116  
Figure 6-3 Comparison of IRI value at 90% reliability for Plant2 0hrs with Plant2 12hrs ..... 117



## List of Tables

Table 2-1 AASHTO specification for selecting binder for RAP mixes .....	14
Table 2-2 Fatigue life performance of virgin and RAP mixture (Oliver, 2001).....	19
Table 2-3 Rutting performance of virgin and RAP mixture (Oliver, 2001) .....	19
Table 3-1 Job mix formula of mixes containing RAP .....	35
Table 3-2 Silo and sampling parameters at Plant 1 and 2.....	35
Table 3-3 volumetric properties tests with their equations and specification numbers .....	41
Table 3-4 Total number of the tested fatigue samples.....	49
Table 4-1 Conditioning time and temperature of the asphalt binder samples .....	53
Table 4-2 The blended samples tested under ESEM .....	57
Table 5-1 Air void content of all the tested materials for rutting test.....	72
Table 5-2 ANOVA for VMA values .....	76
Table 5-3 Fracture temperature and fracture stress for all the tested mixes .....	82
Table 5-4 ANOVA for thermal cracking temperature values.....	90
Table 5-5 ANOVA for fracture stress values .....	90
Table 5-6 Rutting depth results for all the tested mixes .....	91
Table 5-7 ANOVA for rutting test.....	97
Table 5-8 $\epsilon_6$ value for each mix (Peak-to-Peak strain amplitudes).....	105
Table 5-9 ANOVA for fatigue test at 500 $\mu\text{m}$ .....	105
Table 6-1 The structure of each of the four pavements .....	110
Table 6-2 main inputs of the AASHTOWare Pavement ME Design .....	112
Table 6-3 Expected commercial vehicle distribution for municipal roadways (ARA, 2015) ....	114
Table 6-4 Climate inputs for AASHTOWare Pavement ME Design.....	114

Table 6-5 Predicted long-term performance of the Plant1 pavements ..... 115

Table 6-6 Predicted long-term performance of the Plant2 pavements ..... 116

## List of Abbreviation

AASHTO	American Association of State Highway and Transportation Officials
AC	Asphalt Cement
BRD	Bulk Relative Density
BSE	Backscattered Electrons
CPATT	Centre for Pavement and Transportation Technology
ESEM	Environmental Scanning Electron Microscopy
EN	European Standards
$\epsilon_6$	Epsilon 6
HMA	Hot Mix Asphalt
HWTT	Hamburg Wheel-Track Tester
MEPDG	Mechanistic-Empirical Pavement Design Guide
MTO	Ministry of Transportation Ontario
NMAS	Nominal Maximum Aggregate Size
PG	Performance Grading
RAP	Reclaimed Asphalt Pavement
SE	Secondary Electrons
TSRST	Thermal Stress Restrained Specimen Test
$V_a$	Air Voids
VFA	Voids Filled with Asphalt
VMA	Voids in Mineral Aggregate

# 1 Introduction

## 1.1 Background

A pavement is a structure of a set of layers of selected materials that are placed on the foundation soil or subgrade. The primary structural function of a pavement is to support the wheel loads and distribute them to the underlying subgrade (Huang, 1993). The main factors weighed in pavement design are; traffic volume, subgrade type and strength, climate, the range of construction materials available, the desired service life, and the thickness of each layer (McLeod, 1956). There are two main types of pavement based on their design considerations; flexible (asphalt) pavements and rigid (concrete) pavements. Canada has more than 1,420,000 km of roads (TAC, 2014), 200,000 of them are in Ontario (OHMPA, 2012). Approximately 95 percent of paved roads in the world are being constructed of or surfaced with asphalt. A typical flexible pavement structure consists of three main layers; surface course, base course, and sub-base course above the sub-grade (natural ground) as shown in Figure 1-1. The surface course is usually Hot Mix Asphalt (HMA) layer. HMA is a combination of approximately 95% aggregate and 5% asphalt binder. A 150 mm thick and 10 m wide road needs approximately 3750 tonnes of HMA layer (Ektas and Karacasu, 2012). HMA layer can be constructed of one or several different HMA sub-layers (Pavement Interactive, 2010). HMA is the stiffest layer and greatly contributes to pavement strength. The underlying layers are less stiff but are still important to the pavement strength as well as the drainage and frost protection. A typical structural design results in a series of layers that gradually decrease in material quality with depth (NAPA, 2001).

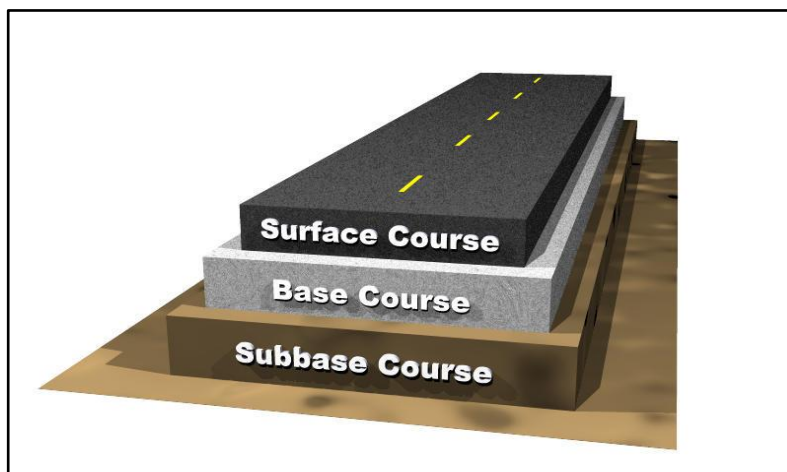


**Figure 1-1 Basic flexible pavement structure**

The cost of the production of asphalt mix is composed of four parts: cost of raw materials, plant production, trucking and lay-down (i.e., construction). Generally, the cost of the materials is the highest among the four costs and represent about 70 percent of the cost to produce HMA as shown in Figure 1-2 (Copeland, 2011).

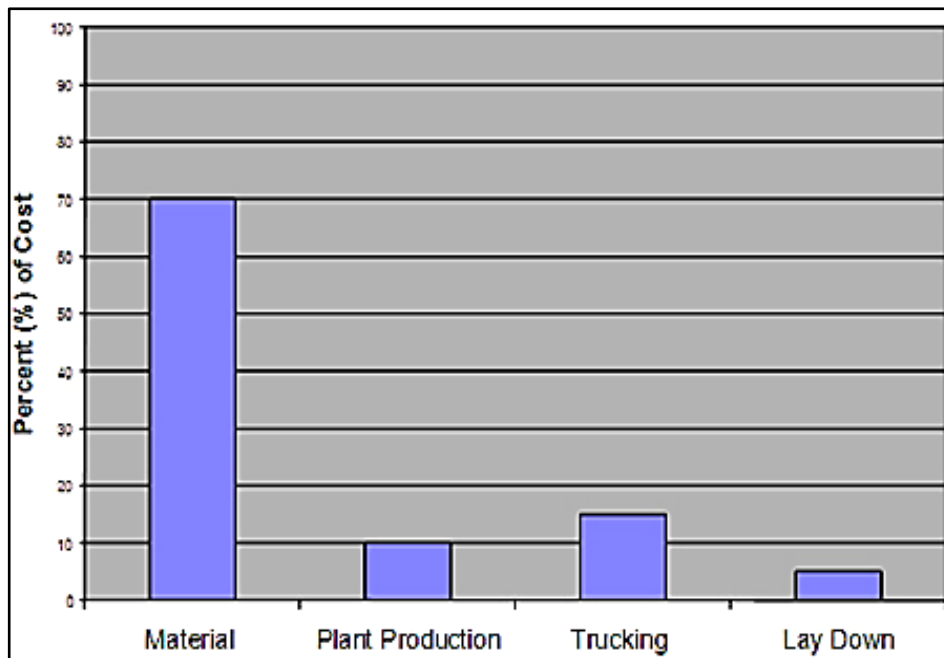


**Figure 1-2 Estimated asphalt production cost categories (Copeland 2011)**

The most expensive and economically variable material in an asphalt mixture is the asphalt binder. As the asphalt binder is a product of crude oil, the road construction industry is strongly associated to the petroleum industry. High volatility has been seen in asphalt binder price over the last few years recent years (NRC, 2011) as shown in Figure 1-3 (OHMPA, 2019). Recycling asphalt pavement creates a cycle of reusing materials and allows a better optimisation of the use of natural resources. Reclaimed asphalt pavement (RAP) is an aged asphalt pavement that has been removed, reprocessed, and combined with virgin material to produce HMA. It is a sustainable alternative to virgin materials because it reduces the need for new asphalt binder and virgin aggregates for the production of asphalt paving mixtures (Emery, 1993). Therefore, the demand to use higher percentages of reclaimed asphalt pavement in the production of hot mix asphalt pavements has increased in the last few decades (Copeland, 2011).

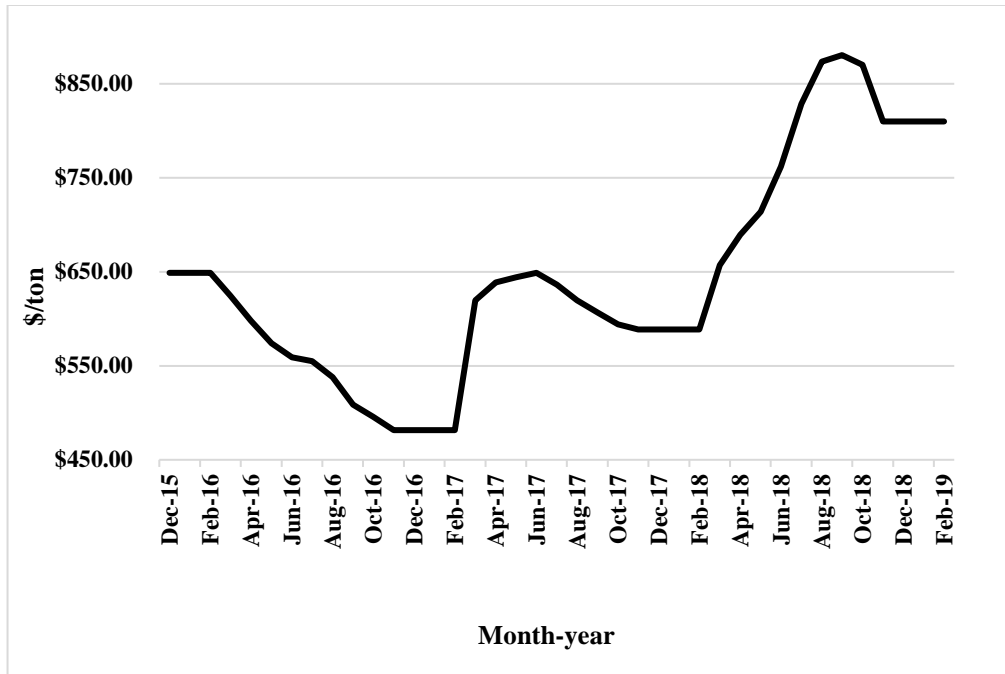


Figure 1-3 MTO asphalt binder price index (OHMPA, 2019)

## 1.2 Research Hypothesis

This research study is based on the following hypothesis:

- During the mixing process of HMA, only a partial blending between virgin and RAP binders occurs.

Some researchers indicated that at least some partial blending occurs during mixing process of the HMA. However, it depends on different components, such as mixing time and temperature (Gaitan, 2012; Huang et al., 2005; Shirodkar et al., 2011).

- Full blending of the two binders might happen over time.

In their recent study, (Pavel Kriz et al., 2014) showed that the diffusion between the in-contact layers of the aged and the virgin binders may explain the blending process. As a significant part of the blending takes place during the mix production, storage and placement of binder, but diffusion continues and drives further blending during road service. While prolonged silo-storage may result in a homogeneous binder blending within few hours, it makes the binder susceptible to significant aging during storage.

- Time-temperature effect of the silo-storage on HMA containing RAP can optimize the blending between virgin and RAP binders.

In 1890, Arrhenius law states that higher temperatures accelerate reactions and blending between the molecules. In addition, it was assumed that the time affects the average distance that the molecules travel to interact with its neighbours (Aquilanti et al., 2010).

- Improving blending efficiency of RAP and virgin binders could potentially offer a solution to enhance the durability performance of RAP mixes.

The aged binder in RAP causes an increase in the mixture stiffness for the mixtures with high in RAP content. Mixture stiffness then leads to a reduced durability and performance of RAP mixtures due to fatigue and thermal cracking (Mogawer et al., 2015). Thus, increasing the blending efficiency between aged and virgin binder, and get the maximum contribution of the aged binder in the mixture would help decreasing the stiffness and, therefore, increasing the durability of the pavement.

### **1.3 Scope and Objectives**

The main objectives of this research are as follow:

- To study the kinematics of blending of aged and virgin binders by considering the time-temperature effect during mixing and silo-storage,
- to evaluate the thermo-mechanical behavior of asphalt mixes containing RAP at different blending/diffusion states,
- to unveil correlations between time-temperature effects and mixture performance,
- to develop an innovative asphalt binder characterization approach using the Environmental Scanning Electron Microscopy.

### **1.4 Novelty of the Work**

It is necessary to investigate innovative approaches to accelerate the diffusion and enhance binder blending in RAP mixes. The literature showed that several researchers focused on evaluating the behaviour of RAP mixes without investigating methods to enhance this behaviour. Even though the use of additives or rejuvenators to enhance binder blending has also been investigated but this solution may be expensive and the long term efficacy of the rejuvenators remains an issue (Al-Qadi et al., 2007; Carpenter and Wolosick, 1980; Mogawer et al., 2013). Few studies have

investigated the asphalt diffusion in RAP mixes, however, all these studies were limited to the use of lab mixes and binders. Therefore, the novelty of this research work remains in the fact that it is the very first study focusing on diffusion in a larger scale during the production and storage stages. As it is estimated that increasing the time in the silo-storage will enhance the blending between the old and new binder. Thus, this study is a complete study to investigate the effect of the silo-storage on the diffusion rate and, consequently, the behaviour and performance of the HMA.

In addition to this, the use of ESEM for the characterisation of asphalt binders is not a common technique. Developing such an approach would also be very innovative and the results obtained are certainly very promising.

## **1.5 Research Methodology**

The objectives of this research were achieved through a comprehensive laboratory evaluation of asphalt binder and RAP-HMA. This is to take into consideration the time-temperature effect on the blending between aged and virgin binder. The laboratory testing was performed at the state-of-the-art testing facility at the Centre for Pavement and Transportation Technology (CPATT) at the University of Waterloo. Moreover, characterization of the corresponding rheological and physicochemical properties of the recovery of binder from the collected mixes are analyzed by Sarnia Technology Application and Research Center of Imperial Oil Ltd, Ontario, Canada. In addition, a long-term performance prediction of the RAP-HMA was conducted for 20-year service life. The research methodology is explained in details in Chapter 3.

## **1.6 Organization of the thesis**

This thesis is organized into chapters with following contents:

**Chapter 1: Introduction** - This chapter provides the scope and overall objectives of this research project.

**Chapter 2: Literature Review** - A comprehensive review into details on current state of knowledge on concepts and methods associated with materials characterization, mix design, test methods, and field performance relating to hot mix asphalt containing recycled asphalt pavement.

**Chapter 3: Research Methodology** - The methodology used to examine the blending between aged and virgin binder and evaluate the hot mix asphalt containing recycled asphalt pavement is



explained in this chapter in terms of: (1) material collection, (2) sample preparation, and (3) details of performing laboratory testing and protocols for both asphalt binder and HMA.

**Chapter 4: Asphalt binder Testing Analysis and Discussion** – The results of ESEM images for virgin, aged and blended binders are analysed and discussed. In addition, the rheological characterization of the asphalt binders considering the effect of the silo-storage time was investigated.

**Chapter 5: HMA Performance Testing Analysis and Discussion** - Laboratory evaluation of the RAP-HMA is presented, discussed, and analysed statistically.

**Chapter 6: Long-Term Field Performance Prediction** - Long-term field performance of the collected samples are predicted by utilizing AASHTOWare Pavement Mechanistic-Empirical Design for 20 years of service.

**Chapter 7: Conclusions, recommendations, and future research** - This chapter provides a general conclusion and summary of key findings of the research. Recommendations for future research guidelines are also highlighted.

## 2 Literature Review

Due to mostly economic and environmental considerations, Reclaimed Asphalt Pavement (RAP) has been commonly used in asphalt paving mixtures for pavement construction and maintenance activities since the 1970s (Copeland, 2011). As a first step in this research, an in-depth study of the literature related to blending between RAP asphalt binder and virgin asphalt binder is performed. In addition, the main properties and performance tests are explained in this chapter.

### 2.1 The Basic Theory of Diffusion

The RAP binder is a thin layer that coats RAP aggregates and does not exist as a free mass in the mixture. Therefore, it may be unreasonable to assume mechanical blending between the aged binder and virgin binder during the mixing process. The blending can be described using other phenomena which can help the two binders blend at proper temperatures for a required time (Pavel Kriz et al., 2014; P. Kriz et al., 2014). This mechanism is called diffusion, which allows molecules transfer in the matter when they have enough energy to move. Crank has defined the diffusion of a material as below:

*“Diffusion is the process by which matter is transported from one part of a system to another as a result of random molecular motion”* (Crank, 1975).

For an atom (or a molecule) to make such a move, two requirements must be met. Firstly, there must be an empty adjacent site. Secondly, the atom (or molecule) must have sufficient energy to break bonds with its neighbor atoms and then cause some lattice distortion during the displacement. At a specific temperature, some small fraction of the total number of atoms is capable of diffusive motion. This fraction increases with rising temperature. In other words, diffusion is the thermal movement of all particles at temperatures above absolute zero. The rate of this movement is a function of temperature, the viscosity of the fluid, and the size of the particles. As the temperature rises, the average speed at which the molecules of a material are moving increases. In addition, the time affects the average distance that the molecules travels to interact with its neighbours. Diffusion explains the flow of molecules from a region of a higher concentration to that of a lower concentration. Once the concentrations are equal, the molecules continue to move, but since there is no concentration gradient the process of molecular diffusion has stopped and is rather directed by the process of self-diffusion, starting from the random motion of the molecules. The result of diffusion is a gradual mixing of material such that the distribution of molecules is uniform. The

diffusion can be influenced by several factors such as shape and size of molecules, temperature, forces between molecules, and the structural rigidity of diffusing molecules (William and Callister, 2007).

There are two mechanisms of diffusion: Vacancy Diffusion and Interstitial Diffusion. Vacancy diffusion involves the interchange of an atom from a normal lattice position to a nearby empty lattice site or vacancy as illustrated by Figure 2-1 (a). As diffusing atoms and vacancies switch positions, the diffusion of atoms in one direction corresponds to the movement of vacancies in the reverse direction. On the other hand, interstitial diffusion in Figure 2-1 (b), is usually faster than vacancy diffusion, and involves atoms that transfer from an interstitial position to a neighboring one that is empty. Interstitial diffusion is found for inter-diffusion of impurities such as hydrogen, carbon, and oxygen, which have atoms that are small enough to implement into the interstitial positions (Krishan and Abromeit 1984).

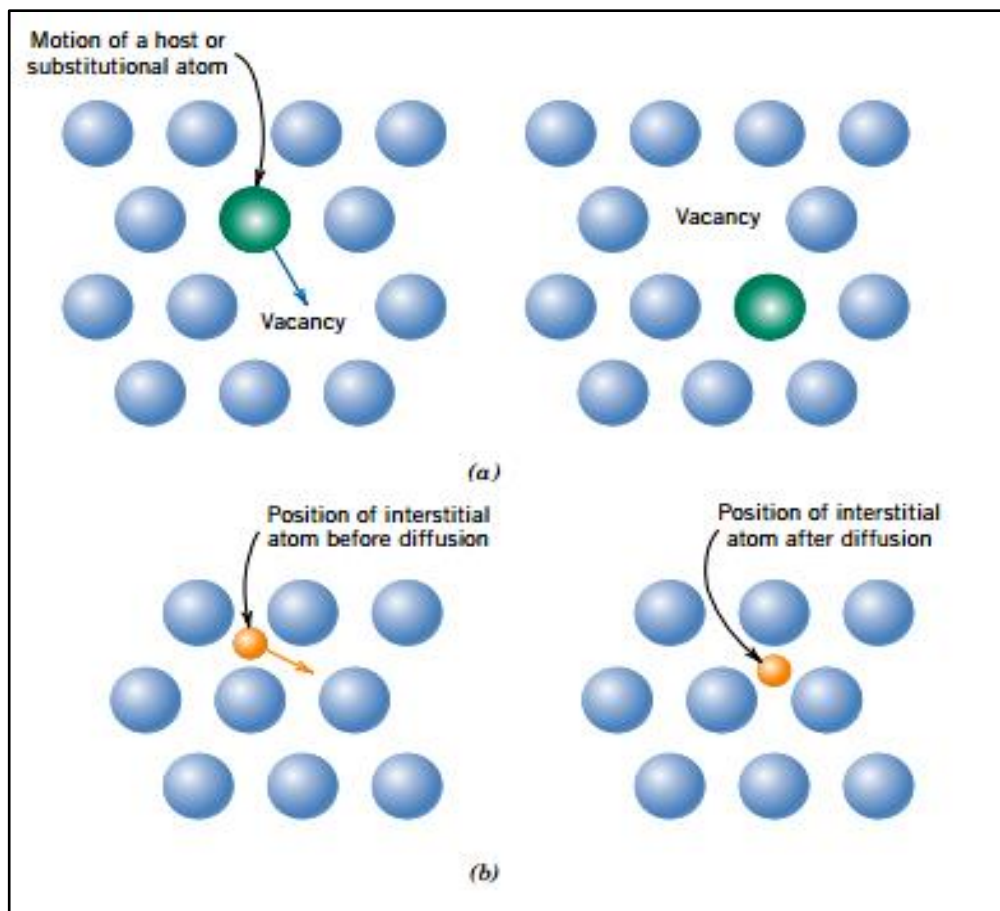


**Figure 2-1 Schematic representations of (a) vacancy diffusion and (b) interstitial (William and Callister 2007)**

Cussler states that the diffusion rate has an inverse relationship with the viscosity of the material. The diffusion of material is described by the diffusion coefficient, which demonstrates the mobility of material caused by diffusion. Diffusion coefficient is assigned as the amount of diffusing material across a unit area during 1 second. Theoretically, the diffusion coefficient is determined using first and second Fick's laws. The assumption of the mathematical theory of diffusion is an isotropic substance (Cussler, 2009). The rate of transfer of diffusing matter over the unit area is equivalent to the perpendicular gradient of concentration measured in the section as shown in the equation below which was adjusted by Fick and called Fick's first equation (Fick, 1855):

**Equation 2-1**

$$F = -D \frac{\partial c}{\partial x}$$

where:

F = rate of transfer per unit of area,

C = concentration of diffusing material,

x = space coordinate,

D = diffusion coefficient.

Diffusion coefficients can be modeled using Arrhenius equation. In 1899, the Swedish chemist Svante Arrhenius (1859-1927) developed one of the most important empirical relationships in physical chemistry:

**Equation 2-2**

$$K = Ae^{-\left(\frac{E_a}{RT}\right)}$$

where:

A = pre-exponential factor,

E<sub>a</sub> = activation energy,

RT = average kinetic energy,

$e^{-\left(\frac{E_a}{RT}\right)}$  = the fraction of reactant molecules.

At higher temperatures, the likelihood that two molecules will interact is greater. This higher interaction rate leads to a higher kinetic energy, which has an effect on the activation energy (E<sub>a</sub>). E<sub>a</sub> is the amount of energy demanded to ensure that a reaction occurs (Aquilanti et al., 2010). When

the activation energy (temperature) is zero, or the kinetic energy of all molecules exceeded  $E_a$ , the  $K$  can be expressed as Equation 2-3 below:

**Equation 2-3**

$$k=A$$

Yet, limited studies have been accomplished on diffusion mechanism between virgin and RAP binders, and none of them have utilized Arrhenius law to estimate the degree of blending between the two binders in a large scale during the production process of RAP-HMA.

## **2.2 Properties of the materials**

### **2.2.1 Elasticity, Viscosity, and Plasticity**

Elasticity is the ability of a substance to deform under an applied load and to return to the original size and shape, instantaneously, when the load is removed. Solid objects will deform when forces are applied to them. If the material is elastic, it will return to its initial shape and size when these forces are removed. Perfect elasticity does not exist in the real world as few materials remain purely elastic even after very small deformations (Saad, 2005). In engineering, the elasticity of a material is characterized using two major properties, namely Elastic (aka Young's) modulus and the elastic limit. The former is also an indication of the resistance to deformation. For instance, a higher modulus indicates that the material is harder to deform. The latter is a measure of the limit of stress beyond which the material no longer behaves elastically and permanent deformation of the material will take place. This means that when the stress is released, the material will elastically return to a permanently deformed shape instead of going back to its original shape. To properly compare two materials, both the modulus and the elastic limit should be considered. For instance, rubbers have a low modulus and high elastic limit comparing to metals which typically have high modulus but low elastic limit. Thus, rubber tends to stretch significantly and then return to its original shape (Landau and Lipshitz, 1959).

The viscosity of a fluid is a measure of its resistance to continuous deformation, or flow, under the effect of shear stress or tensile stress. For fluids, it corresponds to the informal concept of thickness; for instance, honey has a much higher viscosity than water. Viscosity is a property arising from collisions between neighboring particles of a fluid that are moving at different velocities. For a given velocity pattern, the stress required is proportional to the fluid's viscosity. A fluid that has

no resistance to shear stress is known as an ideal or inviscid fluid. Zero viscosity is recognized only at very low temperatures in superfluids. Yet, a liquid would be considered to be viscous if its viscosity is greater than that of water, and may be described as mobile if its viscosity is less than water (Mohammadi and A. McCulloch, 2014). The main characteristic of the viscous behavior is time-temperature dependency

Plasticity describes the deformation of a material undergoing non-reversible changes of shape in response to applied forces. In engineering, the transition from elastic behavior to plastic behavior is called yield (Symon, 1971). Plastic deformation is recognized in most materials, especially metals, soils, rocks, and concrete. Yet, a wide range of physical mechanisms can contribute to inducing plastic deformation. In brittle materials such as concrete, plasticity is caused by slip at microcracks (Aifantis, 1987). For many ductile metals, tensile loads applied to a sample would lead to an elastic response. Any increase in load can be characterized by an equivalent increment in extension. While in the elastic region, the sample recovers to its original size after removing the load. However, if the load exceeds the yield strength of the sample, the extension develops more rapidly as compared to the case of the elastic region. In this case, when the load is removed, some degrees of extension would remain (Kapoor, 1994).

### **2.2.2 Viscoelastic Materials**

Viscoelasticity is the property of substances that exhibit both viscous and elastic characteristics when undergoing deformation. Viscous materials resist shear flow and strain linearly with time when a stress is employed. Elastic materials, on the other hand, strain when stretched and then restore their original shape once the load is excluded. Viscoelastic materials have components of both characteristics, and they show time-dependent strain (Chawla, 1999).

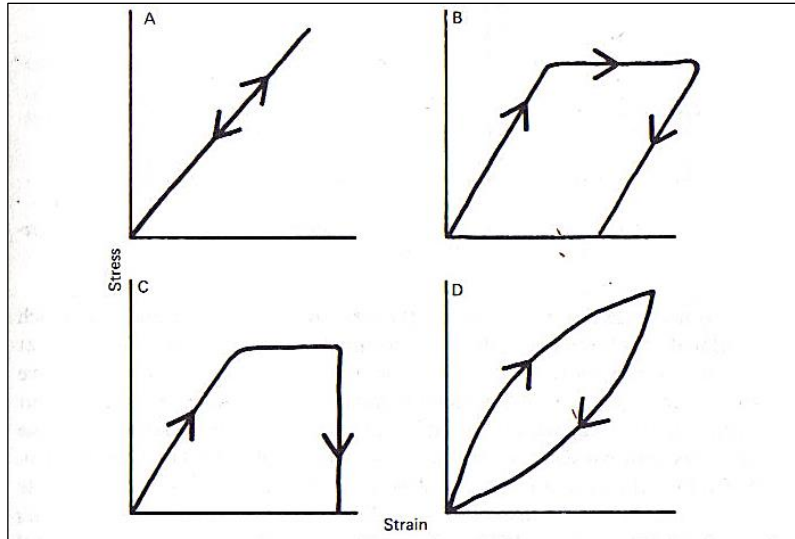


**Figure 2-2 Stress-strain curve A) an elastic material B) an Elastic-Plastic material C) a Plastic material D) a viscoelastic material (Chawla, 1999)**

The behavior of asphalt is generally assumed to be viscoelastic in the domain of small strains ( $<10^{-4}$  mm/mm) (Airey et al., 2003; Benedetto et al., 2007). However, the property that asphalt displays depends on temperature and time of loading. The flow behavior of an asphalt could be the same for one hour at 60°C or 10 hours at 25°C as shown in Figure 2-3 below. This means that the effects of time and temperature are related; the behavior at high temperatures over short time periods is equivalent to what occurs at lower temperatures and longer times. This is often referred to as the time-temperature shift or superposition concept of asphalt binder (Benedetto et al., 2007).

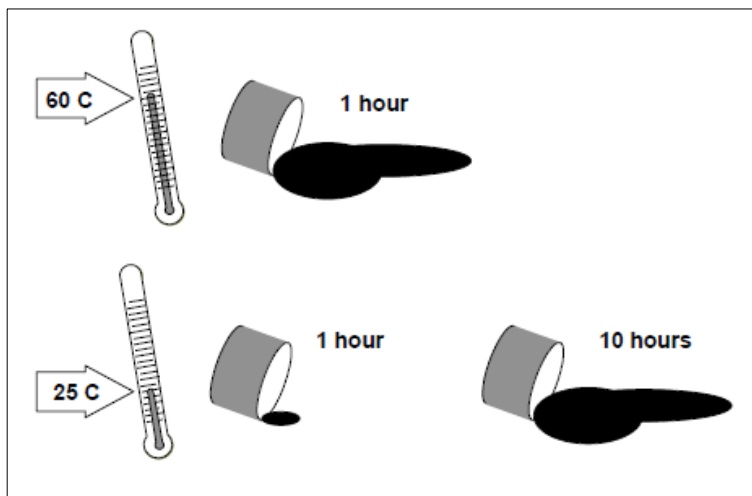


**Figure 2-3 Asphalt behavior at different temperatures (McGennis et al., 1994)**

### 2.3 SuperPave Performance Grade Binder System (PG)

Asphalt binder is a thermoplastic substance that behaves as an elastic solid at low temperatures, and viscous liquid at high temperatures. It may be obtained in natural deposits or may be a refined product; it is a substance classified as a pitch. The most common procedure to evaluate asphalt binder in North America is the SuperPave performance grade (PG) binder system which is a relatively new Asphalt Binder Specification for deciding the appropriate binder for pavement performance concerning rutting, fatigue cracking, and thermal cracking. PG system is based on climate and traffic loading (OHMPA, 1999). The standard notation for PG binder is PG XX-YY where XX is the average-seven day maximum pavement design temperature and YY is the minimum pavement design temperature. For instance, the most common PG in the southern Ontario is PG 58-28, as the average extreme temperatures are 58 and -28. Design temperatures for PG are in increments of 6 degrees. PG binders that differ in the high and low temperature specification by 90°C or more generally require some sort of modification such as polymer and oil as shown in Figure 2-4.

		High Temperature, °C				
		52	58	64	70	76
Low Temperature, °C	-16	52-16	58-16	64-16	70-16	76-16
	-22	52-22	58-22	64-22	70-22	76-22
	-28	52-28	58-28	64-28	70-28	76-28
	-34	52-34	58-34	64-34	70-34	76-34
	-40	52-40	58-40	64-40	70-40	76-40

	= Crude Oil
	= High Quality Crude Oil
	= Modifier Required

Figure 2-4 Prediction of PG grades for different crude oil blends (Pavement Interactive, 2010)

Once the binder is selected, several tests are utilized to define the asphalt binder’s temperature-viscosity relationship such as Rotational Viscosity, Dynamic Shear Rheometer, and Direct Tension (Walker, 2011).



## 2.4 Recycled Asphalt Pavement

RAP was first practiced in 1915 in the United States (Kandhal and Foo, 1997). It has become more popular in the last two decades due to a general rise in crude oil prices as well as environmental waste considerations (Pratheepan and Hajj, 2008). Recently, the use of RAP in asphalt mixes is becoming a common practice by asphalt paving industries. Mixes containing up to 20% RAP are commonly considered to have similar behaviour to virgin mixes (McDaniel and Anderson, 2001). However, the use of RAP is usually limited by recycling capability of asphalt plants and the restrictions in the specifications. In Canada, the use of RAP into new HMA is a regular practice. For example, the Ministry of Transportation Ontario (MTO) allows up to 20% RAP as a standard content in many asphalt mixes and up to 40% RAP in some other mixes such as binder base layer (OHMPA, 2007). MTO regulates the use of virgin binders according to the climate zone and the RAP content in accordance with the American Association of State Highway and Transportation Officials (AASHTO) recommendations. According to AASHTO M323 mix design specification for HMA containing RAP, the binder grade selection depends on the RAP content as shown in Table 2-1 below. Yet, the long term performance of asphalt mixtures is still the key challenge, especially when RAP is used in the mix design.

**Table 2-1 AASHTO specification for selecting binder for RAP mixes**

<b>Recommended fresh asphalt binder grade</b>	<b>RAP %</b>
No change in grade	< 15
One grade softer than normal	15 to 25
Follow recommendations from blending charts	> 25

Some researchers (Baaj et al., 2013, 2011, 2004; Tapsoba et al., 2014) have studied the impact of recycled asphaltic materials (Recycled Asphalt Pavement and Recycled Asphalt Shingles) on the Linear Visco-Elastic behaviour and on the performance (fatigue cracking, rutting, low temperature cracking and moisture resistance) of asphalt mixtures. These studies showed the great potential of using these recycled materials as both substitution material and mixture behaviour modifier. By analyzing the rheological behaviour of HMA produced with up to 40% binder substitution, the authors concluded that the overall performance of the RAP-modified mixes were almost equivalent to the control one. Hence, mixes with RAP should provide more

economical pavement designs using empirical or mechanistic pavement design methods. Other researchers have examined an organic rejuvenator solution to accelerate binder diffusion and enhance the blending (Ech et al. 2014).

Researchers have also been working on projects to establish a guideline for using RAP based on its performance assessments under local climate conditions (Ambaiowei, 2014; Sanchez, 2014; Yang et al., 2013). For example, the performance of laboratory-prepared SuperPave™ SP12.5 mixtures with varying percentages of RAP contents were investigated by exposing the specimens to repetitive loading, low temperature cracking and rutting (Sanchez, 2014). Although these studies have shown the potential of using RAP with minimal negative impacts on the behavior of asphalt mixes with respect to rutting and fatigue, it appears that the low temperature cracking performance remains a major challenge. This can be to some extent attributed to insufficient (inefficient) blending between the aged RAP and virgin binders.

#### **2.4.1 Current Studies on Blending**

The rheological behavior of the aged binder differs from the virgin binder due to the gradual loss of some of its components during the pavement construction process and over the service life of pavements. Therefore, it is important to control the blending process between old and new binders. (Kandhal and Mallick, 1998) concluded that the use of 5-20% of RAP in HMA does not affect the properties of the blend of new and RAP binder. However, more than 20% of RAP can significantly affect the properties of the blend and may change the stiffness of the binder.

A serious concern directly affecting the performance of HMA that incorporates RAP relates to the level of blending that occurs between the residual and virgin asphalt binders. The level of blending affects both the performance of the produced HMA and the economic competitiveness of the recycling process. If the mix designer assumes that full blending happens between the two sources of binders while the RAP is actually behaving as a black rock, the binder will not be stiff enough and the mix will have deficient asphalt binder content. Many design methods including the Illinois Department of Transportation (IDOT) design method assume that the aged binder effectively contributes to the blend (Lighting, 2013). Hence, the amount of virgin asphalt binder can be decreased in the mix design by the full amount of the RAP binder for the percentage specified (Al-Qadi et al., 2007). In contrast, if it is assumed that RAP does not blend with the virgin asphalt binder when it is actually blending, then the binder will be more viscous than expected.

The problem can be further complicated when considering that the blending process may take some time to occur and that it is also influenced by the rejuvenating agent (Carpenter and Wolosick, 1980). Despite some differences between the mix design procedure for a conventional mix and a mix containing RAP, both mixtures should have acceptable characteristics and deliver the required pavement performance.

In NCHRP 9-12 study, three scenarios of blending between aged and virgin binders were examined experimentally: black rock (0% blending), total blending (100% blending), and actual practice (blending as it usually occurs over time). In all three cases, the overall gradation and total asphalt binder content were kept constant. The maximum and minimum percentages of RAP used were 40% and 10% respectively. Reclaimed asphalt pavement was extracted from sources in Arizona, Connecticut, and Florida. Produced mixtures were compared using SuperPave™ performance parameters obtained from the frequency sweep test, the simple shear test, and the repeated shear at constant height test. The indirect tensile creep and strength tests were also used to evaluate the HMA performance at low temperature. The results of this study indicate that 10% RAP content in the mixture shows no significant difference in terms of using different blending assumptions. However, at a RAP content of 40%, the black rock case was statistically different from the actual practice and total blending cases Figure 2-5. These results indicate that no change in binder grade is required at low RAP contents; though, total blending was not likely at a higher RAP content (McDaniel and Anderson, 2001).

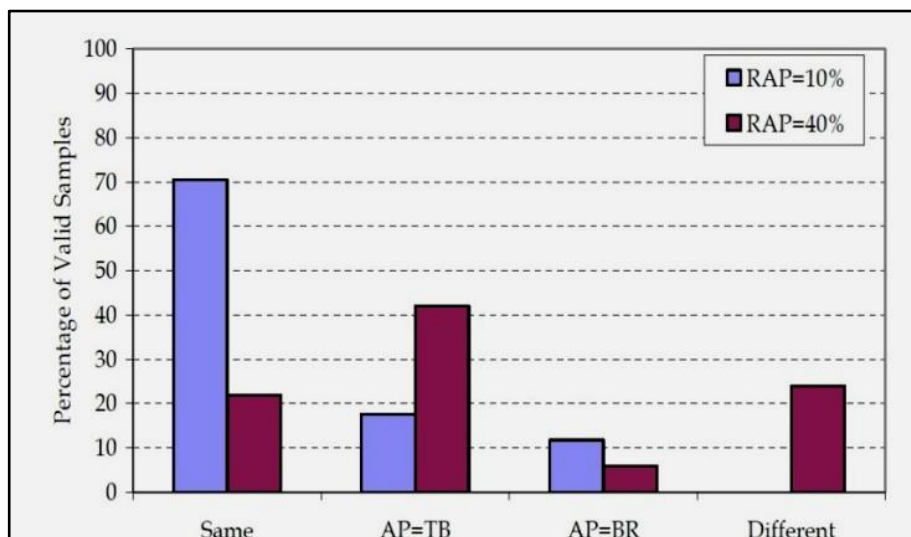


**Figure 2-5 Statistical results of interaction between aged and virgin binders evaluated in NCHRP 9-12 study**

Where,

Same: Actual Practice = Total Blending = Black Rock

AP = TB: Actual Practice = Total Blending ≠ Black Rock

AP = BR: Actual Practice = Black Rock ≠ Total Blending

Different: Actual Practice ≠ Black Rock ≠ Total Blending

In summary, three possible scenarios can be considered: no-blending, partial blending, and complete blending as shown in **Figure 2-6** (Moghaddam and Baaj, 2016b)

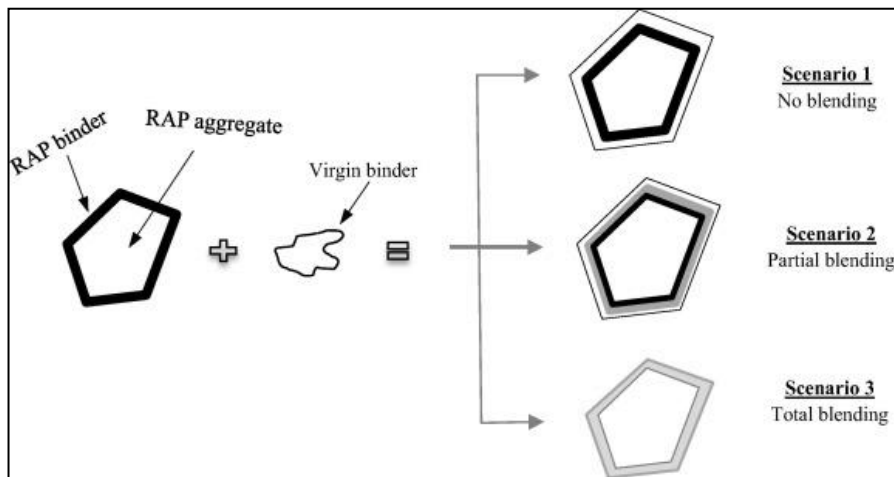


**Figure 2-6 RAP binder and virgin binder blending scenarios (Moghaddam and Baaj, 2016b)**

In parallel to McDaniel and Anderson's work, an experimental program was carried out by (Stephens et al., 2001) to assess the effects of blending between RAP aged and virgin binders on the asphalt mixture. Eleven mixes were prepared with the same gradation, RAP percentage (15%), and virgin binder. The only difference between the samples was the RAP preheating time (0-540 minutes) before being added to virgin aggregates and binder. Another sample with no RAP was prepared for comparison purposes. As shown in Figure 2-7, the preheating time had a significant effect on the asphalt mixture strength, confirming that blending does occur between aged and virgin binders. Besides, when comparing the mix with no preheating to control mix with only virgin materials, an improvement in the indirect tensile strength is recognized upon adding the RAP to the virgin materials even without any preheating (Stephens et al., 2001).

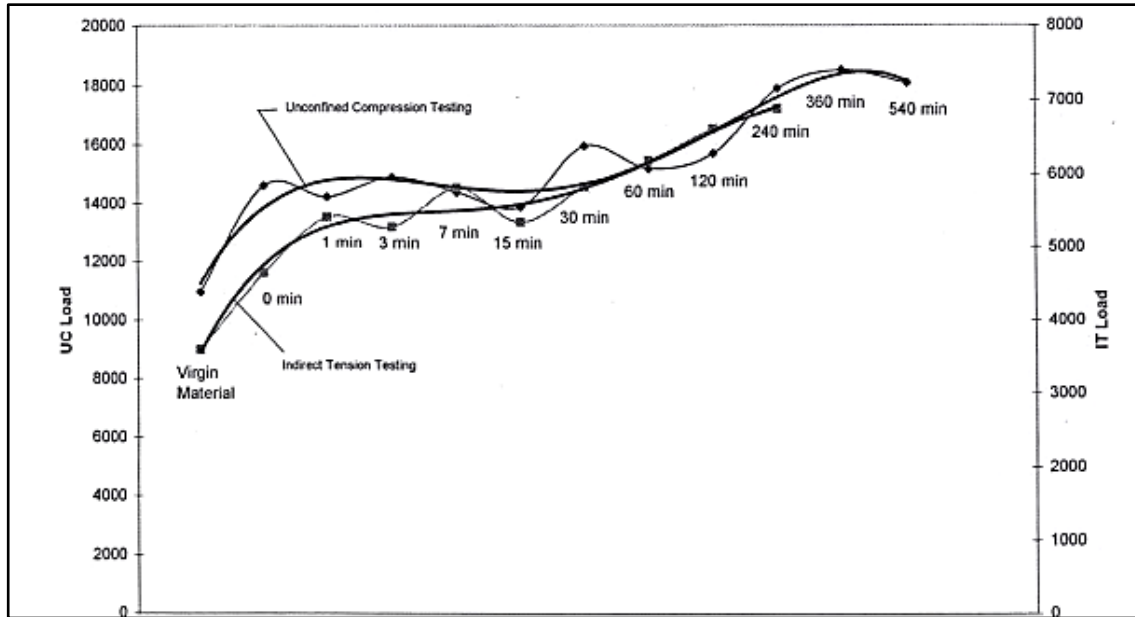


**Figure 2-7 RAP preheat time before mixing comparing the unconfined compression and indirect tension**

Karlsson and Isacson have done a series of studies of the mechanism of blending in asphalt binder and diffusion rate utilizing Fourier Transform Infrared Spectroscopy (FTIR-ATR) and Dynamic Shear Rheometer (DSR) tests. The results of the FTIR-ATR analysis revealed that the increase in polarity and molecular size of the binder molecules as a result of further distillation of bitumen to stiffer grades reduces the rate of diffusion. They also presumed that the diffusion rate is examined by the viscosity of maltene phase rather than the whole binder. They hypothesized that aging has small effect on viscosity of the maltenes as diffusion process is not affected considerably by aging (Karlsson and Isacson, 2003). In this study, they used DSR to determine the diffusion coefficient by studying the rheological properties of the binders. Their findings showed that diffusion determined by FTIR-ATR method happens with the change in rheological properties of the binder after aging. The significant outcome of this study is the indication that the time scales for diffusion identified by FTIR-ATR and rheological changes due to diffusion are of the same order of magnitude. Hence, confirming the prior conclusions that the rate of diffusion in the binder is enough to contribute to the production of isotropically recycled binders during the recycling process (Karlsson et al., 2007).

The National Center for Asphalt Technology (NCAT) at Auburn University also conducted a comprehensive study where the performances of sections of asphalt concrete pavements

containing at least 30% RAP and built with entirely virgin asphalt concrete at the same time were compared. The selected pavements for this study were built between 1990 and 2000 in sixteen states in the U.S. and two Canadian provinces. Most selected sections with RAP showed similar performance or even better than the ones constructed using only virgin asphalt in terms of resisting rutting, cracking, ravelling, and other defects (West and Willis, 2014).

Oliver has also investigated the blending process between aged and virgin asphalt binders utilizing mechanical testing (fatigue and rutting performance tests) in 2001. Results of laboratory testing indicated that the 50% RAP mix showed higher fatigue and lower rutting performance than the virgin HMA. Table 2-2 shows that the fatigue life of the RAP mixture is approximately 37.5% longer than the virgin mixture. On the other hand, Table 2-3 shows that the tracking rate, defined as the rutting depth per 1,000 cycles, was lower for the virgin mix than for the RAP mix and; thus, more likely the RAP mix will have higher rutting in the field. Based on these results, (Oliver, 2001) concluded that aged and virgin binders might not fully blend in HMA due to the formation of agglomerates of aggregate and filler, making it difficult for the fresh binder to penetrate into the RAP binder. Therefore, incomplete blending between virgin and aged binder was presumed to create regions with soft binder in the mixture. This results in an overall softer binder than regular HMA.

**Table 2-2 Fatigue life performance of virgin and RAP mixture (Oliver, 2001)**

Average fatigue life (Cycle at 20° C)		Average air void content %	
Mixture with 50% RAP	Virgin mixture	Mixture with 50% RAP	Virgin Mixture
238,375	89,485	2	2.6

**Table 2-3 Rutting performance of virgin and RAP mixture (Oliver, 2001)**

Average wheel tracking rate at 60°C (mm/Kcycle)		Average air void content %	
Mixture with 50% RAP	Virgin mixture	Mixture with 50% RAP	Virgin Mixture
0.27	0.18	5.1	5.4

(Huang et al., 2005) examined the blending between aged and virgin binders in HMA containing RAP. For the RAP, only the materials passing through the No. 4 sieve were used. For the virgin aggregates, only the particles retained on the No. 4 sieve were used. To evaluate the blending due to mechanical mixing, RAP materials were mixed with virgin aggregates without adding any virgin binder. After mixing, it was resolved that the asphalt binder was decreased by approximately 11% from the RAP materials due to pure mechanical mixing. The authors conducted staged extractions to obtain asphalt binders from various layers coating the RAP aggregates. Results showed that after blending, outside layers of asphalt binder around RAP aggregates were softer than the inside layers of binder. Approximately 60% of the aged binder did not blend with the virgin binder while 40% of the outside binder was a blend between aged and virgin binders. Despite the fact that the authors admitted that the mixtures utilized in that study do not reflect the common HMA used in fields, it was evident that the level of contribution of the residual asphalt binder should be considerably lower than 100% blending for the given mixing procedure.

(Kandhal and Foo, 1997) assumed that if the RAP binder does not blend with the virgin binder; the pavement performance could be compromised. More than 15% of RAP makes the Performance Grade (PG) of the virgin binder decreased due to the increasing in the stiffness of the mixture.

(Poulikakos et al., 2014) employed a methodology (Figure 2-8), for calculating the degree of partial blending in the HMA containing RAP. They concluded that the mixtures containing RAP have a lower cumulative stress and strain rate than the virgin mixtures. It was revealed that despite the differences in chemical and micro-structural characteristics, a well-designed mixture containing RAP up to 40% can perform as well mechanically as the virgin mixture in laboratory tests.

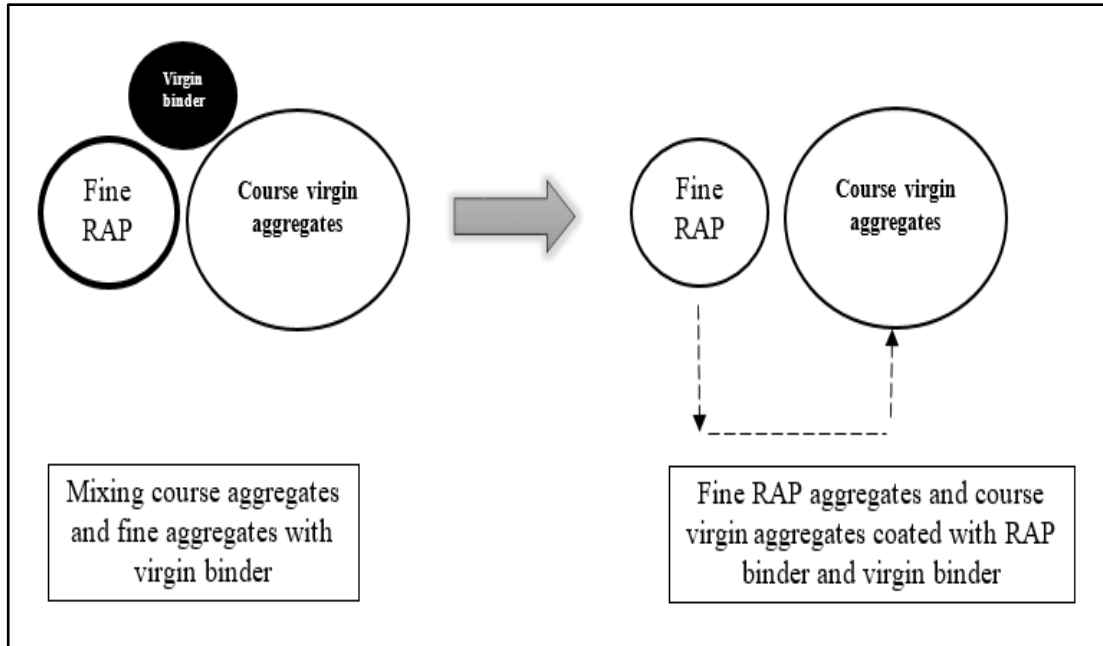


**Figure 2-8 Schematic representation of procedure of blending study (Poulikakos et al., 2014)**

(Shirodkar et al., 2011) concluded that there is a partial blending between aged and virgin binder and the degree of this blending is independent of binder testing temperature. They pointed out that the degree of blending for 25% RAP content with PG 70-28 virgin binder is 70%. The degree of partial blending for 35% RAP with PG 58-28 virgin binder is 96%. Yet, the author stated that these results should not be generalized as they depend on various factors such as RAP and virgin binder properties, gradation, and mixing temperature.

Literature indicates that two factors can have significant impact on the blending process between aged and new binders in RAP-containing HMA mixes: i) mechanical blending, and ii) diffusion between aged and new binders. While mechanical blending is mainly controlled by production conditions, higher temperatures can provide enhanced driving force for blending between binders (Alavi et al., 2015; Pavel Kriz et al., 2014; P. Kriz et al., 2014; Rad et al., 2014). The previous work done by Kriz et al. has contributed to the understanding of the blending phenomenon. Their research showed that the diffusion between the in-contact layers of the aged and the virgin binders may explain the blending process. Also, it has been stated that a significant part of blending can take place during the mix production, storage, and placement of the asphalt mix, where diffusion continues at a much slower rate, during road service life. In asphalt plants,



silo-storage is a staging platform where higher temperatures coupled with longer curing times can facilitate the progress of blending.

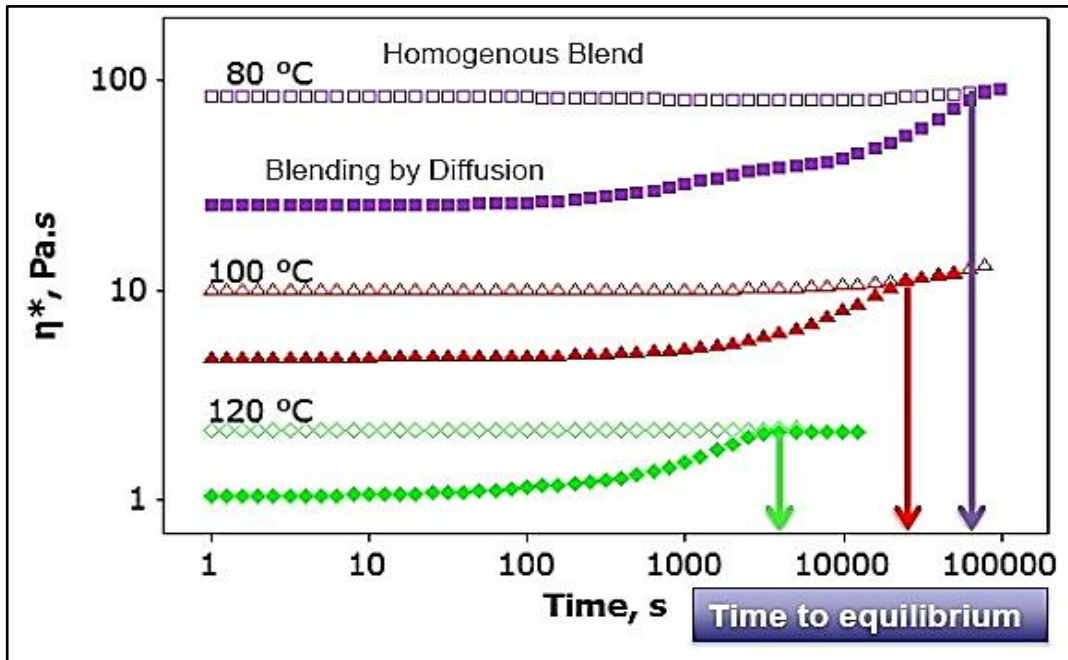


Figure 2-9 Diffusion at varying temperature. (Kriz et al, 2014)

Conversely, the analysis of the Dynamic Modulus Test results of a another study indicate that there was a general increase in the stiffness of HMA containing RAP with the increase of the silo-storage time to 7.5 hours due to oxidation. This indicated that the silo conditions play a key role in changing the HMA characteristics and would lead to some aging. This aging would have a negative impact on the overall performance and durability of the RAP-HMA (Jacques et al., 2016). (West and Willis, 2014) tested the chemical and physical differences of asphalt mixture made with binder and RAP using Differential Scanning Calorimetry (DSC) and the Automated Flocculation Titrimeter (AFT). They determined that the PG of the virgin binder plays a crucial role in the blending efficiency between the virgin and aged binder.

Yousefi (2013) utilized another experimental study to quantify the time and temperature responsiveness of the diffusion rate and final degree of blending that happens between aged and fresh binders. In this study, it is confirmed that at conditioning temperatures below 100°C very limited blending occur between the fresh and RAP binder occurs. Thus, increasing the temperature could enhance the blending phenomena (Yousefi, 2013).

Bowers (2013) found that different additives, such as foaming, can improve the blending efficiency of RAP in mixtures which results in a better pavement performance. He has also examined the impact of mixing time and mixing temperature on blending efficiency using rheological testing and Gel permeation chromatography (GPC). All mixing factors were found to influence the asphalt mixture. Blending efficiency, determined with a blending ratio, was less than 80% in all cases.

Bressi et al. (2015) have produced a multiple regression models at different temperatures (30, 40, 50 and 60°C) for the prediction of the complex modulus and phase angle of binder blends. The models examine four variables at the same time: the source of virgin and aged binders, the percentage of aged binder, the loading frequency, and the temperature. They have confirmed that in the high-temperature domain binders are more sensitive to blending than in the low temperature domain.

Results of another laboratory study reveal that during mixing process aged RAP binder and virgin binder do not blend completely and only partial blending occurs. The degree of partial blending was determined by utilizing the rheological tests such as complex modulus and phase angle conducted in Dynamic Shear Rheometer (DSR) (Liphardt et al., 2015).

To conclude this part, mixing time and temperature, RAP content, asphalt binder content, the presence of the additives can play a significant role in the blending process between the aged and virgin binder in RAP-HMA.

#### **2.4.2 Microstructure of virgin and aged binder**

The blending of RAP binder with the virgin binder is an essential factor in the characteristic of RAP mixtures. Microstructure analysis was utilized in several studies to understand the physical and chemical processes of the interaction between the aged binder and the virgin binder. Atomic Force Microscopy (AFM) (Nahar et al., 2013; Zhao et al., 2015) and Environmental Scanning Electron Microscope (ESEM) (El Béze et al., 2012; Mohajeri et al., 2014; Navaro et al., 2012; Rinaldini et al., 2014) have been used for this purpose in the last few years. Hence, the microstructure of the blending zone between virgin and aged binder can be examined using ESEM.

ESEM utilizes a high-pressure gas in the chamber to accommodate a relatively natural state in which materials may be scanned analogously to a standard SEM, but without routine preparation for compatibility (Poulikakos and Partl, 2010). Due to the viscous and volatile nature of the asphalt

cement, certain issues would be encountered when an electron beam is focused on the sample in high vacuum. For instance, the use of the Energy-Dispersive X-Ray Spectrometry (EDS) attachment is restricted due to the carbon atoms that flood the observation chamber from the efflorescence in high vacuum, considerably altering the accuracy of the analysis. Furthermore, the presence of vaporized carbon matter can be a serious concern for the vacuum pumps of the device that is originally designed for crystalline materials (Mikhailenko et al., 2016). Moreover, the viscous nature of bitumen makes it challenging to implement a conductive coating as is performed for SEM observation (Yousefi, 2013).

Furthermore, ESEM utilizes an electron beam and electromagnetic microscopes to focus and direct the beam on the specimen surface. A very small focused electron point is examined in a raster form over a small specimen area. The beam electrons interact with the specimen surface and produce numerous signals that are collected with proper detectors (Michon et al., 1998). ESEM can be utilized to examine wet, oil-bearing, and insulating materials without prior specimen preparation or application of a conductive coating allowing for a gaseous environment in the specimen chamber (Stangl et al., 2006).

The use of ESEM to examine the blending between aged and virgin binder has been investigated in few studies. Analysis of the ESEM images in (Rinaldini et al., 2014) study, confirm that the blending of new bitumen and RAP is location dependent. The boundary between the RAP and virgin materials are observed in Figure 2-10. This figure shows weak spots that can create micro-cracks at this border, which may be an evidence of poor adhesion between old and new material. The results show that it is not possible to clearly see the blending between the two binders, however, there is evidence of a good blending of virgin binder and RAP.

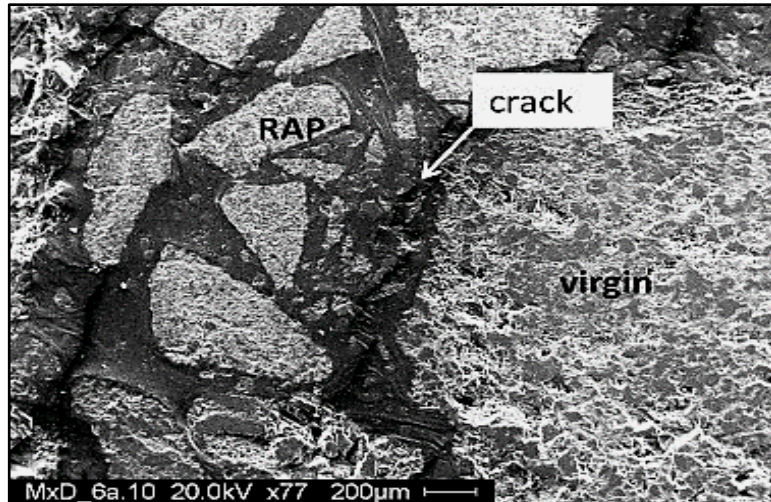


**Figure 2-10 ESEM image showing the crack formation at the border between RAP and virgin materials (Rinaldini et al., 2014)**

In another experimental study (Mohajeri et al., 2014) employed ESEM and other tests towards fundamental understanding of blending phenomenon between RAP binder and virgin binder. They stated that a “blending zone” between aged and virgin binder could be difficultly recognised by utilising ESEM in micro- and nano-scales.

Stangl et al. (2006) used ESEM to examine the impact of environmental conditions (temperature and aging) on the mechanical properties of asphalt binder. In their study, the characterization of binder, comprising the binder chemistry, its microstructure, and its viscoelastic properties were examined considering the fresh and aged states. The final results of their study provide new insight into the durability performance of binders, revealed by the changes in the microstructure properties of asphalt binder as shown in Figure 2-11 (Stangl et al., 2006).

Saturate, Aromatic, Resin and Asphaltene are the four main fraction of the asphalt binder. The fibril microstructure of the asphalt binder under ESEM is likely a combination of these fractions, most likely the asphaltenes and the resins. It should be noted that ESEM images are formed after the upper surface layer oil (Saturate and Aromatic) are removed by the electron beam of the ESEM (Rozeveld et al., 1997).

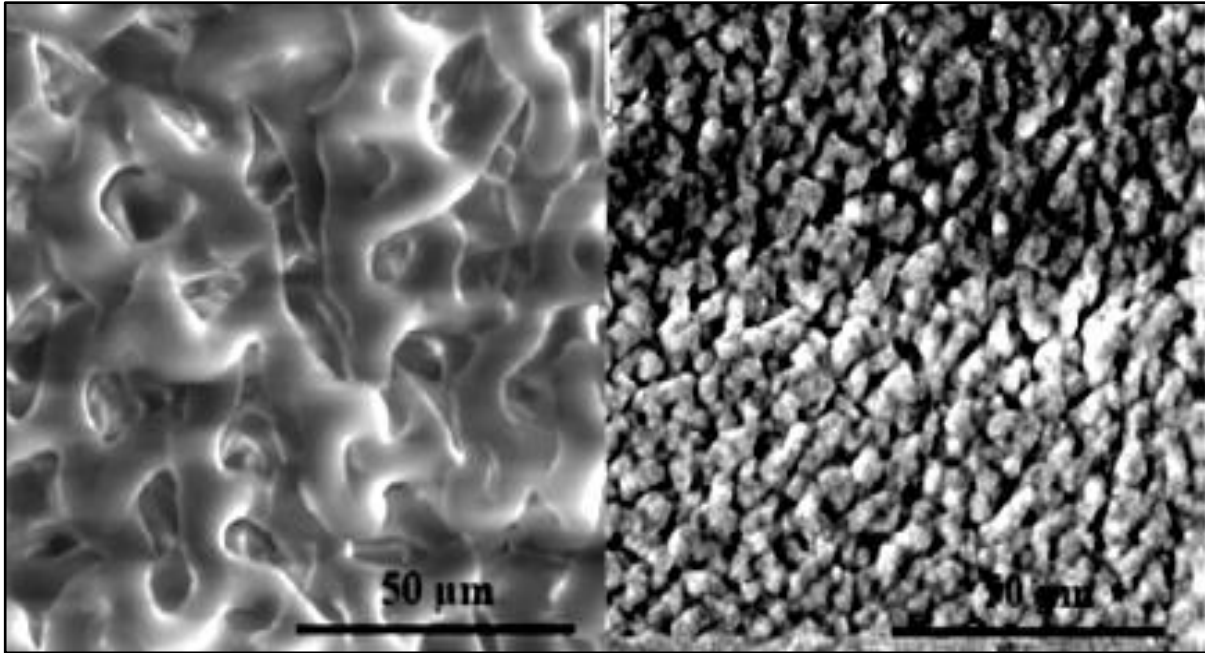


**Figure 2-11 ESEM images, Left: fresh binder. Right: aged binder (Stangl et al., 2006)**

## **2.5 HMA performance Tests**

An ideal HMA mixture is workable, flexible, impermeable, highly resistant to permanent deformation and fatigue cracking, and capable of providing a suitable surface texture. HMA is designed to deliver an expected service life with good resistance to deformation under predicted traffic loads. When these mixture properties are not supported at sufficient levels, HMA can be subject to distresses such as fatigue cracking, thermal cracking, and rutting (TDT, 2011).

### **2.5.1 Dynamic Modulus Test**

The dynamic modulus ( $E^*$ ) is a linear viscoelastic test for HMA that was first developed at Ohio State University. The dynamic modulus changes with temperature, the speed rate of traffic, and age. The dynamic modulus of an asphalt mixture can be determined by utilizing laboratory tests in either a stress-controlled or a strain-controlled mode (Dougan et al., 2003).  $E^*$  can be determined as the stress amplitude divided by the strain amplitude and represents the absolute value of the complex modulus  $|E^*| = (\sigma_o) / (\epsilon_o)$ .

Another output variable of this test is the phase angle ( $\phi$ ). The phase angle is a direct indicator of the elastic-viscous properties of the mix. The value of ( $\phi$ ) = 0 is indicative that the material is performing as a perfectly elastic material. Whereas, a value of ( $\phi$ ) = 90 indicates a perfectly viscous material (Loulizi et al., 2006). The time-temperature superposition principle can

be used for constructing an HMA master curve if the measured values are shifted horizontally from the measured temperature to the chosen reference temperature. A shift factor can be measured as the ratio of two frequencies or times at both temperatures (Zhu et al., 2011). Below (Figure 2-12) is an example of a master curve for eight samples containing different percentage of RAP conditioning at a set of temperature range with 10 °C as a reference temperature (Baaj et al., 2013).

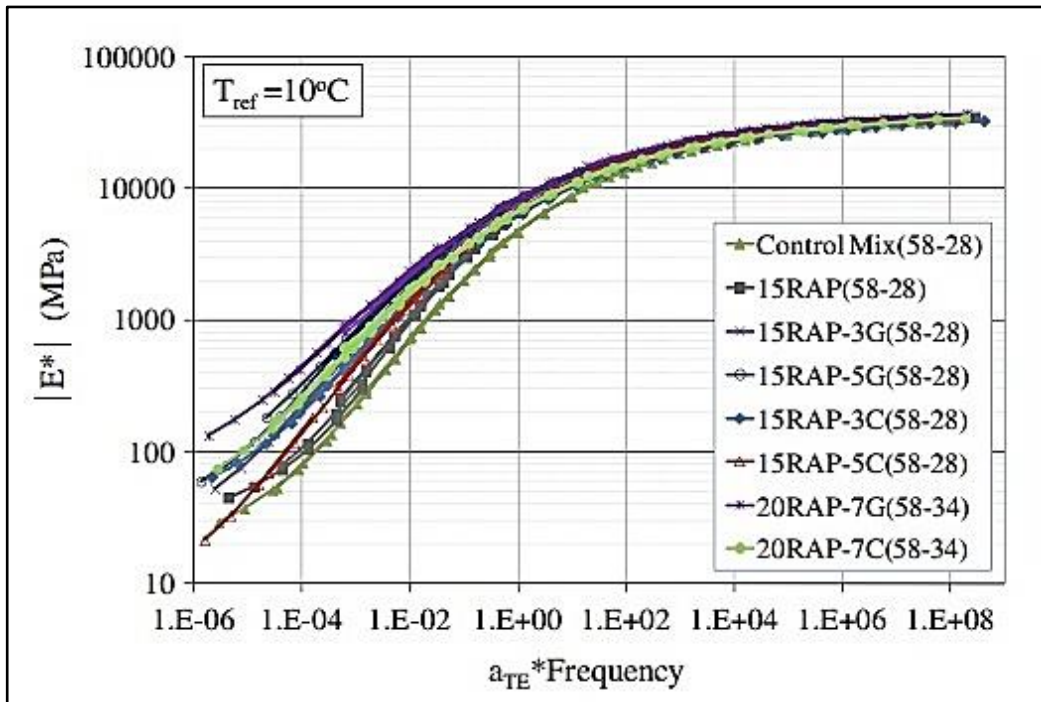


**Figure 2-12 Master curve of the complex modulus of asphalt mixes (Baaj et al., 2013)**

Temperature and frequency have a significant influence on both  $|E^*|$  and  $(\phi)$ . For instance, at a constant temperature of 20°C,  $|E^*|$  increases as the loading frequency and RAP content increase. However,  $(\phi)$  decreases as the loading frequency and RAP content increase.  $|E^*|$  of HMA containing RAP could be as high as twice the dynamic modulus of HMA without RAP. On the other hand, the temperature has an inverse relationship with  $|E^*|$  and positive relationship with  $(\phi)$  at a constant frequency (Rahman and Tarefder, 2014).

### 2.5.2 Thermal Cracking Test

Thermal cracking is a serious concern in the cold regions in the world as it is associated with the growth of high tensile stresses under repetitive exposures to extremely low temperatures (below 4°C) or moderate daily temperature cycles. Thermal cooling cycle shrinkage in an asphalt bound layer restrained, thus, tensile stresses will develop. It is stated that using RAP in HMA likely

decreases the rutting, but increases the possibility of thermal cracking at low temperatures (Gardiner and Wagner, 1999). The Thermal Stress Restrained Specimen Test (TSRST) is utilized to determine the low-temperature cracking of HMA. TSRST was developed at Oregon State University (OSU) in the 1990s, and the test method got included in AASHTO TP10 (Jung and Vinson, 1994). During TSRST test, the temperature and the tensile stress are recorded, and the thermal stress temperature curve is plotted as shown in Figure 2-13 (Baaj et al., 2013). Three or four thermistors are attached to the surface of the specimen to measure the specimen temperature and a resistance temperature detector is used to monitor the temperature of the chamber and to control the cooling at a chosen rate (1, 2, 5, and 10 °C/hr) (Marasteanu et al., 2007).

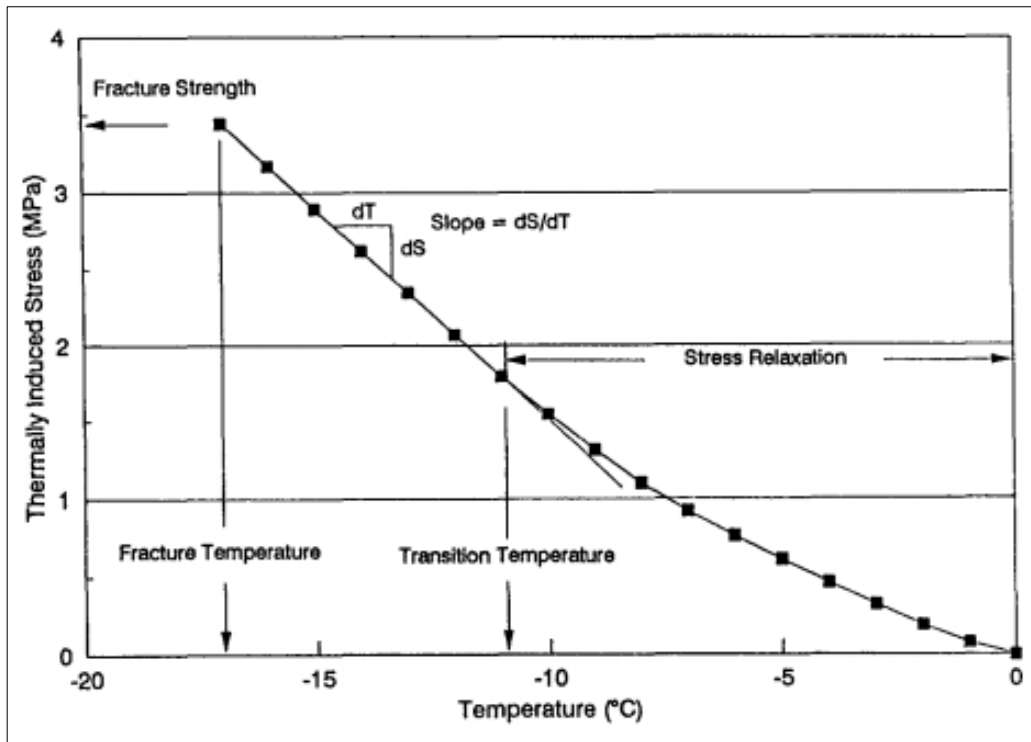


**Figure 2-13 Typical results from the TSRST test (Baaj et al. 2013)**

Various improvements were added to the traditional TSRST method to improve the repeatability of thermal stress measurements as well as provide the ability to measure the thermal strain of an asphalt mixture from an unrestrained specimen. The improvements to the TSRST setup were followed by adjustments to the end plates, gluing technique of the specimens, and the addition of a modular feature for measuring the thermal strain from an unrestrained specimen simultaneously with those of the restrained specimen (Hajj et al., 2015). After implementing these adjustments, the new device was named the Uniaxial Thermal Stress and Strain Test (UTSST) to

be differentiated from the traditional TSRST setup. However, the traditional TSRST was used in this study.

### **2.5.3 Rutting Test**

Permanent deformation or rutting is one of the most common distress modes of asphalt pavements. Rutting is described as progressive accumulation of permanent deformation in one or more layers of the pavement structure due to repetitive loading. Rutting is a primary concern in locations with high in-service temperatures and heavy traffic loads. Laboratory wheel-tracking devices are usually employed to run simulative tests to evaluate HMA rutting performance by rolling small loaded metal or rubber wheels over the surface of compacted asphalt mix samples for several thousands of cycles (usually 20,000) (Izzo and Tahmoressi, 1999; Jr et al., 2000). The performance of the specimens is compared to actual in-service pavement performance.

Studies indicate that using RAP in HMA increases the mix stiffness and, consequently, improves the mix rutting resistance (Haas et al., 2007; Lee et al., 2009). However, it has also been shown that using RAP might lower the rutting resistance when aged and virgin binders are not fully blended. Oliver (Oliver, 2001) investigated the blending process between aged and virgin asphalt binders utilizing mechanical testing (fatigue and rutting tests). The results indicated that the tracking rate, defined as the rutting depth per 1,000 cycles, was lower for the virgin mix than for the RAP mix and; thus, more likely the RAP mix will have higher rutting in the field. It was then concluded that the RAP and virgin binders might not fully blend in the HMA due to the formation of agglomerates of RAP aggregate and filler, making it difficult for the virgin binder to penetrate into the RAP binder. As such, incomplete blending between virgin and aged binder was expected to leave softer areas, susceptible to rutting, within the asphalt mixture. This conclusion was later confirmed by other investigations (Chen et al., 2009; Nahar et al., 2013).

Laboratory wheel-tracking devices are usually employed to run simulative tests that measure HMA performance by rolling a small loaded wheel device frequently across asphalt samples. The performance of the test specimen is compared to actual in-service pavement performance. Most commonly, the 47 mm wide wheel is tracked across a submerged sample for 20,000 cycles using a 158 lb load. Rut depth is measured with a series of linear variable displacement transducers (LVDTs) on the sample (Kandhal and Cooley, 2002).



## 2.5.4 Fatigue Testing

Fatigue cracking, also known as alligator cracking, is the phenomenon that occurs due to the repeated tensile strain at the bottom of the HMA pavements generated by heavy vehicles (Tapsoba et al., 2015). It is generally believed that RAP has an adverse effect on the HMA regarding fatigue resistance. Literature confirms that RAP offers inconsistent fatigue cracking in comparison to virgin mixes (Huang et al., 2005, 2004). Thus, it is important to achieve comprehensive blending between aged and virgin binders in RAP-containing HMA to improve the resistance to permanent deformation as well as to fatigue cracking. The flexural fatigue test is one of the methods used to identify the fatigue life of HMA at intermediate pavement operating temperatures (20°C) (Kingery, 2004). During the test, the beam is placed in a 4-point loading machine and a repeated is applied as shown below. The load frequency is usually set at 1 to 10 Hz. The deflection caused by the loading is measured at the center of the beam. The number of loading cycles to failure can then give an estimate of the fatigue life for the HMA beam. Another parameter that can be calculated through fatigue testing is the dissipated energy of specimen which is a measure of the energy that is lost to the material or developed through mechanical work, heat generation, or damage to the sample (Vukosavljevic, 2006). Figure 2-14 shows a schematic of flexural fatigue test (Pavement Interactive, 2010).

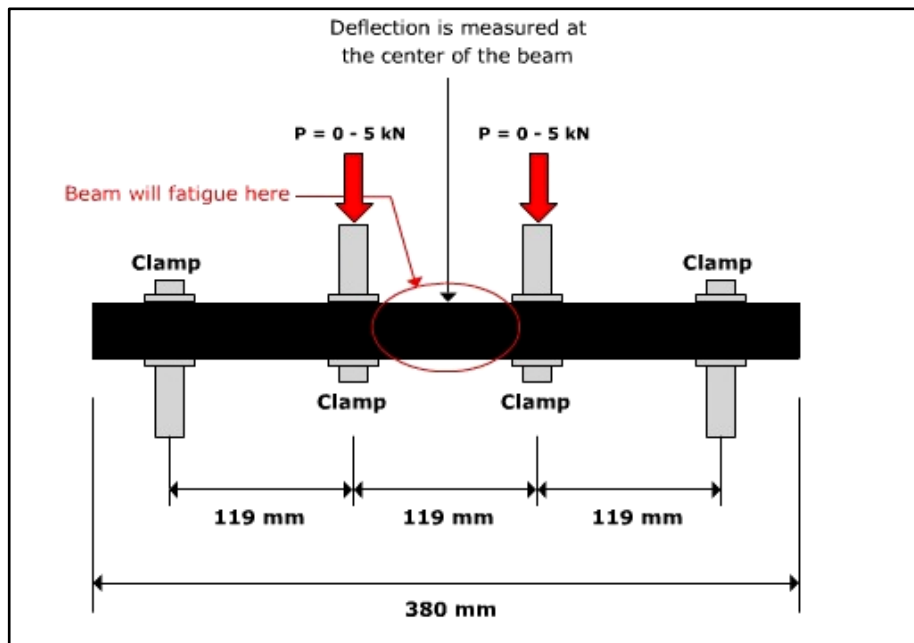


Figure 2-14 Schematic flexural fatigue test (Pavement Interactive, 2010)

## 2.6 Asphalt Plants and Silo-Storage

The effect of silo-storage on properties of HMA has been a topic of investigations since introduction of silos to industry around 1960s (Middleton et al., 1967; Tuttle, 1966). Early silos were found to be prone to mix segregation, asphalt migration and heat loss, which resulted in remodels of silos in 1970s. Storage silos can improve efficiency of asphalt plant production and transportation of material. However, keeping the asphalt mix at higher temperatures, i.e. around 140°C or above, for extended periods posed questions about aging and hardening of the stored material (Kandhal and Wenger, 1973; Middleton et al., 1967; Tuttle, 1966). Early studies shown that long storage times, within 5-10 days, of HMA results in changes in properties of asphalt, such as viscosity increase. The extent of property change, however, was dependent on factors such as type of atmosphere in the silo, source and chemistry of the asphalt binder, additives, asphalt mix gradation, temperature and duration of storage. In cases where hardening was observed, a majority of hardening occurred within the first 24-48 hours of storage (Middleton et al., 1967; Tuttle, 1966). A majority of earlier plant studies on impact of silos were carried out on virgin mixes that contained no RAP (Middleton et al., 1967; Tuttle, 1966). In a recent study, Jacques (2016) confirmed that an increase in silo storage time caused an increase in stiffness for both virgin and RAP HMA. Moreover, the difference in the stiffness of the mixture was statistically significant for the samples that been collected at a storage time of 7.5 hours (Jacques et al., 2016). However, the increase in the stiffness of those samples in that case might be due to the silo conditions or the sampling process.

The most common types of asphalt plants are batch (pug mill) and continuous (drum) plant. Conventional batch plants are common around the world as they offer more operational flexibility, for instance when high RAP content is desired in the mix (Kennedy and Huber, 1985). The full mixing time in this plant usually takes 40-50 seconds. On the other hand, there is no interruption in the production cycle of the continuous plants. The final asphalt mixture is fed into storage silos, for later discharge into trucks and transport to the site. Generally, the manufacturing procedures can be modified to satisfy the client requirements, while keeping a high level of quality. It is worth mentioning that storage silos are usually insulated and sealed airtight to prevent heat loss and to prevent mixture oxidation (Mengel, 1994).

## **2.7 Summary of the Literature Review**

From the above literature study, the blending efficiency of the RAP and the virgin binder is still unexplored clearly. Some researchers believe that the blending efficiency depends on the percentage of RAP in the asphalt mixture, mixing temperature, and duration of mixing. Others believe the blending procedure is temperature independent. Yet, none of the studies to date have focused on diffusion in a larger scale during the production and storage stages.

However, it is clear that the appropriate amount of the RAP aged binder that effectively contributes to RAP-HMA needs to be further investigated. An improved understanding of binder blending would be beneficial in improvement of the thermo-mechanical behaviour of asphalt mixes, which may lead to long lasting and better-performing asphalt pavements.

### 3 Research Methodology

The primary objective of this study was to evaluate the performance of RAP-HMA and examine the blending progress of the aged and virgin binders with respect to the silo-storage time. To achieve overall objectives, the research plan shown in Figure 3-1 was developed.

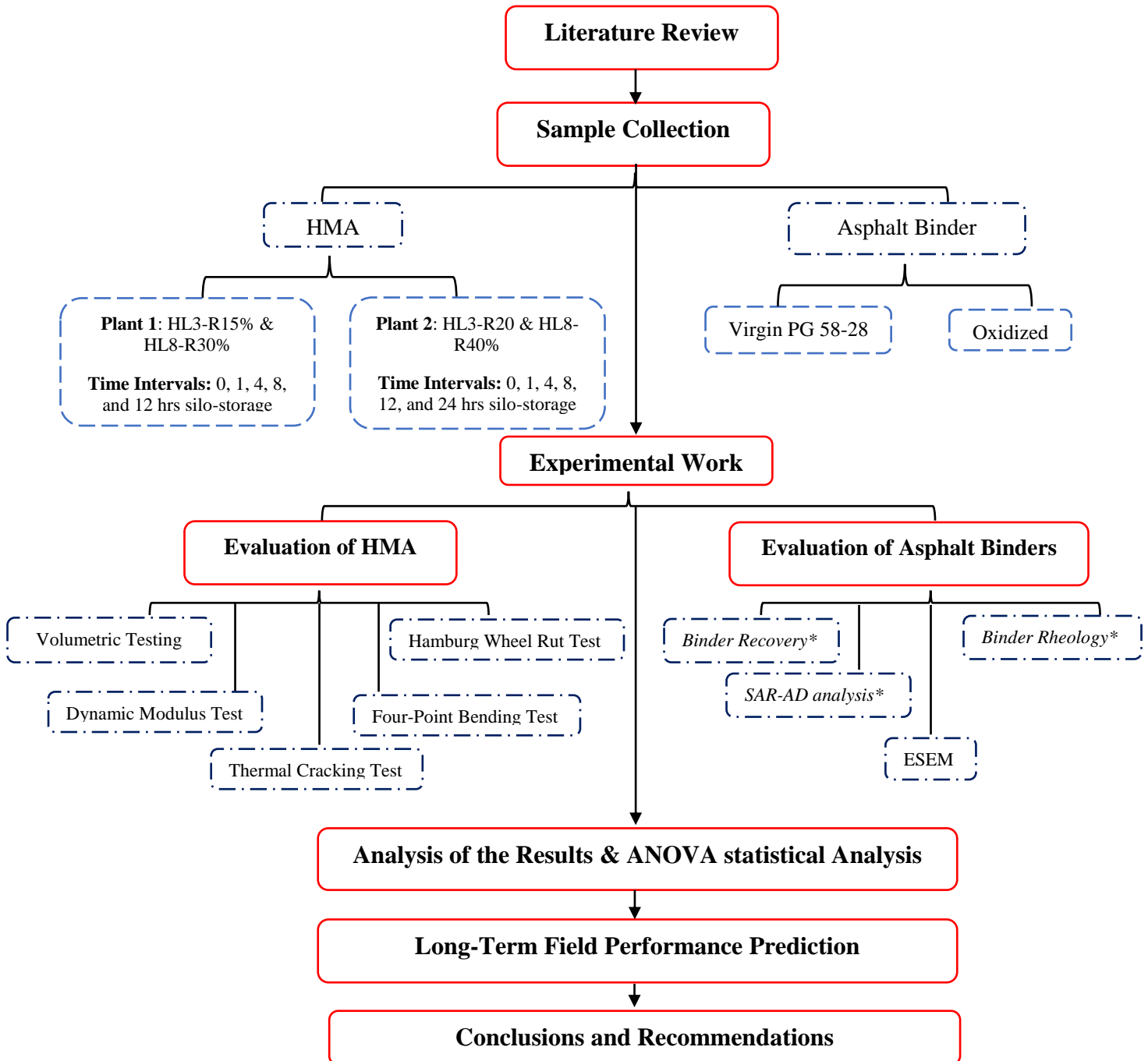


Figure 3-1 Outline of the research methodology

\*These tests were conducted and analyzed by Sarnia Technology Application and Research Center of Imperial Oil Ltd, Ontario, Canada.

### 3.1 Literature Review and state of the current practice

A comprehensive literature review has been conducted in order to enhance the knowledge on RAP binder properties, rejuvenation of recycled binder, and the blending of aged and virgin binders through diffusion. More emphasis was given to understand the thermo-rheological behaviour of asphalt binders and its impact on blending phenomenon, especially with the operations in asphalt plants. Also, experiences of different research groups on the long-term field and laboratory performance of HMA produced with different percentages of RAP were reviewed. For this review, technical reports from different ministries and departments of transportation in Canada and USA, and research papers published in different journals and conference proceedings were surveyed.

### 3.2 Sample collection

Enhanced blending quality of plant-produced mixes could be obtained by utilizing silo-storage facilities. The asphalt mixes used in this study were produced and collected at two plants located in Markham and Cambridge, Ontario, Canada. Figure 3-2 shows the batch and drum asphalt plants (Plant 1) and (Plant 2), respectively.



**Figure 3-2 Plant 1 (left), Plant 2 (right)**

For this research project, two Marshall mixes were produced and collected from Plant 1 including a surface course HL-3 containing 15 percent RAP and a base course HL-8 containing 30 percent RAP. These mixes were labelled as 1HL-3- and 1HL-8 respectively. In addition, two Marshall mixes were produced and collected from Plant 2 including a surface course HL-3 containing 20 percent RAP and a base course HL-8 containing 40 percent RAP. These mixes were labelled as 2HL-3 and 2HL-8 respectively. One should note that HL stands for Hot Load, and the

3 and 8 represents the size of the aggregate used in the mix. Table 3-1 summarizes the job mix formula of these mixes.

**Table 3-1 Job mix formula of mixes containing RAP**

Mix Type	%RAP	% Asphalt Cement (AC)	% Virgin AC	% RAP AC	Virgin AC Grade	Nominal Maximum Aggregate Size (NMAS)	Voids in Mineral Aggregate %	Recommended Compaction Temperature (°C)
1HL-3	15	5	4.4	0.6	PG 58-28	13.2 mm	15.3	135
1HL-8	30	4.7	3.5	1.2	PG 52-34	19 mm	14.6	131
2HL-3	20	5	4.2	0.8	PG 58-28	13.2 mm	15.5	135
2HL-8	40	4.7	3	1.7	PG 52-34	19 mm	14.4	131

Silos at both plants were equipped with a heated oil circulated jacket to heat the bottom of the silo. Sampling was performed from pads of mix collected right after mixing in the plant for 0-hour storage and from silos for stored samples. The main difference between the silos of the two plants is that Plant 1 has an off-loading silo-storage, whereas the silo of Plant 2 is stagnant. Production and sampling conditions of each plant versus the type of the mix sampled are summarized in Table 3-2.

**Table 3-2 Silo and sampling parameters at Plant 1 and 2**

Asphalt course	1HL-3	1HL-8	2HL-3	2HL-8
Ambient day high temperature (°C)	32	34	6	6
Mixing Temperature (°C)	160	160	165	175
Silo Temperature (°C)	140	140	147	147
Production Rate (ton/h)	178	180	180	150
Silo Status	Off-loading	Off-loading	Stagnant	Stagnant

To investigate the impact of storage time on the blending progress and achieving a cohesive final binder, the mix samples were collected as a function of storage time in the silo. The first sampling was done immediately after production (t = 0-hour), and then at several time intervals of silo-storage; i.e., at 1, 4, 8, and 12 hours. For the Plant 2, the samples were additionally collected after 24 hours of storage time. In case of Plant 1, some samples were immediately compacted using SuperPave Gyrotory Compactor at plant's quality assurance laboratory for the dynamic modulus

analysis which was performed later. A refrigerated van was used to transport all the loose and compacted mixes of Plant 1 to the University of Waterloo because of high ambient temperatures during sampling. This was a crucial step to effectively minimize any further diffusion between the time of the sampling and laboratory testing. In case of Plant 2, collected samples were immediately transferred to University of Waterloo for compaction. In both cases, all samples were compacted to reach 7% air void content. After 24 hours of curing time, the BRD test was conducted to calculate the air void content. Then the samples were let to air-dry before storing.

It is worth mentioning that the temperature of the collected mixes was recorded and monitored throughout the whole process of the sampling. All loose mix collected specimens were stored in a refrigerator at University of Waterloo at 7°C until the day of compaction. This was a very important step in this study. Keeping the RAP-HMA samples at constant low temperature eliminates any further potential diffusion between the aged and virgin binder.

In addition to silo-stored samples, RAP samples were collected from both plants. No information on history of the collected RAP samples was available.



**Figure 3-3 Monitoring the temperature of the collected mixes during sampling**

### **3.3 Asphalt Binder Testing**

This section explains the material and method of Micro-mechanical investigation of blending using ESEM, the volumetric properties of the collected HMA, and the performance tests

#### **3.3.1 Microstructure investigation of Asphalt Binder using ESEM**

A microstructure investigation was conducted on the blending phenomenon between aged and virgin binders by utilizing Environmental Scanning Electron Microscope (ESEM). All ESEM tests were performed at the Waterloo Advanced Technology Laboratory (WatLab) at the Chemistry Science Department at the University of Waterloo, Waterloo, Ontario, Canada.

##### ***3.3.1.1 Material***

The virgin asphalt bitumen was an Imperial Oil Scona PG 58-28. The same bitumen was oxidised by air blowing it at approximately 260°C in a lab-scale air blower, with 50 L/kg/min of air for a period of 5 h. With this process, the bitumen was exposed to ageing from heat effects in addition to oxidation from the air. This procedure is used by industry for the aging of roofing materials. It was chosen due to the severity of the method in oxidising the binder. The microstructures were compared with ESEM observation for their relative size, abundance and other characteristics, clearly showing an evolution in the microstructure with different ratios of oxidation.

##### ***3.3.1.2 Sample Holder***

In order to employ a sample holder that fits ESEM testing methods, a sample holder was developed. As it is important to be able to heat the binder during sample preparation, stainless steel was found to be compatible with the needs of both heating the sample on a plate, and observing them in the ESEM. A stainless steel mould was designed and fabricated with a cylindrical opening 8mm in diameter and 2mm in height. The square perimeter of the mould was 10x10mm and a 15mm long handle was also added to be able to move it safely, with a 5mm base to ensure that the mould did not tip over. Figure 3-4 Figure 3-4 Stainless steel sample moulds for ESEM test shows the stainless steel mould for ESEM.



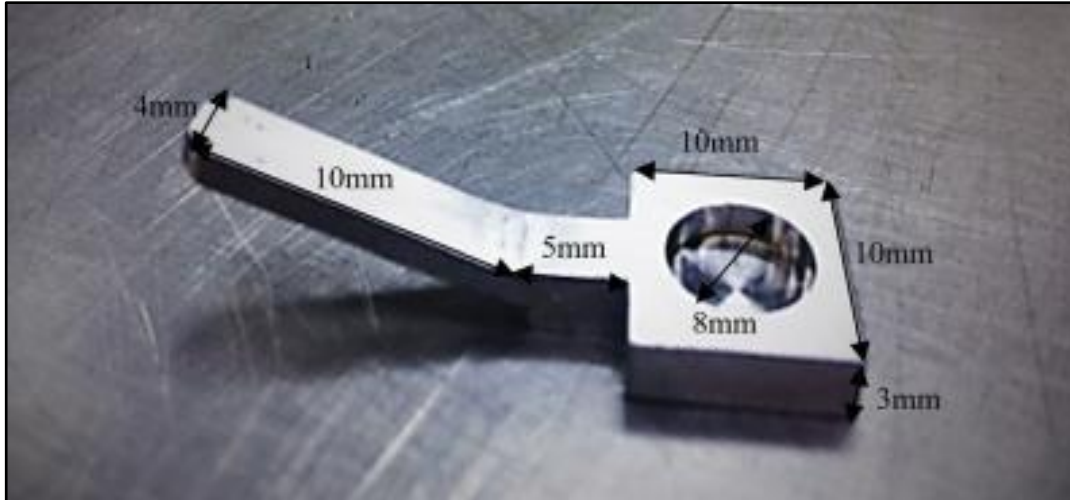


**Figure 3-4 Stainless steel sample moulds for ESEM test**

In addition, stainless steel sample holder with a 2 mm diameter and a 2 mm thick divider in the middle as shown in Figure 3-5 was design and fabricated. The divider was intended to allow for the examination of the evolution of the blending zone at interface of aged and virgin asphalt binder at different temperatures and times intervals. The binder could be added on either side of the wall and heated to make the two binders come into contact. This is used in this study to evaluate the blending of different binders for different time and temperatures All he sample holders were first designed and fabricated at the CPATT (Mikhailenko et al., 2016).

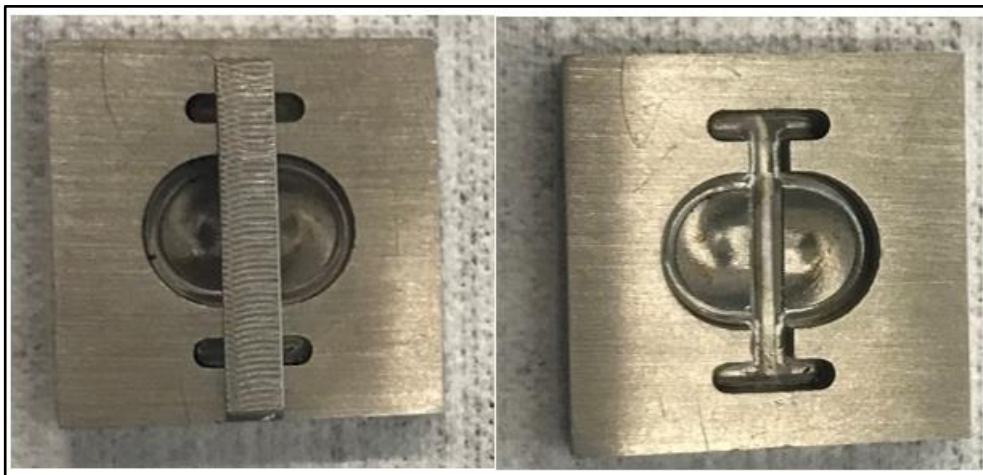


**Figure 3-5 Stainless steel sample mould with divider for ESEM test**

After the test, the sample holders were cleaned by submerging them in a bitumen solvent, and removing the solvent afterwards with a cloth and ethanol.

### 3.3.1.3 Sample Preparation

Three set of samples were prepares for this study. The first set is the virgin and oxidized binders. These binders were prepared separately to examine their microstructure under ESEM. The second set is the blended samples. The virgin and oxidized binder were mixed at different ratio to examine the change in the microstructure with the increase of the oxidized binder ratio. The last set was prepared to examine the evolution in the microstructure of the blending zones at the interface of the aged and virgin binder with respect to the conditioning time and temperature. The preparation of these samples are explained in details in Chapter 4.

### 3.3.1.4 ESEM Observation

The ESEM used was an FEI Quanta 250 FEG at the Watlab of the University of Waterloo, shown in Figure 3-6, with the Energy Dispersive Spectrometer EDS removed since we did not require it.

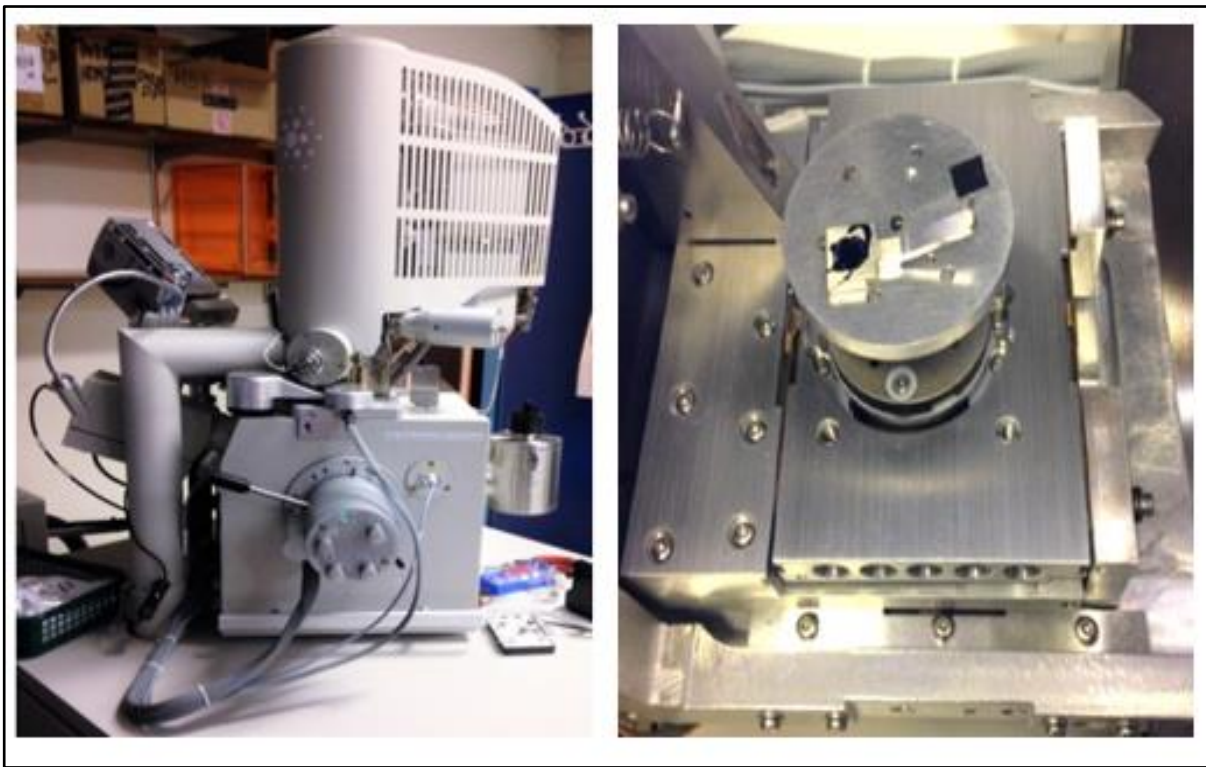


**Figure 3-6 ESEM device at WATLAB**

The observations were conducted in low vacuum mode under room temperature immediately after being removed from the cooler to prevent the contamination with dust. The settings for microscope were an acceleration voltage of 20 keV and a chamber pressure of 0.8 mbar. A lower acceleration

voltage of 10 keV was tried, but the images were found too dark and required a longer observation time to produce the microstructures.

### **3.3.2 Asphalt Binder Recovery**

Recovery of binder from RAP samples and silo-stored samples were performed according to ASTM D2172, using trichloroethylene (TCE). Solvent recovery was then performed according to ASTM D1856. Afterwards, the samples were scanned with X-ray Fluorescence spectroscopy for presence of excess TCE residues in extracted samples.

### **3.3.3 Binder rheology**

Virgin binders were examined for SuperPave assessment according to AASHTO M320. Extracted binders and RAP samples were examined for shear complex modulus to analyse their high temperature performance and monitor potential aging or hardening as a function of storage in silo. Mastercurves of binders were constructed by merging measured complex modulus in the temperature range of -20 and 80°C with a frequency range of 0.1-100 rad/s at each temperature. The reference temperature of the Mastercurve was selected to be 30°C.

### **3.3.4 SAR-AD analysis**

Separation of asphalt samples was performed by HPLC according the patented Saturates Aromatics Resins and Asphaltenes (SAR-AD<sup>TM</sup>) instrument protocol developed by Western Research Institute (Boysen and Schabron, 2013). The instrument separates asphalt into 8 fractions based on application of solvents of varying solvency and valve switching between 4 different columns. The columns were packed according to standard protocols and thermostated to 30 °C. A quality control sample was measured every 8 samples to ensure stability of response from the instrument.

Asphalt (200 mg) was dissolved in 2 mL of chlorobenzene at ambient temperature with periodic shaking (~30 min). After dissolution 20 µL of the 10 % solution was injected onto the HPLC instrument columns. The HPLC system was equilibrated with heptane prior to injection and the sample was passed over the PTFE, glass beads, aminopropyl silica and silica gel columns sequentially with a flow rate of 2.0 mL/min. The representative pressure range for the separation sequence was 10 - 25 bar. The solvent fractions were detected in the order of saturates, naphthene saturates, cyclohexane asphaltenes, toluene asphaltenes, methylene chloride: methanol (98:2) asphaltenes, aromatics 1, aromatics 2 and resins by varying solvents. The separation was complete in 80 min after injection.

### 3.4 HMA Testing

All HMA performance tests were performed at CPATT at the Department of Civil & Environmental Engineering of the University of Waterloo, Waterloo, Ontario, Canada.

#### 3.4.1 Volumetric Properties of the HMA

The volumetric properties of both HL-3 and HL-8 mixes were examined in accordance to AASHTO specifications. Table 3-3 below shows the volumetric properties tests with their equations and specification numbers.

**Table 3-3 volumetric properties tests with their equations and specification numbers**

Test	Equation	AASHTO Specification
Bulk Specific Gravity of the Compacted Mixture ( $G_{mb}$ )	$G_{mb} = A / (B - C)$ Where, $G_{mb}$ = bulk specific gravity of compacted specimen $A$ = mass of dry specimen in air (g) $B$ = mass of the saturated surface-dry specimen in air (g) $C$ = mass of the specimen in water at 25°C (g)	T 166-11
Air Void Content ( $V_a$ )	$V_a = ((G_{mm} - G_{mb}) / G_{mm}) \times 100\%$ Where, $G_{mm}$ = bulk specific gravity of compacted specimen $G_{mb}$ = Theoretical maximum specific	T 269-11
Voids in Mineral Aggregate (VMA%)	$VMA = 100 - (G_{mb} - P_s) / G_{sb}$ Where, $G_{mb}$ = bulk specific gravity of compacted specimen	/

	$P_s$ =aggregate content by weight of mix % $G_{sb}$ =bulk specific gravity of the aggregate	
Voids Filled with Asphalt (VFA)	$VFA = (VMA - V_a) / VMA$ Where, VMA=voids in mineral aggregate $V_a$ =air void content	/

**3.4.1.1 Voids in Mineral Aggregate (VMA)**

VMA represents the volume of void space between the aggregate particles that is available to accommodate the effective asphalt binder and the volume of air voids required in the mixture. Based on the fact that the thicker the asphalt film on the aggregate particles the more durable the mix, specific minimum requirements for VMA are specified in most specifications. Figure 3-7 shows the illustration of VMA in a compacted asphalt mix specimen.

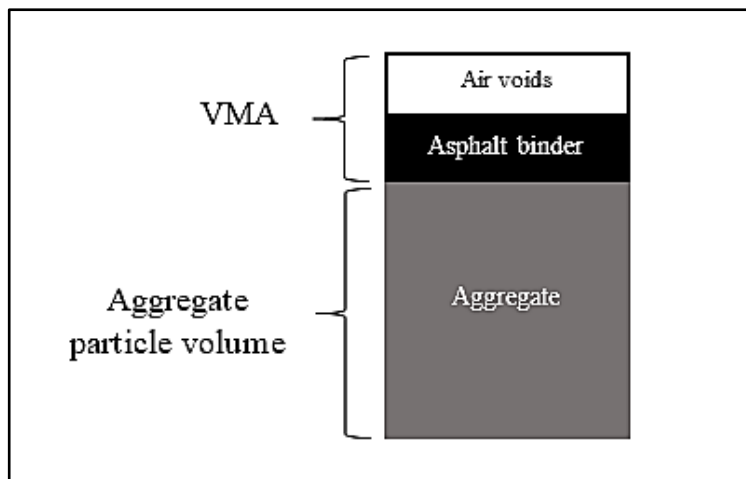


**Figure 3-7 Illustration of VMA in a compacted asphalt mix specimen**

VMA can be defined as the sum of the volume of air voids and effective (i.e., unabsorbed) binder in a compacted asphalt sample (NHI, 2000, p. 13105). As it is assumed that silo-storage time would increase the binder blending in HMA and result in overall less viscous binder, more asphalt binder is absorbed by the aggregate particles in the mix. Hence, VMA decreases. To assess the effect of silo-storage on the VMA of HL-3 and HL-8 mixes, two replicates were examined for 0, 8, and 12-hour samples of each mix.

### **3.4.1.2 Voids Filled with Asphalt (VFA)**

The VFA is the percentage of voids in the compacted aggregate mass that are filled with asphalt binder. It is equivalent to the asphalt-void ratio. The VFA is directly linked to the relative durability. To examine the correlation between the VFA and storage time, two replicates for 0, 8, and 12-hour samples of both HL-3 and HL-8 were calculated.

### **3.4.2 Asphalt Mixture Characterization**

The asphalt mixture characteristics can provide enough data to conclude its field performance. Therefore, an evaluation was conducted on the high, intermediate and low temperature susceptibilities of the collected mixtures containing RAP from the mixing plants. Below are a set of tests planned to evaluate susceptibilities and link the findings with the binder test results:

#### **3.4.2.1 Specimen Compaction**

In case of Plant 1, some samples were immediately compacted at plant's quality assurance laboratory for the dynamic modulus analysis which was performed later. In case of Plant 2, collected samples were immediately transferred to University of Waterloo for compaction. In both cases, all samples for dynamic modulus measurement as well as performance tests were compacted to reach 7%  $\pm$ 1% air void content.

For rutting and dynamic modulus tests, SuperPave Gyratory Compactor at CPATT was used to fabricate the samples. In accordance with AASHTO PP 60-13, "Standard Practice for Preparation of Cylindrical Performance Test Specimens Using the Superpave Gyratory Compactor (SGC) (Montgomery et al., 2009) (AASHTO, 2013), the mixtures were compacted to a 152 mm in diameter and approximately 180 mm in height for the dynamic modulus samples and 63 mm in height for the rutting samples at a pressure of 600 KPa. The mass of the HMA used for the Dynamic Modulus samples and Rutting samples was 6.5 kg and approximately 2.5 kg respectively.

For the Fatigue and Thermal Cracking tests, the mixtures were compacted to 450 mm length, 150 mm width, and approximately 160 mm height at a pressure of 750 KPa using PReSBOX Shearbox Compactor at CPATT. Afterward, the slabs were cut to obtain the samples at the required dimension. The mass of loose HMA used for both Fatigue and Thermal Cracking samples was 18-20 kg. Figure 3-8 shows the both Gyratory and Shearbox compactors. After compaction, the dynamic modulus samples were cut and cored to form the specimens at the

required dimensions. Afterward the specimens were grinded to obtain a smooth leveled surfaces. Figure 3-9 shows the cutting, coring, and grinding machines at CPATT.



**Figure 3-8 SuperPave Gyratory Compactor (left) and ShearBox slab compactor (right)**



**Figure 3-9 (a) coring machine, (b) saw-cutting machine, and (c) grinding machine**

After cutting, coring, and grinding, the compacted bulk specific gravity of the compacted specimen ( $G_{mb}$ ) were determined.  $G_{mb}$  includes the volume of air voids within the specimen.



Determination of  $G_{mb}$  was achieved using an apparatus shown in Figure 3-10 to weight compacted specimen in water.

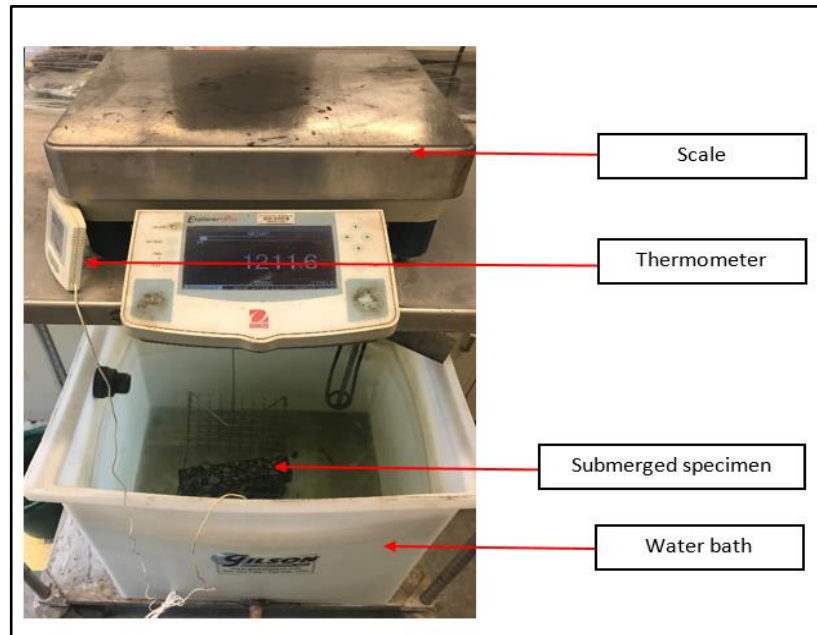


**Figure 3-10 Bulk Relative Density (BRD) apparatus for the compacted HMA**

The test was conducted in accordance with LS-262, “Bulk Relative Density of Compacted Bituminous Mixes” (MTO, 2012b)

#### **3.4.2.2 HMA Performance Tests**

Four performance tests were conducted to evaluate HMA from both asphalt plants. Complex (Dynamic) Modulus test was conducted at different temperatures and frequencies to examine the change in the stiffness with the increase of silo-storage time. Thermal Stress Restrained Specimen Test (TSRST) was also carried out to evaluate the effect of silo-storage time on the thermal properties of the mixes. In addition Hamburg Wheel-Track Testing was employed to examine the improvement in the behaviour of the mixes at different time intervals under high temperature (50 ° C). Finally, the fatigue life of the mixes was examined under different strain levels (500, 400, 300, 250  $\mu$ m) using the four-Point Bending Fatigue Test.

#### **Dynamic (Complex) Modulus Test:**

The dynamic modulus of both HL-3 and HL-8 from both asphalt plants for time intervals at silo-storage were determined using CPATT Material Testing System (MTS) shown in Figure 3-11.



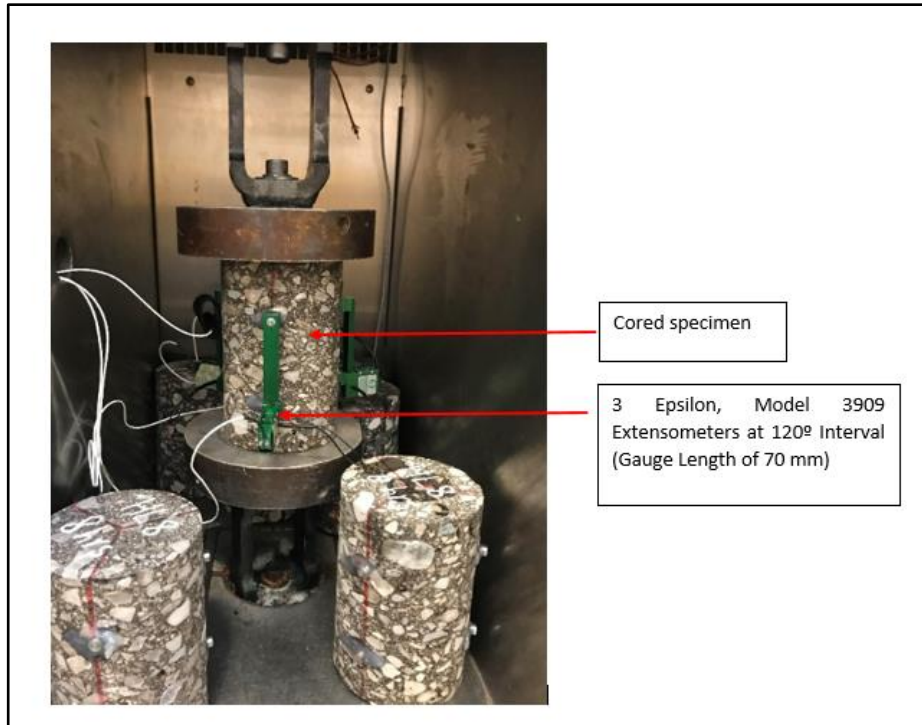


**Figure 3-11 MTS loading farm with dynamic modulus test setup**

The test was performed according to the procedure given in AASHTO TP 62-07, Standard Test Method for Determining Dynamic Modulus of Hot-Mix Asphalt Concrete Mixtures. The test specimens were subjected to a repetitive, compressive, and sinusoidal load. Two Linear Variable Differential Transducers (LVDTs) were used to measure the deformation of test specimen. Triplicate Ø100×150H mm cylinder specimens were used in this test.

All silo time samples were examined at six loading frequencies (0.1, 0.5, 1.0, 5.0, 10.0 and 25 Hz) and five temperatures (-10, 4.4, 21.1, 37.8, and 54.4 °C). Hence, the total number of the tested samples is 66.

**Low temperature cracking susceptibility:**

Low temperature cracking is another major mode of failure of flexible pavements in cold regions as well as in areas with large daily temperature fluctuation. TSRST method was utilized to evaluate the low temperature cracking in asphalt pavement by many researchers. To estimate the low temperature cracking performance of HMA mixtures considering silo-storage time, TSRST was conducted at CPATT using MTS device (Figure 3-12), according to AASTHO TP-10-93 specification, Standard Test Method for Thermal Stress Restrained Specimen Tensile Strength.

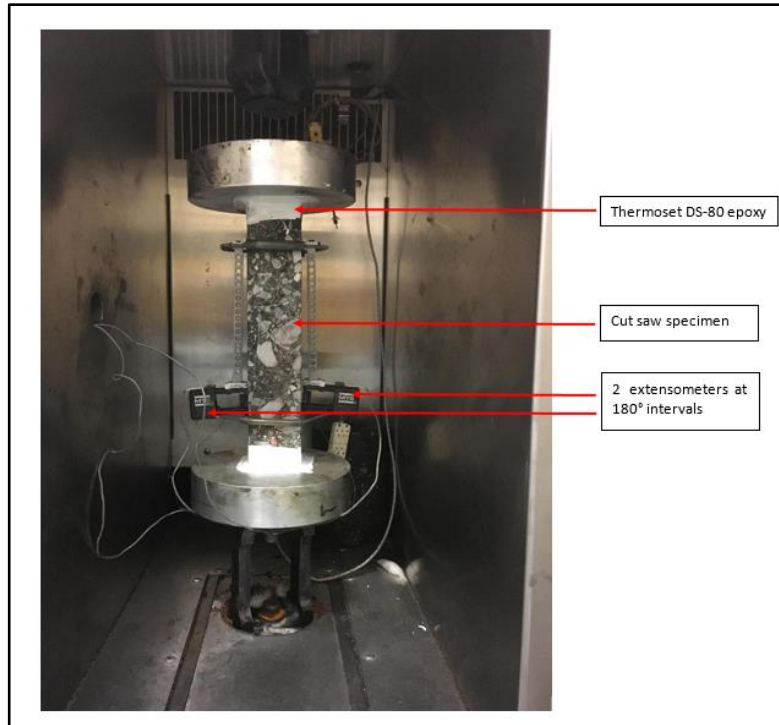


**Figure 3-12 MTS loading farm with TSRST setup**

Three rectangular test specimens (50mm x 50mm x 250mm) were prepared for 0, 8, 12, and 24-hour silo samples for both HL-3 and HL-8. Each specimen were glued to two aluminium end platens with thermoset DC-80 epoxy. The epoxy bond is allowed to cure for at least 6 hours prior to conditioning the test specimen at 5°C in the CPATT MTS-651 environmental test chamber for 3 hours. Actual testing is performed at a constant cooling rate of 10°C/hr. The total number of the tested rutting samples is 42.

**Rutting test:**

The rutting test was conducted in the CPATT (Centre for Pavement and Transportation Technology) lab to evaluate the rutting resistance of different HMA mixes. The test was carried out according to AASHTO T 324-04, Hamburg Wheel-Track Testing of compacted asphalt mixes. The test setup for rutting test is shown in Figure 3-13. Quadruplicate Ø150×63H mm cylinder specimens were used for each run for 0, 8, 12, and 24-hour silo samples for both HL-3 and HL-8. The specimens were tested in wet condition by using solid steel wheels. The test was carried out at the temperature of 50°C. An LVDT device was used to measure the depth of the impression of the wheel (rutting depth). The permanent deformation of specimens was monitored and measured

at least every 400 passes using a data acquisition system. The total number of the tested rutting samples is 56.

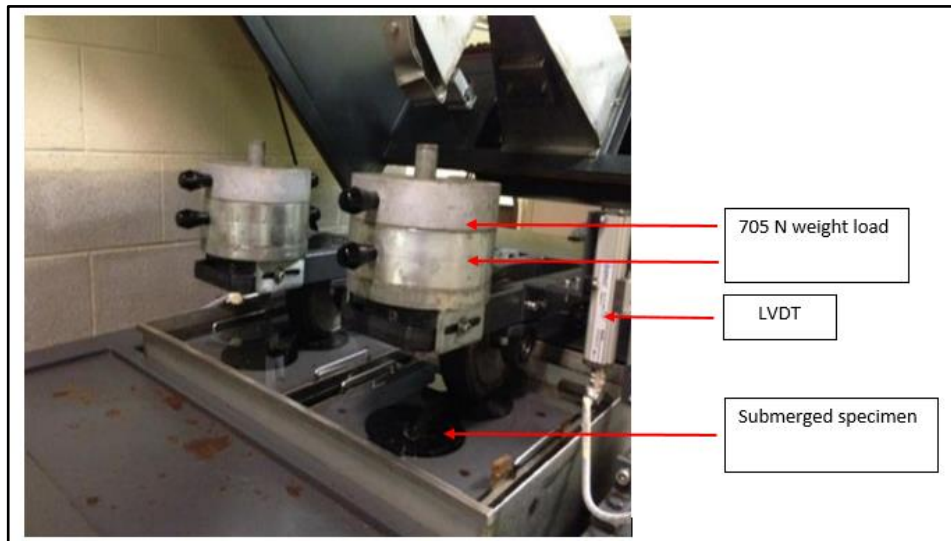


**Figure 3-13 CPATT Hamburg Wheel Tracking Device**

**Flexural beam fatigue test:**

The four-point bending fatigue test was used to determine the fatigue life of different HMA mixtures. The test setup is entirely computer-controlled and consists of a load frame, a closed-loop control, and data acquisition system, as shown in Figure 3-14. The test was carried out in accordance with the AASHTO T 321 procedure “Method for Determining the Fatigue Life of Compacted Hot-Mix Asphalt (HMA) Subjected to Repeated Flexural Bending”. Triplicate 380L×63W×50H mm beam specimens were used in this test for 0, 8, 12, and 24-hour silo samples for both HL-3 and HL-8 from both plants. In a four-point bending frame, the test beams was subjected to repeated flexural loading at a loading frequency of 10 Hz. The deflection level (strain level) was selected to allow the specimen undergo a minimum of 10,000 load cycles before its stiffness is reduced to, at least, 50% of the initial stiffness. The initial stiffness was estimated by applying 50 load cycles at a constant strain level of 250, 300, 400, and 500  $\mu\text{m}/\text{m}$ . The test was performed at a temperature of 20°C.

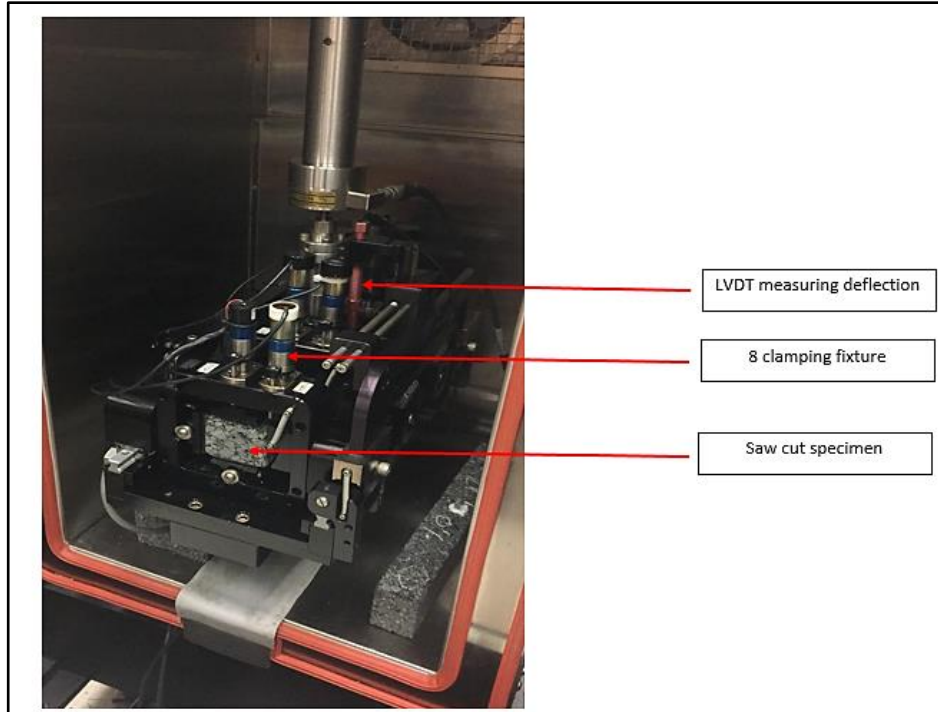


**Figure 3-14 CPATT Repeated Flexural Fatigue Bending Test Setup**

It is worth mentioning here that more than 168 fatigue samples were prepared for the fatigue testing. This is after taking into consideration the desirable air void content. Table 3-4 shows the number of samples prepared for the fatigue testing.

**Table 3-4 Total number of the tested fatigue samples**

Mix	# of strain levels	# of tested silo-storage samples	# of replicates	Total
1HL-3	4	3	3	36
1HL-8	4	3	3	36
2HL-3	4	4	3	48
2HL-8	4	4	3	48
<b>Total = 168</b>				

The results were then analysed using the classical method with the criteria of fatigue failure  $N_f$  50% (WÖHLER curve) as shown in Figure 3-15. In this method,  $\epsilon_6$  is the main criterion which represents the strain level that leads to failure after one million cycles. The higher the value of  $\epsilon_6$ , the higher the fatigue resistance of the asphalt mix. Both  $\epsilon_6$  and the complex (Stiffness) modulus

are used in some Empirical Mechanistic Pavement Design Methods to determine the thickness of asphalt layers.

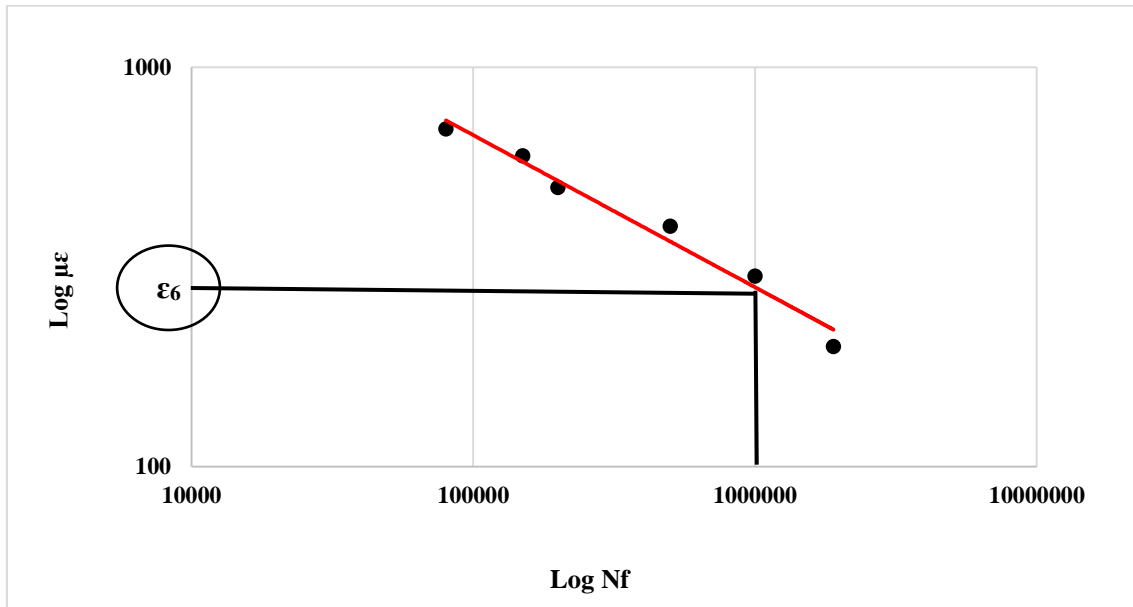


**Figure 3-15 WÖHLER (or fatigue) curve and determination of "ε<sub>6</sub>"**

### 3.5 ANOVA Statistical Analysis

Analysis of Variance (ANOVA) approach was used in order to conduct a statistical analysis on the effect of silo-storage time on the RAP-HMA properties and performance. ANOVA is a statistical tool used for determining the relative difference between means for different data sets. A single factor ANOVA was carried out with the data of all samples with different time intervals (0, 8, 12, 24-hour). The significance level ( $\alpha$ ) or confidence level (%) determines the degree of evidence at which the difference (variability) in the variables is unlikely to have arisen by chance. A 95% confidence level ( $\alpha = 0.05$ ) was used in the study. A null hypothesis ( $H_0$ ) is paired with an alternative hypothesis ( $H_1$ ) to examine the variability of the alternative hypothesis. If  $H_0: \mu_1 = \mu_2$  does not reject the null hypothesis then performance is consistent. However, if  $H_0: \mu_1 \neq \mu_2$ , the null hypothesis is rejected. Montgomery noted that two types of errors are likely with these hypotheses (Montgomery et al., 2009). These include: (1) Type I error where null hypothesis is rejected when it is true and (2) Type II error where null hypothesis is accepted when it is false.

The hypothesis testing was carried out on the assumption that the null hypothesis (i.e. mixes with longer silo-storage time) will perform better than those with shorter or without silo-storage.

The F-test considers the variability in terms of the sum of squares considering the different source of variation. The sum of squares (SS) favors to be greater when the null hypothesis is not true hence SS have to be statistically independent for the F-distribution under null hypothesis to follow. F-value was calculated as shown in Equation 3-1.

**Equation 3-1**

$$F_{\text{calculated}} = (S^2 \text{Control mix}) / (s^2 \text{alternative mix})$$

Where: S2 is the variance of either control or alternative mixes.

If the  $F_{\text{Calculated}} > F_{\text{Critical}}$ , the  $H_0$  is rejected concluding that there were contrasts in the HMA mixes and it is in favor of the alternative mix. On the other hand, if  $F < F_{\text{Critical}}$ , a weak conclusion could be drawn or indicates lack of statistical significant evidence of variation (Montgomery et al., 2009). In this case the control and alternative (i.e. mixes with and without silo-storage) variables are statistically observed to be consistent with each other and perform the same.

## **4 Asphalt Binder Testing Analysis and Discussion**

This chapter focuses on the microstructure analysis of virgin, oxidized, blended asphalt binder, and blending zones under ESEM. In addition, the characterizing of the corresponding rheological and physicochemical properties of the recovered binder from the collected mixes were analyzed at Sarnia Technology Application and Research Center of Imperial Oil Ltd, Ontario, Canada,

### **4.1 Environmental Scanning Electron Microscope (ESEM)**

#### **4.1.1 ESEM Sample Preparation**

Three set of samples were prepares to be tested under ESEM. The preparation protocol of each set is explained in details below.

##### ***4.1.1.1 Virgin and Oxidized Samples***

Following a type of heat-casting method, both virgin and oxidized binders were softened by heating them in an oven for approximately 1h at 110°C inside covered containers in ordered to avoid their oxidization and contamination during the process. Approximately 0.1 g was transferred from the containers into the sample holder with a spatula. The sampling was conducted under a fume hood to reduce the contamination of the sample by dust, which can happen very easily due to the sticky nature of asphalt cement (Mikhailenko, 2015). The sample holder was placed on a heater at 120°C for approximately 10s to flatten the sample and stored in covered plastic containers in a cooler with an electric fan to maintain a constant temperature (8°C).

##### ***4.1.1.2 Blended Samples***

Virgin and oxidized binders were softened by heating them in an oven for approximately 1h at 110°C inside covered containers in order to minimize their oxidation during the heating process. They were then mixed at ratios of 25/75, 50/50 and 75/25 in containers, and then reheated for 10 minutes to be softened again. After that, they were stirred by spatula for 1 minute at 110 °C to get isotropic mixtures. Approximately 0.1g was poured from the containers into the sample holders using a spatula. The sample holder was placed on a heater at 120°C for approximately 10s to flatten the sample. Afterward, the samples were stored in the cooler for 19hrs.

##### ***4.1.1.3 Blending Zone at the Interface of the Aged and Virgin Binder***

Both virgin and oxidized binders were softened by heating them in an oven for approximately 1h at 110°C inside covered containers in ordered to avoid their oxidization and contamination during the heating process. Approximately 0.1 g of each binder was transferred from the containers into

the sample holder with the divider using a spatula. The sampling was conducted under a fume hood. The sample holder was placed on a heater at 120°C for approximately 10s to flatten the sample. Afterward, the divider was removed to allow blending between the two binders. Then, the samples were put in a covered container and stored at the required conditioning time and temperature as specified in Table 4-1. In addition, the sample preparation for the blending zones samples are illustrated in Figure 4-1.

**Table 4-1 Conditioning time and temperature of the asphalt binder samples**

Temperature (°C)	Comments	Storage	Conditioning Time (hours)
25	Room temperature	Fume hood	8, 12, and 24
60	Intermediate temperature	Oven	8 and 12
90	Temperature at which the virgin binder is workable	Oven	8 and 12
120	Temperature at which the aged binder is workable	Oven	8 and 12

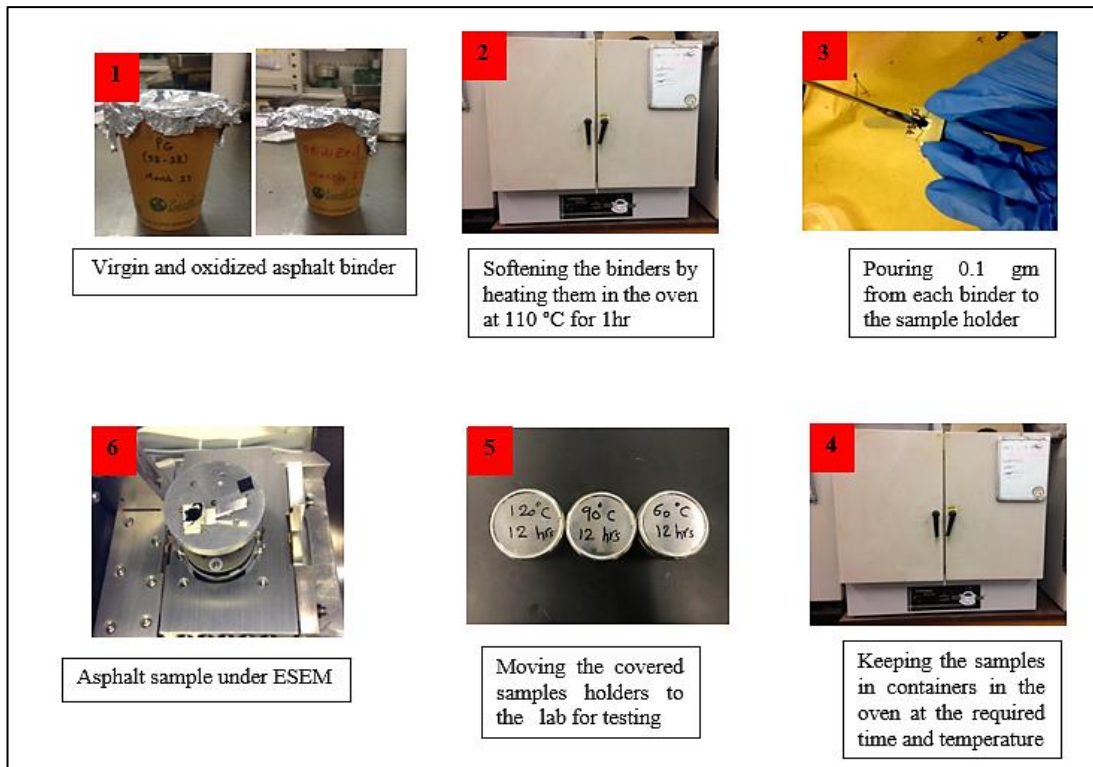


**Figure 4-1 Illustrates the preparation procedure for ESEM samples**



### 4.1.2 Image processing

The resultant ESEM images were processed using MATLAB to measure the fibril size. The developed code of fibril size measurement is shown in Figure 4-2 below. The image received from the ESEM is a result of the interaction of the electron beam with the sample. Due to the interaction with the primary electron beam, the secondary electrons (SE) are released by the sample and interpret the sample topography. Two types of signal are sensed with ESEM; the backscattered electrons (BSE) and the secondary electron (SE). However, SE mode was found to give a clearer image than BSE mode. This is due to the fact that SE mode is able to reveal more of the morphology, whereas the BSE mode is better for designating differences in elemental composition (Milani et al., 2007).

```
clear
clc

geshi={'*.dcm','Dicom image (*.dcm)';...
      '*.bmp','Bitmap image (*.bmp)';...
      '*.jpg','JPEG image (*.jpg)';...
      '*.*','All Files (*.*)'};%%%??????????
[FileName FilePath]=uigetfile(geshi,'Load Image','*.jpg','MultiSelect','on');%%%??????????,?????
if ~isequal([FileName,FilePath],[0,0]);%%%?????????????????
    FileFullName=strcat(FilePath,FileName);
    if ~ischar(FileFullName)
        FileFullName=FileFullName([2:end 1]);
    end
else
    return;
end

    Img = imread(FileFullName);
    figure, imshow(Img)

[x,y] = ginput(2)
stand_value = input('please input the true value: ')
pixel_value_stand = abs(x(2)-x(1))

result = zeros(8,2);

for i = 1:4

[x,y] = ginput(2);
Diameter_pixel = sqrt((x(1)-x(2))^2+(y(1)-y(2))^2);
Diameter_true = Diameter_pixel*stand_value/pixel_value_stand
result(i,:) = [Diameter_pixel Diameter_true];

end
```

Figure 4-2 The developed MATLAB code for fibril size measurement

Saturate, Aromatic, Resin and Asphaltene are the four main fraction of the asphalt binder. The fibril microstructure of the asphalt binder under ESEM is likely a combination of these fractions, most likely the asphaltenes and the resins. It should be noted that ESEM images are formed after the upper surface layer oil (Saturate and Aromatic) are removed by the electron beam of the ESEM (Rozeveld et al., 1997).

### 4.1.3 ESEM Results

#### 4.1.3.1 Virgin Asphalt Binder

Straight run virgin binder PG 58-28 was observed inside the ESEM. The preparation of this sample was previously explained in part (4.1.1.1) of this chapter. Under ESEM, it took approximately 10-15 seconds for the binder to go from flat and featureless to having a visible fibril structure and took another 30s to stabilize. The structure was visible in both Backscattered-Electron (BSE) and Secondary Electrons (SE) modes (Figure 4-3). A magnification of 1000x was found to provide a good overall view of the structure. The fibril size was relatively large at around 15-20  $\mu\text{m}$ , but the structure itself was relatively sparse. Both the SE and BSE modes provided a clear image, but the SE mode image showed more depth. The structure was consistent throughout the sample and the fibril was similar to that found for unaged straight run asphalt binder in (Rozeveld et al., 1997; Stangl et al., 2006) as they also found relatively large and sparse fibrils.

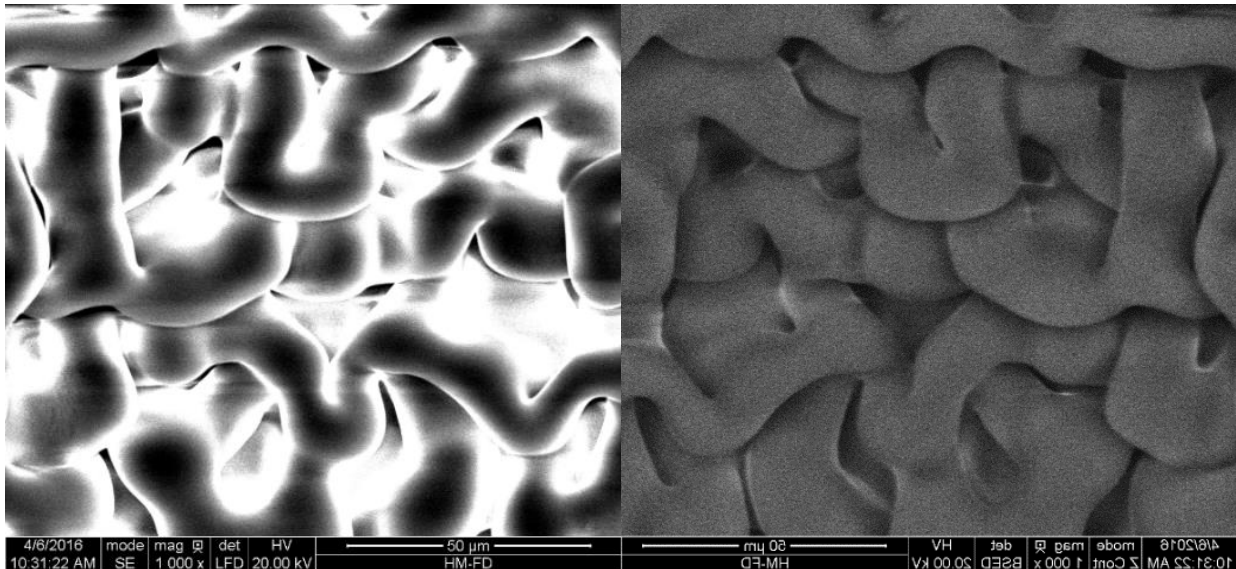


**Figure 4-3 ESEM Images of 58-28 binder with SE (left) and BSE (right) modes at 1000x magnification**

The sample holder was adequate for the testing. The quantity of binder (approximately 0.1g) did not appear to pose a problem for the ESEM. It is worth noting that the height of the handle did require the beam source to be 20 mm away from the surface of the sample as opposed to the standard 10 mm, although this did not appear to be detrimental to the analysis. Additionally, there was a significant presence of dust in some parts of the sample, indicating that the sample preparation could be improved especially during handling the sample from the fume hood to the cooler.

#### 4.1.3.2 Asphalt Binder Oxidation

The preparation of the oxidized binder was explained previously in part (4.1.1.1) of this chapter. In order to determine the validity of the analysis method, the oxidized asphalt binder sample was compared to the virgin one. The resulting images, shown in Figure 4-4, clearly showed an evolution in the fibril structure. As observed by (Rozeveld et al., 1997; Stangl et al., 2006) after aging, the size of the fibrils became smaller (6-10  $\mu\text{m}$ ) and the structure became denser and intertwined. The fibrils also appears to be much more perpendicular and organized.

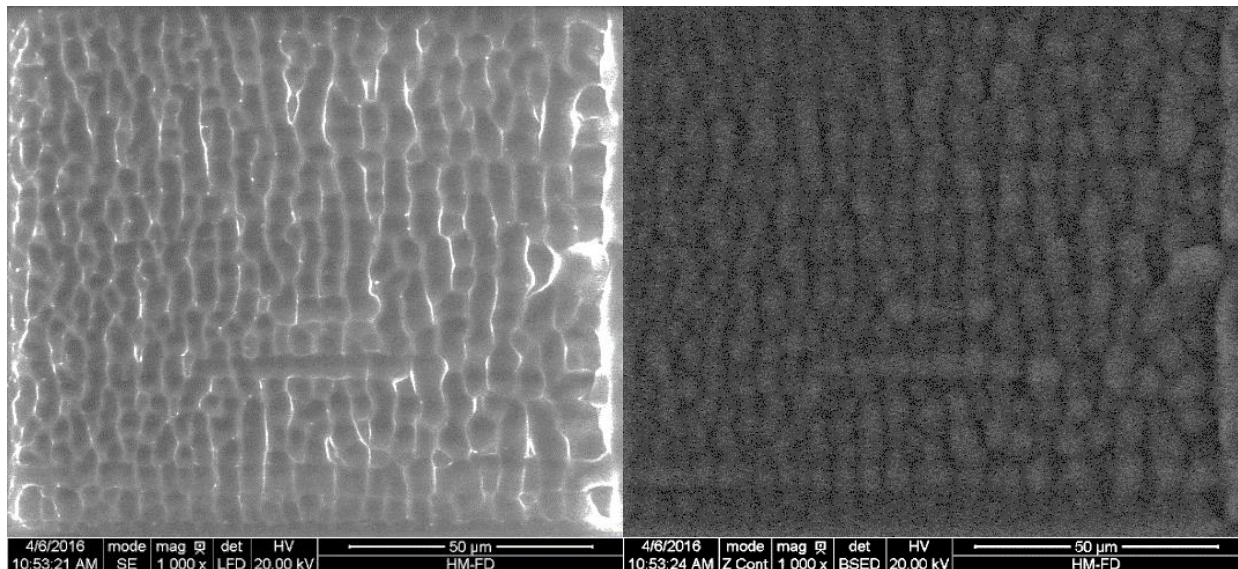


**Figure 4-4 ESEM Images of oxidized 58-28 binder with SE (left) and BSE (right) modes at 1000x magnification**

Although the ESEM images observed in this research is produced by the electron beam, the modification of the structure shows an evolution in the binder misconstruction. Moreover, the evolution of the structure into a denser and connected network of fibrils is consistent with the physical binder hardening observed during oxidation (Lu and Isacsson, 2002; Petersen, 2009). The

change in the structure indeed resembles increase molecular association (Le Guern et al., 2010). It is worth recapping here that the fibril sizes were measured using MATLAB.

#### 4.1.3.3 Blended Samples

The three blended samples were prepared as explained in part (4.1.1.2) in this chapter to be examined under ESEM. This part summarizes the evaluation of the binder structure under SE mode images regarding different binder ratios. Approximately it took 10-15 seconds for the binder to change from flat and featureless structure to having a visible fibril structure and took another 30 seconds to stabilize in the three tested samples. The samples are labeled as shown in Table 4-2 below.

**Table 4-2 The blended samples tested under ESEM**

Label	%Virgin binder content	%Oxidized binder content
B1	75	25
B2	50	50
B3	25	75

B1 sample tended to have relatively comparable fibril size and shape to that of virgin binder (Figure 4-3). Figure 4-5 below shows the microstructure of B1 under ESEM.

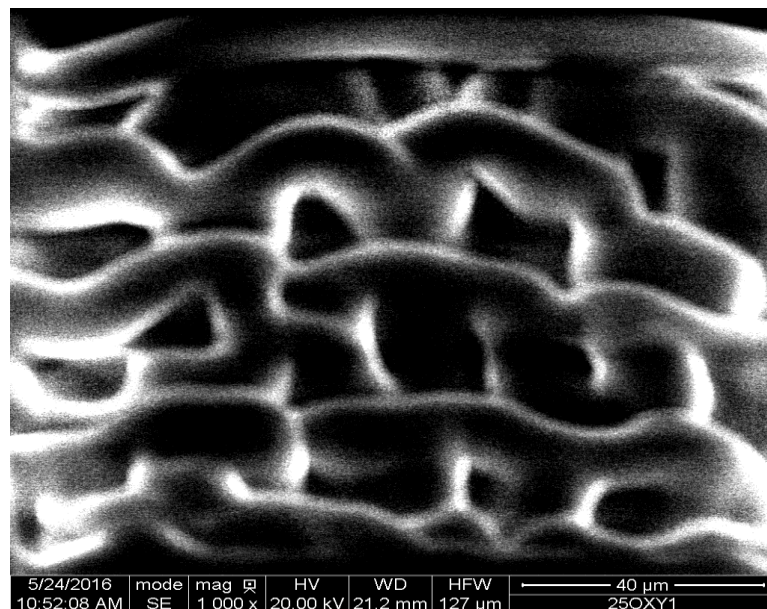


**Figure 4-5 B1 blending sample under ESEM**

Due to the high percentage of virgin binder (75%), sample B1 showed relatively similar microstructure to the virgin binder. Since there is a partial interaction in the properties of the two binders, the effect of oxidized binder appears slightly in the organization and size of the fibrils. Hence, the 75% of the virgin binder dominates the overall structure of the blended sample. Yet, fibrils in B1 image are more organized, connected, and relatively smaller as compared with the virgin binder.

On the other hand, the structure of B2 sample, 50% virgin binder and 50% oxidized binder, showed properties in between parent materials (virgin and oxidized binders). Fibril size appears smaller than the virgin's and larger than the oxidized's with approximately 10-20  $\mu\text{m}$ . Fibril shape looks more connected and denser than the virgin sample; however, it is still unorganized. Overall, the proper mixing temperature (110°C) and time (1 min) of the blended samples results in an isotropic blended sample. Figure 4-6 shows the microstructure of the B2 sample under ESEM.

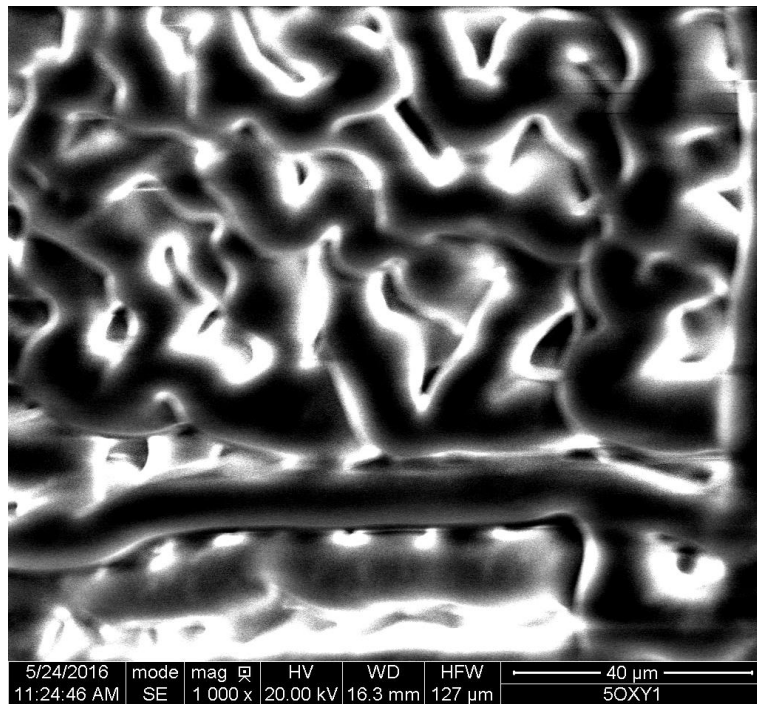


**Figure 4-6 B2 blending sample under ESEM**

Looking at the structure of 75% oxidized 25% virgin blended binder (B3) shown in Figure 4-7, fibril shape tends to appear perpendicular and organized, similar to that of oxidized binder sample. Yet, the fibril size looks large (6-15  $\mu\text{m}$ ) comparing with the oxidized sample.

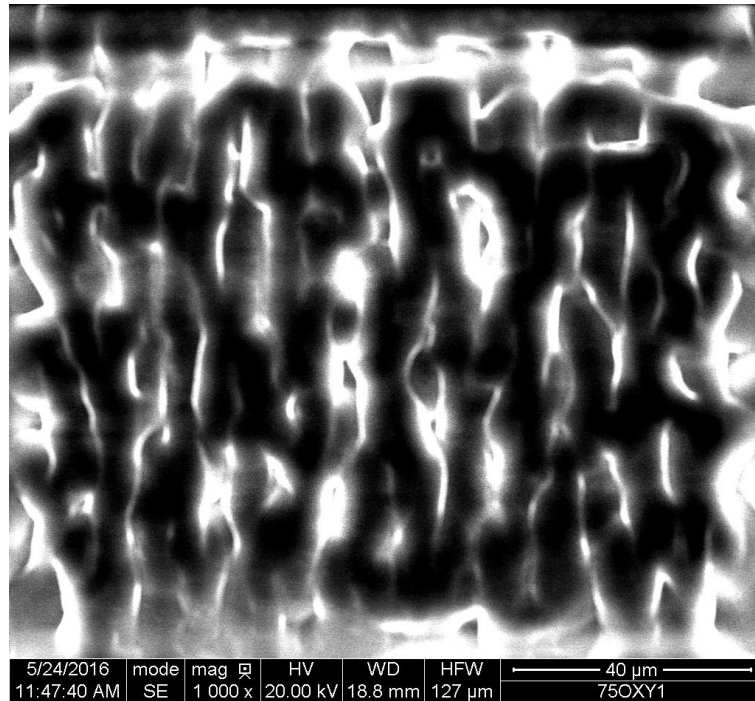


**Figure 4-7 B3 blending sample under ESEM**

As a result of using 75% of oxidized binder in sample B3, fibril structure looks more organized, systematic, perpendicular, and well connected. However, there is still a big leap in terms of the size and shape between sample B3 and the oxidized binder (Figure 4-4). Overall, the proper mixing temperature (110°C) and time (1 min) of the B3 sample makes even the small percentage of virgin binder (25%) affects the structure of the sample.

#### ***4.1.3.4 Blending Zone at the Interface of the Aged and Virgin Binder***

As mentioned previously in part (4.1.1.3), approximately 0.1 g of each virgin and oxidized binder was transferred into the sample holder with the divider using a spatula. The divider was then removed to allow the two binders to blend over different conditioning time and temperatures.

The blending zone was not found (under ESEM) at the interface of aged and virgin asphalt binder even after 24 hours conditioning at 25 °C. This indicated that the room temperature was not sufficient to bring the two binders to contact and blend even over a long period of time. The images in Figure 4-8 show the unblended aged and virgin binders. The average fibril sizes are 14.9 μm and 6 μm for the virgin and oxidized binders, respectively.

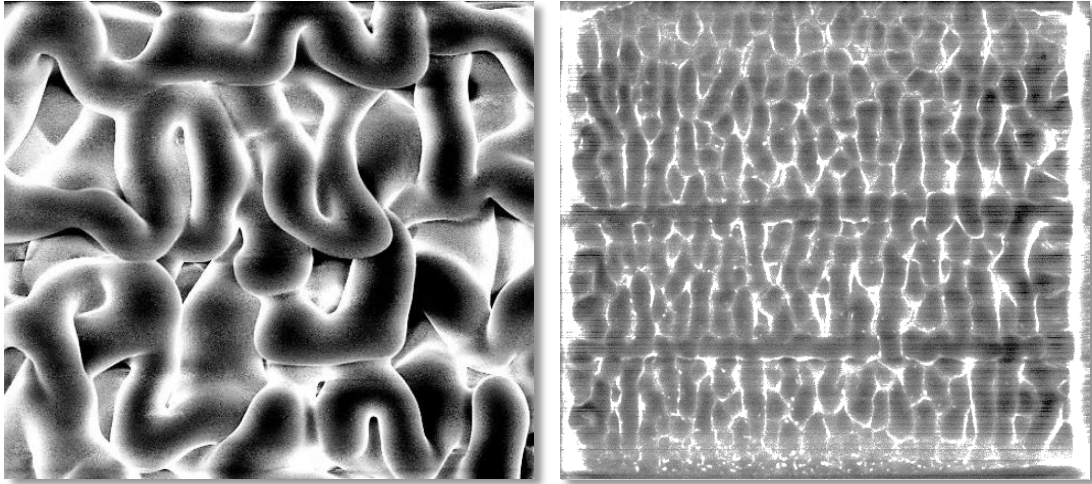


**Figure 4-8 ESEM images of virgin binder (left) and oxidized binder (right)**

Figure 4-9 and Figure 4-10 show the evolution of the blending zone after 8 and 12-hour in the oven at 60 °C. These images clearly show the spatial evolution in the microstructure of the blending zone in terms of fibrils size and their distributions with the increase of conditioning time. For the 8-hour conditioning at 60 °C, the binders are blended partially at the interface as shown in Figure 4-9.

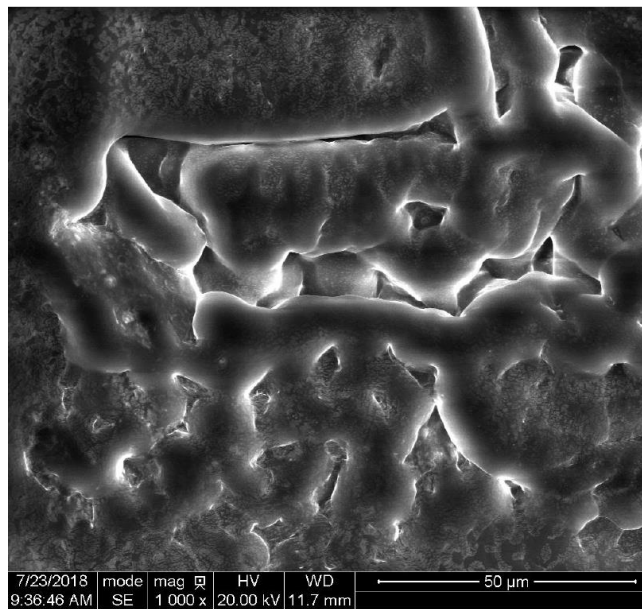


**Figure 4-9 ESEM images of the blended zone for 8hrs sample at 60 °C**



On the other hand, a better blending is observed after 12-hour conditioning time at 60 °C. The fibril structure is more organized and intertwined as shown in Figure 4-10. The average fibril sizes of the binder are 10.3 μm and 9.1 μm for the 8 and 12-hours samples, respectively.

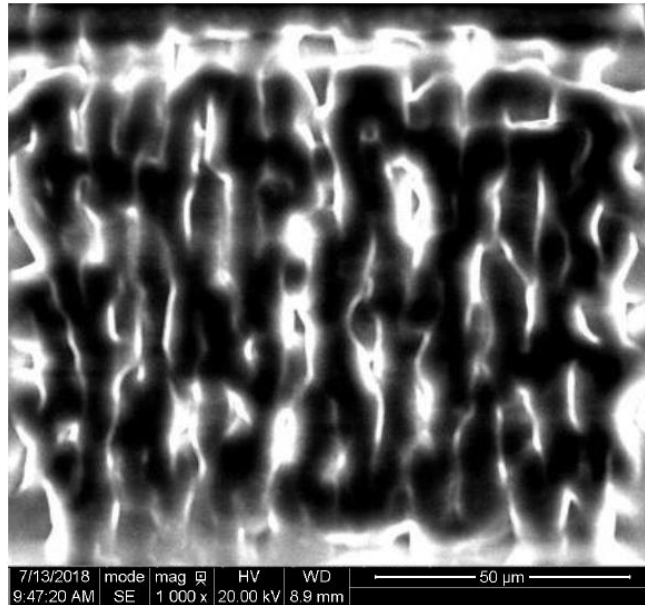


**Figure 4-10 ESEM images of the blended zone for 12hrs sample 60 °C**

For the 90 °C samples, the microstructure of the blending zones appear to be oxidized. The blending zone of the 8-hour sample seems to have similar microstructure as compared with the oxidized samples at 25 °C with slightly larger average fibril size of 7.1 μm as shown in Figure 4-11.



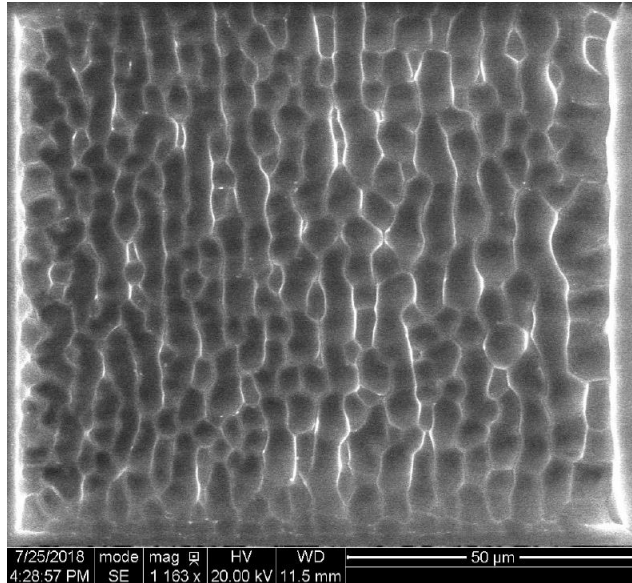


**Figure 4-11 ESEM images of the blended zone for 8hrs sample at 90 °C**

On the other hand, the blending zone of the 12-hour sample (Figure 4-12) has an average fibril size of 2.7 μm which is smaller than the fibril size of the oxidized sample at 25 °C.

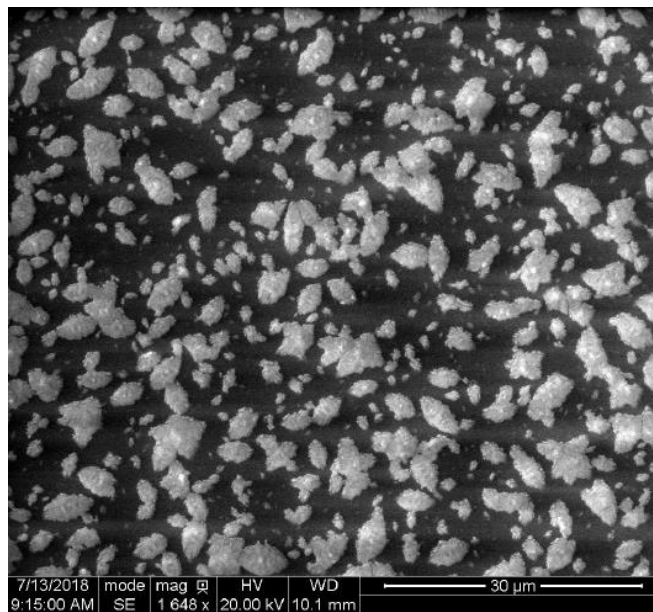


**Figure 4-12 ESEM images of the blended zone for 12hrs sample at 90 °C**

For the 120 °C samples, the microstructure of the blending zones appears to be significantly oxidized due to higher exposure temperature. The microstructure appears to be virtually denser

after 12-hour conditioning. The average fibril sizes of the blending zones at the 8-hour and 12-hour samples are 1.7  $\mu\text{m}$  and 0.5  $\mu\text{m}$ , respectively, as shown in Figure 4-13 and Figure 4-14.

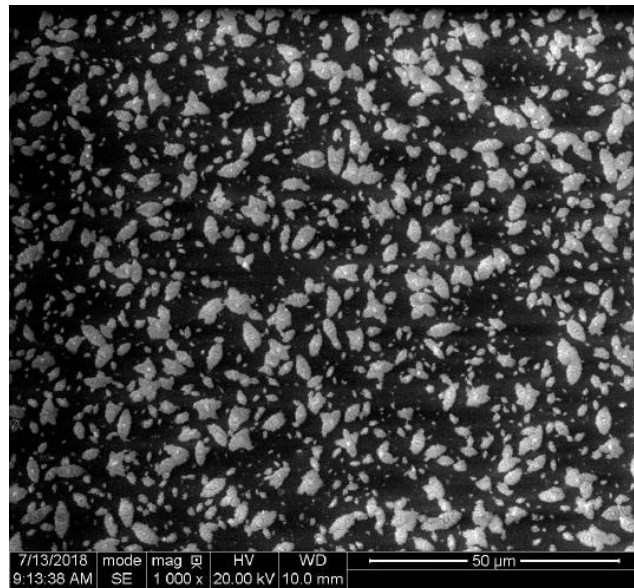


**Figure 4-13 ESEM images of the blended zone for 8 hrs sample at 120 °C**

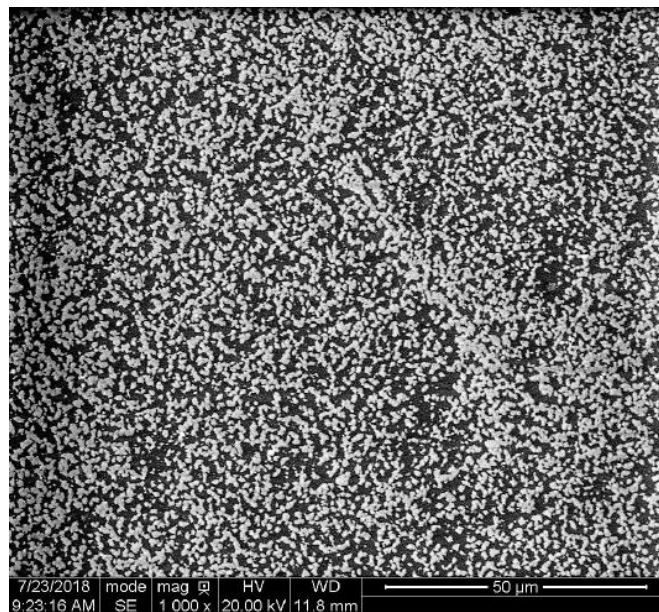


**Figure 4-14 ESEM images of the blended zone for 12 hrs samples at 120 °C**

Overall, it was observed that for a small sample size (0.2 gm), good blending happened after 12-hour storage at 60 °C. Hence, it can be said that a responsible increase in the conditioning time and temperature significantly impacts the blending process between aged and virgin binder. However,

the microstructure images show that the aging dominates after increasing the temperature to a certain level. As the reaction of oxygen with the asphalt binder leads to aging, conducting these tests under oxygen-free environment while conditioning would significantly minimize binder aging. Consequently, a better comparison between of the test results obtained from ESEM images and results of the recovered asphalt binder testing would be drawn.

## **4.2 Binder Characterization**

All binder characterizations were conducted at Sarnia Technology Application and Research Center of Imperial Oil Ltd, Ontario, Canada.

Binders extracted from mixes collected at different silo-storage times were examined for their high temperature PG (HTPG) and low temperature PG (LTPG) performance. This performance was then compared with utilized virgin binders and RAP for each mix, and presented Figure 4-15 and Figure 4-16. This comparison helps tracking evolution of produced mix during storage and whether any aging of the binder occurs during storage.

Data in Figure 4-15 indicates that both surface (HL-3) and base (HL-8) samples from Plant 1 did not experience a significant hardening within 12-hour of silo-storage, i.e. the variations in HTPG are within expected sampling, binder extraction and Superpave performance assessment variations. On the other hand, the 24-hour stored base sample from Plant 1 is showing a trend towards additional hardening.

In case of Plant 2, the surface (HL-3) course samples behaved similarly to those of Plant 1 samples, the HTPG changed variabilities associated with sampling, extraction and Superpave tests. Furthermore, the increase in HTPG between 12 and 24-hour are minimal. However, the base course (HL-8) appears to have a very different binder behavior as a function of silo-storage time. The increase in HTPG spanned about a grade between 0 and 12-hour storage. Furthermore, the increase from 12 to 24-hour storage was very drastic. The HTPG of the base 24-hour sample was comparable to that of recovered RAP binder in Plant 2, indicating that the base course experienced a relatively severe aging during silo-storage. To examine the nature of any observed aging, samples were analyzed for their SARA composition (i.e. saturates, aromatics, resins and asphaltene content). By looking at the constituent binders, it was noticed that the PG 52-34 binder used in Plant 2 is softer than the one used in Plant 1. The unusual softness of this binder was further investigated through compositional analysis.

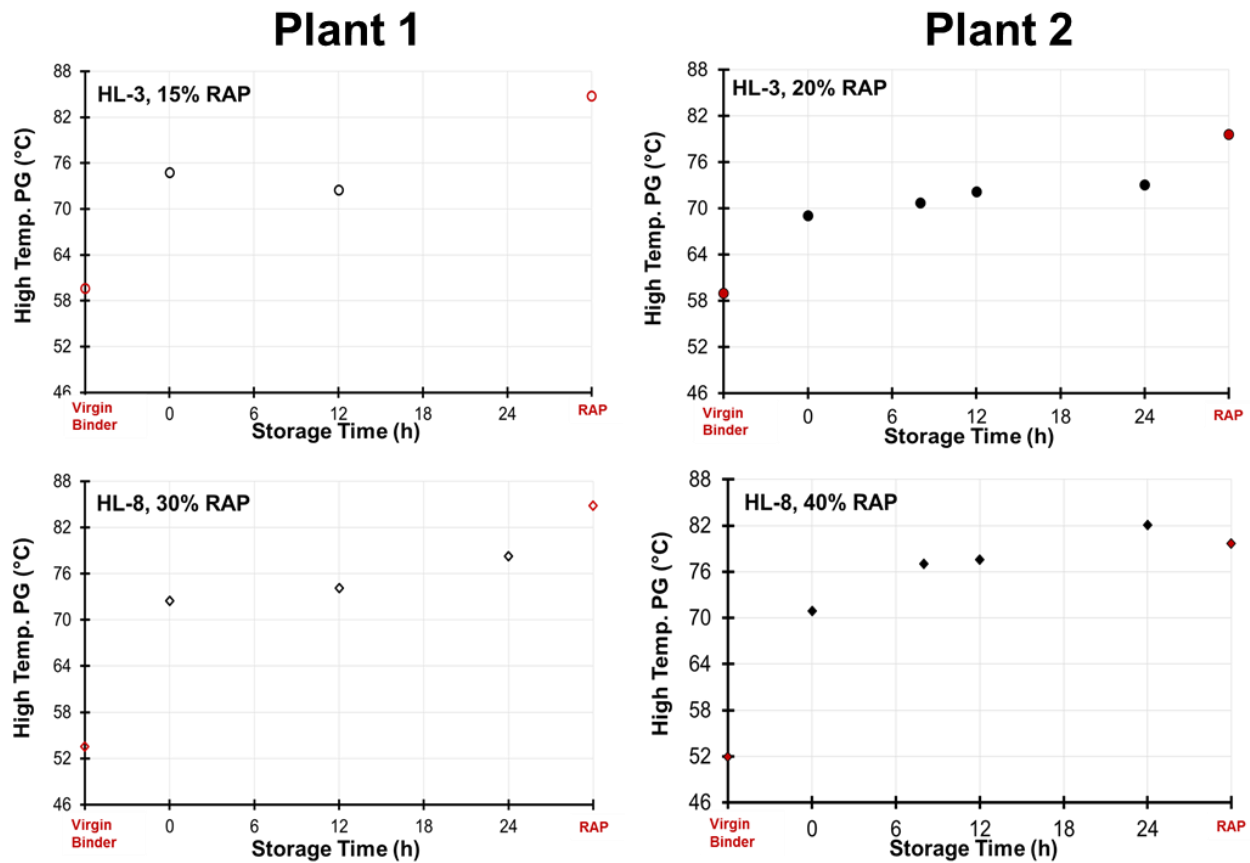


**Figure 4-15 High temperature PG of source and extracted binders for all HL-3 and HL-8**

Low temperature PG performance (LTPG) of all the tested samples are presented in Figure 4-16. Combining HTPG and LTPG of virgin binders utilized for surfaces (HL-3) mixes, it is evident that the PG 58-28 binder used in both plants were very similar. Evolution in LTPG of produced mix was less than half a grade over silo-storage time for both plants. In case of base (HL-8) mixes, the virgin binder from Plant 2 was more than half a grade softer than the virgin binder used in Plant 1. While the starting LTPG of produced base mixes were very similar, Plant 1 LTPG stayed almost the same after 12-hour, while Plant 2 sample lost about half a grade. After 24-hours of storage, however, the produced mixes ended up around a similar LTPG value within resolution of test methods. Nevertheless, similar 24-hour LTPG for a virgin binder with softer grade could be indicative of additional aging experienced during storage time, consistent with HTPG behavior above.

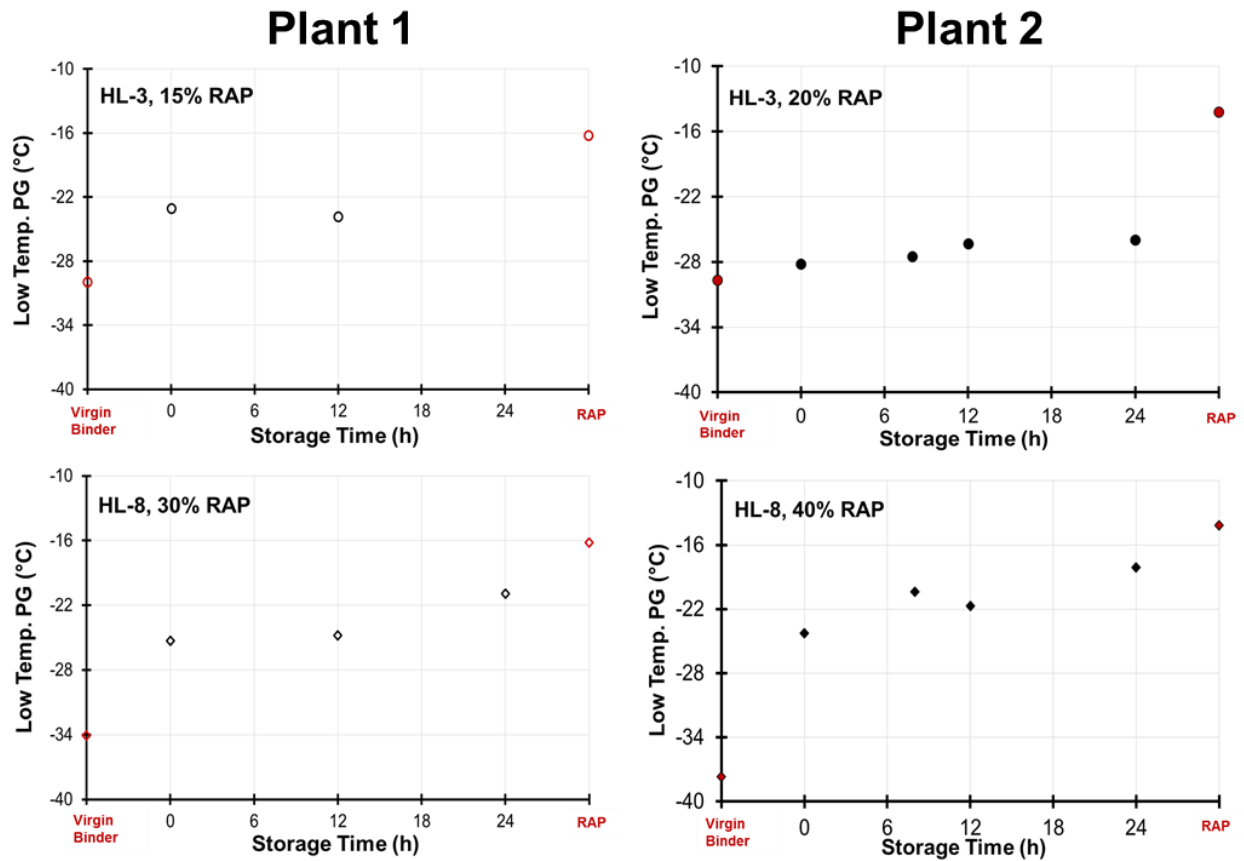


**Figure 4-16 Low temperature PG of source and extracted binders for all HL-3 and HL-8**

Figure 4-17 presents the results of SAR-AD analysis. SAR-AD analysis of virgin and recovered RAP binders from Plants 1 and 2 are presented in the top panels of the figure. Compositional evolution of HL-3 and HL-8 from Plants 1 and 2 are presented in middle and bottom panels, respectively.

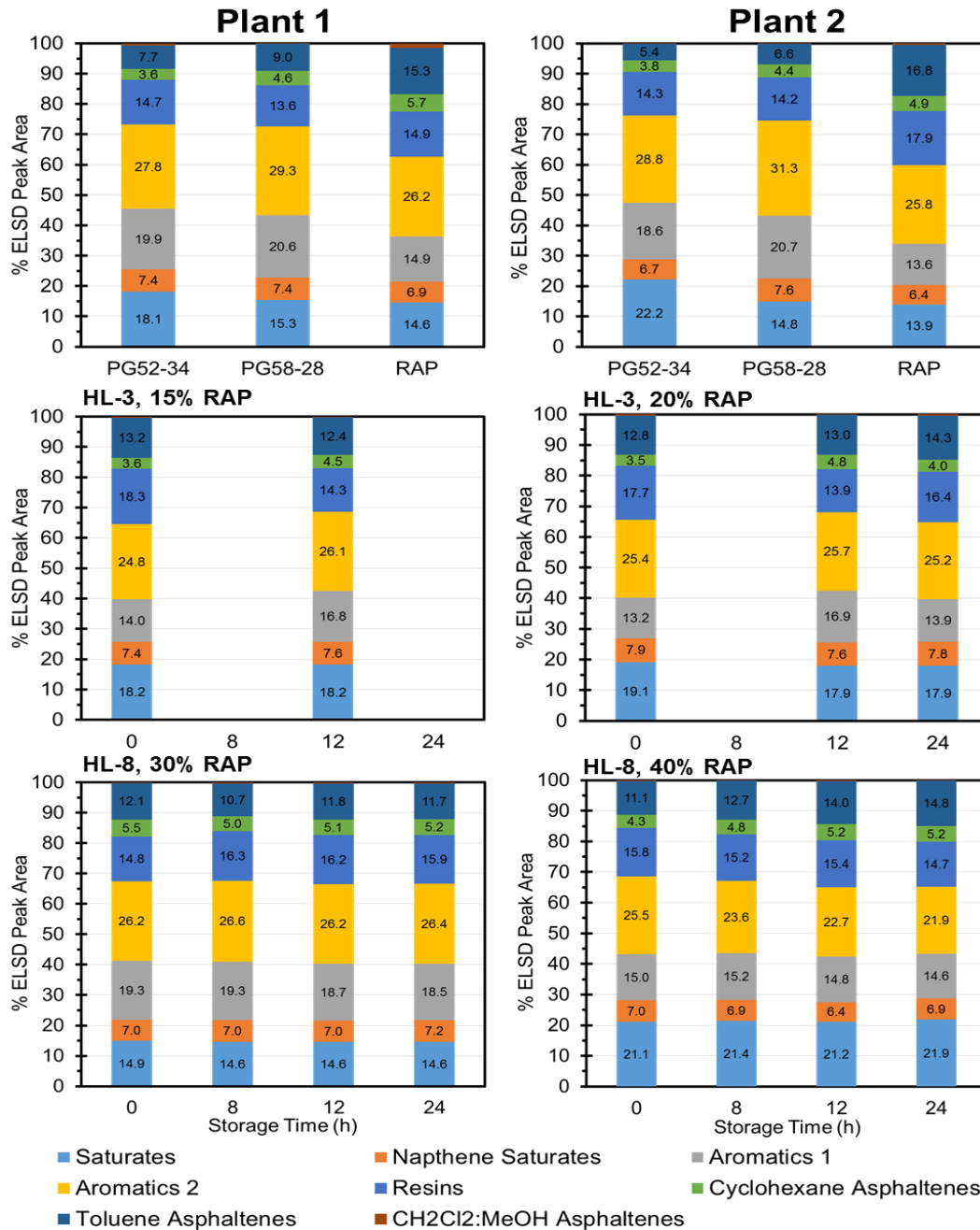


**Figure 4-17 SAR-AD analysis for all the tested asphalt binder**

Data suggest that the PG 58-28 virgin binders and the extracted RAP binders from the two plants have a very similar chemical nature. However, differences are observed between virgin PG 52-34 binders from the two plants. This difference is mainly in the paraffinic components of the two virgin binders. Figure shows that Plant 2 virgin PG 52-34 has 13% higher content of the oil

fraction (Saturates) and 23% lower content of the heavy fraction (Asphaltenes) than the one of Plant 2. These differences indicate the presence of the softener in Plant 2 PG 52-34.

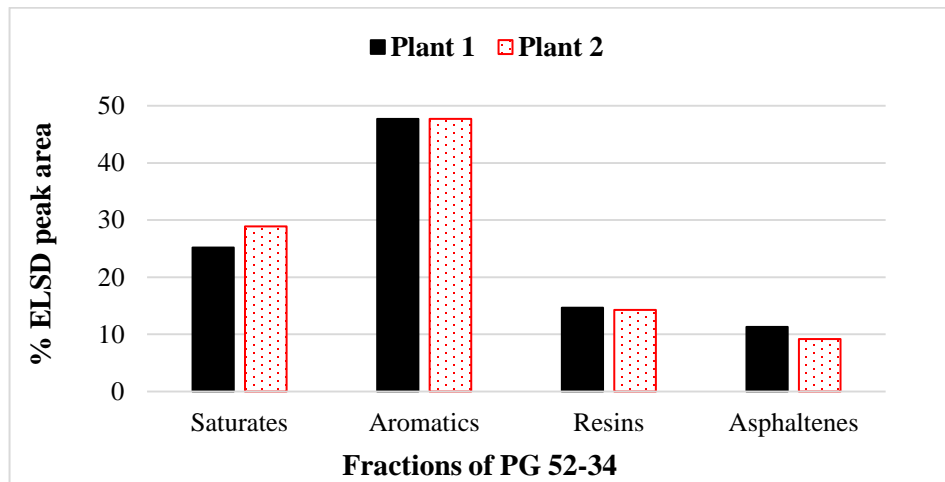


**Figure 4-18 Comparison of virgin PG 52-34 of Plant 1 and Plant 2**

Examining the silo-stored samples, SAR-AD data suggest that the surface and course samples stored at 0 and 12-hour in Plant 1 have almost identical chemistry. Yet, with the base courses of 24-hour sample indicating an increase in asphaltene content supporting the observed hardening in Figure 4-15 and Figure 4-16. Surface (HL-3) samples from Plant 2 present a similar behavior to that of Plant 1 in composition with time. In contrast, base course (HL-8) from Plant 2 point to gradual increase in heavier components, i.e. resins and asphaltenes, directionally supporting the observed hardening in Figure 4-15 and Figure 4-16. A comparison of the asphaltenes content of the extracted binder from the silo-stored mixes is presented in Figure 4-19. As shown in Figure 4-19, the asphaltenes content of the 2HL-8 mixes significantly increased with the increase of silo-storage time. This additional hardening could potentially be due to oxidation. The extracted binder from 24-hour of 2HL-8 had 23% more asphaltenes than the 0-hour 2HL-8. These findings support the presence of binder softeners which result in deteriorating impacts on aging of binders during silo-storage.

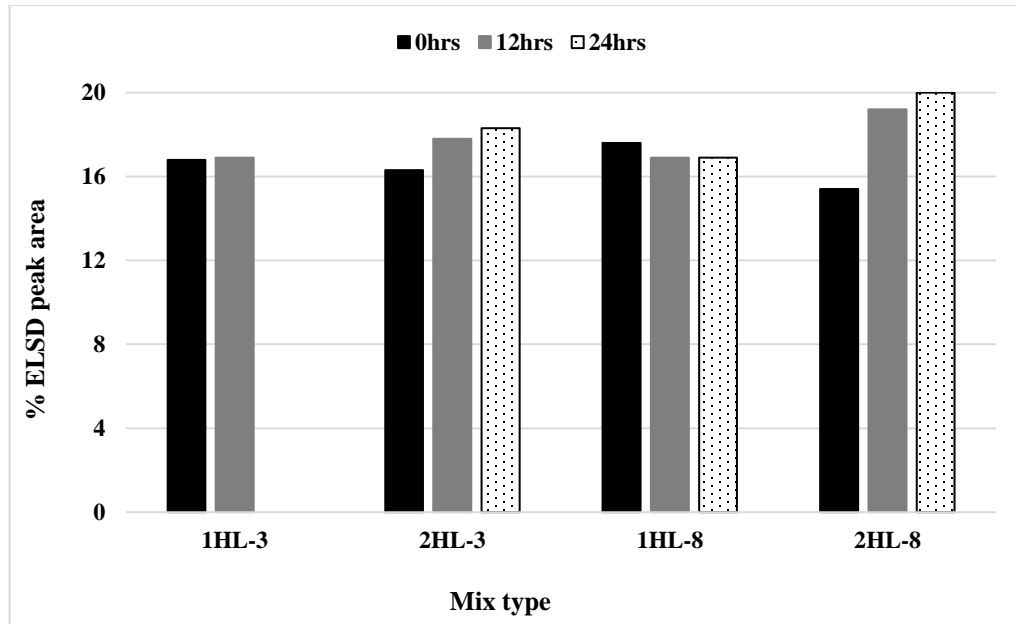


**Figure 4-19 Asphaltenes content of the extracted binder from the silo-stored mixes**

Four fractions of the asphalt binder that are separated by SARA-AD are shown in Figure 4-20.

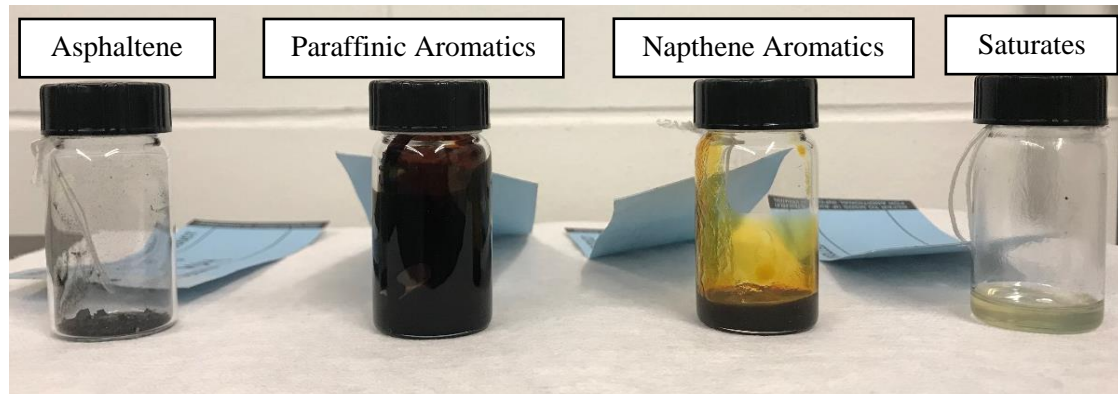


**Figure 4-20 Asphalt binder components from SARA analysis**

### 4.3 Summary of the Results

This chapter presented the laboratory results on the use of the Environmental Scanning Electron Microscope for the observation of asphalt binder microstructure. The following conclusions have been drawn:

- The binder preparation technique for ESEM testing was adequate, and the sample holders were easy to use, handle, and clean. In addition, the divider blending mould design proved



beneficial in the evaluation of the interaction of the two the binders (virgin and oxidized). These sample moulds were designed and fabricated at CPATT.

- The fibril size of the virgin binder tends to be relatively large at around 15-20  $\mu\text{m}$ ; however, the structure is relatively sparse, and the fibrils intersect each other. On the other hand, the fibril size of the oxidized binder are smaller than that of virgin binder (6-10  $\mu\text{m}$ ), and the structure also appears to be much more perpendicular, dense, connected, interviewed, and organized. The more the oxidized binder in the blending sample, the denser, smaller, and more organized fibrils are observed.
- As observed from the ESEM images, the blending between aged and virgin binder is highly impacted by the storage time and temperature. This is in an agreement with Arrhenius law which states that diffusion rate increases with increasing temperature.
- Conducting ESEM tests under oxygen-free environment while conditioning would significantly minimize binder aging.
- Overall, development of innovative asphalt binder characterization approach using the ESEM was achieved in this study. Instead of the visual traditional method, a MATLAB code was developed to accurately measure the fibril size and efficiently detect the change in the microstructure of the blending zones at the interface of the aged and virgin binders with the change in the conditioning time and temperature.
- The data obtained from the rheological analysis of the binders suggests that the time frame required for diffusion to progress towards completion was around 8-12 hours for the mixes examined in this work, which is very close to that of estimated by laboratory-produced mixes by Kriz et al. (Kriz et al., 2014).
- For the base course mixes from Plant 2, the presence of binder softeners, compared to softer grades manufactured from straight run binders, as part of new mix formulation might result in deteriorating impacts on aging of binders during silo-storage.

## **5 HMA Performance Testing Analysis and Discussion**

Using RAP in HMA is a sustainable alternative to virgin materials because it reduces the need for new asphalt binder and virgin aggregates for the production of asphalt paving mixtures (Emery, 1993). Therefore, the demand to use higher percentages of reclaimed asphalt pavement in the production of hot mix asphalt pavements has increased in the last few decades (Copeland, 2011). However, the rheological behavior of the aged binder differs from the virgin binder due to the gradual loss of some of its components during the pavement construction process and over the service life of pavements. In order to improve the overall performance of the asphalt mix with RAP, it would be beneficial to enhance the blending between old and new binders. As explained before, extended silo-storage time would contribute to a better blending; hence, in this chapter, the thermo-mechanical behaviour of the RAP-HMA with respect to different silo-storage time utilizing different performance tests are discussed in details. In addition, ANOVA test was carried out to examine the statistical significance of these findings.

### **5.1 Volumetric Properties**

As the rutting test of HMA have a close relationship with the percentage of the air voids in the asphalt mix (Fontes et al., 2010; Seo Youngguk et al., 2007), a particular attention was given to air void contents in the tested samples. For the rutting test, all samples were intentionally compacted to a target of  $7 \pm 0.3$  percent air content which is narrower than the  $7 \pm 1$  percent specified by AASHTO. This is because the main focus of this study is to examine the influence of silo-storage and eliminate the influence of air voids content on the rutting resistance. Table 5-1 summarizes the air void content values for all the tested samples for the rutting. For the Fatigue, TSRST and Dynamic Modulus testing, the samples were compacted to  $7 \pm 1$  percent air void coming down to  $5 \pm 0.3$  percent after coring and saw cutting. As the sampling of both HL-3 and HL-8 from Plant 1 of 24 hours in the silo-storage was not applicable, it was referred to it as N/A in the table below.

**Table 5-1 Air void content of all the tested materials for rutting test**

Mix type	Storage time (hours)	Air Voids	Mix Type	Storage time (hours)	Air Voids
1HL-3	0	7.10%	2HL-3	0	7.10%
		6.99%			7.14%
		7.10%			7.00%
		7.08%			7.13%
	8	6.88%		8	6.50%
		6.69%			6.97%
		6.99%			7.00%
		7.00%			7.00%
	12	7.20%		12	6.80%
		7.11%			6.76%
		7.12%			6.83%
		7.00%			6.79%
	24	N/A		24	7.00%
		N/A			7.11%
		N/A			7.15%
		N/A			7.15%
1HL-8	0	6.78%	2HL-8	0	7.20%
		6.85%			7.22%
		6.90%			7.34%
		6.90%			7.36%
	8	7.10%		8	7.00%
		7.03%			7.00%
		7.00%			7.13%
		7.20%			7.20%
	12	7.10%		12	6.87%

		7.13%			6.77%
		7.13%			6.69%
		7.14%			6.91%
	24	N/A		24	7.14%
		N/A			7.16%
		N/A			7.11%
		N/A			7.00%

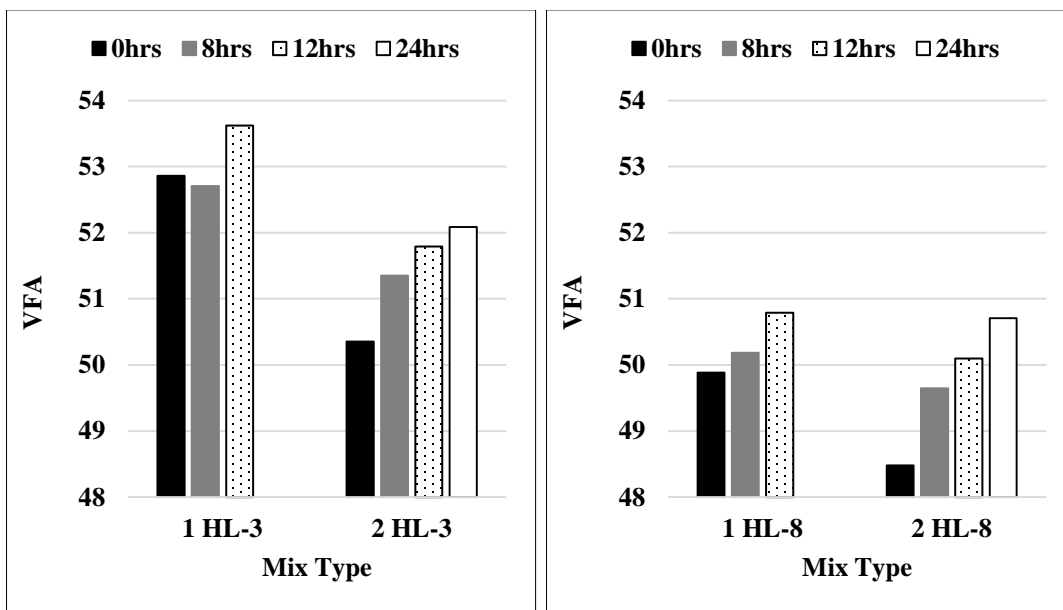


Figure 5-1 and Figure 5-2 illustrate the measured void in mineral aggregate (VMA) and void-filled-with asphalt (VFA) contents of asphalt mixes with respect to the silo-storage time. It is observed that as silo-storage time increases, VMA decreases while VFA increases. This observation is consistent among all the tested samples from both Plant1 and Plant 2.

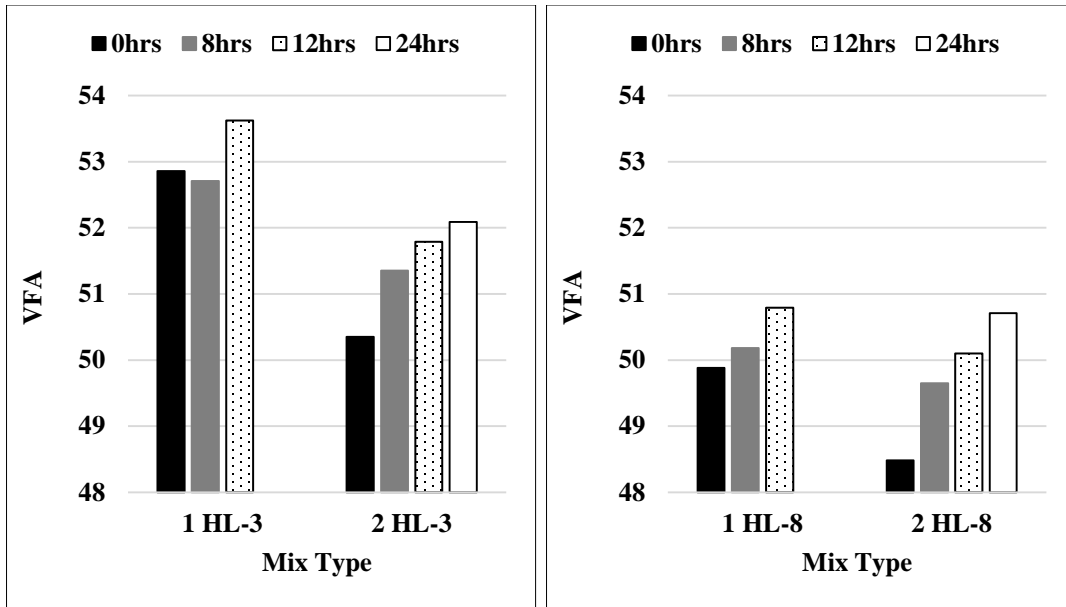


Figure 5-1 Effect of silo-storage time on VFA for (left) HL-3 and (right) HL-8 mixes

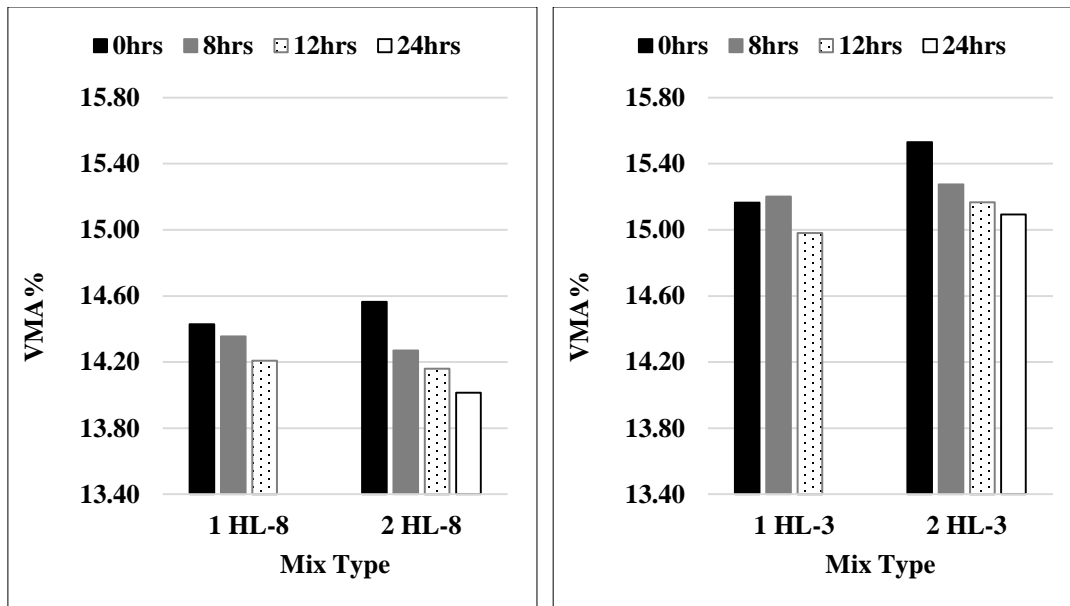
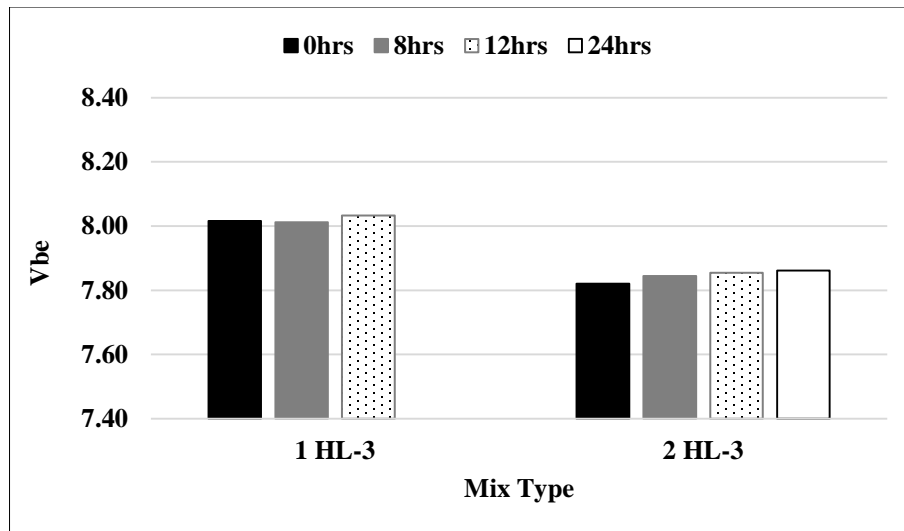


Figure 5-2 Effect of silo-storage time on VMA for (left) HL-3 and (right) HL-8 mixes

One should note here the decrease in VMA value for virgin HMA was also observed in a previous study (Chadbourn et al., 1999). It was determined that the manufacturing temperature playing a key role in the reduction of the viscosity of the asphalt binder, hence further absorption of the binder by aggregates is followed. Further absorption of the asphalt binder would result in VMA reduction (Chadbourn et al., 1999). In the present case, given that RAP aggregates have been through absorption process before, absorption may not essentially be a dominating factor in the

observed changes in volumetric properties (Figure 5-1). Therefore, evolution of volumetric properties in the present mix samples can then point to changes in RAP binder role. At the beginning of production (0-hour storage), RAP acts only as filler or a ‘black rock’ in the mix. At this stage, mix may appear ‘dry’ as the total binder content of the mix is not at its functioning level. This behavior leads to relatively higher VMA and lower VFA content for the 0-hour samples. However, as RAP mix gets heated during production, and is kept heated during storage (140-147 °C), its binder content becomes more fluid and active. This activation of RAP binder helps the diffusion with the added virgin binder to progress further. As more RAP binder diffuses with the virgin binder, its contribution as a filler decreases and binder content of mix increases, i.e. final binder blend approaches its full functional level. As a result, a gradual decrease in VMA and increase in VFA would be expected. Consequently, the effective binder volume ( $V_{be}$ ) slightly increases in the mixes with the increase of the silo-storage time as shown in Figure 5-3 and Figure 5-4. One thing to note is that the effective binder volume in the mix depends considerably on the virgin binder content, RAP content, and aggregate gradation. Hence, both base course mixes exhibited lower  $V_{be}$  as compared with the surface course mixes from both Plant 1 and Plant 2. This is due to the fact that the base course mixes have lower virgin binder content, higher RAP content, and larger NMAS.



**Figure 5-3 Effect of silo-storage time on the  $V_{be}$  for HL-3 mixes**

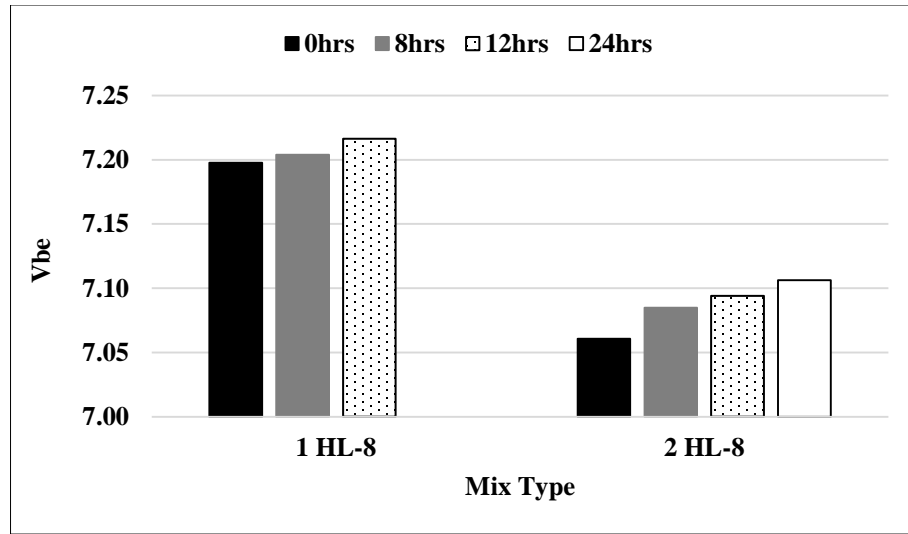


**Figure 5-4 Effect of silo-storage time on the  $V_{be}$  for HL-8 mixes**

It is worth mentioning here that the time it takes binders to diffuse can depend on binder thickness, aggregate properties, and plant processes such as preheating RAP aggregates as well as mixing and storage temperatures.

To assess whether the results obtained from the tests are statistically significant, Variance (ANOVA) single factor analysis was conducted. A 95% confidence level ( $\alpha = 0.05$ ) was used. For the volumetric properties, the null hypothesis was ‘increasing silo-storage time does not affect the VMA% values’ whereas the alternative hypothesis was the opposite. Table 5-2 confirms that the effect of increasing silo time on both VMA% values are statistically significant.

**Table 5-2 ANOVA for VMA values**

Mix Type	F	P-value	F <sub>Critical</sub>	Remark
1HL-3	3863.36	4.67E-10	5.14	statistically significant
1HL-8	2793.44	1.23E-09	5.14	statistically significant
2HL-3	124.23	4.76E-07	4.07	statistically significant
2HL-8	1246.57	5.11E-11	4.07	statistically significant

## 5.2 Dynamic Modulus Test Results

Master curves for all the collected samples were developed with 21 °C as a reference temperature. For Plant 1 and Plant 2 mixes, the master curve for each silo time indicates that complex modulus

of HL-3 samples collected between 0 and 4-hour do not differ significantly as shown in Figure 5 2. Hence, this would indicate that there was no considerable effect of a 4-hour silo-storage on the rheology of this mixture. Each panel presents evolution of  $|E^*|$  versus reduced frequency as a function of silo-storage duration. As observed in Figure 5-5, the change in behavior is more prominent in case of base courses compared with surface ones. It is worth reminding that base courses had higher RAP content compared to surface courses, i.e. 30% and 40% for Plant 1 and Plant 2, respectively.

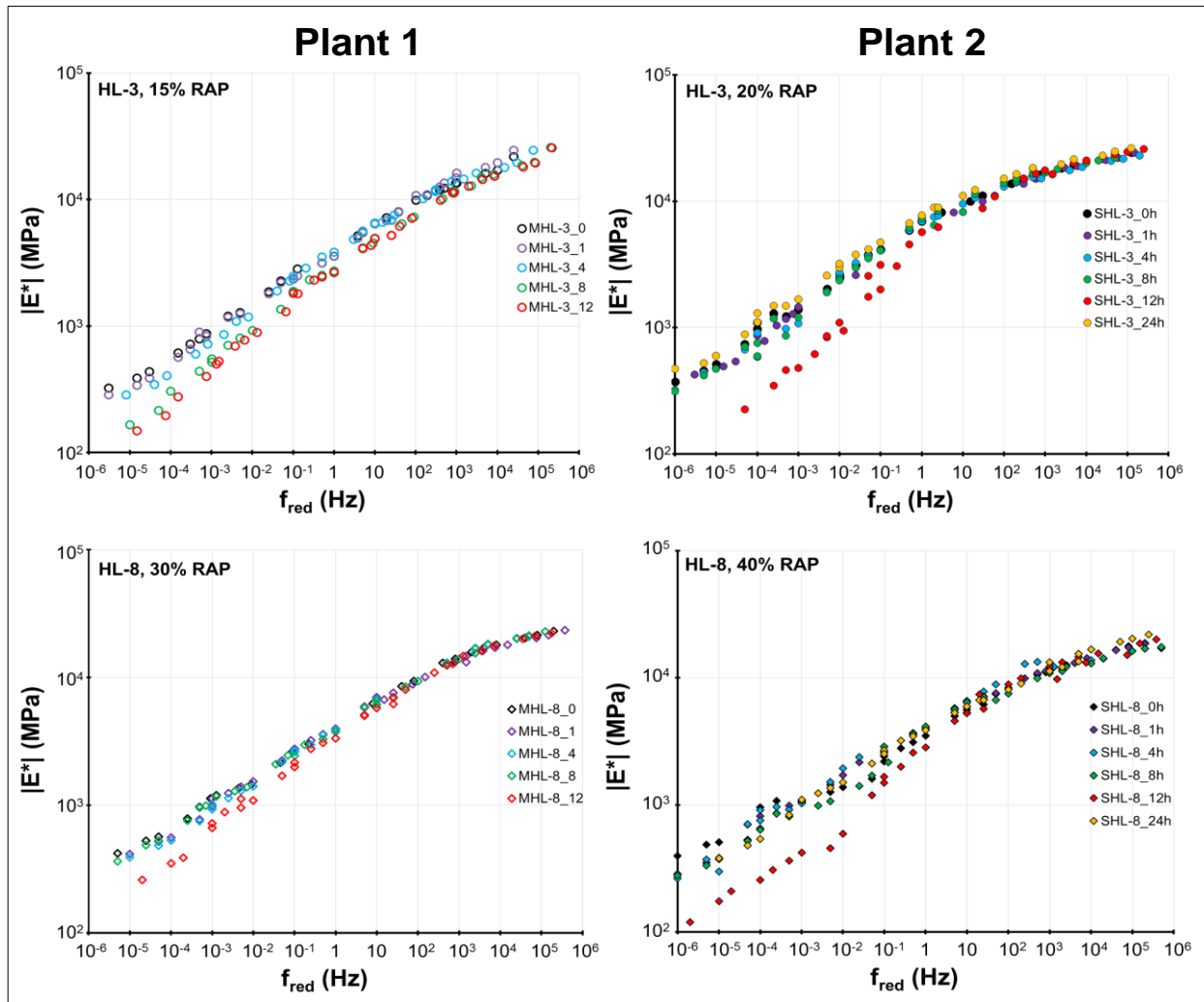


**Figure 5-5 Master curve of HL-3 and HL-8 for all mixes**

An additional feature in the data is the onset time of behavioral change in master curves. It seems that for the surface course from Plant 1, with lowest RAP content of 15%, the mix started to manifest blending progress at around 8-hour (the difference between 8 and 12-hour are



neglectable). However, when the RAP content increased to 20% and above, the impact of blending started to manifest between 8 to 12 hours. As it is difficult to visualize the differences between the samples in the log-log master curve, modulus ratio was used to better represent the influence of the silo-storage on the stiffness. Each ratio value represents the stiffness of the mix without silo storage (called E0) divided by the stiffness of the mix with 12-hour silo-storage for both HL-3 and HL-8 (called E12). Figure 5-6 and Figure 5-7 clearly show that the complex modulus values for 0-hour storage is two times higher than that of 12-hour in the silo-storage for 1HL-3 and 2HL-3 mixes.

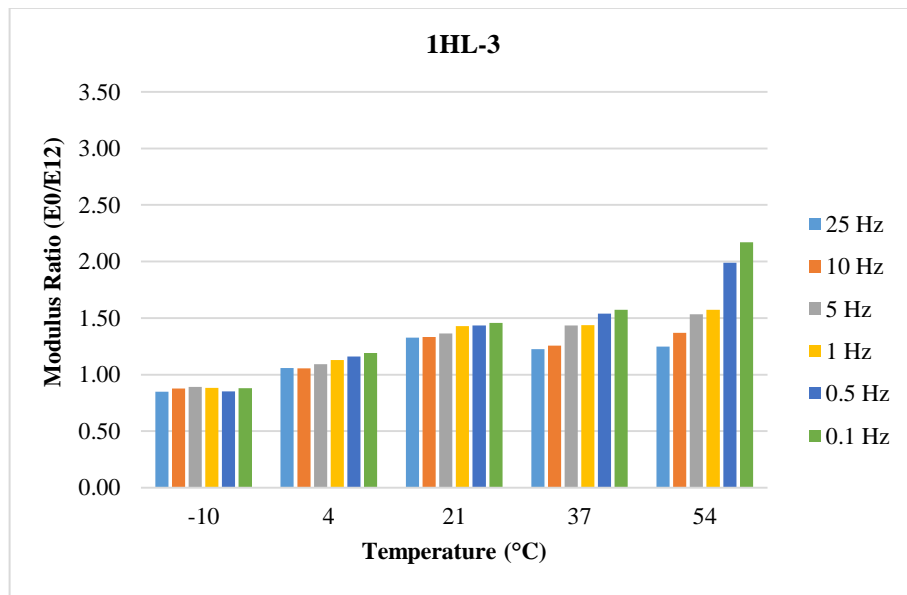
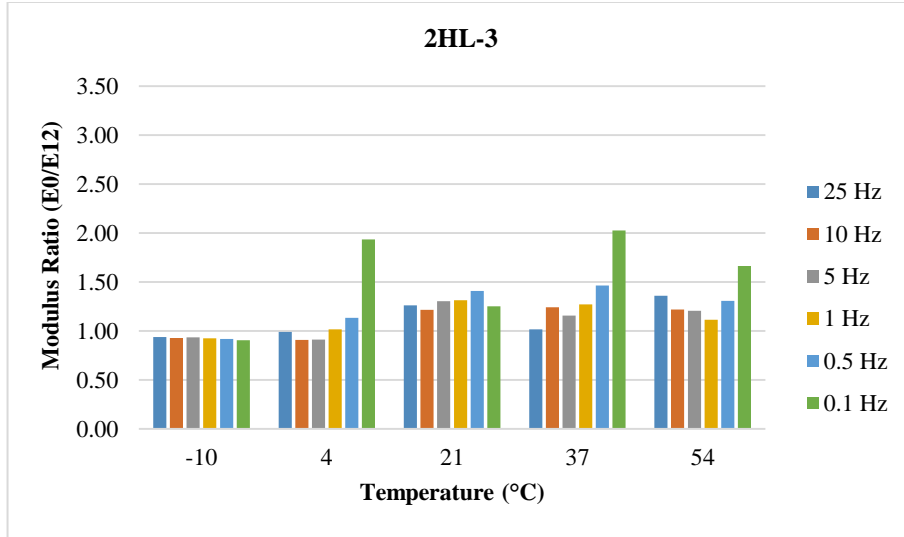
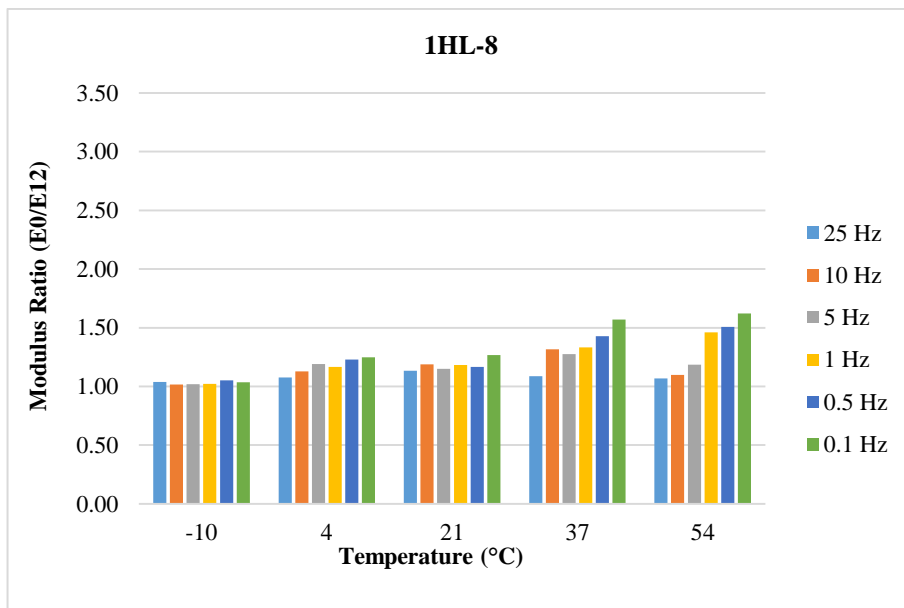


Figure 5-6 Modulus Ratio Values (E0/E12) of 1HL-3 mixes



**Figure 5-7 Modulus Ratio Values (E0/E12) of 2HL-3 mixes**

For the base-course mixes, approximately the complex modulus value for 0-hour storage is 1.6 and 3.3 times higher than that of 12-hour in the silo-storage for 1HL-8 and 2HL-8 mixes, respectively as shown in Figure 5-8 and Figure 5-9, respectively.



**Figure 5-8 Modulus Ratio Values (E0/E12) of 1HL-8 mixes**

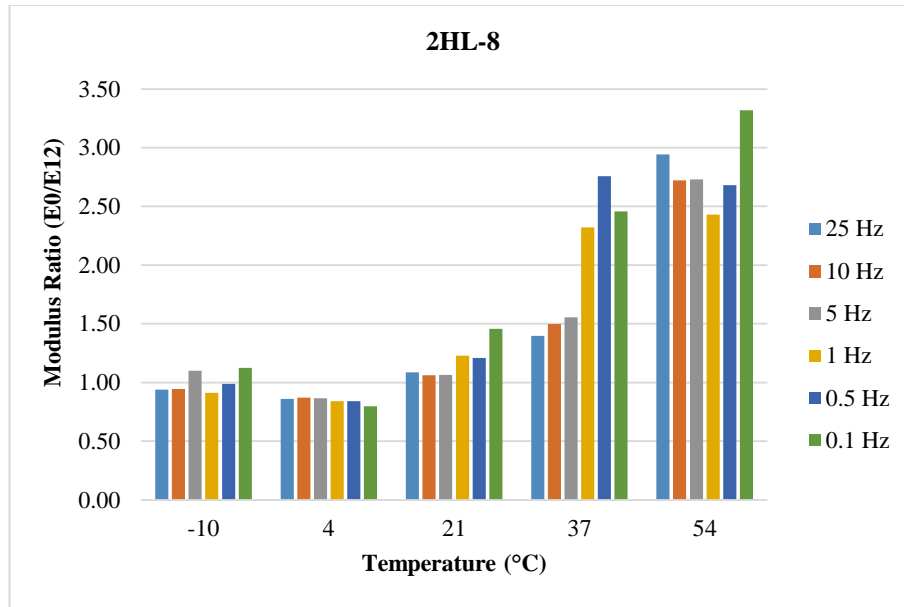


**Figure 5-9 Modulus Ratio Values (E0/E12) of 2HL-8 mixes**

A general observation of Figure 5-6 - Figure 5-9 indicate that the modulus ratio values for the collected mixes are less than 1 at low temperature (-10 °C). One possible explanation of this observation is that the blending at 0-hour silo-storage time is minimal, hence, the virgin binder takes over more of the deformation during the compressive loading at low temperatures. However, the blended binder, which is stiffer than the virgin binder, is not activated at low temperature. Consequently, the stiffness of the 0-hour mixes is less than the one of 12-hour mixes at low temperature. On the hand, more available binder through blending of the 12-hour mixes, as compared with the 0-hour mixes, plays a role at higher temperatures of the test resulting in lower stiffness.

When the 24-hour silo-stored surface and base course mixes from Plant 2 were examined for dynamic modulus, both samples exhibited hardening and elevated stiffness. This behavior suggests that there may be an optimum silo-storage duration for each mix design beyond which hardening occurs. This optimum time appears to be between 8-12 hours for the mixes examined in this field study. Figure 5-10 and Figure 5-11 show that the complex modulus values for 0-hour storage are slightly lower than that of 24-hour in the silo-storage for both 2HL-3 and 2HL-8 mixes.

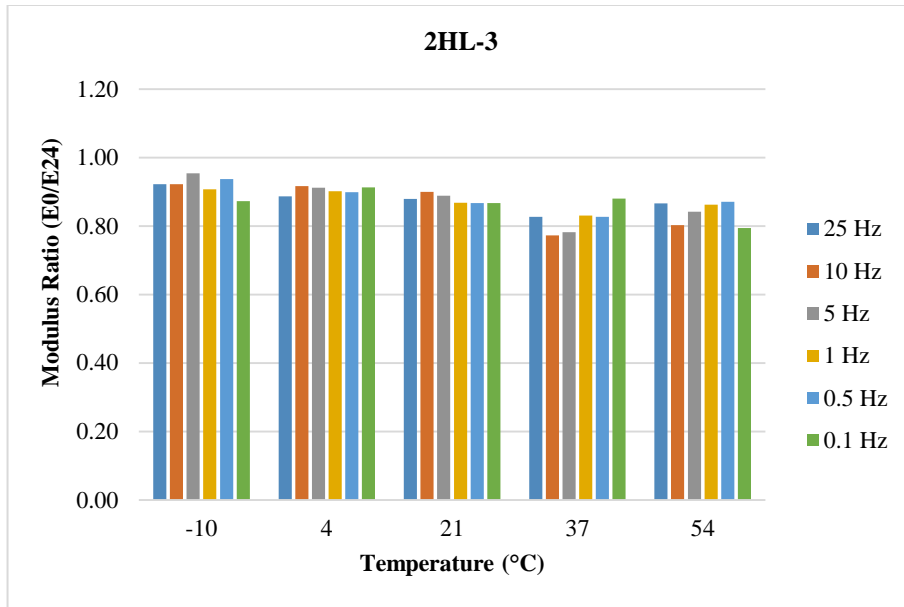


Figure 5-10 Modulus Ratio Values (E0/24) of 2HL-3 mixes

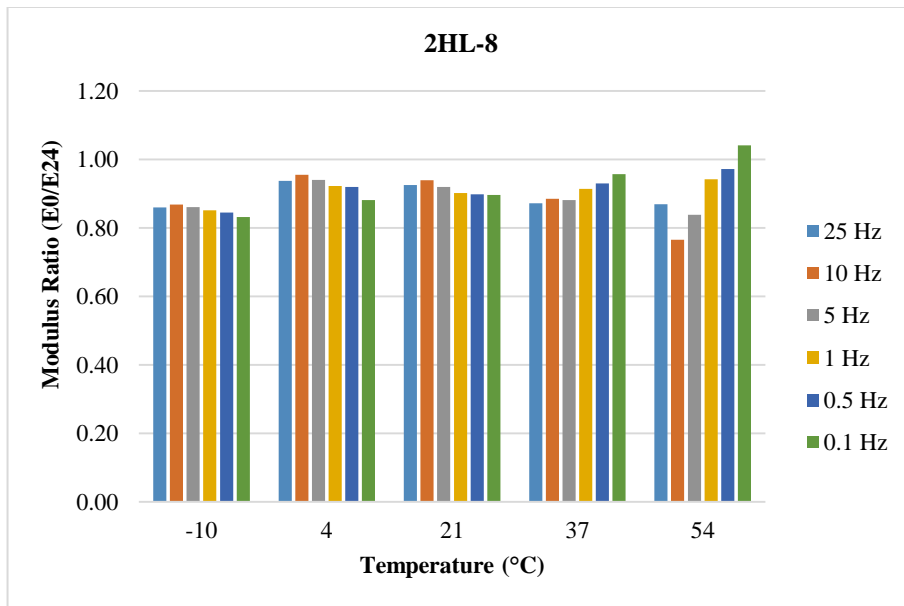


Figure 5-11 Modulus Ratio Values (E0/24) of 2HL-8 mixes

### 5.3 Thermal Cracking Test Results

As the RAP asphalt binder is generally harder than virgin asphalt binder, asphalt mixes with additional recycled materials could then show a brittle behaviour at low temperatures and premature thermal cracking could be exhibited. However, more blending between aged and virgin binder could enhance the thermal cracking behaviour of these mixes. Table 5-3 reports the test

results in terms of the average maximum stress at which the specimen fails (fracture stress) with an average corresponding fracture temperature.

A general observation of the results is that the values of the standard deviations (S.D) for fracture temperature ranged from 0.091 °C to 1.3 °C for the tested mixes of plant 1. Whereas the standard deviations for fracture temperature ranged from 0.03 °C to 0.33 °C for the tested mixes of plant 2. These results indicate that the mixes showed good repeatability in terms of fracture temperature.

**Table 5-3 Fracture temperature and fracture stress for all the tested mixes**

Mix Type	Silo time (hours)	Fracture Temperature (°C)		Fracture Stress (MPa)	
		Average	SD	Average	SD
1HL-3	0	-31.08	1.30	2.00	0.66
	8	-31.41	0.52	2.10	0.22
	12	-34.93	0.091	1.70	0.50
1HL-8	0	-31.65	0.61	2.80	0.15
	8	-32.82	0.92	2.78	0.70
	12	-34.99	0.86	2.10	0.19
2HL-3	0	-28.04	0.27	3.36	0.36
	8	-29.49	0.33	3.53	0.21
	12	-35.48	0.34	2.76	0.32
	24	-29.75	0.35	4.11	0.19
2HL-8	0	-28.25	0.09	3.62	0.26
	8	-29.34	0.31	4.11	0.04
	12	-35.90	0.03	3.51	0.16
	24	-28.47	0.40	3.58	0.51

The examination of the results confirms that the fracture temperature of the 0-hour mix with PG 58-28 binder surpassed the critical low temperature grade of the virgin binder by 3.08 °C

for the surface mix of plant 1 (1HL-3). For the second surface mix from plant 2 (2HL-3) the average fracture temperature was 28.04 °C, which is very close to the critical low temperature grade of 28°C. Whereas both base mixes (1HL-8 and 2HL-8), with the PG 52-34 binder, failed to meet the anticipated -34 °C limit for mix fracture temperature.

In case of plant 1, the fracture temperatures of the 8-hour samples of 1HL-3 and 1HL-8 mixes have reached -31.41°C and -32.82 °C respectively. Additionally, the fracture temperatures of the 12-hour samples for both mixes have exceeded the critical low grade of the virgin binders by 6.93 °C and 0.99 °C respectively. In case of plant 2, the fracture temperatures of the 8-hour samples of both 2HL-3 and 2HL-8 mixes have reached -31.41 °C and -29.34 °C, respectively. Moreover, the fracture temperatures of the 12-hour samples for both mixes have exceeded the critical low grade of the virgin binders by 7.48 °C and 1.9 °C respectively.

Although the 8-hour silo-storage enhanced the thermal cracking resistance of the mixes, the fracture temperature for both base course mixes from both asphalt plants failed to meet the critical low grade of the virgin binders (-34 °C). In addition, the 24-hour samples have observed an increase in their fracture temperature as compared with the 12-hour samples. This is because the 24-hour mixes exhibited an increase in the stiffness that would be attributed to aging and then lower thermal cracking performance is observed. Figure 5-12 below shows the effect of silo-storage time on the fracture temperature of the mixes.

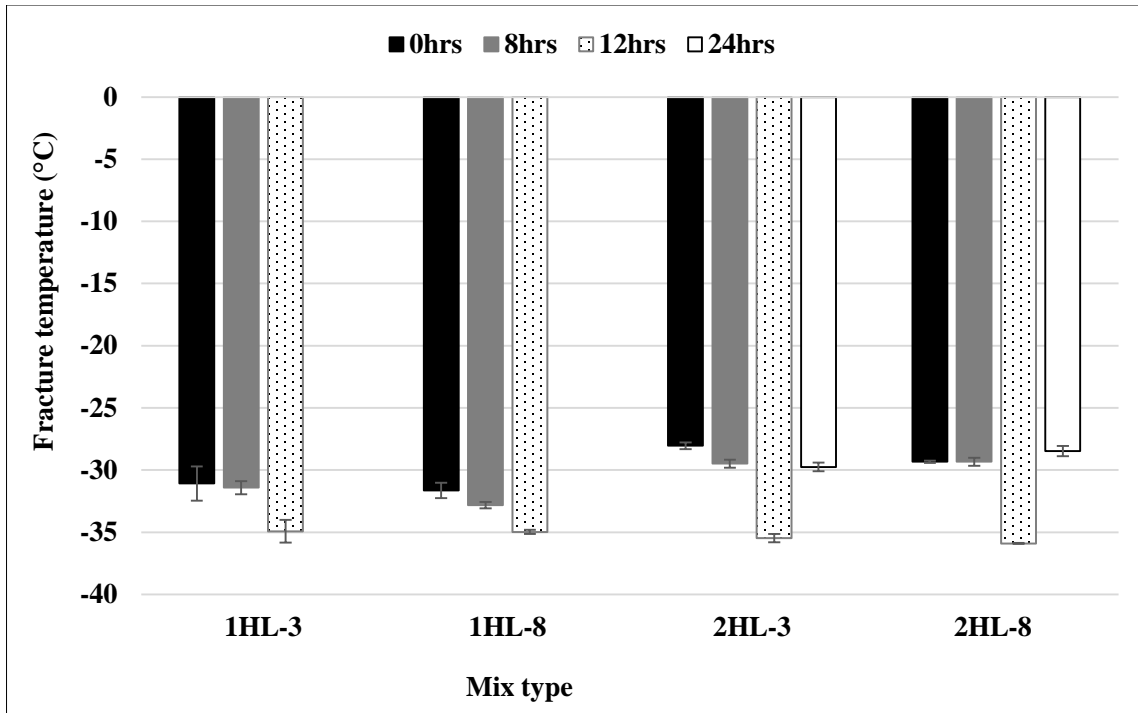


**Figure 5-12 Average fracture temperature for all the tested mixes**

Therefore, it appears that the increased silo-storage time has improved the performance of the binder which primarily controls the thermal crack resistance of the HMA at low temperatures. The examination of the results shows that although the difference between the results at 0-hour and 8-hour do not appear to be significantly different, the results obtained at 12-hour are significantly different and confirm the trend of the improvement of the critical cracking temperature for all mixes. However, the 24-hour mixes exhibited a higher thermal cracking temperature due to the negative impact of aging.

Generally, a decrease in the fracture stress was found with the improvement of the thermal resistance of all HL-3 and HL-8 from both asphalt plants. It is also noted that a lower fracture stress is exhibited for the surface course mixes compared to the base course mixes. It was also found that the 12-hour samples for all HL-3 and HL-8 mixes from both asphalt plants have the lowest fracture stress comparing with 0, 8, and 24-hour storage mixes. Figure 5-13 represents the reduction of the fracture stress with the increase of silo-storage time. However, due to the fact that the standard deviation values for fracture stress were high, it seems that the decrease of the stress is not significantly different of most of the cases.

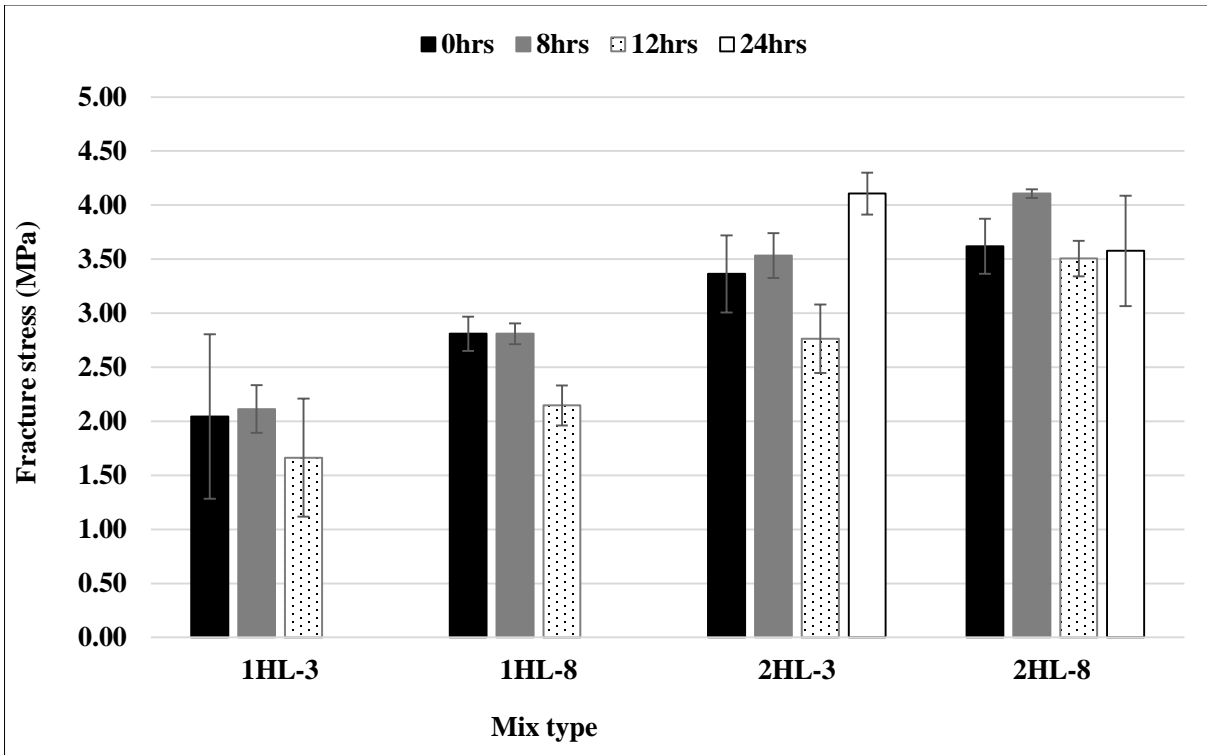


**Figure 5-13 Average fracture stress for all the tested mixes**

The examination of the results of the fracture tensile stress shown in Figure 5-13 demonstrated that in general the base-course mixes (HL-8) showed higher fracture stresses values than the surface-course mixes (HL-3). This is more possibly because HL-8 had less virgin asphalt content, more RAP content, and larger Nominal Maximum Aggregate Size (NMAS), which results in a stiffer overall mixture. Higher stiffness mixes could exhibit higher build-up of cracking. However, it is noted that more silo time has a positive influence on the fracture temperature and fracture stress of all HL-3 and HL-8 from both asphalt plants. This is due to the improved degree of blending between aged and virgin binder and greater homogeneity in the mixture with higher storage time. Hypothetically, more blending would result in increasing the thickness of the film of the “efficient” binder on the aggregates and enhancing the adhesion of the mix. This is more likely because the RAP binder had an increased contribution to the efficient asphalt binder used within the mixture, which is a major criterion of the thermal crack initiation in HMA. This would improve the quality of the HMA and enhance thermal cracking resistance. Figure 5-14, Figure 5-15, Figure 5-16, and Figure 5-17 graphically show the fracture curve behaviour of 1HL-3 and 1HL-8 for the three replicates of 0 and 12-hour silo-storage time.



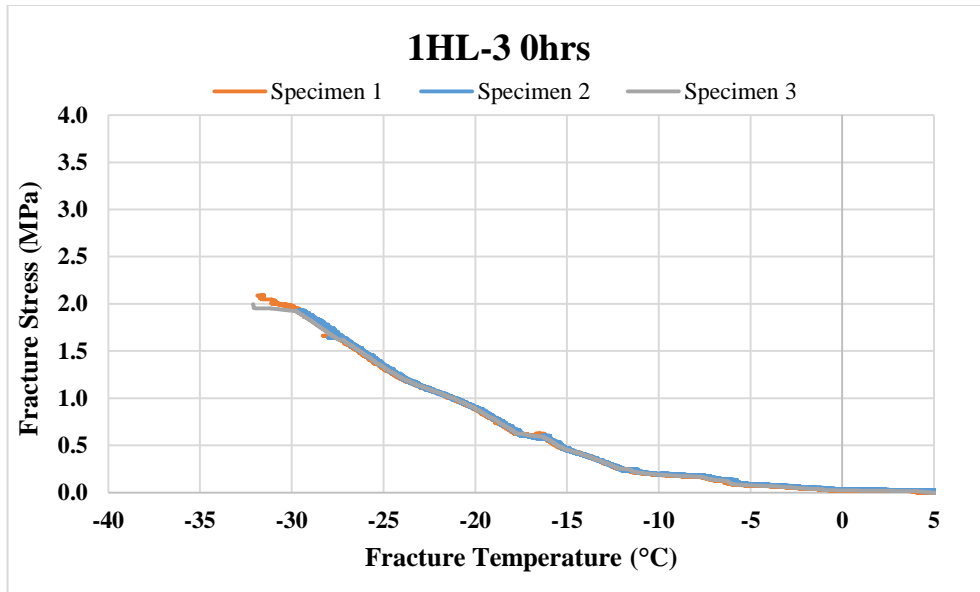


Figure 5-14 Fracture curve behavior of the three replicates of 1HL-3 0hrs

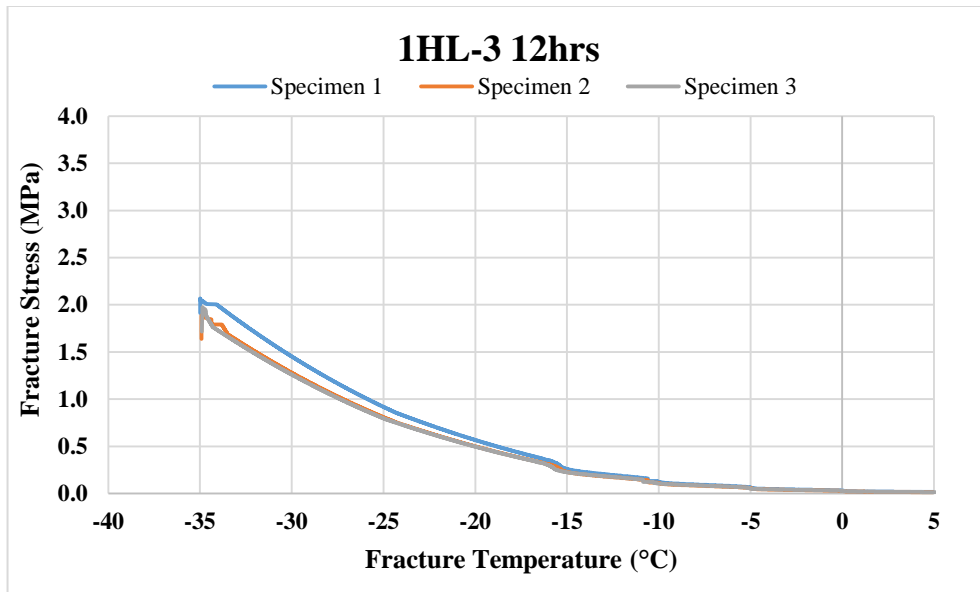


Figure 5-15 Fracture curve behavior of the three replicates of 1HL-3 12hrs

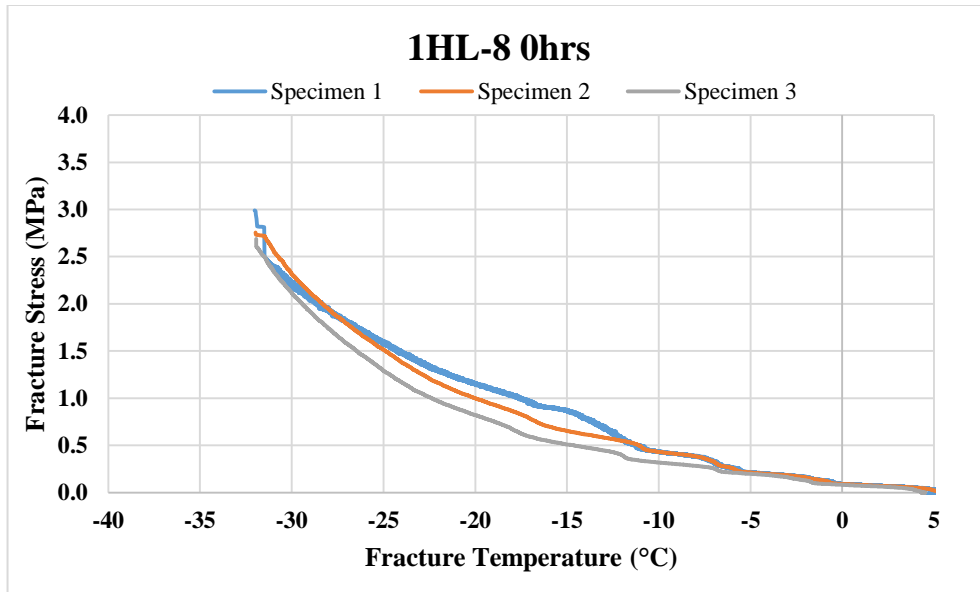


Figure 5-16 Fracture curve behavior of the three replicates of 1HL-8 0hrs

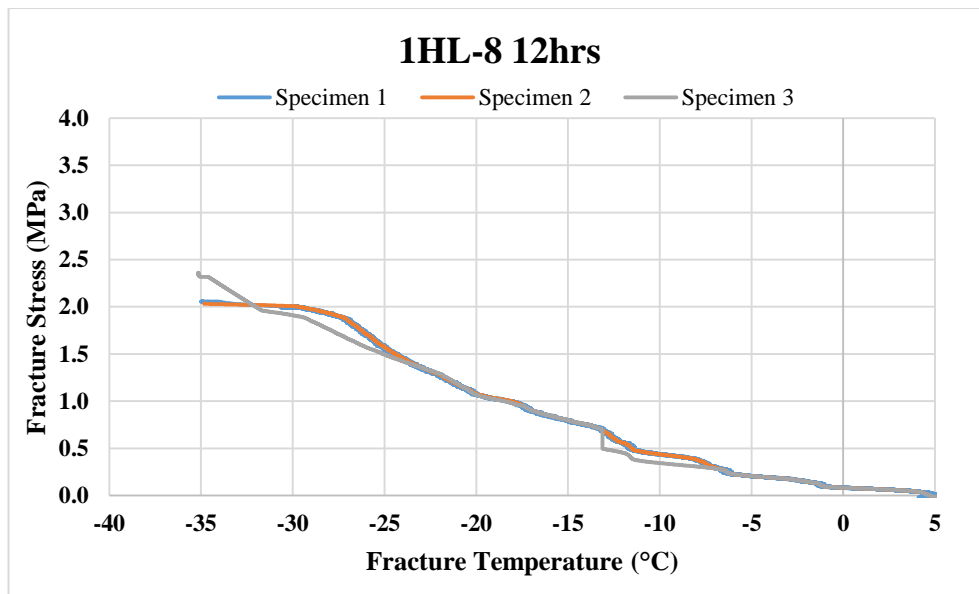
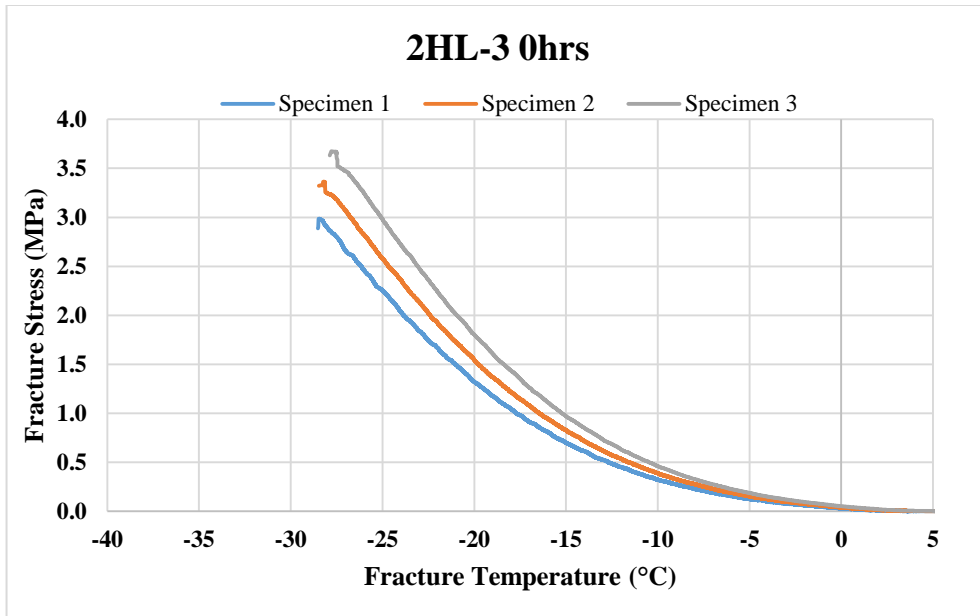
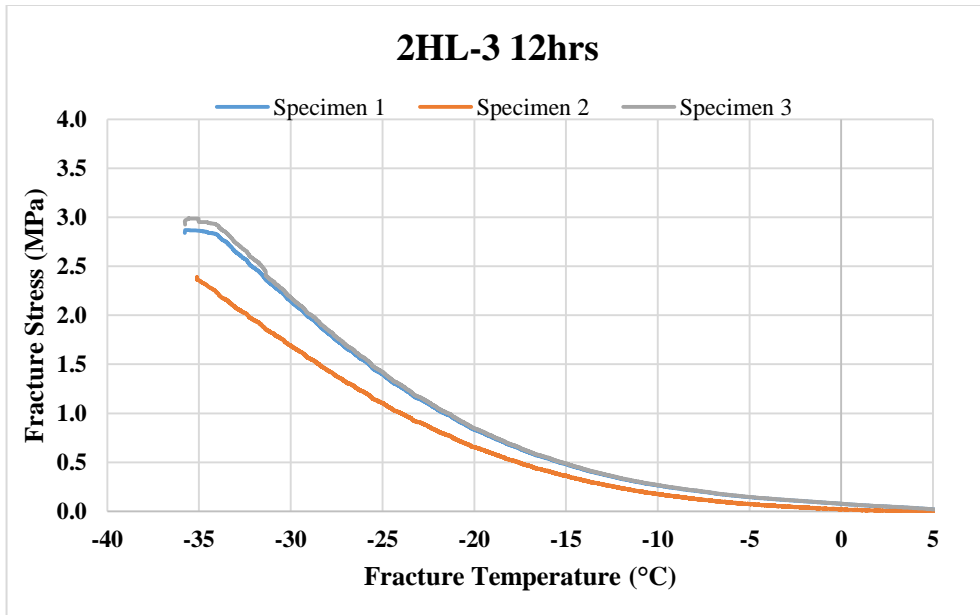


Figure 5-17 Fracture curve behavior of the three replicates of 1HL-8 12hrs

It is worth mentioning that the variability of the test results within the same mix was due to an issue with the valve control of the cooling system. However, the final results were not impacted significantly by this issue. For the Plant 2 mixes, the variability of the test results within the same mix was less. Figure 5-18, Figure 5-19, Figure 5-20, and Figure 5-21 graphically show the fracture curve behaviour of 1HL-3 and 1HL-8 for the three replicates of 0 and 12-hour silo-storage time. The fracture curves of the other storage time mixes are presented in the Appendix.



**Figure 5-18 Fracture curve behavior of the three replicates of 2HL-3 0hrs**



**Figure 5-19 Fracture curve behavior of the three replicates of 2HL-3 12hrs**

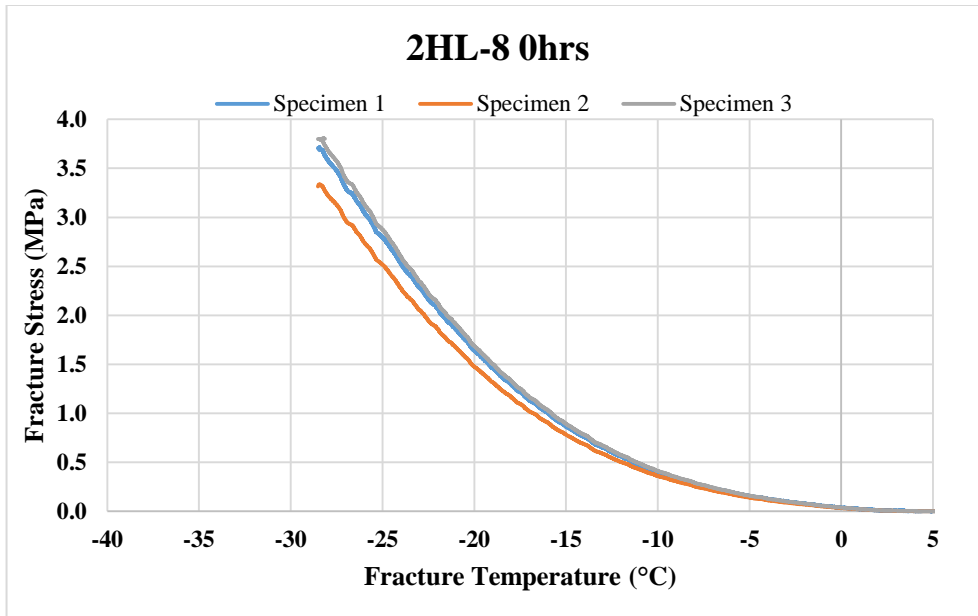


**Figure 5-20 Fracture curve behavior of the three replicates of 2HL-8 0hrs**

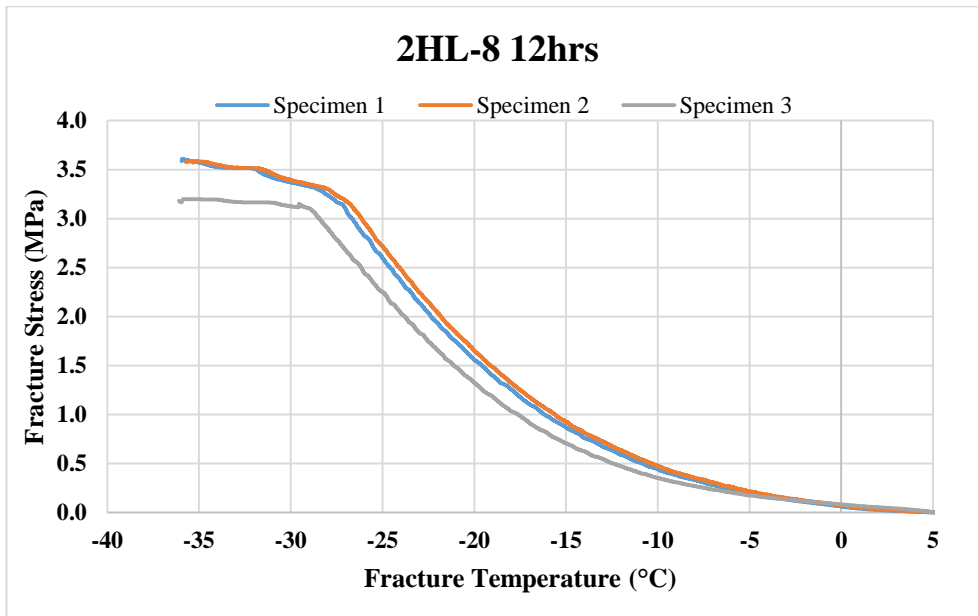


**Figure 5-21 Fracture curve behavior of the three replicates of 2HL-8 12hrs**

As a final point, the results of the TSRST indicated that the 12-hour specimens had a better resistance to the thermal cracking than the ones without silo-storage for both HL-3 and HL-8 due to more homogeneous binder blending for the 12-hour mixes.

To statistically analyse the thermal cracking test results, the null hypothesis was ‘increasing silo-storage time does not affect the thermal cracking temperature’ whereas the alternative hypothesis was the opposite. Table 5-4 confirms that the effect of increasing silo time on the thermal cracking temperature of both HL-3 and HL-8 is statistically significant.

**Table 5-4 ANOVA for thermal cracking temperature values**

<b>Mix Type</b>	<b>F</b>	<b>P-value</b>	<b>F<sub>Critical</sub></b>	<b>Remark</b>
1HL-3	13.55	5.96E-03	5.14	Statistically Significant
1HL-8	55.35	1.36E-04	5.14	Statistically Significant
2HL-3	308.66	1.32E-08	4.07	Statistically Significant
2HL-8	592.80	9.88E-10	4.07	Statistically Significant

In addition, ANOVA test was carried out to statistically examine the fracture stress results of all the mixes. The null hypothesis was ‘increasing silo-storage time does not affect the fracture stress’ whereas the alternative hypothesis was the opposite. As shown in the Table 5-5, the effect of the silo-storage on both 1HL-3 and 2HL-8 mixes was statistically insignificant. This is due to the high variability in the results for the both mixes as shown previously in Figure 5-13. The standard deviation of 1HL-3 mixes reached 0.66 (for the 0-hour samples), whereas, the standard deviation of 2HL-8 mixes reached 0.51 (for the 24 hours samples).

**Table 5-5 ANOVA for fracture stress values**

<b>Mix Type</b>	<b>F</b>	<b>P-value</b>	<b>F<sub>critical</sub></b>	<b>Remark</b>
1HL-3	0.569686	0.593573	5.143253	<b>statistically insignificant</b>
1HL-8	18.30631	0.002792	5.143253	statistically significant
2HL-3	11.86798	0.002575	4.066181	statistically significant
2HL-8	2.53034	0.130668	4.066181	<b>statistically insignificant</b>

#### **5.4 Rutting Test Results**

Despite the fact that the specimens with 8 and 12-hour of silo-storage exhibited lower complex modulus than 0-hour specimens at higher temperatures, the results indicate that these specimens

tend to demonstrate better resistance to rutting distress for all the tested samples. Additionally, the rutting resistance tends to marginally improve after 24-hour of storage for both the 2HL-3 and 2HL-8 mixes. Despite the fact that the specimens with 8 and 12-hour of silo-storage exhibited lower complex modulus than 0-hour specimens at higher temperatures, the results indicate that these specimens tend to demonstrate better resistance to rutting distress for all the tested samples. Additionally, the rutting resistance tends to marginally improve after 24-hour of storage for both the 2HL-3 and 2HL-8 mixes. Table 5-6 reports the rutting depths and the associated standard deviation (SD) values for all the tested materials.

**Table 5-6 Rutting depth results for all the tested mixes**

<b>Mix Type</b>	<b>Silo-Storage Time (hrs)</b>	<b>Rut Depth (mm)</b>	<b>S.D</b>
1HL-3	0	4.30	0.40
	8	4.23	0.10
	12	4.00	0.44
1HL-8	0	3.79	0.43
	8	3.70	0.10
	12	3.43	0.33
2HL-3	0	4.15	0.07
	8	2.77	0.11
	12	2.14	0.02
	24	2.03	0.01
2HL-8	0	3.15	0.23
	8	2.26	0.09
	12	1.76	0.02
	24	1.31	0.01

Although the specimens with 8 and 12-hour of silo-storage exhibited lower complex modulus than 0-hour specimens at higher temperatures, the results indicate that these specimens tend to demonstrate better resistance to rutting distress for all the tested samples. Additionally, the

rutting resistance tends to marginally improve after 24-hour of storage for both the 2HL-3 and 2HL-8 mixes.

Better blending between the aged and the virgin binders can be the reason for observed improvement in rutting resistance. Maintained higher mix temperatures (140°C for Plant 1 and approximately 147°C for Plant 2) and longer incubation time in-silo enabled further blending of the binders. These conditions probably enabled the virgin binder to have an extended effective diffusion distance and further engage the RAP binder in the produced mix samples.

As a result, the samples with higher silo-storage time provide slightly better resistance to permanent deformation. Figure 5-22, Figure 5-23, Figure 5-24, and Figure 5-25 graphically present the results of HWTD test for all the tested mixes.

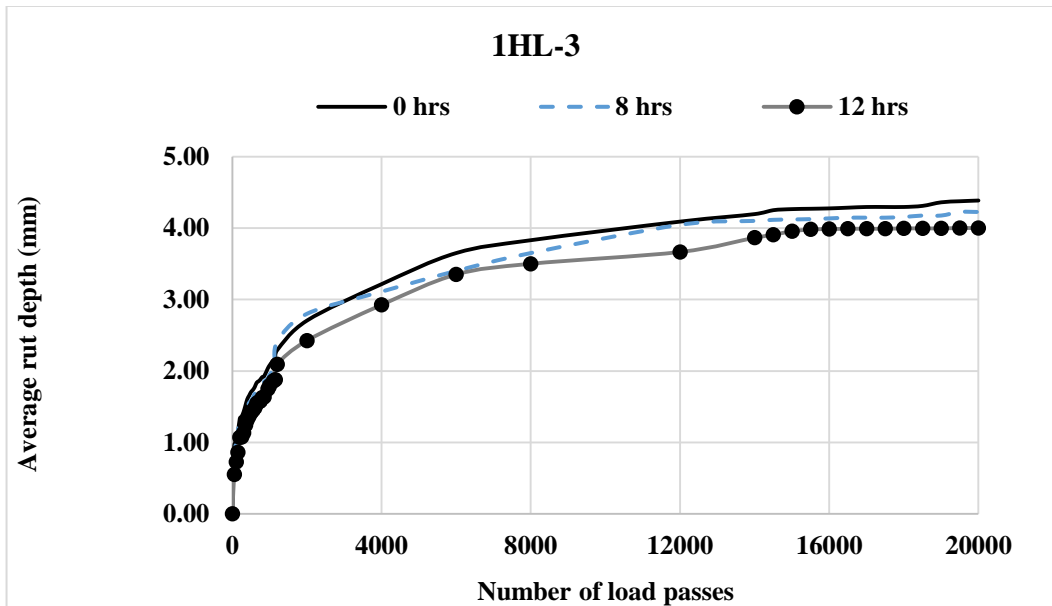


Figure 5-22 Hamburg Wheel Track rutting results of 1HL-3

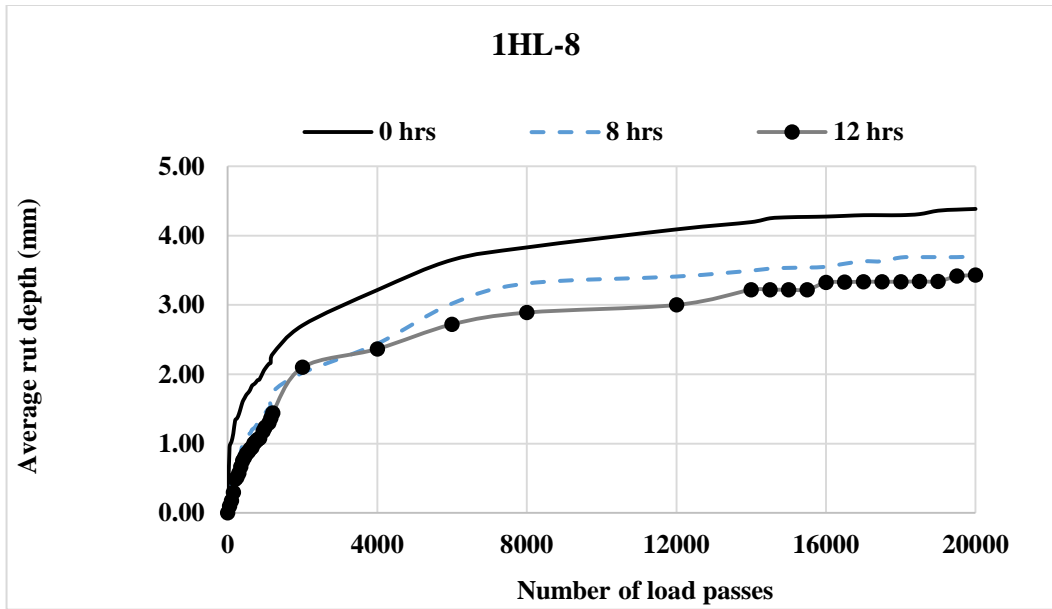


Figure 5-23 Hamburg Wheel Track rutting results of 1HL-8

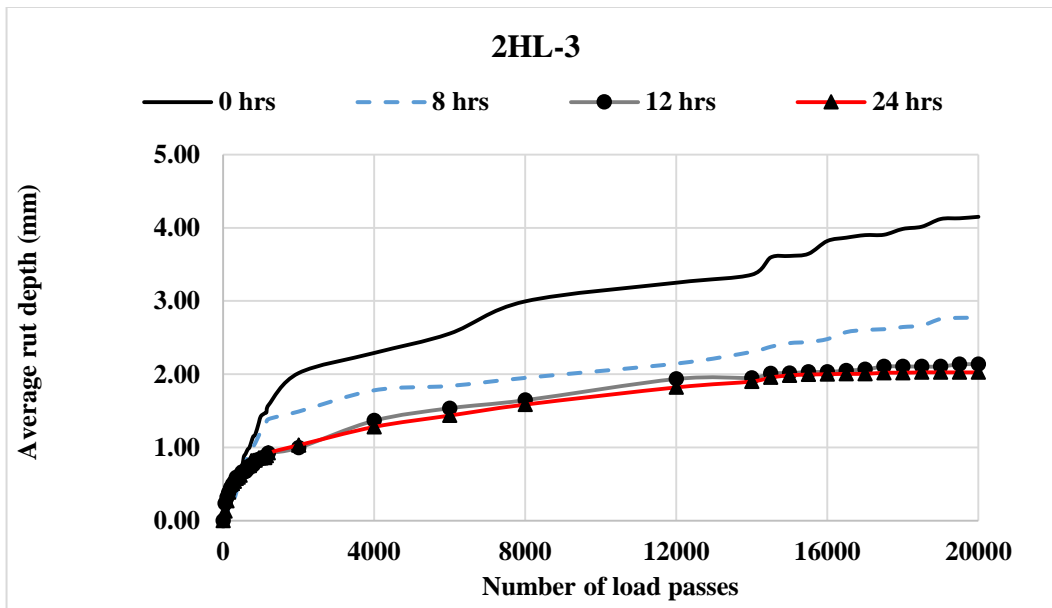


Figure 5-24 Hamburg Wheel Track rutting results of 2HL-3



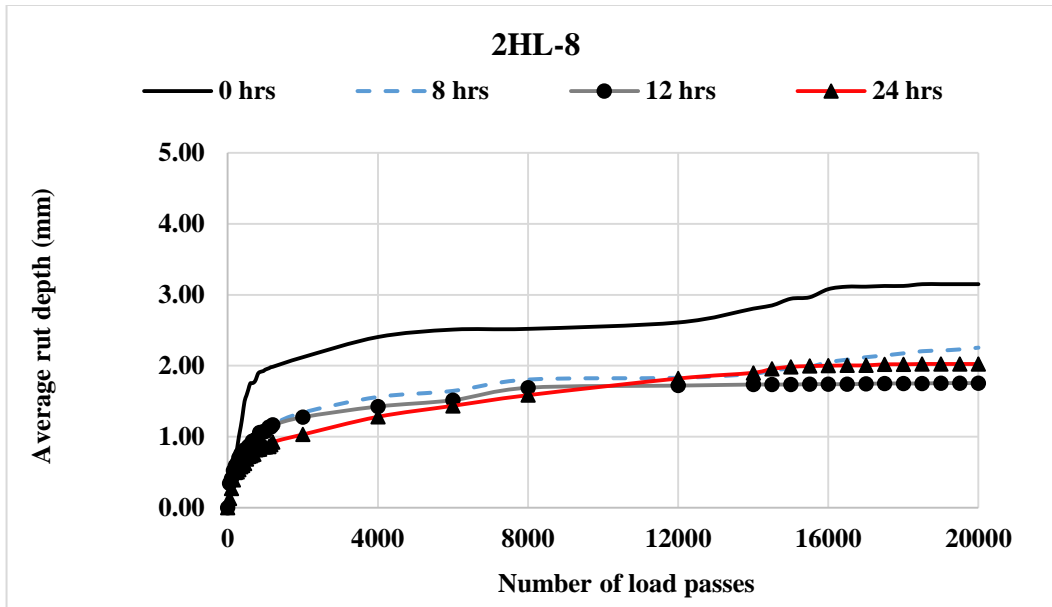


Figure 5-25 Hamburg Wheel Track rutting results of 2HL-8

Based on the results obtained for the four tested materials, the HWTD showed that the rutting resistance of the base course mixture (1HL-8 and 2HL-8) was slightly better than that of the surface course mixtures (1HL-3 and 2HL-3). Although the number of tested materials is limited, this trend would be explained by the fact that the RAP contents in HL-8 mixtures were higher than those in HL-3 mixtures, resulting in a stiffer overall mixture and providing better shear resistance. In addition, the HL-8 mixtures had a lower asphalt binder content and larger Nominal Maximum Aggregate Size (NMAS) that provides a smaller surface area to be coated by the asphalt binder. This probably resulted in better adhesion of HL-8 mixtures in comparison to the HL-3 mixtures. Moreover, HL-8 had a softer virgin binder (PG52-34) compared to HL-3 which had a PG58-28 binder. This might help more softening of the RAP and better adhesion of the mix. Overall, it can be said that the combination of reduced binder content and softer virgin binder appears to have resulted in improved rutting resistance for the HL-8 mixes as compared with the HL-3 mixes.

It has also been observed that all 2HL-3 and 2HL-8 samples exhibited lower rut depth comparing with the 1HL-3 and 1HL-8 samples, respectively. The analysis of the results indicates that 2HL-3-0hrs had 5.5 percent lower rutting as compared with the 0-hour samples of 1HL-3. Additionally, 2HL-8-0hrs had 16.9 percent lower rut depth than 1HL-8-0hrs. This is more likely

because the 2HL-3 and 2HL-8 samples contain higher RAP content (20 and 40 percent, respectively) than the 1HL-3 and 1HL-8 samples (15 and 30 percent, respectively) leading to stiffer mixtures. Further, the 2HL-3-12hrs samples exhibited 46.5 percent lower rut depth than 1HL-3-12hrs. Similarly, the 2HL-8-12hrs samples exhibited 48.7 percent lower rut depth as compared with 1HL-8-hrs possibly due to more binder blending. Contributing factors may also include higher temperature during production and storage which would contribute to faster diffusion, oxidation, evaporation and absorption, which could contribute to improved cohesion until oxidation becomes predominant. Based on recent work by (Pirzadeh et al., 2018) the binder also experiences oxidation during silo-storage. This could possibly lead to better rutting resistance with increased silo time.

Furthermore, 24-hr samples significantly reduced the rutting depth by 51.1 and 58.4 percent for the 2HL-3 and 2HL-8, respectively as compared with their 0-hour samples. This could be that after 8, 12, and 24-hour more blending occurred between the virgin and aged binder and more homogenous mixture was obtained. Another reason could be that 24-hour samples might experience extensive aging leading to stiffer mixtures, and that could have been why rutting depth decreased after 12-hour.

Based on the results observed from Table 5-6, all tested specimens for 2HL-3 and 2HL-8 showed good repeatability in terms of rut depth as the value of the standard deviation for the rut depth range from 0.01 to 0.23 mm. However, for 1HL-3 and 1HL-8 a variability was observed in their measured rut depth, reflected in their corresponding standard deviations ranging from 0.1 to 0.44 mm. These values are relatively high as the average rut depth values vary from 4.3 to 3.43 mm. Figure 5-26 illustrates mean rut depth with the standard deviation error bar of the tested samples. Error bars represent mean plus or minus standard deviation of uncertainty.

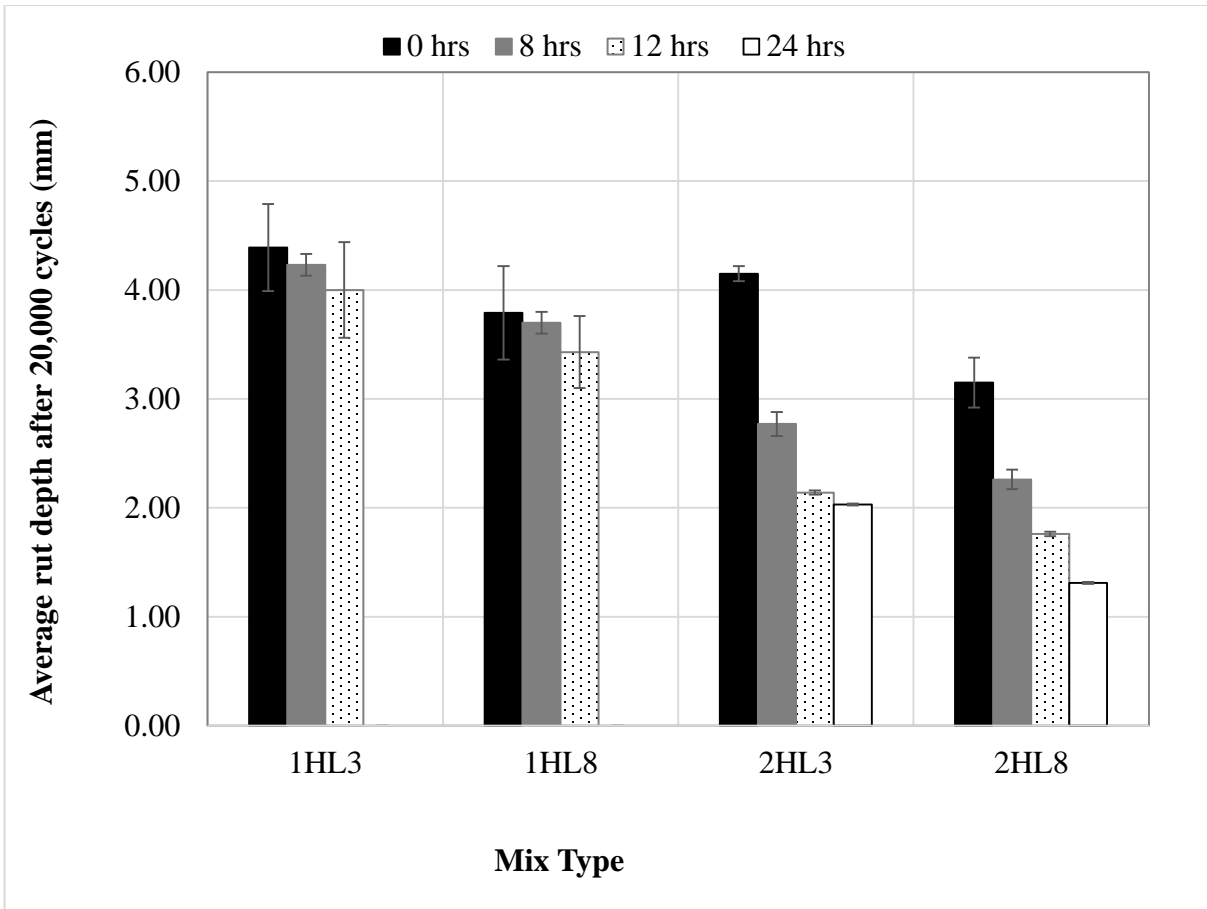


**Figure 5-26 Rut depth with the standard deviation error bar for all the tested mixes**

For the rutting test results, the null hypothesis was ‘increasing silo-storage time does not affect the rutting depth’ whereas the alternative hypothesis was the opposite. Table 5-7 confirms that the effect of increasing silo time on the rutting depth of both 2HL-3 and 2HL-8 is statistically significant. However, the effect of increasing silo time on the rutting depth of both 1HL-3 and 1HL-8 is statistically insignificant. As it has been observed earlier, the improvements in the rut depth after 12-hour of silo-storage for the mixes from plant 1 are 0.3 mm and 0.36 mm for 1HL-3 and 1HL-8, respectively. This observation is confirmed with the statistical analysis as shown in the table below.

**Table 5-7 ANOVA for rutting test**

Mix Type	F	P-value	F <sub>Critical</sub>	Remark
1HL-3	0.54	6.32E-01	9.55	<b>Statistically Insignificant</b>
1HL-8	0.69	5.65E-01	9.55	<b>Statistically Insignificant</b>
2HL-3	417.14	1.90E-05	6.59	Statistically Significant
2HL-8	11.44	1.97E-02	6.59	Statistically Significant

### 5.5 Flexural Beam Fatigue Test Results

The results of the fatigue life to failure ( $N_f$ ) of the three replicates samples for each silo time at different strain levels for both HL-3 and HL-8 are presented in Figure 5-27, Figure 5-28, Figure 5-29, and Figure 5-30. It is worth to notice that  $N_f$  represents the 50% reduction of the initial stiffness value.

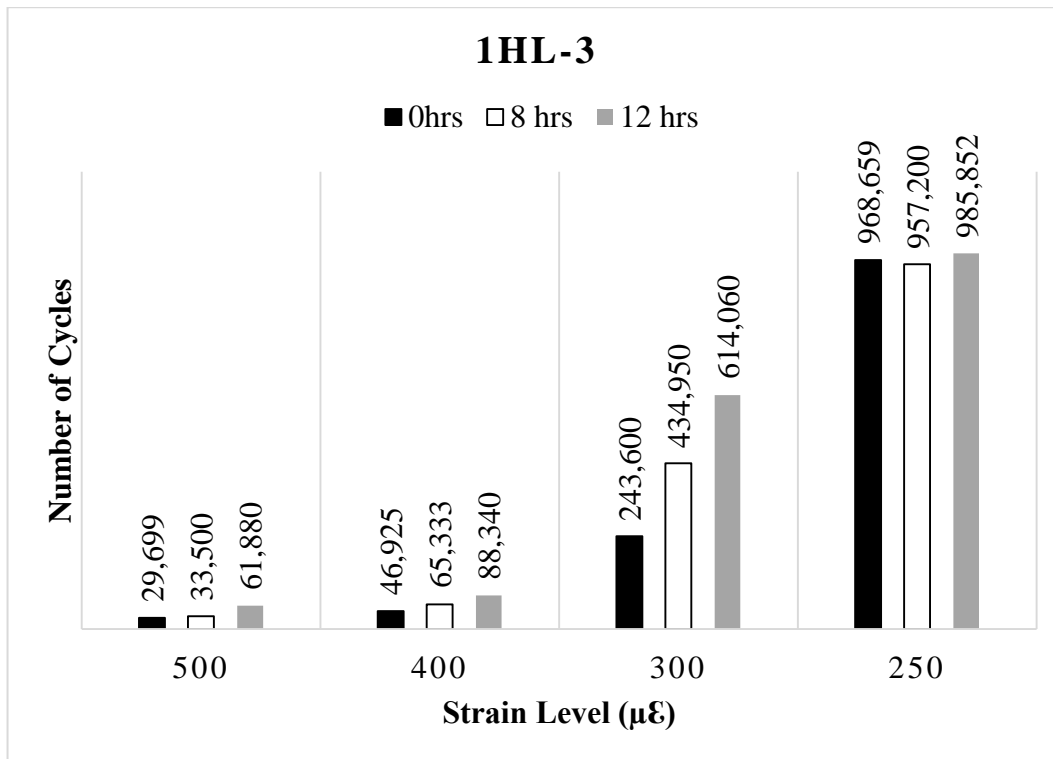


**Figure 5-27 Fatigue life at different strain levels for 1HL-3**

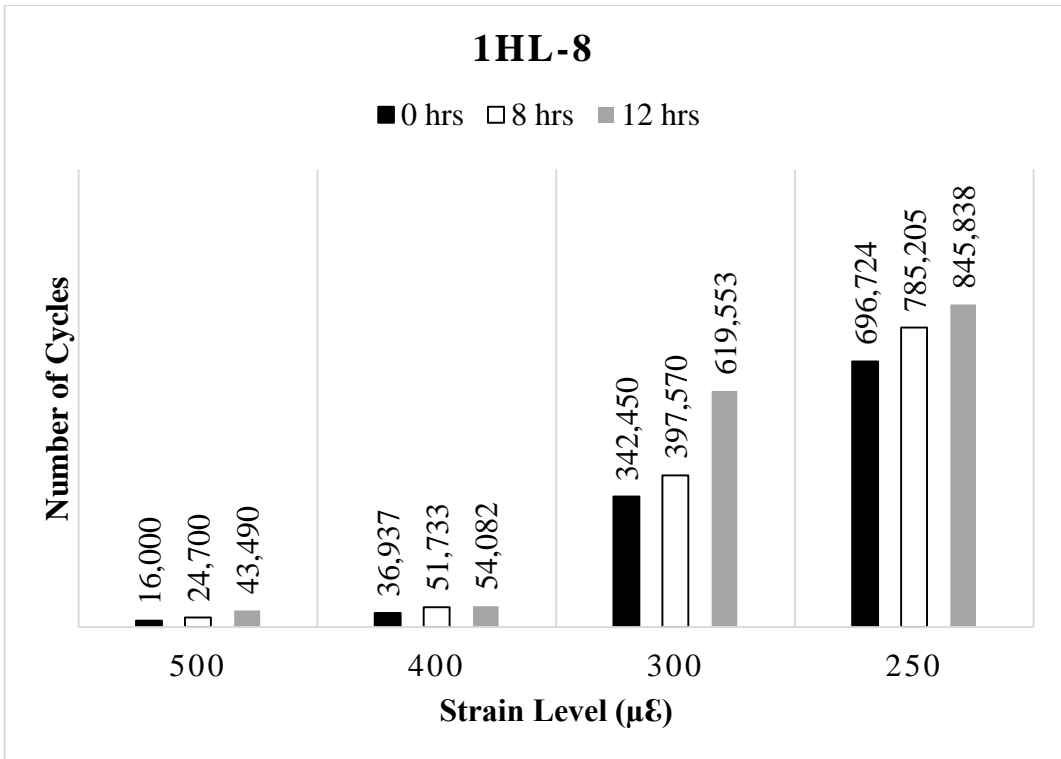


Figure 5-28 Fatigue life at different strain levels for 1HL-8

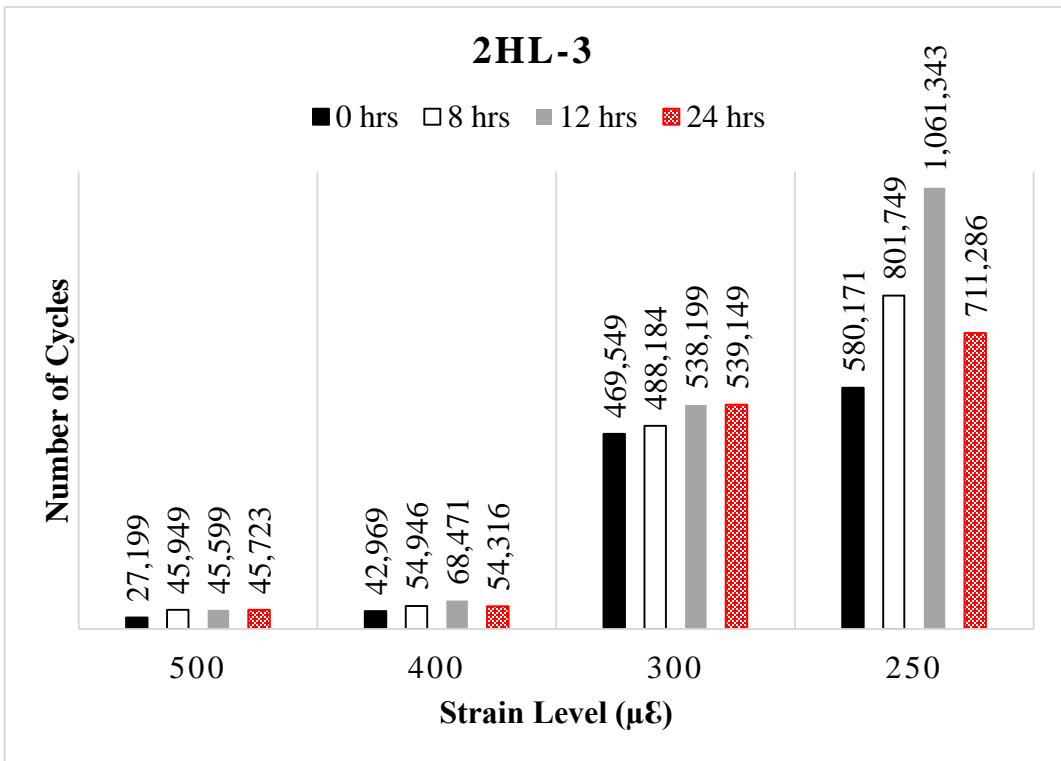
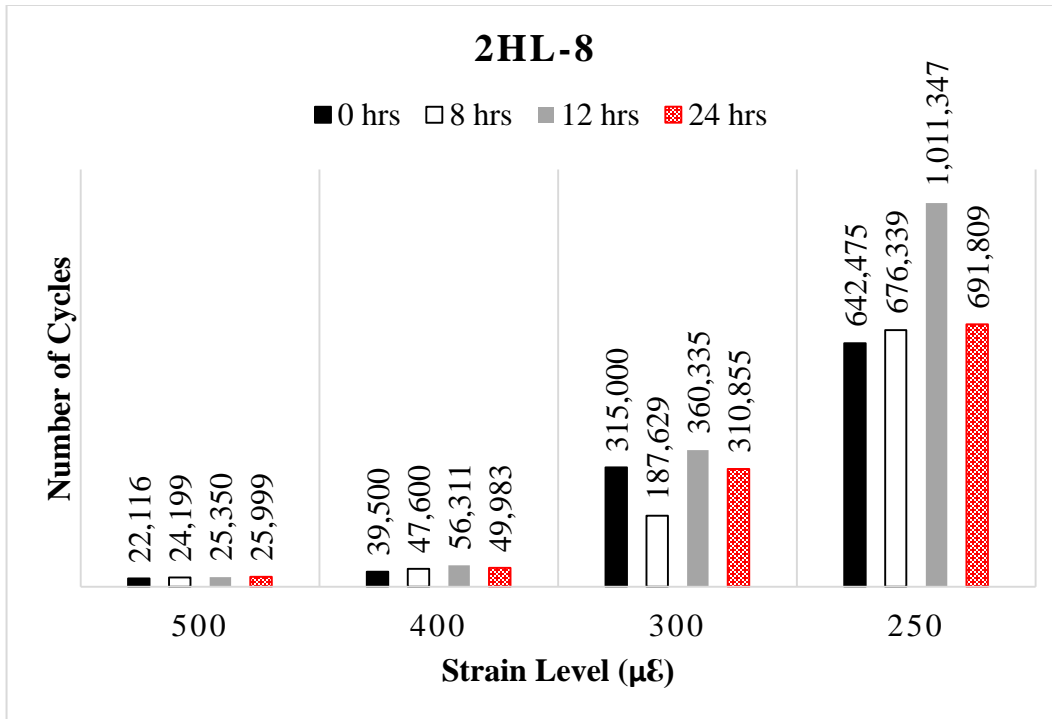


Figure 5-29 Fatigue life at different strain levels for 2HL-3



**Figure 5-30 Fatigue life at different strain levels for 2HL-8**

Data clearly indicate that fatigue life cycles increase with the increase of silo-storage time (up to 12 hours in this case) for all mixes. The trend in fatigue data indicates that the cohesion of the corresponding mix samples was still evolving as a function of storage time, and the response is dominated by relatively softer virgin mix, i.e. lower RAP content. This observation may imply an incomplete diffusion between RAP and virgin binders in samples. In addition, the results were analysed using the classical method with the criterion of fatigue failure  $N_f$  50% (WÖHLER curve). WÖHLER curves considering controlled strain tests are shown in Figure 5-31- Figure 5-44.

In this method, epsilon 6 ( $\epsilon_6$ ) is the main criterion which represents the strain level that leads to failure after one million cycles. The higher the value of  $\epsilon_6$  the higher the fatigue resistance of the asphalt mix. This method is very applicable as both  $\epsilon_6$  and the complex (Stiffness) modulus are used in some Empirical Mechanistic Pavement Design Methods to determine the thickness of asphalt layers. It is important to mention that the strain amplitudes  $\epsilon_6$  are peak-to-peak amplitudes as specified by AASHTO standard (AASHTO, 2017) and should be divided by 2 if compared strain amplitudes used by other specifications such as European Standards (EN, 2012).

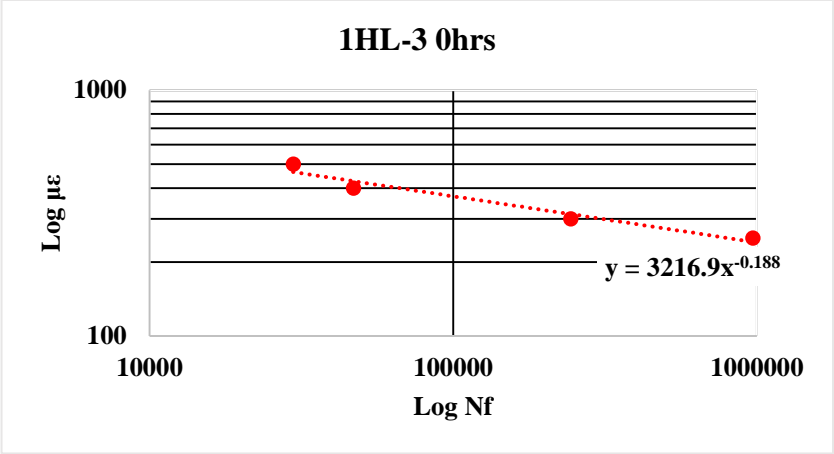


Figure 5-31 WÖHLER curve for 1HL-3 0hrs

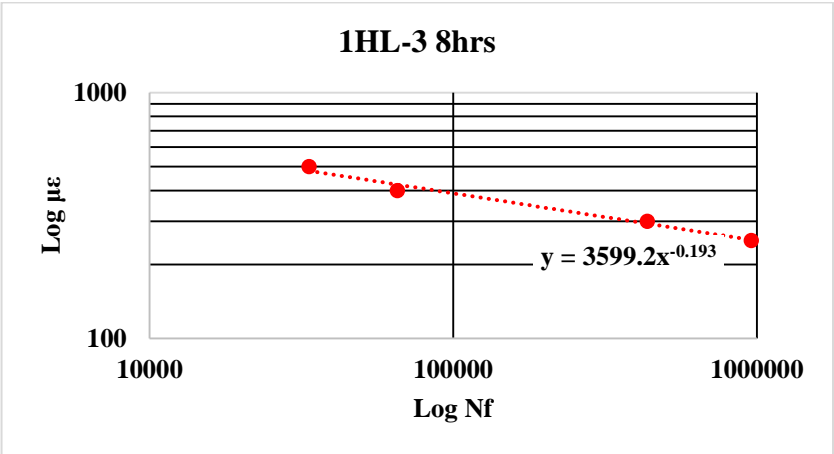


Figure 5-32 WÖHLER curve for 1HL-3 8hrs

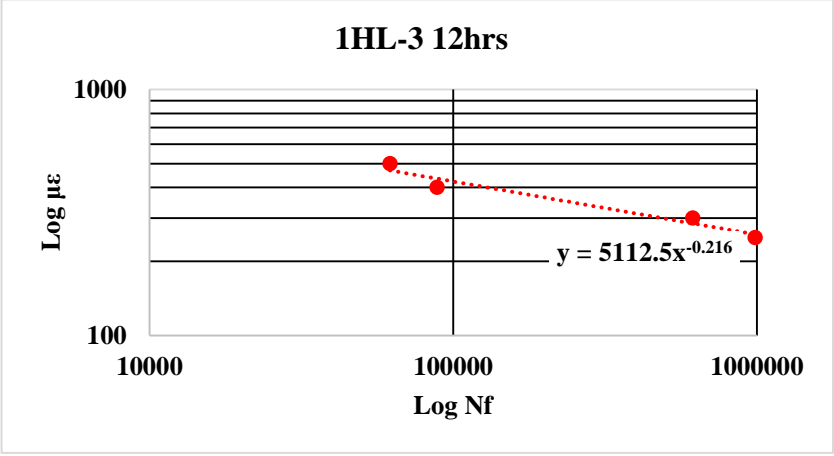


Figure 5-33 WÖHLER curve for 1HL-3 12hrs

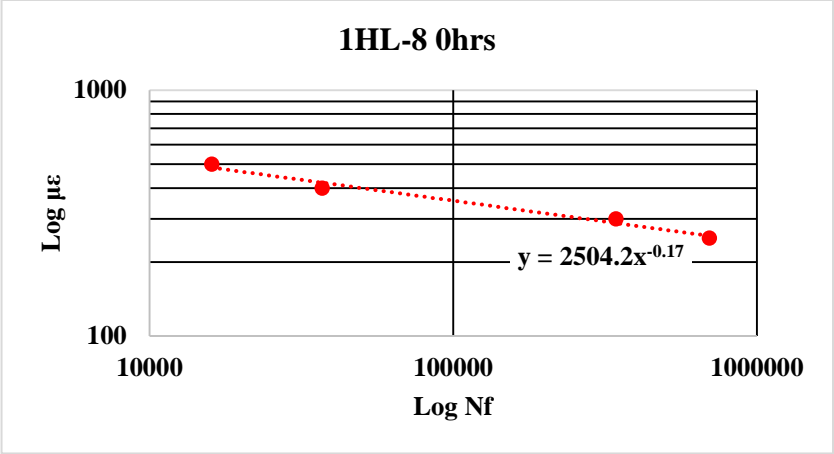


Figure 5-34 WÖHLER curve for 1HL-8 0hrs

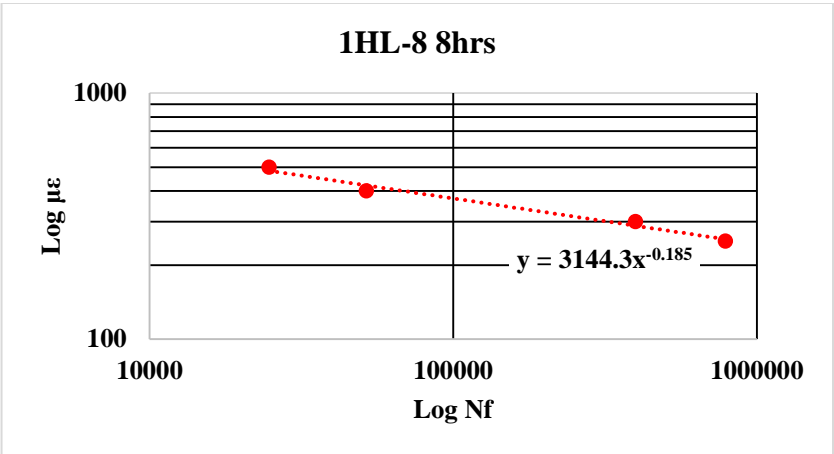


Figure 5-35 WÖHLER curve for 1HL-8 8hrs

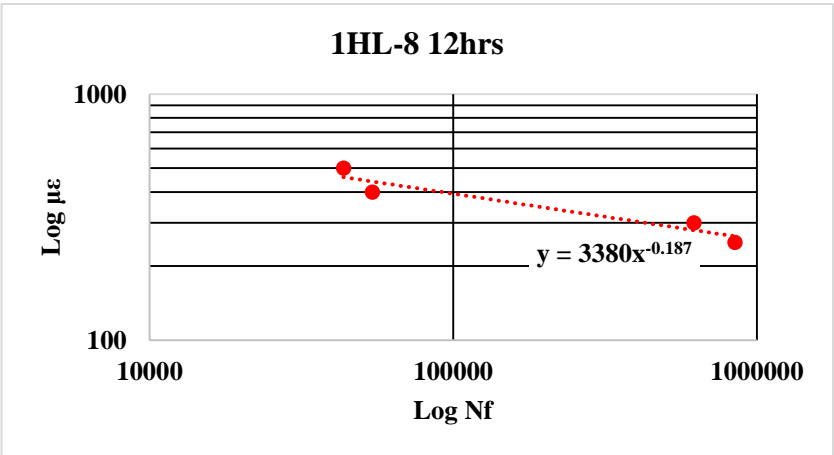


Figure 5-36 WÖHLER curve for 1HL-8 12hrs



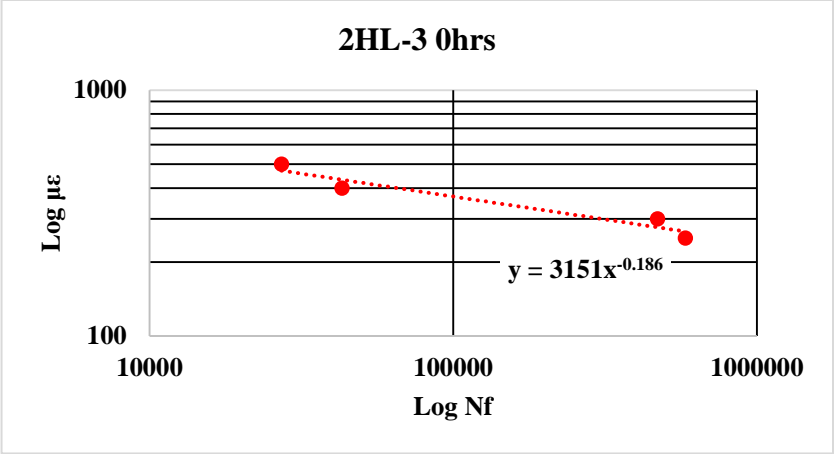


Figure 5-37 WÖHLER curve for 2HL-3 0hrs

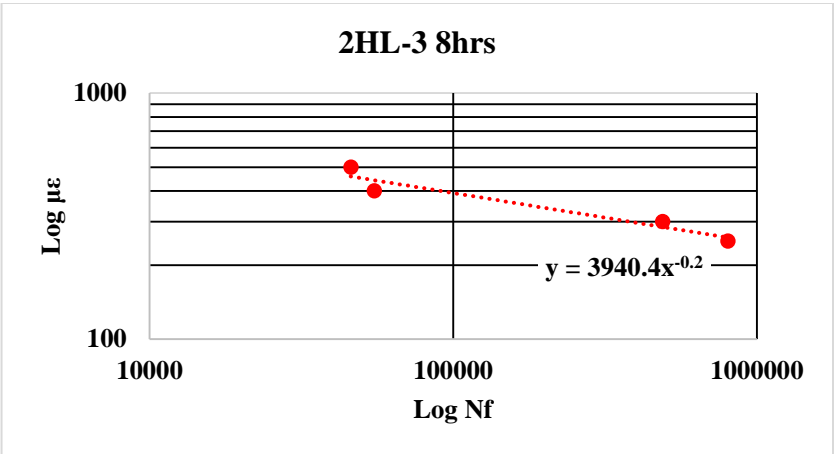


Figure 5-38 WÖHLER curve for 2HL-3 8hrs

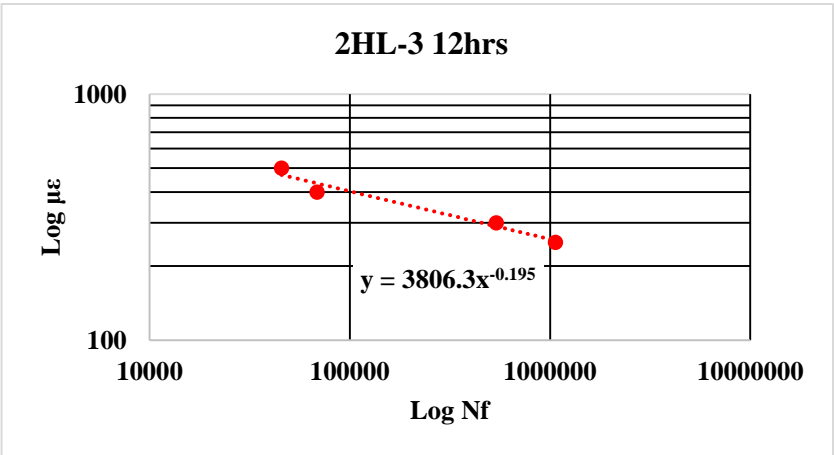


Figure 5-39 WÖHLER curve for 2HL-3 12hrs

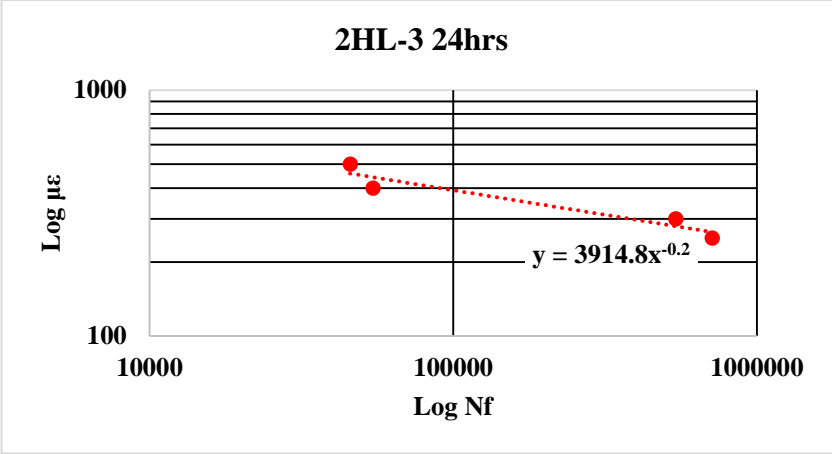


Figure 5-40 WÖHLER curve for 2HL-3 24hrs

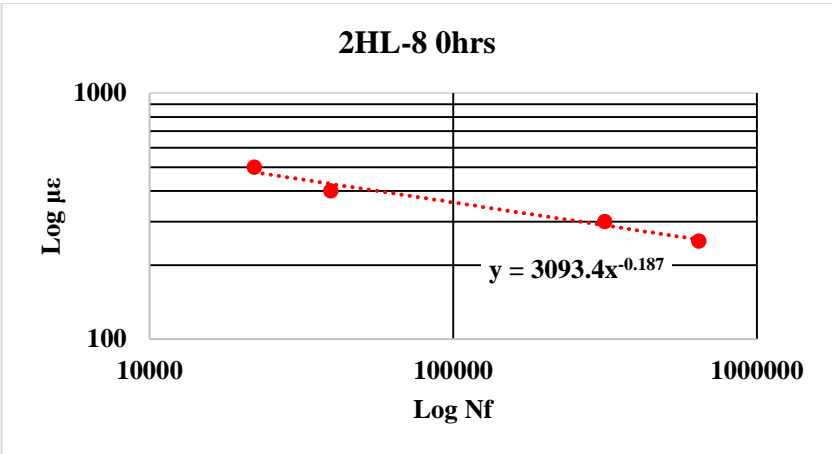


Figure 5-41 WÖHLER curve for 2HL-8 0hrs

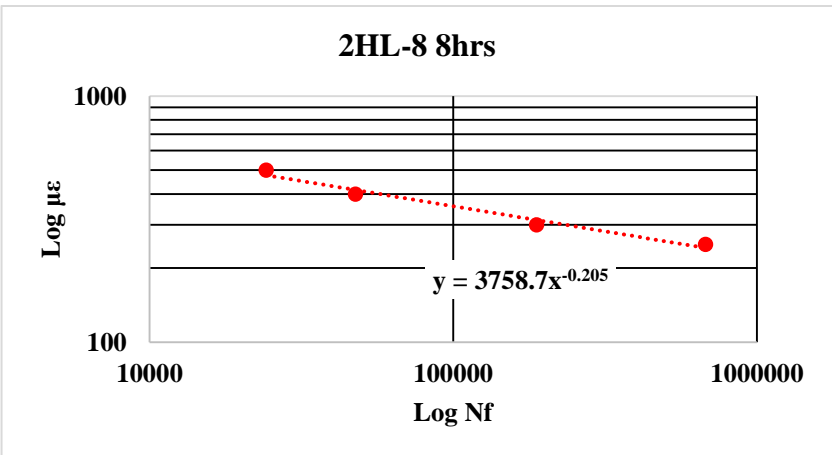


Figure 5-42 WÖHLER curve for 2HL-8 8hrs

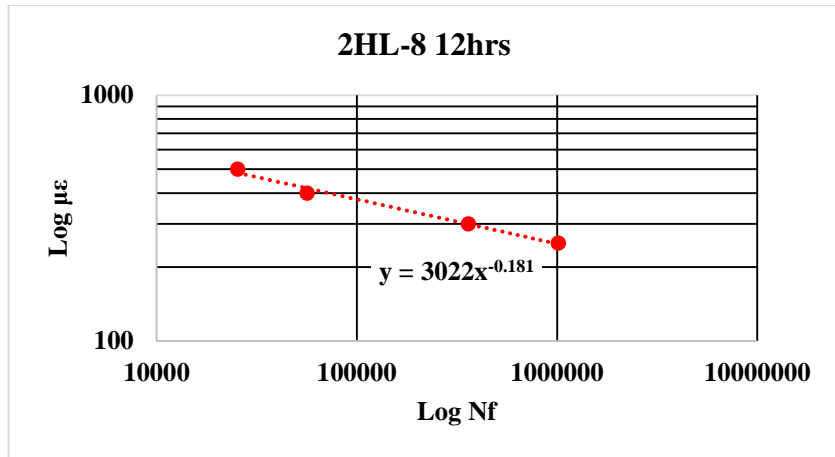


Figure 5-43 WÖHLER curve for 2HL-8 12hrs

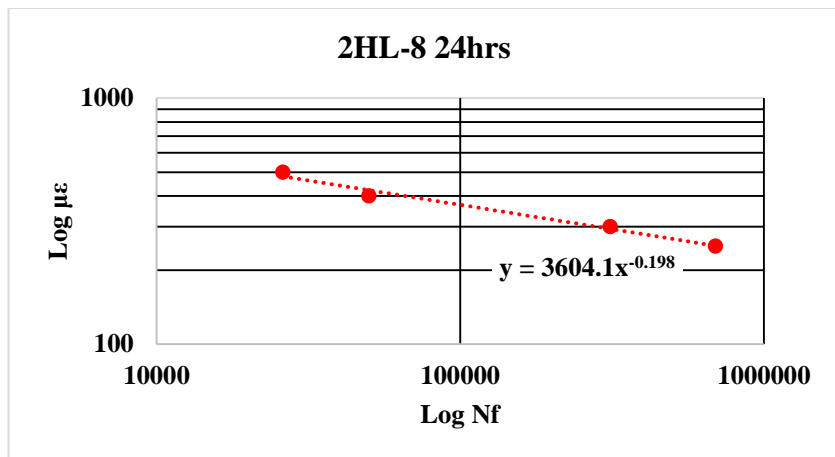


Figure 5-44 WÖHLER curve for 2HL-8 24hrs

For all mixes, the WÖHLER curve method has shown that the addition storage time improves the fatigue life. Overall, higher storage time results in a final binder blend with more uniform cohesiveness, and improved adherence to aggregates. This enhanced cohesiveness and adherence reflects itself in better fatigue cracking performance of the stored mix. The value of  $\epsilon_6$  for each mix is presented in Table 5-8. It was noted that 1HL-3 with 12-hour storage time has the greatest  $\epsilon_6$  value (258.60) among all mixes. This could be due to higher storage time, lower RAP content as well as smaller NMAAS as compared with the HL-8 mix. These factors might result in a better homogenous mix and consequently higher fatigue life.

**Table 5-8  $\epsilon_6$  value for each mix (Peak-to-Peak strain amplitudes)**

Mix Type	Silo-storage time (hrs)	$\epsilon_6$ value	Improvement of $\epsilon_6$ value after 12 hrs
1HL-3	0	239.57	7.4%
	8	250.15	
	12	258.60	
1HL-8	0	239.15	6.3%
	8	244.08	
	12	255.22	
2HL-3	0	241.24	6.3%
	8	248.62	
	12	257.34	
	24	247.01	
2HL-8	0	233.58	5.8%
	8	221.33	
	12	247.91	
	24	233.77	

To evaluate whether the effect of the silo-storage on the fatigue life is statistically significant, the null hypothesis was ‘increasing silo-storage time does not affect the fatigue life’ whereas the alternative hypothesis was the opposite. The highest strain level (500  $\mu\text{m}$ ) was selected for this test.

**Table 5-9 ANOVA for fatigue test at 500  $\mu\text{m}$**

Mix Type	F	P-value	F <sub>Critical</sub>	Remark
1HL-3	1159.01	4.65E-05	9.55	Statistically Significant
1HL-8	317.03	3.23E-04	9.55	Statistically Significant
2HL-3	509.19	1.28E-05	6.59	Statistically Significant
2HL-8	5.51	6.64E-02	6.59	Statistically Insignificant

Table 5-9 above indicates that the effect of increasing silo time on the fatigue life of both HL-3 and HL-8 is statistically significant for all the mixes excluding 2HL-8. It should be noted that that the improvement in  $E_6$  value of the 2HL-8 after 12 hours silo-storage time was only 5.8%.

## 5.6 Summary of the Results

In this Chapter, the laboratory performance testing results for all HMA samples from both Plant 1 and Plant 2 were presented, analyzed and discussed in accordance with the thesis methodology and research objectives.

The examination of the volumetric properties values, obtained at different silo-storage times, showed that a slight decrease in VMA and  $V_{be}$  values was generally found with respect to increasing the silo-storage time for all HMA samples. This could be explained by assuming that when better blending happens during silo-storage, this would lead to increasing the aged-binder contribution to the efficient binder in the mixture.

For all the collected HMA samples, there was no significant change in the complex modulus values of samples that were collected at 0, 1 and 4-hour of silo-storage. Hence, this would indicate that there was no considerable effect of the storage up to 4-hour on the rheology of this mixture. On the other hand, a decrease in the stiffness at high temperatures/lower frequencies was observed in the samples collected after 8 and 12-hour of silo-storage. Theoretically, more blending would result in an enhanced adhesion between the binder and the aggregates and would improve the quality of the HMA and enhance resistance to permanent deformation. This is more likely because the RAP binder had an increased contribution to the efficient asphalt binder used within the mixture due to increased overall blending. Yet, the 24-hour mixes from Plant 2 exhibited an increase in their stiffness that would attributed to aging.

The fracture temperatures of both HL-3 and HL-8 mixes were generally affected by their virgin binder grades. All HL-8 samples slightly exhibited lower fracture temperature than HL-3 samples due to their softer virgin asphalt binder. For both HL-3 and HL-8, an improvement of the thermal resistance was found for the 8 and 12-hour samples as compared with the 0-hour samples. On the other hand, the 24-hour mixes exhibited an increase in the stiffness that would attributed to aging. Hence, lower thermal cracking resistance was observed

The results of the HWTD test appeared to point that the base course mixes (1HL-8 and 2HL-8) exhibited lower rut depth percentages compared with the surface course mixes (1HL-3 and 2HL-3). This would be due to higher RAP content, larger NMAS, softer virgin binder, lower overall asphalt content, or a combination of different factors. Partially, due to higher RAP content, 2HL-3 and 2HL-8 showed a significantly better rutting resistance as compared with the 1HL-3 and 1HL-8, respectively. However, other factors play roles such as; blending rate in the mix, aggregate gradation of the mix, binder type, and binder content. These results are promising and suggest that higher storage time for the given mixes and silo conditions could potentially improve the blending of RAP and virgin binders, which positively affect the rutting resistance of HMA-RAP mixtures. Yet, it should be noted that aging can also result in smaller rutting depth values for the samples that have been kept for extended period (24-hrs) in silo-storage.

The results of the fatigue test indicated that increasing silo-storage time can extend the fatigue life of the both HL-3 and HL-8. WÖHLER curve method has shown that the addition storage time improves the fatigue life. In addition, higher  $E_6$  values can significantly affect the pavement design positively as it is used to determine the thickness of asphalt layer in some Empirical Mechanistic Pavement Design. Overall, higher storage time resulted in a final binder blend with more uniform cohesiveness, and improved adherence to aggregates. This enhanced cohesiveness and adherence reflects itself in better fatigue cracking performance of the stored mix.

Previous work of Kriz et al. (P. Kriz et al., 2014), where diffusion in lab-produced mix samples were studied, suggested that diffusion between RAP and virgin binders was completed in about 10 hours. This estimated time scale for completion of diffusion perfectly matches the observed time scale of evolutions in  $|E^*|$  and mix performance properties (particularly in Plant 2 samples) in the present field work. This consistency between earlier theoretical work (P. Kriz et al., 2014a), lab-scale mix (P. Kriz et al., 2014b) and the present work highlights the important role of diffusion in utilizing RAP in production of new mix.

Overall, silo of Plant 2 was stagnant during storage; this stagnancy helps the stored mix to retain a larger heat capacity relative to an off-loading silo of Plant 1. The higher heat capacity benefits the material by decreasing the rate of cooling, which further assists blending and diffusion progress. Improved diffusion enables achieving a more homogeneous blend within the silo-storage time frame. It should be also noted that binder chemistry could have also played a role in faster

rate of aging during silo-storage in case of Plant 2 base mix. Therefore, further investigation is required to further resolve the confounding impacts of binder chemistry and longer storage time for RAP-containing asphalt mixes.

## 6 Long-Term Field Performance Prediction

In this chapter, the 20-years field performance prediction was evaluated using the AASHTOWare Pavement Mechanistic-Empirical Design model. This method was first developed in 2002 under the Mechanistic-Empirical Pavement Design Guide (MEPDG). It was developed by the National Cooperative Highway Research Program (NCHRP) Project 1-37A (Darter et al., 2006). MEPDG was introduced to address the limitations of the AASHTO 1993 method. This method was then revised to address some technical limitation in 2011 under the name AASHTOWare.

In this method, the design of the desired pavement structure is first considered on trial data, accompanying with inputs for traffic and climate. AASHTOWare Pavement ME Design can measure how the trial design will perform under the load and different environmental stresses. This leads to an estimate of the level of damage the pavement will support over its service life, in terms of pavement distresses and deterioration in ride quality and comfort. It should be noted that the International roughness index (IRI) is used as the main indicator of pavement performance. IRI is one of the common indexes. IRI is a standard roughness measurement measured from the records of a specific type of road meter installed on vehicles (Sayers and Karamihas, 1996). It is usually observed that the IRI value rises by increasing pavement age due to the effect of deterioration elements (Sobhani et al., 2016). It is assumed that at least improvement of the IRI values would be detected for the pavements that are constructed with the mixes that were stored at 12-hour at the silo-storage.

However, the users of AASHTOWare Pavement ME Design should be mindful of the limitation of this method. For instance, HMA is a viscoelastic material. Simplification is made essentially owe to the time-dependent characteristic of a viscoelastic material is always very challenging. In other words, AASHTOWare Pavement ME Design incorporates the dynamic modulus values of the HMA at different temperatures and frequencies which are measured under very small strain level within the linear viscoelastic domain of the HMA. Yet, the pavement distresses (rutting and cracking) are formed due to larger strain level. Hence, the simplified mechanistic is a drawback of this method. Additionally, flexible pavement is a multi-layered structure which adds additional complicates to the modeling tasks. Therefore, researchers are regularly developing models to adequately reflect the influence of viscosity, plasticity and other nonlinear characteristics on pavement structures (Chen, 2009).



The lab performance test results of this study indicate that the 12-hour storage mixes exhibited a significant enhancement in terms of rutting and cracking resistance. Yet, it is equally required to estimate the field performance of these mixes to draw more solid conclusions. Therefore, the comparison between 0-hour mixes and 12-hour mixes were carried out for both mixes from Plant1 and Plant 2.

## 6.1 Inputs

AASHTOWare Pavement ME Design was utilized to examine the effect of the 12-hour silo-storage time on the long term performance of the pavements. Four pavements have been designed for this purpose namely; Plant1 0hrs, Plant1 12hrs, Plant2 0hrs, and Plant2 12 hrs. These pavements have the same structure of their granular A, granular B, and the subgrade. Yet, the properties of the first layer (surface course and base course) is a silo storage-dependent. Table 6-1 describes the structure of these four pavement sections. In addition, the information about the layer thicknesses and properties are presented in Table 6-2. A systematic structure of all the designed pavements is shown in Figure 6-1.

**Table 6-1 The structure of each of the four pavements**

<b>Pavement</b>	<b>Structure</b>
Plant 1 0hrs	Surface course: 1HL-3 @0hrs Base course: 1HL-8 @0hrs Granular A Granular B Subgrade
Plant 1 12hrs	Surface course: 1HL-3 @12hrs Base course: 1HL-8 @12hrs Granular A Granular B Subgrade

Plant 2 0hrs	Surface course: 2HL-3 @0hrs Base course: 2HL-8 @0hrs Granular A Granular B Subgrade
Plant 2 12hrs	Surface course: 2HL-3 @12hrs Base course: 2HL-8 @12hrs Granular A Granular B Subgrade

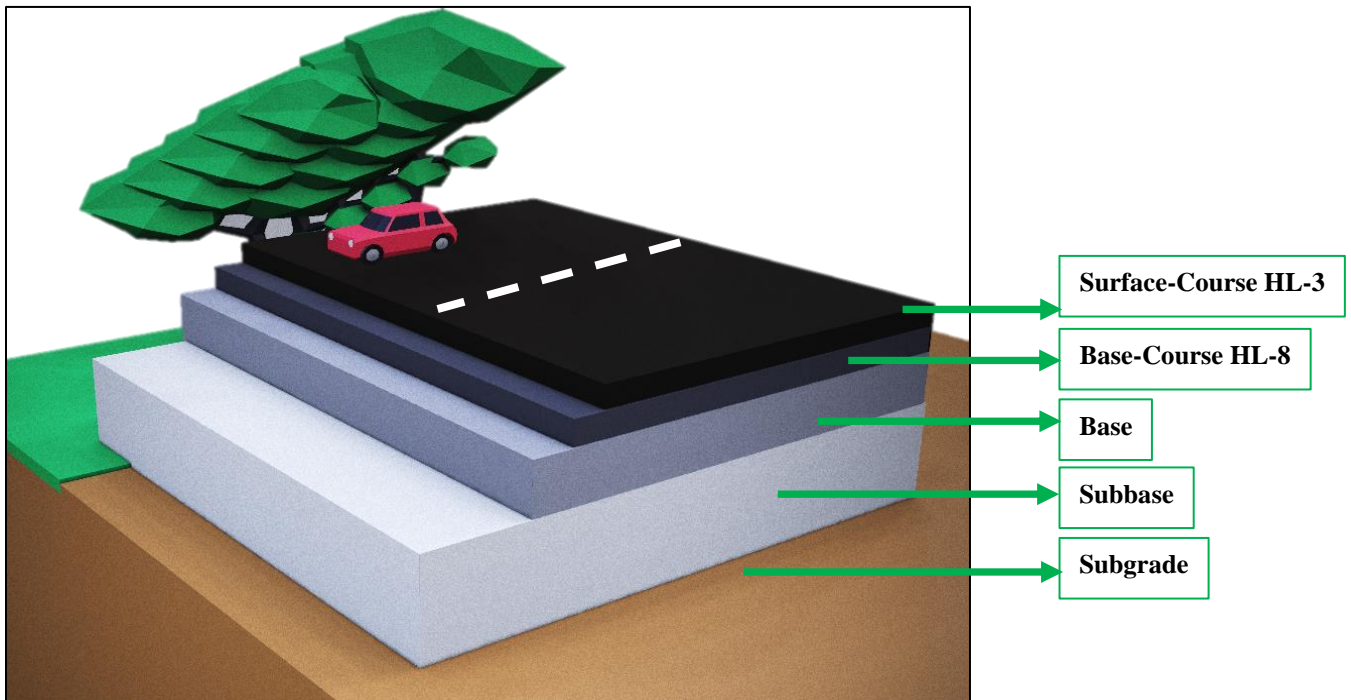


**Figure 6-1 A systematic structure of all the designed pavements**

These four flexible pavements with a 3.7 m design lane were designed and compared in accordance with the Typical Ontario Pavement Designs Report (ARA, 2015) and Canadian Guide: Default Parameters for AASHTOWare Pavement ME Design (TAC, 2014).

Three levels of performance analysis may apply in AASHTOWare Pavement ME Design depending on the availability of data and importance of the project. These levels are as follows:

**Level 1:** This is the most solid and trustworthy of all levels. It is usually used for the most heavily trafficked projects where the safety of the users and the financial consequences of early pavement failures are critical. The input of this level requires the stiffness of both binder and HMA at different temperatures.

**Level 2:** the inputs are based on insufficient testing and/or are chosen from the values given by the agency. Such values are usually determined empirically. Thus, this level is less reliable than level 1.

**Level 3:** the least reliable of all levels. Inputs are user selected default values.

For this study, Level 1 was applied for the performance analysis. For this Level, the dynamic modulus values of the 0hrs and 12 hrs mixes at different temperatures and frequencies were input. In addition, the stiffness of the virgin binders were used in this analysis.

The main inputs are highlighted in the Table 6-2.

**Table 6-2 main inputs of the AASHTOWare Pavement ME Design**

<b>Criterion</b>	<b>Input</b>
Subgrade resilient modulus (MPa)	50
Subbase thickness (mm)	300
Subbase resilient modulus (MPa)	200
Base thickness (mm)	150
Base resilient modulus (MPa)	240
Base course thickness (mm)	80
Surface course thickness (mm)	40
Air voids (%)	4











Age (year)	20
Target terminal International Roughness Index IRI (m/km)	2.7
Target permanent deformation - total pavement (mm)	19
Target AC bottom-up fatigue cracking (%)	20
Target AC thermal cracking (m/km)	190
Target AC top-down fatigue cracking (m/km)	380

As the stiffness of RAP-HMA samples were affected significantly by the 12-hour silo-storage time, level 1 input of performance analysis was chosen.

### 6.1.1 Traffic Input

The AASHTOWare Pavement ME Design uses a complex process to predict the traffic loads on a roadway. To complete this part of the process, the traffic volume for each month is divided into the 13 vehicle classes. However, light vehicles, class 1 through 3, are disregarded as their load impact on the roadway is negligible. Table 6-3 below shows the distribution of the commercial vehicles as specified by the US Federal Highway Administration (FHWA) (ARA, 2015). As the collected mixes were RAP mixes, it is decided to use them in minor arterial roads with 1,000 initial Annual Average Daily Traffic (AADT) per year for one lane in design direction. A linear traffic growth rate of 2% was used in this process. The percent of trucks in design lane is assumed to be 80% and the design speed was 100 km/hrs.

**Table 6-3 Expected commercial vehicle distribution for municipal roadways (ARA, 2015)**

FHWA Class	Commercial Vehicle		Distribution of Commercial Vehicles		
			Collector	Minor Arterial	Major Arterial
4		Two or Three Axle Buses	2.9 %	3.3 %	1.8 %
5		Two-Axle, Six-Tire, Single Unit Trucks	56.9 %	34.0 %	24.6 %
6		Three-Axle Single Unit Trucks	10.4 %	11.7 %	7.6 %
7		Four or More Axle Single Unit Trucks	3.7 %	1.6 %	0.5 %
8		Four or Less Axle Single Trailer Trucks	9.2 %	9.9 %	5 %
9		Five-Axle Single Trailer Trucks	15.3 %	36.2 %	31.3 %
10		Six or More Axle Single Trailer Trucks	0.6 %	1.0 %	9.8 %
11		Five or Less Axle Multi-Trailer Trucks	0.3 %	1.8 %	0.8 %
12		Six-Axle Multi-Trailer Trucks	0.4 %	0.2 %	3.3 %
13		Seven or More Axle Multi-Trailer Trucks	0.3 %	0.3 %	15.3 %

### 6.1.2 Climate input

As climate is one of the most significant factor influencing the performance of pavements, a typical climate representing Southern Ontario was chosen. Table 6-4 shows the main climate inputs.

**Table 6-4 Climate inputs for AASHTOWare Pavement ME Design**

Criterion	Input
The mean annual air temperature (°C)	7.51
The mean annual precipitation (mm)	1057.15
The average annual number of freeze/thaw cycles	76.99
The water table depth (m)	10

## 6.2 Performance Prediction and Analysis

All the four pavements passed the target criteria of the 20-years performance prediction. In addition, the performance predication indicates that increasing silo-storage time improves the

overall long-term performance. Table 6-5 shows that Plant1 12hrs pavement exhibited an improvement in all criteria as compared with the Plant1 0hrs pavement.

The improvement in IRI value, permanent deformation, and top-down fatigue cracking for the 12hrs silo-storage HMA after 20-year service life are 11%, 4.5%, and 12.4% respectively.

**Table 6-5 Predicted long-term performance of the Plant1 pavements**

Criteria	Distress @ 90% Reliability		
	Target	Predicted for Plant1 0hrs	Predicted for Plant1 12hrs
Target terminal IRI (m/km)	2.7	2.49	2.21
Target permanent deformation - total pavement (mm)	19	16.5	15.75
AC bottom-up fatigue cracking (%)	20	1.46	1.45
AC thermal cracking (m/km)	190	40.98	40
AC top-down fatigue cracking (m/km)	380	96.26	87.66

Figure 6-2 represents a comparison of IRI value at 90% reliability for Plant1 0hrs with Plant1 12hrs. The reduction in the IRI value for the Plant 1 12hrs pavement is 11% as compared with the Plant 1 0hrs. The results of pavement performance predication in Table 6-6 and Figure 6-3 below indicate improvements in Plant2 12hrs with respect to all criteria as compared with the Plant2 0hrs pavement. The improvement in IRI value, permanent deformation, and top-down fatigue cracking for the 12hrs silo-storage HMA after 20-year service life are 13.6%, 9.2%, and 2%, respectively. Moreover, the thermal cracking has improved by 25.6% for the Plant2 12hrs pavement. Overall, plant1 pavements have higher IRI values as compared with the Plant2 pavements. This is because silo of Plant 2 was stagnant during storage; this stagnancy helps the stored mix to retain a larger heat capacity relative to an off-loading silo. The higher heat capacity benefits the material by decreasing the rate of cooling, which further assists blending and diffusion progress. Improved diffusion enables achieving a more homogeneous blend within the silo-storage time frame. Hence, better predicted performance is observed with the Plant 2 pavements.

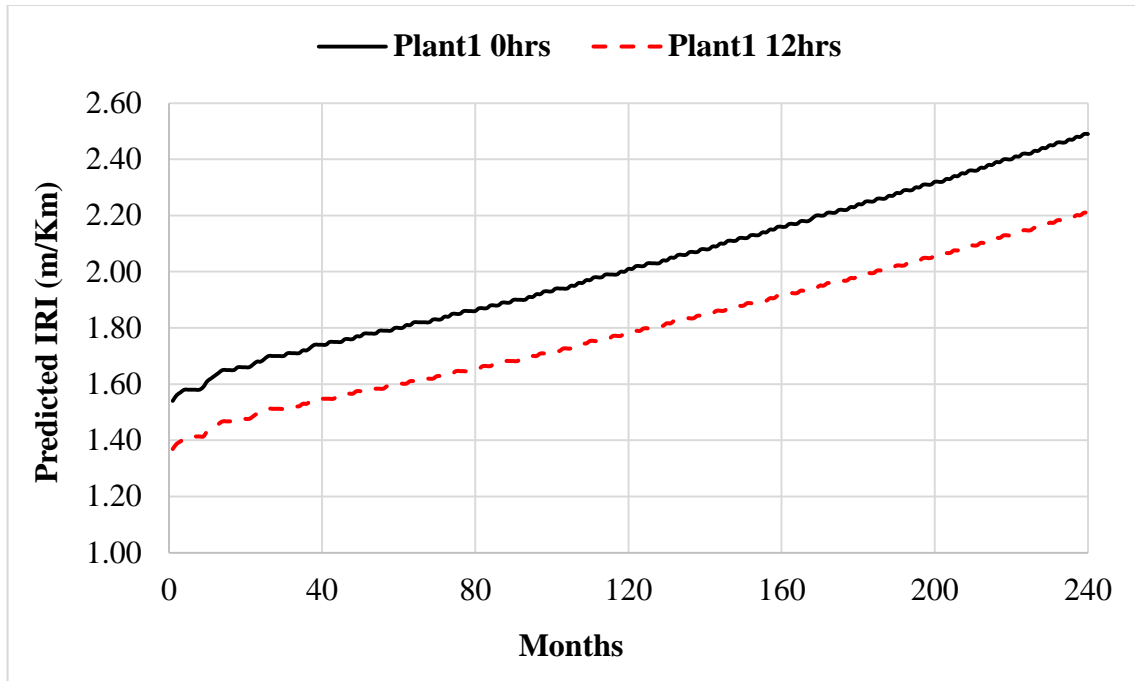
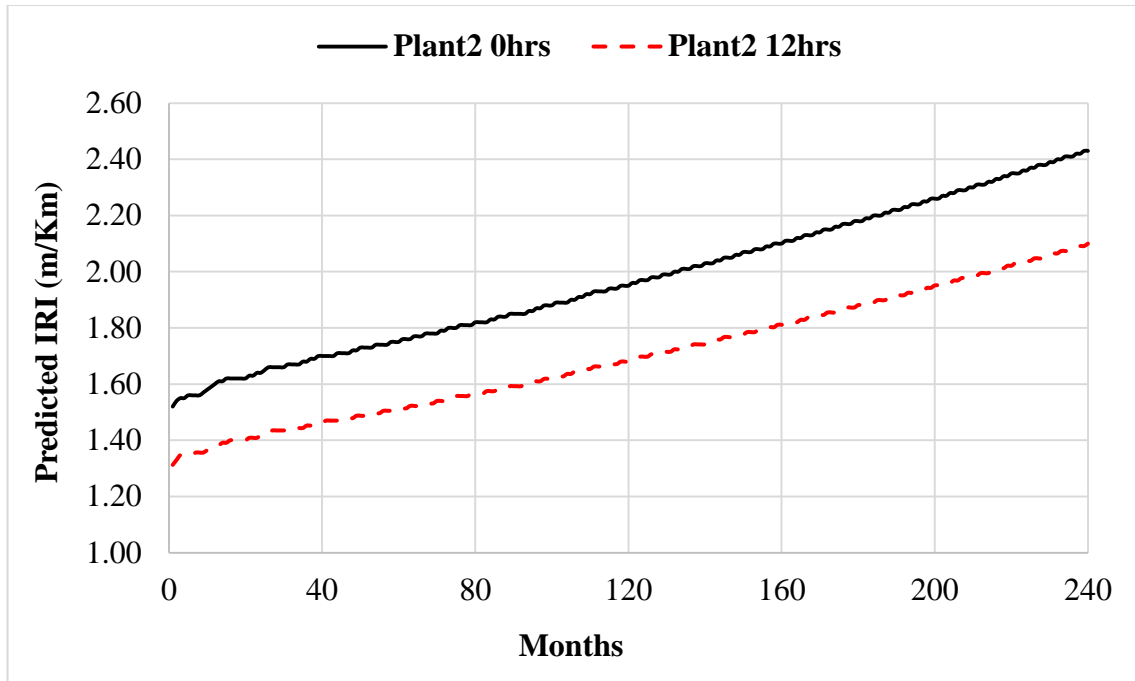


Figure 6-2 Comparison of IRI value at 90% reliability for Plant1 0hrs with Plant1 12hrs

Table 6-6 Predicted long-term performance of the Plant2 pavements

Criteria	Distress @ 90% Reliability		
	Target	Predicted for Plant2 0hrs	Predicted for Plant2 12hrs
Target terminal IRI (m/km)	2.7	2.43	2.1
Target permanent deformation - total pavement (mm)	19	14.39	13.06
AC bottom-up fatigue cracking (%)	20	1.5	1.45
AC thermal cracking (m/km)	190	54.97	40.9
AC top-down fatigue cracking (m/km)	380	91.79	89.93



**Figure 6-3 Comparison of IRI value at 90% reliability for Plant2 0hrs with Plant2 12hrs**

Despite the fact that the long term performance predication shows only a slight improvement for pavements that have been designed with the 12-hour storage mixes, it indicates that the silo-storage could actually enhance the overall performance and durability of the pavements. Yet, it should be noted that AASHTOWare Pavement ME Design does not capture the effect of blending in pavement performance. Therefore, a better calibration to incorporate the blending parameters within the AASHTOWare Pavement ME Design method is recommended to improve the long-term performance prediction.

The obtained results of the RAP-HMA testing suggest that higher storage time for the given mixes and silo conditions could potentially improve the blending of RAP and virgin binders, which positively affect the performance of the mixes. However, it should be noted that aging can be the dominant process at different silo-storage conditions. Therefore, the insights provided by this study can be expanded to the incorporation of other stiffer material such as oxidized asphalt (e.g. shingles) and reclaimed asphalt shingles (RAS) in new pavement asphalt mix as well. These data along with the percentage of RAP content for each layer and silo and sampling parameters should be incorporated within AASHTOWare Pavement ME Design for a better prediction of the performance of the RAP-HMA pavements.



## 7 Conclusions, Outcome, and Future Research

### 7.1 Summary of Findings and Conclusions

This research has investigated the practicability of using extended silo-storage times in order to improve the durability of asphalt mixes produced with RAP by enhancing binder blending. Results obtained from the comprehensive laboratory performance characterization satisfied the research hypothesis stipulating that silo-storage would help improving the blending of the aged and virgin asphalt binders in the RAP-HMA mixes. Consequently, this blending improves the mixture's stability, durability, workability, and flexibility. The following findings have therefore been drawn:

- The binder preparation technique for ESEM testing was adequate, and the sample moulds were easy to use, handle, and clean. In addition, the divider blending mould design proved beneficial in the evaluation of the interaction of the two the binders (virgin and oxidized). These moulds were designed and fabricated at CPATT.
- The fibril size of the virgin binder tends to be relatively large at around 15-30  $\mu\text{m}$ ; however, the structure is relatively sparse, and the fibrils intersect each other. On the other hand, the fibril size of the oxidized binder (6-10  $\mu\text{m}$ ) is smaller than that of virgin binder, and the structure also appears to be much more perpendicular, dense, connected, intertwined, and organized.
- The examination of the volumetric properties values, obtained at different silo-storage times, showed that a slight decrease in VMA and  $V_{be}$  values was generally found with respect to the increase of the silo-storage time for all HMA samples. The decrease of the VMA values was statistically significant.
- For all the collected HMA samples, there was no significant change in the complex modulus values of samples that were collected at 0, 1 and 4-hour of silo-storage. Hence, this indicated that there was no considerable effect of up to 4-hour of silo-storage on the rheology of these mixes. However, a significant decrease in the stiffness was observed in the samples collected after 8 and 12-hour of silo-storage. In other words, the stiffness of 0-hour storage was more than two times higher than that of 12-hour in the silo-storage for some mixes.

- The 24-hour mixes from Plant 2 exhibited an increase in their stiffness that would be attributed to aging.
- The fracture temperatures obtained from the TSRST of both HL-3 and HL-8 mixes were generally affected by their virgin binder grades. All HL-8 samples slightly exhibited lower fracture temperature than HL-3 samples due to their softer virgin asphalt binder. For both HL-3 and HL-8, an improvement of the thermal resistance was found for the 8 and 12-hour samples as compared with the 0-hour samples.
- The 24-hour mixes exhibited an increase in the stiffness that could be attributed to aging. Hence, lower thermal cracking resistance was observed.
- The results of the HWTD test appeared to point that the base course mixes (1HL-8 and 2HL-8) exhibited lower rut depth percentages compared with the surface course mixes (1HL-3 and 2HL-3). This is due to higher RAP content, larger NMAS, better activation of the RAP binder with a softer virgin binder, lower overall asphalt content, or a combination of different factors.
- Partially, due to higher RAP content, mixes 2HL-3 and 2HL-8 showed a significantly better rutting resistance as compared with mixes 1HL-3 and 1HL-8, respectively.
- Aging can also result in lower rutting depth values for the samples that have been kept for extended period (24-hrs) in silo-storage.
- The results of the fatigue test and WÖHLER curve method indicated that increasing silo-storage time can extend the fatigue life of the all the tested mixes.

In addition, the major conclusions of this study are summarized below:

- As observed from the ESEM images, the blending between aged and virgin binder is highly impacted by the storage time and temperature. This finding is in agreement with the Arrhenius law which states that diffusion rate increases significantly with increasing temperature.

- Overall, 12-hour silo-storage would be the optimum time, for the given silo-storage conditions, at which the performance of the asphalt mixtures with RAP was notably improved.
- The silo in Plant 2 was stagnant during storage; this stagnancy helps the stored mix to retain a larger heat capacity relative to the off-loading silo used in Plant 1. The higher heat capacity benefits the material by decreasing the rate of cooling, which further assists blending and diffusion progress. Improved diffusion enables achieving a more homogeneous blend within the silo-storage time frame. Hence, lower rate of production can enhance RAP-binder activation and accelerate initial diffusion rates. In addition, higher constant silo temperature, i.e. stagnant versus continuous off-loading operation, can help diffusion to progress faster toward completion.
- The AASHTOWare Pavement ME Design does not appear to capture the effect of blending on the pavement performance. A better calibration to incorporate blending parameters within the AASHTOWare Pavement ME Design method would improve the long-term performance prediction and lead to more accurate pavement designs.
- On the evidence of the findings of this study, the optimization of the use of the recycled asphalt materials (up to 40%) will allow the asphalt paving industry to adjust the production operations, enhance the quality of RAP-mixes and increase the recycling rates. The enhancement of the quality of the RAP-mixes would lead to more durable and sustainable pavements and to a larger acceptance of recycling by transportation agencies and municipalities.

## **7.2 Scientific Contribution**

The main scientific contributions of this research study are:

- The investigation of the applicability of the concepts of Arrhenius empirical relationship of diffusion in the context of asphalt recycling. The findings from this study confirm that diffusion of virgin and RAP-binders is highly influenced by time and temperature.
- Characterization of the thermo-mechanical behavior of asphalt mixes containing RAP at different blending/diffusion states.

- Development of innovative asphalt binder characterization approach using the Environmental Scanning Electron Microscopy. Moreover, a MATLAB code was developed to accurately measure the fibril size and efficiently detect the change in the microstructure of the binder with the change in the conditioning time and temperature.
- Unveil correlations between time-temperature effects and mixture performance.
- Recommendations for a better use of RAP in pavement industry.

### **7.3 Future Research Opportunities**

Based on research work obtained from this thesis, the followings are potential areas for future research that would be beneficial to the better use of RAP-HMA:

- The obtained results of the RAP-HMA testing are promising and suggest that higher storage time for the given mixes and silo conditions could potentially improve the blending of RAP and virgin binders, which positively affect the performance of the mixes. Yet, it should be noted that aging can be the dominant process at different silo-storage conditions. Therefore, the insights provided by this study can be expanded to incorporation of other recycled materials with stiffer asphalt such as post-manufacturer asphalt shingle waste or post-consumer asphalt shingles waste.
- The increased use of recycled materials in asphalt mixes, without having negative impact of the behaviour of those mixes, will significantly reduce the cost of these mixes. However, conducting Life-Cycle Cost Analysis (LCCA) of the use of 12-hour silo-storage mixes would be advantageous to draw a solid conclusion on the estimation of the economic impact of the 12 hours RAP-HMA.
- The preservation of non-renewable raw materials such as high quality aggregates and asphalt binder is a very important environmental benefit. However, keeping the mixes for 12-hour in the silo-storage could associate with some environmental impact. Hence, Environmental Impact Assessment (EIA) can be conducted to analyse the effect of the 12-hour silo-storage mixes on the global CO<sub>2</sub> emissions of the asphalt industry.
- The incorporation of the percentage of the RAP content and the silo-storage conditions within the AASHTOWare Pavement ME Design method would significantly enhance the performance prediction of this method.

- As the ESEM samples exhibited higher oxidation during conditioning as compared with the recovered binders from the silo mixes, preparing and thermally conditioning ESEM samples under oxygen-free environment would significantly minimize binder aging.

## Publications

- **Kadhim, H.**, Mikhailenko, P., Baaj, H., and Tighe, S. “The Effect of the Silo-Storage on the Rheological Behavior of a Surface Course Asphalt Mix Containing Reclaimed Asphalt Pavement (RAP), *In Proceedings of Candian Society for Civil Engineering (CSCE)*: Vancouver, BC, (2017).
- Mikhailenko, P., **Kadhim, H.**, Baaj, H., and Tighe, S. "Observation of asphalt binder microstructure with ESEM." *Journal of microscopy* 267, no. 3 (2017): 347-355.
- Mikhailenko P, **Kadhim H.**, Baaj, H. Observation of bitumen microstructure oxidation and blending with ESEM. *Road Materials and Pavement Design*. (2017): 216-25.
- **Kadhim, H.**, and Baaj, H. "Evaluation of the Impact of Silo-Storage on Thermal Cracking of the Hot Mix Asphalt with RAP." *TAC 2018: Innovation and Technology: Evolving Transportation-2018 Conference and Exhibition of the Transportation Association of Canada* (2018).
- **Kadhim, H.**, Baaj. H., and Pirzadeh, P. "Evaluating Permanent Deformation in Asphalt Mixes Containing Reclaimed Asphalt Pavement by Considering the Effect of Silo-Storage Time" *the 13th ISAP Conference on Asphalt Pavements*. Fortaleza, Ceará, Brazil (2018).
- **Kadhim, H.**, and Baaj, H. “Evaluating the Performance of the Asphalt Mixes Containing Reclaimed Asphalt Pavement by Considering the Effect of Silo-Storage Time” Submitted to *the Journal of Testing and Evaluation (JTE)*. (2019).
- Pirzadeh, P., **Kadhim, H.**, Grant, D.L., Webb, J. D., Baaj, H., Kriz, P., “Impact of Hot Mix Asphalt Plant Silo-Storage Conditions on Blending and Diffusion between Virgin and RAP Binders” submitted to *Road Materials and Pavement Design* . (2019).

## References

AASHTO, S.T., 2007. Standard method of test for determining the fatigue life of compacted hot-mix asphalt (HMA) subjected to repeated flexural bending. *T321-03*.

Aifantis, E.C., 1987. The physics of plastic deformation. *International Journal of Plasticity*, 3(3), pp.211-247.

Airey, G.D., Rahimzadeh, B. and Collop, A.C., 2003. Viscoelastic linearity limits for bituminous materials. *Materials and Structures*, 36(10), pp.643-647.

Alavi, M.Z., He, Y., Harvey, J. and Jones, D., 2015. *Evaluation of the combined effects of Reclaimed Asphalt Pavement (RAP)* (No. CA16-2827A).

Al-Qadi, I.L., Elseifi, M. and Carpenter, S.H., 2007. *Reclaimed asphalt pavement—a literature review*.

Ambaiowei, D., 2014. Innovative Evaluation of Crumb Rubber Asphalt and Recycled Asphalt Pavement.

Aquilanti, V., Mundim, K.C., Elango, M., Kleijn, S. and Kasai, T., 2010. Temperature dependence of chemical and biophysical rate processes: Phenomenological approach to deviations from Arrhenius law. *Chemical Physics Letters*, 498(1-3), pp.209-213.

Applied Research Associate, 2011. Methodology for the Development of Equivalent Pavement Structural Design Matrix for Municipal Roadways: Including Maintenance and Rehabilitation Schedules and Life Cycle Cost Analysis.

Baaj, H., Di Benedetto, H. and Chaverot, P., 2005. Effect of binder characteristics on fatigue of asphalt pavement using an intrinsic damage approach. *Road Materials and Pavement Design*, 6(2), pp.147-174.

Baaj, H., Di Benedetto, H. and Chaverot, P., 2004. Different experimental approaches and criteria for fatigue of asphalt mixes. In *Proceedings of the Forty-Ninth Annual Conference of the Canadian Technical Asphalt Association (CTAA)-Montreal, Quebec*.

Baaj, H., Ech, M., Tapsoba, N., Sauzeat, C. and Di Benedetto, H., 2013. Thermomechanical characterization of asphalt mixtures modified with high contents of asphalt shingle modifier (ASM®) and reclaimed asphalt pavement (RAP). *Materials and structures*, 46(10), pp.1747-1763.

Benedetto, H.D., Delaporte, B. and Sauzéat, C., 2007. Three-dimensional linear behavior of bituminous materials: experiments and modeling. *International Journal of Geomechanics*, 7(2), pp.149-157.

Boysen, R.B. and Schabron, J.F., 2013. The automated asphaltene determinator coupled with saturates, aromatics, and resins separation for petroleum residua characterization. *Energy & Fuels*, 27(8), pp.4654-4661.

Bowers, B.F., 2013. Investigation of asphalt pavement mixture blending utilizing analytical chemistry techniques.

Bressi, S., Dumont, A.G., Carter, A. and Bueche, N., 2015, June. A multiple regression model for developing a RAP binder blending chart for stiffness prediction. In *6th International Conference Bituminous Mixtures and Pavements, Thessaloniki (Greece)*.

Callister, W.D. and Rethwisch, D.G., 2007. *Materials science and engineering: an introduction* (Vol. 7, pp. 665-715). New York: John Wiley & Sons.

Carpenter, S.H. and Wolosick, J.R., 1980. Modifier influence in the characterization of hot-mix recycled material. *Transportation research record*, (777).

Chawla, K.K. and Meyers, M.A., 1999. *Mechanical behavior of materials* (Vol. 627). Upper Saddle River, NJ, USA: Prentice Hall.

Chadbourn, B.A., Skok Jr, E.L., Newcomb, D.E., Crow, B.L. and Spindle, S., 1999. The effect of voids in mineral aggregate (VMA) on hot-mix asphalt pavements.

Chen, J.S., Wang, C.H. and Huang, C.C., 2009. Engineering properties of bituminous mixtures blended with second reclaimed asphalt pavements (R2AP). *Road Materials and Pavement Design*, 10(sup1), pp.129-149.

Chen, Y., 2009. *Viscoelastic modeling of flexible pavement* (Doctoral dissertation, University of Akron).

Christensen Jr, D.W., Pellinen, T. and Bonaquist, R.F., 2003. Hirsch model for estimating the modulus of asphalt concrete. *Journal of the Association of Asphalt Paving Technologists*, 72.



Copeland, A., 2011. *Reclaimed asphalt pavement in asphalt mixtures: State of the practice* (No. FHWA-HRT-11-021).

Crank, J., 1979. *The mathematics of diffusion*. Oxford university press.

Cussler, E.L., 2009. *Diffusion: mass transfer in fluid systems*. Cambridge university press.

Li, J., Pierce, L. and Uhlmeier, J., 2009. Calibration of flexible pavement in mechanistic-empirical pavement design guide for Washington State. *Transportation Research Record: Journal of the Transportation Research Board*, (2095), pp.73-83.

Dougan, C.E., Stephens, J.E., Mahoney, J. and Hansen, G., 2003. *E\*-dynamic modulus: test protocol-problems and solutions* (No. CT-SPR-0003084-F-03-3,).

Ektas, S. and Karacasu, M., 2012. Use of Recycled Concrete in Hot Mix Asphalt and an ANN model for Prediction of Resilient Modulus. *Ekoloji Dergisi*, 21(83).

El Béze, L., Rose, J., Mouillet, V., Farcas, F., Masion, A., Chaurand, P. and Bottero, J.Y., 2012. Location and evolution of the speciation of vanadium in bitumen and model of reclaimed bituminous mixes during ageing: Can vanadium serve as a tracer of the aged and fresh parts of the reclaimed asphalt pavement mixture?. *Fuel*, 102, pp.423-430.

Emery, J.J., 1993. Asphalt concrete recycling in Canada. *Transportation Research Record*, (1427).

EN, 2012. Bituminous mixtures - Test methods for hot mix asphalt - Part 24: Resistance to fatigue (No. 12697-24).

Fick, A., 1855. V. On liquid diffusion. *The London, Edinburgh, and Dublin Philosophical Magazine and Journal of Science*, 10(63), pp.30-39.

Fontes, L.P., Triches, G., Pais, J.C. and Pereira, P.A., 2010. Evaluating permanent deformation in asphalt rubber mixtures. *Construction and Building Materials*, 24(7), pp.1193-1200.

Gaitan, L., 2012. Evaluation of the degree of blending of reclaimed asphalt pavement (RAP) binder for warm mix asphalt.

Stroup-Gardiner, M. and Wagner, C., 1999. Use of reclaimed asphalt pavement in Superpave hot-mix asphalt applications. *Transportation research record: journal of the transportation research board*, (1681), pp.1-9.

Haas, R., Tighe, S., Dore, G. and Hein, D., 2007, October. Mechanistic-empirical pavement design: Evolution and future challenges. In *Annual Conference and Exhibition of the Transportation Association of Canada, Saskatoon, SK*.

Hajj, E.Y., Sebaaly, P.E., Alavi, M.Z. and Morian, N.E., 2015. Evaluation of Thermal Cracking Resistance of Asphalt Mixtures.

Hofko, B., Porot, L., Cannone, A.F., Poulidakos, L., Huber, L., Lu, X., Mollenhauer, K. and Grothe, H., 2018. FTIR spectral analysis of bituminous binders: reproducibility and impact of ageing temperature. *Materials and Structures*, 51(2), p.45.

Huang, B., Li, G., Vukosavljevic, D., Shu, X. and Egan, B.K., 2005. Laboratory investigation of mixing hot-mix asphalt with reclaimed asphalt pavement. *Transportation Research Record*, 1929(1), pp.37-45.

Huang, B., Zhang, Z., Kingery, W. and Zuo, G., 2004, May. Fatigue crack characteristics of HMA mixtures containing RAP. In *Proceeding 5th Int. Conf. on Cracking in Pavements, RILEM* (pp. 631-638).

Huang, Y.H., 1993. *Pavement analysis and design*.

Lighting, H., 2002. Bureau of design and environment manual. *December*, 56(2), p.56.

Izzo, R.P. and Tahmoressi, M., 1999. Use of the Hamburg wheel-tracking device for evaluating moisture susceptibility of hot-mix asphalt. *Transportation Research Record*, 1681(1), pp.76-85.

Jacques, C., Daniel, J.S., Bennert, T., Reinke, G., Norouzi, A., Ericson, C., Mogawer, W. and Kim, Y.R., 2016. Effect of Silo Storage Time on the Characteristics of Virgin and Reclaimed Asphalt Pavement Mixtures. *Transportation Research Record: Journal of the Transportation Research Board*, (2573), pp.76-85.

Cooley, L.A., Kandhal, P.S., Buchanan, M.S., Fee, F. and Epps, A., 2000. *Loaded wheel testers in the United States: State of the practice*. Transportation Research Board, National Research Council.

Jung, D.H. and Vinson, T.S., 1994. *Low-temperature cracking: test selection* (No. SHRP-A-400).

Kandhal, P.S. and Wenger, M.E., 1973. Storage of bituminous concrete in inert gas. *Highway Research Record*, (468).

Kandhal, P.S. and Cooley, L.A., 2002. Evaluation of permanent deformation of asphalt mixtures using loaded wheel tester. *Asphalt Paving Technology*, 71, pp.739-753.

Kandhal, P.S. and Foo, K.Y., 1997. Designing recycled hot mix asphalt mixtures using Superpave technology. In *Progress of Superpave (Superior Performing Asphalt Pavement): Evaluation and Implementation*. ASTM International.

Kandhal, P.S. and Mallick, R.B., 1998. *Pavement Recycling Guidelines for State and Local Governments: Participant's Reference Book* (No. FHWA-SA-98-042).

Kapoor, A., 1994. A re-evaluation of the life to rupture of ductile metals by cyclic plastic strain. *Fatigue & fracture of engineering materials & structures*, 17(2), pp.201-219.

Karlsson, R. and Isacson, U., 2003. Application of FTIR-ATR to characterization of bitumen rejuvenator diffusion. *Journal of Materials in Civil Engineering*, 15(2), pp.157-165.

Karlsson, R., Isacson, U. and Ekblad, J., 2007. Rheological characterisation of bitumen diffusion. *Journal of materials science*, 42(1), pp.101-108.

Kennedy, T.W. and Huber, G.A., 1984. *The Effect of Mixing Temperature and Stockpile Moisture on Asphalt Mixtures* (No. FHWA/TX-85/49+ 358-1). The Center.

Kingery, W.R., 2004. Laboratory study of fatigue characteristics of HMA surface mixtures containing recycled asphalt pavement (RAP).

Kriz, P., Grant, D.L., Gale, M., Lavorato, S. and Pahalan, A., 2014. Reclaimed Asphalt Pavement-Virgin Binder Diffusion in Asphalt Mixes. In *Proceedings of the Fifty-Ninth Annual Conference of the Canadian Technical Asphalt Association (CTAA): Winnipeg, Manitoba*.

Kriz, P., Grant, D.L., Veloza, B.A., Gale, M.J., Blahey, A.G., Brownie, J.H., Shirts, R.D. and Maccarrone, S., 2014. Blending and diffusion of reclaimed asphalt pavement and virgin asphalt binders. *Road Materials and Pavement Design*, 15(sup1), pp.78-112.

Landau, L., Lipshitz, E., 1959. *Theory of Elasticity*.

Le Guern, M., Chailleux, E., Farcas, F., Dreessen, S. and Mabilie, I., 2010. Physico-chemical analysis of five hard bitumens: Identification of chemical species and molecular organization before and after artificial aging. *Fuel*, 89(11), pp.3330-3339.

Lee, S.J., Amirkhanian, S.N. and Kim, K.W., 2009. Laboratory evaluation of the effects of short-term oven aging on asphalt binders in asphalt mixtures using HP-GPC. *Construction and Building Materials*, 23(9), pp.3087-3093.

Liphardt, A., Radziszewski, P. and Król, J., 2015. Binder blending estimation method in hot mix asphalt with reclaimed asphalt. *Procedia Engineering*, 111, pp.502-509.

Loulizi, A., Flintsch, G.W., Al-Qadi, I.L. and Mokarem, D., 2006. Comparing resilient modulus and dynamic modulus of hot-mix asphalt as material properties for flexible pavement design. *Transportation Research Record*, 1970(1), pp.161-170.

Lu, X. and Isacsson, U., 2002. Effect of ageing on bitumen chemistry and rheology. *Construction and Building materials*, 16(1), pp.15-22.

Marasteanu, M., Zofka, A., Turos, M., Li, X., Velasquez, R., Li, X., Buttlar, W., Paulino, G., Braham, A., Dave, E. and Ojo, J., 2007. Investigation of low temperature cracking in asphalt pavements national pooled fund study 776.

McDaniel, R.S. and Anderson, R.M., 2001. *Recommended use of reclaimed asphalt pavement in the Superpave mix design method: technician's manual* (No. Project D9-12 FY'97). National Research Council (US). Transportation Research Board.

McGennis, R.B., Anderson, R.M., Kennedy, T.W. and Solaimanian, M., 1994. *Background of Superpave Asphalt Mixture Design & Analysis. Final Report* (No. FHWA-SA-95-003).

McLeod, N.W., 1956. Flexible pavement thickness requirements. *Association of Asphalt Paving Technologists*.

Mengel, W.F., Mengel and William F., 1996. *Container transportation system*. U.S. Patent 5,580,211.

Michon, L.C., Williams, T.M., Miknis, F.P., Planche, J.P. and Martin, D., 1998. Use of the environmental scanning electron microscope to investigate three polymer modified asphalts. *Petroleum science and technology*, 16(7-8), pp.797-809.

Middleton, S.C., Goodknight, J.C. and Eaton, J.S., 1967, February. The Effects of Hot Storage on an Asphaltic Concrete Mix. In *Assoc Asphalt Paving Technol Proc.*

Mikhailenko, P., 2015. *Valorization of by-products and products from agro-industry for the development of release and rejuvenating agents for bituminous materials* (Doctoral dissertation, Université Paul Sabatier-Toulouse III).

Mikhailenko, P., Kadhim, H., Baaj, H. and Tighe, S., 2017. Observation of asphalt binder microstructure with ESEM. *Journal of microscopy*, 267(3), pp.347-355.

Milani, M., Drobne, D. and Tatti, F., 2007. How to study biological samples by FIB/SEM. *Modern Research and Educational Topics in Microscopy*, pp.787-794.

Mogawer, W.S., Austerman, A.J., Pauli, T., Salmans, S. and Planche, J.P., 2016. *Determination of the Binder Grade and Performance of High Percentage RAP-HMA Mixes* (No. SPR11-15-57946). Massachusetts. Dept. of Transportation. Office of Transportation Planning.

Mogawer, W.S., Booshehrian, A., Vahidi, S. and Austerman, A.J., 2013. Evaluating the effect of rejuvenators on the degree of blending and performance of high RAP, RAS, and RAP/RAS mixtures. *Road Materials and Pavement Design*, 14(sup2), pp.193-213.

Moghaddam, T.B. and Baaj, H., 2016. The use of rejuvenating agents in production of recycled hot mix asphalt: A systematic review. *Construction and Building Materials*, 114, pp.805-816.

Mohajeri, M., Molenaar, A.A.A. and Van de Ven, M.F.C., 2014. Experimental study into the fundamental understanding of blending between reclaimed asphalt binder and virgin bitumen using nanoindentation and nano-computed tomography. *Road Materials and Pavement Design*, 15(2), pp.372-384.

Mohammadi, H. and McCulloch, C.A., 2014. Impact of elastic and inelastic substrate behaviors on mechanosensation. *Soft Matter*, 10(3), pp.408-420.

Montgomery, D.C., Runger, G.C. and Hubele, N.F., 2009. *Engineering statistics*. John Wiley & Sons.

Nahar, S.N., Mohajeri, M., Schmets, A.J.M., Scarpas, A., Van de Ven, M.F.C. and Schitter, G., 2013. First observation of blending-zone morphology at interface of reclaimed asphalt binder and virgin bitumen. *Transportation Research Record*, 2370(1), pp.1-9.

NAPA, 2001. HMA Pavement Mix Type Selection Guide.

NRC, 2011. Canadian Crude Oil, Natural Gas and Petroleum Products. URL <http://www.nrcan.gc.ca/sites/www.nrcan.gc.ca/files/energy/pdf/eneene/sources/crubru/revrev/pdf/revrev-09-eng.pdf>

Navaro, J., Bruneau, D., Drouadaine, I., Colin, J., Dony, A. and Cournet, J., 2012. Observation and evaluation of the degree of blending of reclaimed asphalt concretes using microscopy image analysis. *Construction and Building Materials*, 37, pp.135-143.

OHMPA, 2018. MTO AC Price Index [WWW Document]. Ontario Hot Mix Producers Association. URL <http://www.ohmpa.org/mtopriceindex/> (accessed 3.22.16).

OHMPA, 2012. OHMPA Asphalt Fact Sheet - Why asphalt is the better way to pave.

OHMPA, 2007. The ABCs of Asphalt Pavement Recycling.

OHMPA, 1999. The ABCs of PGAC: The Use of Performance Graded Asphalt Cements in Ontario.

Oliver, J.W., 2001. The influence of the binder in RAP on recycled asphalt properties. *Road Materials and Pavement Design*, 2(3), pp.311-325.

Pavement Interactive, 2010. HMA Pavement. URL <http://www.pavementinteractive.org/article/hma-pavement/> (accessed 3.28.16)

Petersen, J.C., 2009. A review of the fundamentals of asphalt oxidation: chemical, physicochemical, physical property, and durability relationships. *Transportation Research Circular*, (E-C140).

Pirzadeh, P., Kadhim, H., Grant, D.L., Webb, J.D., Baaj, H., Kriz, P., 2018. Impact of Hot Mix Asphalt Plant Silo Storage Conditions on Blending and Diffusion between Virgin and RAP Binders. Submitted to *The Association of Asphalt Paving Technologists (AAPT)*.

Poulikakos, L.D. and Partl, M.N., 2010. Investigation of porous asphalt microstructure using optical and electron microscopy. *Journal of microscopy*, 240(2), pp.145-154.

Poulikakos, L.D., dos Santos, S., Bueno, M., Kuentzel, S., Hugener, M. and Partl, M.N., 2014. Influence of short and long term aging on chemical, microstructural and macro-mechanical properties of recycled asphalt mixtures. *Construction and Building Materials*, 51, pp.414-423.

Pratheepan, K., 2008. *Use of reclaimed asphalt pavements (RAP) in airfield HMA pavements*. University of Nevada, Reno.

Rad, F.Y., Sefidmazgi, N.R. and Bahia, H., 2014. Application of diffusion mechanism: Degree of blending between fresh and recycled asphalt pavement binder in dynamic shear rheometer. *Transportation Research Record*, 2444(1), pp.71-77.

Rahman, A. and Tarefder, R.A., 2014. Effect of Binder Performance Grade on the Dynamic Modulus Mastercurves of SP III Superpave Mixes in New Mexico. In *Advanced Characterization of Asphalt and Concrete Materials* (pp. 9-16).

Rinaldini, E., Schuetz, P., Partl, M.N., Tebaldi, G. and Poulikakos, L.D., 2014. Investigating the blending of reclaimed asphalt with virgin materials using rheology, electron microscopy and computer tomography. *Composites Part B: Engineering*, 67, pp.579-587.

Rozeveld, S.J., Shin, E.E., Bhurke, A., France, L. and Drzal, L.T., 1997. Network morphology of straight and polymer modified asphalt cements. *Microscopy research and technique*, 38(5), pp.529-543.

Sadd, M.H., 2009. *Elasticity: theory, applications, and numerics*. Academic Press.

Sanchez, X., 2014. Effect of Reclaimed Asphalt Pavement on Ontario Hot Mix Asphalt Performance.

Sayers, M.W., 1998. The little book of profiling: basic information about measuring and interpreting road profiles.

Seo, Y., El-Haggan, O., King, M., Joon Lee, S. and Richard Kim, Y., 2007. Air void models for the dynamic modulus, fatigue cracking, and rutting of asphalt concrete. *Journal of Materials in Civil Engineering*, 19(10), pp.874-883.

Shirodkar, P., Mehta, Y., Nolan, A., Sonpal, K., Norton, A., Tomlinson, C., Dubois, E., Sullivan, P. and Sauber, R., 2011. A study to determine the degree of partial blending of reclaimed asphalt pavement (RAP) binder for high RAP hot mix asphalt. *Construction and Building Materials*, 25(1), pp.150-155.

Ziari, H., Sobhani, J., Ayoubinejad, J. and Hartmann, T., 2016. Prediction of IRI in short and long terms for flexible pavements: ANN and GMDH methods. *International Journal of Pavement Engineering*, 17(9), pp.776-788.

Stangl, K., Jäger, A. and Lackner, R., 2006. Microstructure-based identification of bitumen performance. *Road Materials and Pavement Design*, 7(sup1), pp.111-142.

Stephens, J.E., Mahoney, J. and Dippold, C., 2001. *Determination of the PG Binder Grade to Use in a RAP Mix*(No. JHR 00-278). Connecticut. Dept. of Transportation.

Symon, K.R., 1971. *Mechanics*, 3rd edition. Wesley Publishing Company.

TAC, 2014. Canadian Guide: Default Parameters for AASHTOWare Pavement ME Design | Road Surface | Traffic. URL <https://www.scribd.com/document/304718258/Canadian-Guide-Default-Parameters-for-AASHTOWare-Pavement-ME-Design> (accessed 2.10.19)

Tapsoba, N., Sauzéat, C., Di Benedetto, H., Baaj, H. and Ech, M., 2014. Behaviour of asphalt mixtures containing reclaimed asphalt pavement and asphalt shingle. *Road Materials and Pavement Design*, 15(2), pp.330-347.

Tapsoba, N., Sauzéat, C., Di Benedetto, H., Baaj, H. and Ech, M., 2015. Three-dimensional analysis of fatigue tests on bituminous mixtures. *Fatigue & Fracture of Engineering Materials & Structures*, 38(6), pp.730-741.

TDT, 2011. *Pavement Design Guide*. Texas Department of Transportation

Tuttle, L., 1966. Investigation of the Effects of Holding Hot Bituminous Mixtures in Storage Hoppers for Short and Extended Periods of Time. *Canadian Technical Asphalt Association, Proceeding*.

Vukosavljevic, D., 2006. Fatigue characteristics of field HMA surface mixtures containing recycled asphalt pavement (RAP).

Walker, D., 2011. Refining Superpave asphalt binder characterization. *Asphalt*, 26(2).

West, R.C. and Willis, J.R., 2014. *Case Studies on Successful Utilization of Reclaimed Asphalt Pavement and Recycled Asphalt Shingles in Asphalt Pavements* (No. NCAT Report 14-06).

Yang, J., Ddamba, S., UL-Islam, R., Safiuddin, M. and Tighe, S.L., 2013. Investigation on use of recycled asphalt shingles in Ontario hot mix asphalt: a Canadian case study. *Canadian Journal of Civil Engineering*, 41(2), pp.136-143.



Yousefi Rad, F., 2013. *Estimating blending level of fresh and RAP binders in recycled hot mix asphalt* (Doctoral dissertation).

Zhao, S., Nahar, S.N., Schmets, A.J., Huang, B., Shu, X. and Scarpas, T., 2015. Investigation on the microstructure of recycled asphalt shingle binder and its blending with virgin bitumen. *Road Materials and Pavement Design*, 16(sup1), pp.21-38.

Zhu, H., Sun, L., Yang, J., Chen, Z. and Gu, W., 2011. Developing master curves and predicting dynamic modulus of polymer-modified asphalt mixtures. *Journal of Materials in Civil Engineering*, 23(2), pp.131-137.

## Appendix (A) – HMA Test Results

### Average Dynamic Modulus Test Results: 1HL-3

Temp.	Time-Intervals	Freq.	Dynamic Modulus (MPa)	Temp.	Dynamic Modulus (MPa)	Temp.	Dynamic Modulus (MPa)	Temp.	Dynamic Modulus (MPa)	Temp.	Dynamic Modulus (MPa)
-10.00	0.00	25.00	21839.37	4.00	13537.31	21.00	6914.85	37.00	2843.43	54.00	869.95
		10.00	17082.65		11956.16		6550.81		2279.21		724.20
		5.00	16150.00		10779.90		5594.77		1870.89		613.41
		1.00	13594.19		8051.43		3800.10		1280.02		436.32
		0.50	12334.82		7183.36		3511.16		1197.82		390.52
		0.10	9930.84		5204.90		2646.18		793.02		324.13
Temp.	Time-Intervals	Freq.	Dynamic Modulus (MPa)	Temp.	Dynamic Modulus (MPa)	Temp.	Dynamic Modulus (MPa)	Temp.	Dynamic Modulus (MPa)	Temp.	Dynamic Modulus (MPa)
-10.00	1.00	25.00	24606.08	4.00	14923.31	21.00	6881.25	37.00	2499.99	54.00	832.99
		10.00	19629.77		12627.87		6435.14		2206.92		656.92
		5.00	18050.48		10977.49		5505.29		1806.07		567.07
		1.00	16248.24		7995.94		3586.03		1255.67		389.67
		0.50	13542.21		6843.33		3166.16		1177.35		342.35
		0.10	10849.59		4959.84		2361.52		895.84		285.84
Temp.	Time-Intervals	Freq.	Dynamic Modulus (MPa)	Temp.	Dynamic Modulus (MPa)	Temp.	Dynamic Modulus (MPa)	Temp.	Dynamic Modulus (MPa)	Temp.	Dynamic Modulus (MPa)
-10.00	4.00	25.00	24606.08	4.00	13923.31	21.00	6937.11	37.00	2885.92	54.00	857.67
		10.00	19629.77		11627.87		6563.62		2277.47		720.69
		5.00	18050.48		10177.49		5661.02		1899.60		601.01
		1.00	16248.24		7595.94		3841.57		1188.14		406.16
		0.50	14542.21		6643.33		3528.98		1097.51		346.36
		0.10	11949.59		4859.84		2493.26		719.88		286.36
Temp.	Time-Intervals	Freq.	Dynamic Modulus (MPa)	Temp.	Dynamic Modulus (MPa)	Temp.	Dynamic Modulus (MPa)	Temp.	Dynamic Modulus (MPa)	Temp.	Dynamic Modulus (MPa)
-10.00	8.00	25.00	25824.81	4.00	12923.31	21.00	5237.11	37.00	2335.92	54.00	707.67
		10.00	19846.10		11627.87		4963.62		1877.47		550.69
		5.00	18631.98		10177.49		4161.02		1359.60		441.01
		1.00	15897.04		7295.94		2741.57		928.14		306.16
		0.50	14971.21		6443.33		2528.98		807.51		216.36
		0.10	11658.93		4559.84		1893.26		519.88		166.36

Temp.	Time-Intervals	Freq.	Dynamic Modulus (MPa)	Temp.	Dynamic Modulus (MPa)	Temp.	Dynamic Modulus (MPa)	Temp.	Dynamic Modulus (MPa)	Temp.	Dynamic Modulus (MPa)
-10.00	12.00	25.00	25750.82	4.00	12804.25	21.00	5211.59	37.00	2319.22	54.00	697.67
		10.00	19449.30		11341.10		4915.73		1812.79		528.69
		5.00	18143.85		9879.24		4105.16		1303.57		399.91
		1.00	15381.99		7126.65		2660.66		890.03		277.16
		0.50	14482.39		6190.07		2447.82		778.49		196.36
		0.10	11272.55		4365.00		1815.86		503.80		149.36

### Average Dynamic Modulus Test Results: 1HL-8

Temp.	Time-Intervals	Freq.	Dynamic Modulus (MPa)	Temp.	Dynamic Modulus (MPa)	Temp.	Dynamic Modulus (MPa)	Temp.	Dynamic Modulus (MPa)	Temp.	Dynamic Modulus (MPa)
-10.00	0hrs	25.00	23020.62	4.00	15777.54	21.00	7022.78	37.00	3009.92	54.00	1198.84
		10.00	21488.84		14017.85		6871.68		2623.36		973.02
		5.00	20457.93		12975.39		5849.32		2167.03		788.74
		1.00	18025.72		9402.99		3956.80		1457.99		566.27
		0.50	17053.69		8537.48		3591.05		1369.30		527.72
		0.10	13270.36		6263.10		2745.82		1134.44		422.43
Temp.	Time-Intervals	Freq.	Dynamic Modulus (MPa)	Temp.	Dynamic Modulus (MPa)	Temp.	Dynamic Modulus (MPa)	Temp.	Dynamic Modulus (MPa)	Temp.	Dynamic Modulus (MPa)
-10.00	1hrs	25.00	23473.89	4.00	16198.40	21.00	7607.54	37.00	3230.27	54.00	1246.62
		10.00	21468.92		14757.53		7028.87		2759.98		979.17
		5.00	20439.12		13123.58		5930.39		2238.65		773.62
		1.00	17989.23		10068.31		3978.45		1530.32		557.84
		0.50	17128.52		8829.19		3600.26		1395.03		518.72
		0.10	13239.48		6694.00		2675.49		1127.73		415.40
Temp.	Time-Intervals	Freq.	Dynamic Modulus (MPa)	Temp.	Dynamic Modulus (MPa)	Temp.	Dynamic Modulus (MPa)	Temp.	Dynamic Modulus (MPa)	Temp.	Dynamic Modulus (MPa)
-10.00	4hrs	25.00	22918.04	4.00	15610.02	21.00	6967.72	37.00	2969.09	54.00	1142.28
		10.00	20908.30		13990.85		6782.24		2608.54		929.46
		5.00	20443.03		12878.73		5801.37		2169.67		754.92
		1.00	17991.34		9391.08		3883.17		1407.75		530.17
		0.50	16813.75		8480.58		3540.56		1303.56		485.10

		0.10	13112.30		6205.39		2679.63		1019.65		392.65
Temp.	Time-Intervals	Freq.	Dynamic Modulus (MPa)	Temp.	Dynamic Modulus (MPa)	Temp.	Dynamic Modulus (MPa)	Temp.	Dynamic Modulus (MPa)	Temp.	Dynamic Modulus (MPa)
-10.00	8hrs	25.00	22897.33	4.00	15521.69	21.00	6921.19	37.00	2965.86	54.00	1177.05
		10.00	21294.68		14001.24		6636.04		2464.66		960.48
		5.00	20076.93		12782.63		5786.24		2097.95		759.37
		1.00	18306.78		9356.48		3739.50		1384.50		526.65
		0.50	16971.50		8455.66		3286.35		1288.30		486.51
		0.10	12639.47		6088.28		2448.00		992.54		364.51
Temp.	Time-Intervals	Freq.	Dynamic Modulus (MPa)	Temp.	Dynamic Modulus (MPa)	Temp.	Dynamic Modulus (MPa)	Temp.	Dynamic Modulus (MPa)	Temp.	Dynamic Modulus (MPa)
-10.00	12hrs	25.00	22185.31	4.00	14668.13	21.00	6194.90	37.00	2765.86	54.00	1121.64
		10.00	21121.32		12422.28		5778.95		1994.66		885.65
		5.00	20082.41		10903.34		5082.58		1697.95		665.30
		1.00	17636.65		8057.57		3346.41		1094.50		387.83
		0.50	16218.84		6946.49		3079.80		958.30		350.24
		0.10	12802.46		5023.06		2165.97		722.54		260.41

### Average Dynamic Modulus Test Results: 2HL-3

Temp.	Time-Intervals	Freq.	Dynamic Modulus (MPa)	Temp.	Dynamic Modulus (MPa)	Temp.	Dynamic Modulus (MPa)	Temp.	Dynamic Modulus (MPa)	Temp.	Dynamic Modulus (MPa)
-10.00	0hrs	25	24326.47515	4.00	16305.12685	21.00	7843.878833	37.00	3119.551295	54.00	1285.5054
		10	22832.48908		15046.38999		6939.705608		2480.362084		1040.3897
		5	21945.12294		13799.09337		5957.922465		2022.446734		743.44504
		1	19460.33608		11103.24976		4108.790757		1394.020451		514.64646
		0.5	18365.76669		9981.472712		3610.116391		1228.921768		455.17586
		0.1	15887.85011		8167.701335		2600.448825		973.6498453		374.20627
Temp.	Time-Intervals	Freq.	Dynamic Modulus (MPa)	Temp.	Dynamic Modulus (MPa)	Temp.	Dynamic Modulus (MPa)	Temp.	Dynamic Modulus (MPa)	Temp.	Dynamic Modulus (MPa)
-10.00	1hrs	25	24292.77989	4.00	16303.12023	21.00	7843.622338	37.00	2599.544697	54.00	1286.0705
		10	21972.19304		15041.58142		6939.518785		2658.952302		1042.2625
		5	21202.12277		13767.42873		5957.711769		1902.568721		783.34946
		1	18973.66879		11101.88593		4109.026649		1455.662137		539.58118

		0.5	18340.0277		9990.211765		3609.87854		1174.258555		495.11545
		0.1	15865.62288		8151.726689		2601.053083		863.9356123		424.15452
<b>Temp.</b>	<b>Time-Intervals</b>	<b>Freq.</b>	<b>Dynamic Modulus (MPa)</b>	<b>Temp.</b>	<b>Dynamic Modulus (MPa)</b>	<b>Temp.</b>	<b>Dynamic Modulus (MPa)</b>	<b>Temp.</b>	<b>Dynamic Modulus (MPa)</b>	<b>Temp.</b>	<b>Dynamic Modulus (MPa)</b>
-10.00	4hrs	25	22940.06961	4.00	15496.62893	21.00	7665.176776	37.00	3248.900021	54.00	1181.4996
		10	21635.72248		14063.17336		6978.835851		2714.314634		906.48615
		5	20810.70115		13087.69103		5935.596859		1933.081859		667.34678
		1	18680.61303		10637.49824		4119.339863		1082.609423		475.20394
		0.5	17586.10029		9559.259736		3704.13457		980.8027753		440.58036
		0.1	15167.65753		7533.522099		2580.796656		585.4867665		319.58602
<b>Temp.</b>	<b>Time-Intervals</b>	<b>Freq.</b>	<b>Dynamic Modulus (MPa)</b>	<b>Temp.</b>	<b>Dynamic Modulus (MPa)</b>	<b>Temp.</b>	<b>Dynamic Modulus (MPa)</b>	<b>Temp.</b>	<b>Dynamic Modulus (MPa)</b>	<b>Temp.</b>	<b>Dynamic Modulus (MPa)</b>
-10.00	8hrs	25	22128.03188	4.00	16523.56137	21.00	8397.392884	37.00	2974.459423	54.00	1177.1458
		10	21033.58384		15126.78622		7335.447239		2358.375186		752.66618
		5	20050.0506		13999.12644		6202.869446		1904.558361		704.52324
		1	17916.62888		11401.13248		4058.53779		1207.312896		472.19136
		0.5	16785.16209		8238.756308		3547.347374		862.8275663		419.1256
		0.1	14478.28039		6462.495175		2431.068989		594.7350018		312.36035
<b>Temp.</b>	<b>Time-Intervals</b>	<b>Freq.</b>	<b>Dynamic Modulus (MPa)</b>	<b>Temp.</b>	<b>Dynamic Modulus (MPa)</b>	<b>Temp.</b>	<b>Dynamic Modulus (MPa)</b>	<b>Temp.</b>	<b>Dynamic Modulus (MPa)</b>	<b>Temp.</b>	<b>Dynamic Modulus (MPa)</b>
-10.00	12hrs	25	25897.24926	4.00	16480.4072	21.00	6216.537404	37.00	3066.755917	54.00	946.83625
		10	24581.75574		16577.54517		5713.42642		1999.160029		854.26142
		5	23515.29166		15112.50676		4564.941164		1750.113988		616.39769
		1	21037.70753		10943.32699		3129.773803		1096.905318		462.2836
		0.5	20035.1463		8808.398114		2562.312703		839.0613239		348.32709
		0.1	17567.54879		4224.780942		2080.18184		480.5012191		224.88508
<b>Temp.</b>	<b>Time-Intervals</b>	<b>Freq.</b>	<b>Dynamic Modulus (MPa)</b>	<b>Temp.</b>	<b>Dynamic Modulus (MPa)</b>	<b>Temp.</b>	<b>Dynamic Modulus (MPa)</b>	<b>Temp.</b>	<b>Dynamic Modulus (MPa)</b>	<b>Temp.</b>	<b>Dynamic Modulus (MPa)</b>
-10.00	24hrs	25	26379.39309	4.00	18383.97284	21.00	8921.509215	37.00	3773.948973	54.00	1485.0234
		10	24770.24193		16424.92403		7717.944176		3211.500035		1296.3206
		5	23008.82067		15136.14422		6705.190839		2586.175713		882.9059
		1	21448.46287		12321.05851		4732.645549		1678.172759		597.09299
		0.5	19611.09442		11104.97285		4164.099985		1485.83681		522.64241
		0.1	18218.26577		8948.64333		2999.027459		1106.461688		471.35935

## Average Dynamic Modulus Test Results: 2HL-8

Temp.	Time-Intervals	Freq.	Dynamic Modulus (MPa)	Temp.	Dynamic Modulus (MPa)	Temp.	Dynamic Modulus (MPa)	Temp.	Dynamic Modulus (MPa)	Temp.	Dynamic Modulus (MPa)
-10.00	0	25	18857.29444	4.00	12602.45178	21.00	6187.0958	37.00	2799.93506	54.00	1076.5014
		10	17704.47426		11608.98252		5611.8131		2237.05698		842.82288
		5	16589.13927		10608.14217		4880.9867		1864.35969		702.74725
		1	14243.6207		8314.930285		3493.3661		1379.89558		510.05993
		0.5	13058.71462		7470.681971		3117.1087		1263.26736		468.60023
		0.1	11031.32719		5913.464623		2426.786		1039.14068		397.31693
Temp.	Time-Intervals	Freq.	Dynamic Modulus (MPa)	Temp.	Dynamic Modulus (MPa)	Temp.	Dynamic Modulus (MPa)	Temp.	Dynamic Modulus (MPa)	Temp.	Dynamic Modulus (MPa)
-10.00	1	25	18543.65747	4.00	12156.24749	21.00	7085.4885	37.00	2175.23288	54.00	860.46825
		10	17418.54255		10934.88979		6477.3836		1722.72286		653.50843
		5	16493.14575		9896.325529		5678.6192		1440.18552		531.22867
		1	14296.87323		7568.999893		4120.0766		1066.72263		382.5652
		0.5	13136.38453		6786.878938		3691.9918		990.54412		352.0019
		0.1	11352.70101		5336.61013		2881.944		817.192124		286.32218
Temp.	Time-Intervals	Freq.	Dynamic Modulus (MPa)	Temp.	Dynamic Modulus (MPa)	Temp.	Dynamic Modulus (MPa)	Temp.	Dynamic Modulus (MPa)	Temp.	Dynamic Modulus (MPa)
-10.00	4	25	17171.7584	4.00	12269.68254	21.00	7150.3417	37.00	2389.79094	54.00	966.78674
		10	17031.26189		13351.74333		6623.1723		1948.1147		915.43194
		5	16268.17759		12899.6034		5645.6803		1523.75227		706.76422
		1	14193.66859		8912.17707		3969.4365		1034.38037		300.00322
		0.5	13753.20782		7822.366203		3584.2723		920.246501		372.19453
		0.1	11852.35386		5781.654841		2615.7682		752.817625		265.64454
Temp.	Time-Intervals	Freq.	Dynamic Modulus (MPa)	Temp.	Dynamic Modulus (MPa)	Temp.	Dynamic Modulus (MPa)	Temp.	Dynamic Modulus (MPa)	Temp.	Dynamic Modulus (MPa)
-10.00	8	25	17545.88654	4.00	12266.28799	21.00	7113.4726	37.00	2165.83002	54.00	851.72138
		10	17000.55325		10881.86574		6422.7636		1711.16775		638.87469
		5	16323.3875		9916.878677		5673.1076		1411.87483		520.67158
		1	14298.47982		7530.176879		4132.2687		1072.86328		376.55466
		0.5	12981.73284		6685.06544		3633.6724		988.734748		333.88755
		0.1	11322.8735		5293.724829		2877.6662		812.453874		277.84566
Temp.	Time-Intervals	Freq.	Dynamic Modulus (MPa)	Temp.	Dynamic Modulus (MPa)	Temp.	Dynamic Modulus (MPa)	Temp.	Dynamic Modulus (MPa)	Temp.	Dynamic Modulus (MPa)

-10	12.00	25	20085.30605	4.00	14645.46072	21.00	5694.9006	37.00	2005.85526	54.00	365.76763
		10	18721.32486		13306.94063		5278.9544		1494.66097		309.76287
		5	15082.40874		12255.65535		4582.58		1197.9487		257.32599
		1	15636.64779		9897.575544		2846.4078		594.498859		209.87642
		0.5	13218.8398		8894.426801		2579.7962		458.299368		174.76347
		0.1	9802.464443		7415.445565		1665.9661		422.787677		119.76283
<b>Temp.</b>	<b>Time-Intervals</b>	<b>Freq.</b>	<b>Dynamic Modulus (MPa)</b>	<b>Temp.</b>	<b>Dynamic Modulus (MPa)</b>	<b>Temp.</b>	<b>Dynamic Modulus (MPa)</b>	<b>Temp.</b>	<b>Dynamic Modulus (MPa)</b>	<b>Temp.</b>	<b>Dynamic Modulus (MPa)</b>
-10	24.00	25	21934.49869	4.00	13437.07131	21.00	6684.7387	37.00	3210.49827	54.00	1238.0866
		10	20379.98542		12147.75241		5973.3648		2526.61042		1100.3513
		5	19268.8124		11283.50058		5308.8594		2115.74738		838.27482
		1	16725.39378		9009.99789		3871.7381		1509.2278		541.4388
		0.5	15452.41724		8121.451389		3469.0988		1358.19348		481.90579
		0.1	13255.38343		6706.548601		2708.1979		1085.81882		381.63007

### TSRST Results:

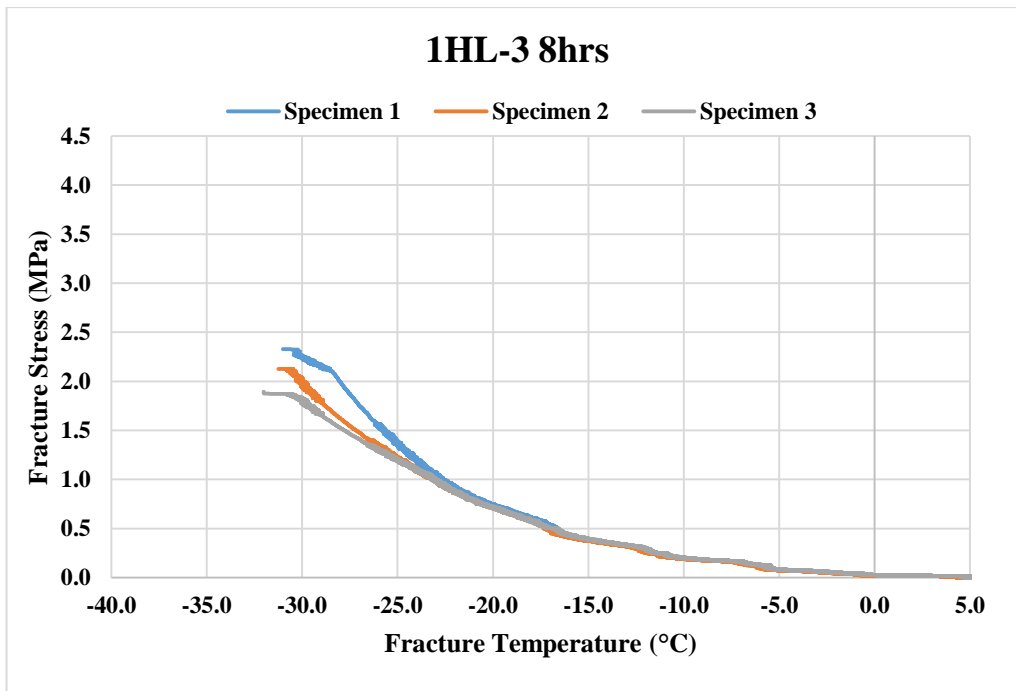
Mix type	Silo Time	Fracture Temperature (°C)			Fracture Stress (MPa)		
		Temperature	Average	S.D	Stress	Average	S.D
1HL-3	0hrs	-32.11	-31.09	1.38	2.78	2.04	0.76
		-29.52			1.26		
		-31.63			2.09		
	8hrs	-31.23	-31.42	0.53	2.12	2.11	0.22
		-32.01			1.89		
		-31.01			2.33		
	12hrs	-33.99	-34.93	0.92	1.89	1.66	0.55
		-34.98			2.06		
		-35.82			1.04		
1HL-8	0	-30.94	-31.65	0.61	2.69	2.81	0.16
		-31.98			2.75		
		-32.02			2.99		

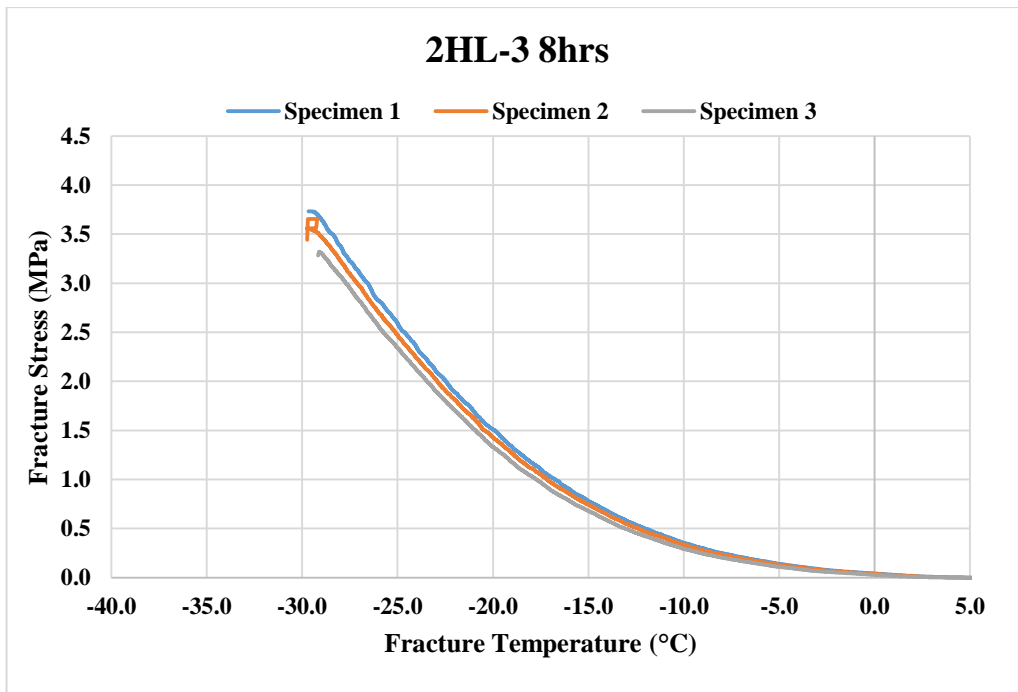
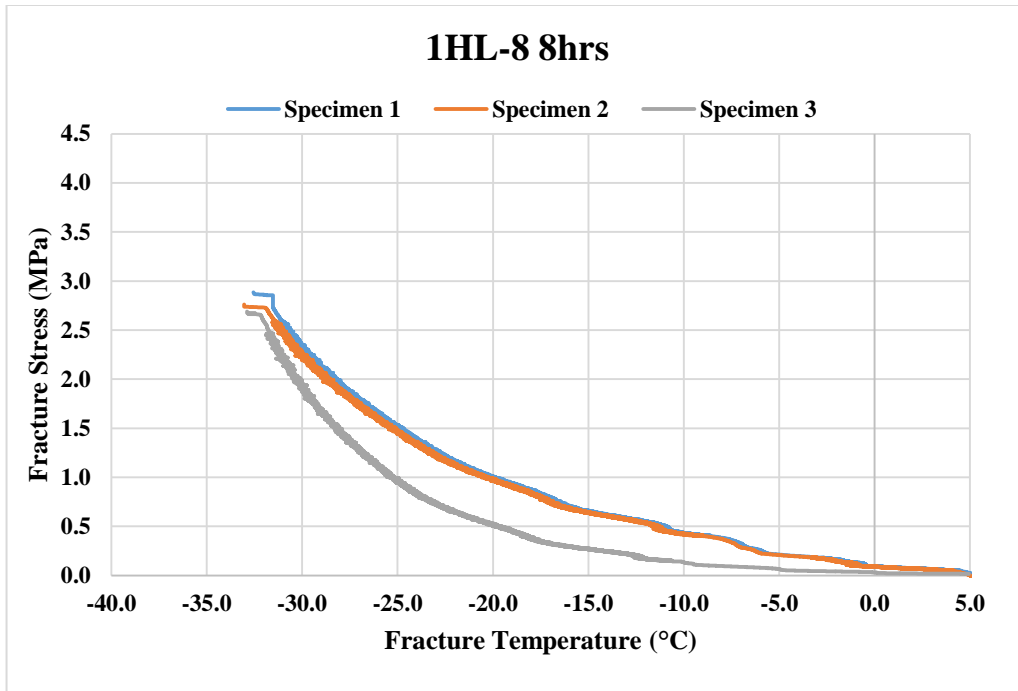
	8	-33.04	-32.82	0.25	2.76	2.78	0.10
		-32.55			2.88		
		-32.88			2.69		
	12	-35.15	-34.98	0.17	2.36	2.15	0.19
		-34.82			2.03		
		-34.97			2.05		

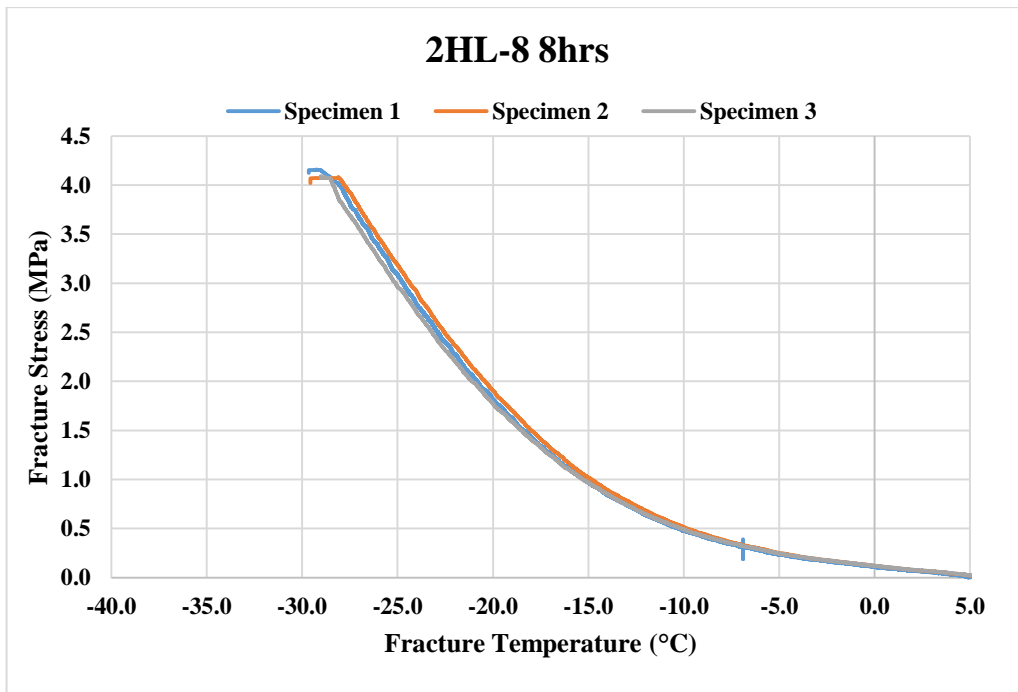
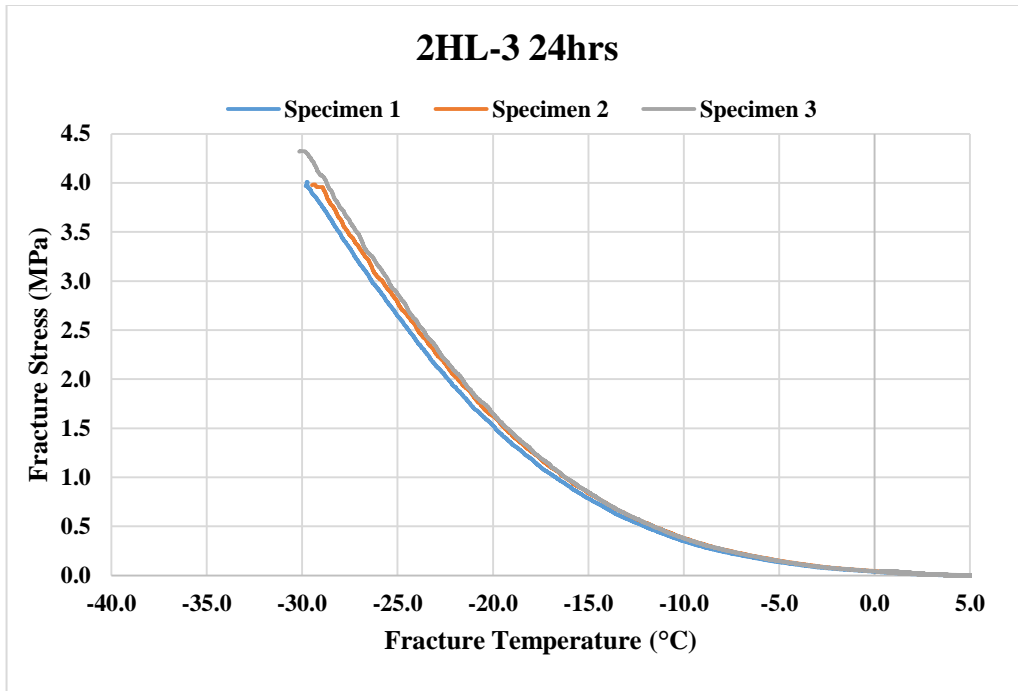
Mix type	Silo Time	Fracture Temperature (°C)			Fracture Stress (MPa)		
		Temperature	Average	S.D	Stress	Average	S.D
2HL-3	0	28.03	28.04	0.27	3.40	3.36	0.36
		28.32			2.99		
		27.78			3.70		
	8	29.11	29.49	0.33	3.30	3.53	0.21
		29.70			3.60		
		29.66			3.70		
	12	35.77	35.48	0.34	2.90	2.76	0.32
		35.11			2.40		
		35.56			2.99		
	24	30.11	29.75	0.35	4.33	4.11	0.19
		29.73			4.01		
		29.41			3.98		
2HL-8	0	28.22	28.25	0.09	3.72	3.62	0.26
		28.35			3.33		
		28.18			3.81		
	8	29.03	29.34	0.31	4.10	4.11	0.04
		29.33			4.07		
		29.65			4.15		

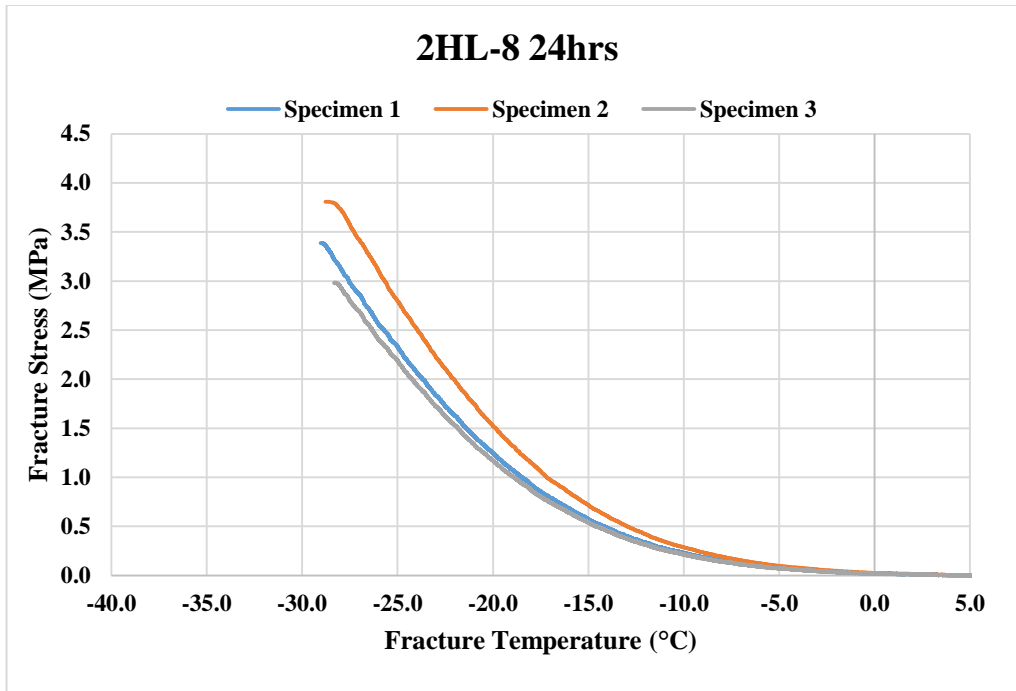


	12	35.91	35.90	0.03	3.61	3.51	0.16
		35.92			3.59		
		35.87			3.32		
	24	28.75	28.47	0.40	3.93	3.58	0.51
		28.66			3.81		
		28.01			2.99		









**Rutting Results:**

#Passes	1HL-3 0hrs			1HL-3 8hrs			1HL-3 12 hrs		
	Depth 1	Depth 2	Average	Depth 1	Depth 2	Average	Depth 1	Depth 2	Average
0	0.00	0.00	0.00	0.53	1.07	0.80	0.00	0.00	0.00
50	0.87	1.03	0.95	0.63	1.12	0.88	0.50	0.60	0.55
100	0.92	1.13	1.03	0.76	1.23	1.00	0.63	0.82	0.73
150	1.03	1.26	1.15	0.81	1.56	1.19	0.77	0.95	0.86
200	1.36	1.31	1.34	0.86	1.57	1.22	1.07	1.07	1.07
250	1.37	1.36	1.37	0.94	1.61	1.28	1.08	1.07	1.08
300	1.41	1.44	1.43	0.97	1.76	1.37	1.12	1.15	1.14
350	1.56	1.47	1.52	1.12	1.79	1.46	1.30	1.18	1.24
400	1.59	1.62	1.61	1.14	1.87	1.51	1.30	1.33	1.32
450	1.67	1.64	1.66	1.20	1.91	1.56	1.38	1.35	1.37
500	1.71	1.70	1.71	1.21	1.96	1.59	1.42	1.41	1.42
550	1.76	1.71	1.74	1.28	1.97	1.63	1.47	1.42	1.45
600	1.77	1.78	1.78	1.36	2.01	1.69	1.48	1.49	1.49
650	1.81	1.86	1.84	1.38	2.03	1.71	1.50	1.59	1.55
700	1.83	1.88	1.86	1.39	2.07	1.73	1.54	1.59	1.57
750	1.87	1.89	1.88	1.40	2.13	1.77	1.55	1.60	1.58
800	1.93	1.90	1.92	1.41	2.13	1.77	1.64	1.61	1.63
850	1.94	1.91	1.93	1.50	2.20	1.85	1.65	1.62	1.64
950	2.00	2.07	2.04	1.59	2.20	1.90	1.71	1.78	1.75

1000	2.05	2.11	2.08	1.60	2.30	1.95	1.76	1.82	1.79
1100	2.10	2.20	2.15	1.72	2.31	2.02	1.81	1.91	1.86
1150	2.11	2.22	2.17	1.80	2.31	2.06	1.82	1.93	1.88
1200	2.11	2.47	2.29	2.50	2.31	2.41	2.00	2.18	2.09
2000	2.38	3.03	2.71	2.70	2.90	2.80	2.11	2.74	2.43
4000	3.02	3.41	3.22	3.00	3.22	3.11	2.73	3.12	2.93
6000	3.10	4.20	3.65	3.50	3.30	3.40	2.79	3.91	3.35
8000	3.38	4.28	3.83	3.70	3.60	3.65	3.01	3.99	3.50
12000	3.76	4.42	4.09	4.08	4.01	4.05	3.20	4.13	3.67
14000	3.81	4.58	4.20	4.12	4.08	4.10	3.44	4.29	3.87
14500	3.88	4.62	4.25	4.13	4.10	4.12	3.48	4.33	3.91
15000	3.90	4.63	4.27	4.13	4.11	4.12	3.57	4.34	3.96
15500	3.91	4.63	4.27	4.13	4.12	4.13	3.62	4.34	3.98
16000	3.92	4.63	4.28	4.14	4.13	4.14	3.63	4.34	3.99
16500	3.93	4.64	4.29	4.15	4.14	4.15	3.64	4.34	3.99
17000	3.94	4.65	4.30	4.15	4.14	4.15	3.64	4.34	3.99
17500	3.94	4.65	4.30	4.15	4.14	4.15	3.64	4.34	3.99
18000	3.94	4.65	4.30	4.15	4.16	4.16	3.65	4.34	4.00
18500	3.96	4.66	4.31	4.15	4.20	4.18	3.65	4.34	4.00
19000	4.06	4.66	4.36	4.15	4.20	4.18	3.65	4.34	4.00
19500	4.09	4.66	4.38	4.15	4.30	4.23	3.65	4.35	4.00
20000	4.10	4.67	4.39	4.15	4.30	4.23	3.65	4.35	4.00

1HL-8 0hrs				1HL-8 8 hrs			1HL-8 12 hrs		
#Passes	Depth 1	Depth 2	Average	Depth 1	Depth 2	Average	Depth 1	Depth 2	Average
0	0.00	0.00	0.00	0.00	0.00	0.00	0	0	0.00
50	0.29	0.32	0.31	0.39	0.22	0.31	0.09	0.11	0.10
100	0.34	0.55	0.45	0.44	0.35	0.40	0.14	0.21	0.18
150	0.45	0.68	0.57	0.45	0.45	0.45	0.25	0.34	0.30
200	0.78	0.73	0.76	0.78	0.53	0.66	0.58	0.39	0.49
250	0.79	0.78	0.79	0.89	0.57	0.73	0.59	0.44	0.52
300	0.83	0.86	0.85	0.90	0.66	0.78	0.63	0.52	0.58
350	0.98	0.89	0.94	1.08	0.68	0.88	0.78	0.55	0.67
400	1.01	1.04	1.03	1.12	0.86	0.99	0.81	0.7	0.76
450	1.09	1.10	1.10	1.19	0.90	1.05	0.89	0.72	0.81
500	1.13	1.12	1.13	1.27	0.92	1.10	0.93	0.78	0.86
550	1.18	1.13	1.16	1.28	1.00	1.14	0.98	0.79	0.89
600	1.19	1.20	1.20	1.29	1.00	1.15	0.98	0.86	0.92
650	1.23	1.28	1.26	1.32	1.08	1.20	1.03	0.86	0.95

700	1.25	1.30	1.28	1.34	1.10	1.22	1.05	0.96	1.01
750	1.29	1.31	1.30	1.38	1.12	1.25	1.09	0.97	1.03
800	1.35	1.31	1.33	1.45	1.13	1.29	1.14	0.98	1.06
850	1.36	1.33	1.35	1.46	1.13	1.30	1.16	0.99	1.08
950	1.42	1.49	1.46	1.49	1.29	1.39	1.2	1.16	1.18
1000	1.47	1.53	1.50	1.55	1.33	1.44	1.27	1.2	1.24
1100	1.52	1.62	1.57	1.58	1.44	1.51	1.32	1.28	1.30
1150	1.53	1.64	1.59	1.59	1.44	1.52	1.33	1.41	1.37
1200	1.53	1.89	1.71	1.70	1.79	1.75	1.33	1.55	1.44
2000	1.80	2.41	2.11	1.73	2.31	2.02	2.09	2.11	2.10
4000	2.44	2.60	2.52	2.54	2.34	2.44	2.24	2.49	2.37
6000	2.52	3.62	3.07	2.62	3.42	3.02	2.24	3.2	2.72
8000	2.80	3.70	3.25	2.90	3.72	3.31	2.5	3.28	2.89
12000	3.18	3.84	3.51	3.28	3.54	3.41	2.7	3.3	3.00
14000	3.30	3.99	3.65	3.3	3.69	3.50	3.02	3.42	3.22
14500	3.30	4.04	3.67	3.31	3.74	3.53	3.02	3.42	3.22
15000	3.32	4.05	3.69	3.32	3.75	3.54	3.02	3.42	3.22
15500	3.33	4.05	3.69	3.33	3.75	3.54	3.02	3.42	3.22
16000	3.34	4.05	3.70	3.35	3.75	3.55	3.02	3.63	3.33
16500	3.35	4.06	3.71	3.44	3.75	3.60	3.02	3.64	3.33
17000	3.36	4.07	3.72	3.51	3.75	3.63	3.02	3.65	3.34
17500	3.36	4.07	3.72	3.51	3.75	3.63	3.02	3.65	3.34
18000	3.36	4.07	3.72	3.62	3.75	3.69	3.02	3.65	3.34
18500	3.38	4.08	3.73	3.63	3.75	3.69	3.02	3.66	3.34
19000	3.38	4.08	3.73	3.63	3.75	3.69	3.02	3.66	3.34
19500	3.38	4.08	3.73	3.63	3.75	3.69	3.17	3.66	3.42
20000	3.48	4.09	3.79	3.65	3.75	3.70	3.2	3.66	3.43

2HL-3 0hrs				2HL-3 8hrs			2HL-3 12hrs		
#Passes	Depth 1	Depth 2	Average	Depth 1	Depth 2	Average	Depth 1	Depth 2	Average
0	0.00	0.00	0.00	0.00	0.00	0.00	0.00	0.00	0.00
50	0.00	0.03	0.02	0.11	0.13	0.12	0.24	0.23	0.24
100	0.10	0.09	0.10	0.12	0.13	0.13	0.33	0.31	0.32
150	0.16	0.19	0.18	0.15	0.15	0.15	0.39	0.37	0.38
200	0.17	0.29	0.23	0.18	0.19	0.19	0.46	0.43	0.45
250	0.38	0.39	0.39	0.23	0.21	0.22	0.50	0.49	0.50
300	0.38	0.48	0.43	0.31	0.29	0.30	0.55	0.51	0.53
350	0.48	0.55	0.52	0.39	0.37	0.38	0.59	0.59	0.59
400	0.52	0.60	0.56	0.48	0.50	0.49	0.60	0.59	0.60
450	0.60	0.74	0.67	0.57	0.54	0.56	0.62	0.63	0.63

500	0.66	0.76	0.71	0.61	0.65	0.63	0.67	0.66	0.67
550	0.72	1.02	0.87	0.69	0.69	0.69	0.67	0.66	0.67
600	0.79	1.04	0.92	0.75	0.79	0.77	0.68	0.66	0.67
650	0.88	1.06	0.97	0.89	0.88	0.89	0.72	0.74	0.73
700	0.91	1.09	1.00	0.90	0.93	0.92	0.73	0.74	0.74
750	0.97	1.18	1.08	0.93	0.93	0.93	0.74	0.74	0.74
800	1.08	1.22	1.15	1.00	1.02	1.01	0.76	0.76	0.76
850	1.08	1.26	1.17	1.04	1.07	1.06	0.80	0.81	0.81
950	1.22	1.46	1.34	1.20	1.13	1.17	0.83	0.84	0.84
1000	1.24	1.61	1.43	1.22	1.20	1.21	0.85	0.84	0.85
1100	1.31	1.62	1.47	1.29	1.21	1.25	0.88	0.85	0.87
1150	1.33	1.63	1.48	1.30	1.29	1.30	0.89	0.87	0.88
1200	1.42	1.73	1.58	1.47	1.30	1.39	0.95	0.89	0.92
2000	1.80	2.23	2.02	1.51	1.47	1.49	1.05	0.94	1.00
4000	1.80	2.78	2.29	1.66	1.90	1.78	1.41	1.32	1.37
6000	2.12	2.99	2.56	1.69	1.99	1.84	1.58	1.49	1.54
8000	3.00	2.99	3.00	1.80	2.10	1.95	1.67	1.62	1.65
12000	3.41	3.09	3.25	1.99	2.30	2.15	1.96	1.91	1.94
14000	3.54	3.18	3.36	2.31	2.30	2.31	1.99	1.91	1.95
14500	3.74	3.45	3.60	2.45	2.30	2.38	2.03	1.99	2.01
15000	3.74	3.49	3.62	2.55	2.30	2.43	2.03	2.00	2.02
15500	3.79	3.50	3.65	2.58	2.30	2.44	2.05	2.01	2.03
16000	3.83	3.81	3.82	2.63	2.33	2.48	2.05	2.01	2.03
16500	3.92	3.81	3.87	2.78	2.37	2.58	2.06	2.04	2.05
17000	3.92	3.88	3.90	2.78	2.43	2.61	2.06	2.07	2.07
17500	3.92	3.89	3.91	2.78	2.45	2.62	2.12	2.09	2.11
18000	3.95	4.02	3.99	2.83	2.46	2.65	2.12	2.09	2.11
18500	3.99	4.04	4.02	2.84	2.49	2.67	2.12	2.09	2.11
19000	4.04	4.20	4.12	2.85	2.66	2.76	2.12	2.09	2.11
19500	4.06	4.20	4.13	2.85	2.69	2.77	2.12	2.15	2.14
20000	4.10	4.20	4.15	2.85	2.69	2.77	2.12	2.15	2.14
20000	4.10	4.20	4.15	2.85	2.69	2.77	2.12	2.15	2.14

2HL-8 0hrs				2HL-8 8hrs			2HL-8 12hrs		
#Passes	Depth 1	Depth 2	Average	Depth 1	Depth 2	Average	Depth 1	Depth 2	Average
0	0	0	0.00	0	0.00	0.00	0.00	0.00	0.00
50	0.34	0.37	0.36	0.17	0.27	0.22	0.37	0.31	0.34
100	0.42	0.52	0.47	0.19	0.39	0.29	0.49	0.33	0.41
150	0.44	0.54	0.49	0.26	0.50	0.38	0.57	0.47	0.52
200	0.68	0.69	0.69	0.27	0.54	0.41	0.63	0.55	0.59
250	0.77	0.89	0.83	0.33	0.55	0.44	0.65	0.61	0.63

300	0.9	1.11	1.01	0.38	0.64	0.51	0.72	0.68	0.70
350	1.1	1.19	1.15	0.39	0.66	0.53	0.78	0.73	0.76
400	1.35	1.28	1.32	0.71	0.70	0.71	0.79	0.78	0.79
450	1.5	1.5	1.50	0.75	0.73	0.74	0.81	0.82	0.82
500	1.57	1.59	1.58	0.75	0.73	0.74	0.81	0.82	0.82
550	1.64	1.69	1.67	0.83	0.81	0.82	0.86	0.87	0.87
600	1.78	1.72	1.75	0.84	0.83	0.84	0.86	0.89	0.88
650	1.79	1.72	1.76	0.84	0.86	0.85	0.92	0.95	0.94
700	1.79	1.74	1.77	0.86	0.88	0.87	0.93	0.95	0.94
750	1.83	1.78	1.81	0.89	0.88	0.89	0.96	0.96	0.96
800	1.88	1.88	1.88	0.94	0.90	0.92	0.99	0.98	0.99
850	1.89	1.93	1.91	0.95	0.97	0.96	1.02	1.10	1.06
950	1.92	1.93	1.93	0.99	1.02	1.01	1.02	1.12	1.07
1000	1.94	1.95	1.95	1.02	1.02	1.02	1.02	1.12	1.07
1100	1.96	1.97	1.97	1.11	1.05	1.08	1.02	1.25	1.14
1150	1.98	1.98	1.98	1.19	1.16	1.18	1.02	1.25	1.14
1200	1.99	1.98	1.99	1.19	1.17	1.18	1.02	1.31	1.17
2000	2.04	2.2	2.12	1.24	1.44	1.34	1.21	1.34	1.28
4000	2.4	2.41	2.41	1.61	1.51	1.56	1.43	1.42	1.43
6000	2.59	2.43	2.51	1.64	1.65	1.65	1.54	1.49	1.52
8000	2.59	2.45	2.52	1.76	1.85	1.81	1.75	1.63	1.69
12000	2.73	2.49	2.61	1.78	1.88	1.83	1.75	1.69	1.72
14000	2.88	2.73	2.81	1.88	1.89	1.89	1.75	1.72	1.74
14500	2.89	2.81	2.85	1.91	1.96	1.94	1.75	1.72	1.74
15000	2.93	2.96	2.95	1.95	1.97	1.96	1.75	1.72	1.74
15500	2.94	2.99	2.97	1.98	1.99	1.99	1.76	1.72	1.74
16000	2.97	3.19	3.08	2.1	2.00	2.05	1.76	1.72	1.74
16500	2.97	3.26	3.12	2.17	2.00	2.09	1.76	1.72	1.74
17000	2.97	3.26	3.12	2.2	2.04	2.12	1.76	1.73	1.75
17500	2.99	3.26	3.13	2.23	2.06	2.15	1.77	1.73	1.75
18000	2.99	3.26	3.13	2.23	2.12	2.18	1.77	1.73	1.75
18500	2.99	3.31	3.15	2.26	2.15	2.21	1.77	1.73	1.75
19000	2.99	3.31	3.15	2.28	2.15	2.22	1.77	1.74	1.76
19500	2.99	3.31	3.15	2.29	2.17	2.23	1.77	1.74	1.76
20000	2.99	3.31	3.15	2.32	2.19	2.26	1.77	1.74	1.76

2HL-3 24hrs				2HL-8 24hrs		
#Passes	Depth 1	Depth 2	Average	Depth 1	Depth 2	Average
0	0.00	0.00	0.00	0.00	0.00	0.00
50	0.16	0.10	0.13	0.14	0.10	0.12



100	0.32	0.22	0.27	0.20	0.19	0.20
150	0.41	0.37	0.39	0.26	0.27	0.27
200	0.50	0.49	0.50	0.30	0.33	0.32
250	0.52	0.49	0.51	0.33	0.38	0.36
300	0.57	0.50	0.54	0.39	0.39	0.39
350	0.59	0.56	0.58	0.45	0.49	0.47
400	0.60	0.59	0.60	0.50	0.56	0.53
450	0.61	0.63	0.62	0.53	0.57	0.55
500	0.69	0.68	0.69	0.55	0.59	0.57
550	0.71	0.73	0.72	0.56	0.62	0.59
600	0.71	0.75	0.73	0.58	0.65	0.62
650	0.72	0.77	0.75	0.59	0.65	0.62
700	0.73	0.77	0.75	0.60	0.67	0.64
750	0.80	0.83	0.82	0.60	0.68	0.64
800	0.80	0.84	0.82	0.60	0.68	0.64
850	0.80	0.85	0.83	0.62	0.69	0.66
950	0.82	0.89	0.86	0.63	0.71	0.67
1000	0.82	0.89	0.86	0.63	0.73	0.68
1100	0.83	0.89	0.86	0.66	0.78	0.72
1150	0.88	0.89	0.89	0.69	0.78	0.74
1200	0.94	0.91	0.93	0.69	0.78	0.74
2000	1.04	1.02	1.03	0.73	0.80	0.77
4000	1.30	1.26	1.28	0.81	0.82	0.82
6000	1.49	1.38	1.44	1.01	1.01	1.01
8000	1.62	1.55	1.59	1.08	1.10	1.09
12000	1.88	1.76	1.82	1.09	1.11	1.10
14000	1.93	1.87	1.90	1.09	1.12	1.11
14500	2.01	1.90	1.96	1.10	1.13	1.12
15000	2.01	1.96	1.99	1.10	1.15	1.13
15500	2.01	1.98	2.00	1.10	1.15	1.13
16000	2.02	1.98	2.00	1.14	1.15	1.15
16500	2.03	1.98	2.01	1.14	1.17	1.16
17000	2.03	1.98	2.01	1.18	1.17	1.18
17500	2.03	2.01	2.02	1.19	1.19	1.19
18000	2.03	2.01	2.02	1.23	1.23	1.23
18500	2.03	2.02	2.03	1.24	1.25	1.25
19000	2.03	2.02	2.03	1.25	1.26	1.26
19500	2.03	2.02	2.03	1.27	1.28	1.28
20000	2.03	2.02	2.03	1.30	1.31	1.31

**Fatigue Test Results:**

<b>1HL-3 0hrs</b>					
<b>Strain Level</b>	<b>Nf1</b>	<b>Nf2</b>	<b>Nf3</b>	<b>Average Nr</b>	<b>S.D Nr</b>
500	29898	30500	28699	29699	916.8429527
400	44590	48199	47985	46924.66667	2024.709938
300	235750	251449		243599.5	11100.86936
250	950288	987030		968659	25980.51735
<b>1HL-3 8hrs</b>					
<b>Strain Level</b>	<b>Nf1</b>	<b>Nf2</b>	<b>Nf3</b>	<b>Average Nr</b>	<b>S.D Nr</b>
500	30500	31799	38201	33500	4122.66916
400	63299	66750	65949	65332.66667	1806.170073
300	428120	441779		434949.5	9658.371524
250	942850	971550		957200	20293.96462
<b>1HL-3 12hrs</b>					
<b>Strain Level</b>	<b>Nf1</b>	<b>Nf2</b>	<b>Nf3</b>	<b>Average Nr</b>	<b>S.D Nr</b>
500	59899	60900	64841	61880	2612.688462
400	99880	97150	67990	88340	17676.39952
300	620120	607999		614059.5	8570.841295
250	978155	993549		985852	10885.20179

<b>1HL-8 0hrs</b>					
<b>Strain Level</b>	<b>Nf1</b>	<b>Nf2</b>	<b>Nf3</b>	<b>Average Nr</b>	<b>S.D Nr</b>
500	15900	16399	15701	16000	359.5844824
400	33940	37910	38960	36936.66667	2647.76006
300	328949	355950		342449.5	19092.5902
250	713569	679879		696724	23822.42746
<b>1HL-8 8hrs</b>					
<b>Strain Level</b>	<b>Nf1</b>	<b>Nf2</b>	<b>Nf3</b>	<b>Average Nr</b>	<b>S.D Nr</b>
500	25455	26305	22340	24700	2087.540419
400	49099	52150	53949	51732.66667	2451.785132
300	400849	394290		397569.5	4637.913378
250	798150	772259		785204.5	18307.70167
<b>1HL-8 12hrs</b>					
<b>Strain Level</b>	<b>Nf1</b>	<b>Nf2</b>	<b>Nf3</b>	<b>Average Nr</b>	<b>S.D Nr</b>
500	45600	42999	41871	43490	1912.373133
400	52599	53149	56499	54082.33333	2110.884491
300	636770	602335		619552.5	24349.22201
250	859525	832150		845837.5	19357.04813

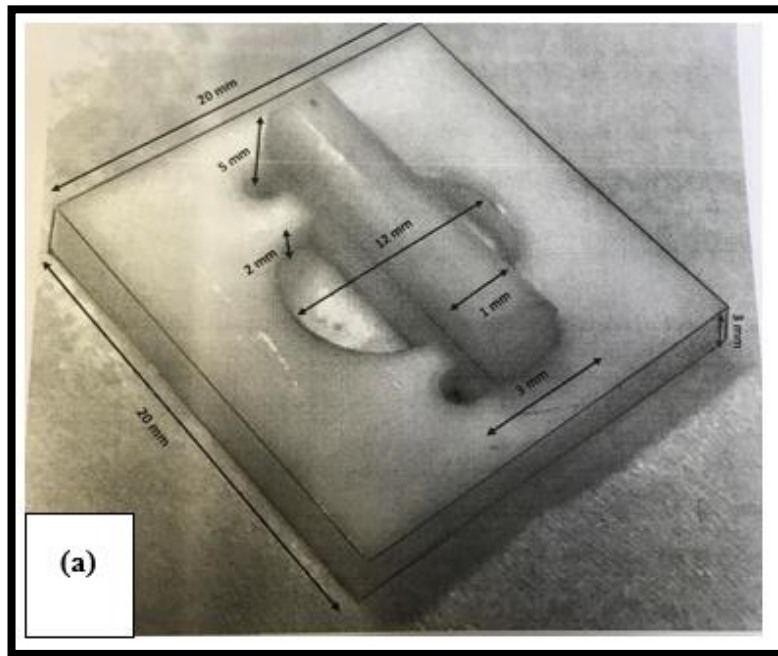
<b>2 HL-3 0hrs</b>
--------------------

Strain Level	Nf1	Nf2	Nf3	Average Nr	S.D Nr
500	26000	25935	29662	27199	2133.26815
400	40959	42150	45799	42969.33333	2521.880317
300	440975	498122		469548.5	40409.03122
250	589622	570720		580171	13365.73238
<b>2 HL-3 8hrs</b>					
Strain Level	Nf1	Nf2	Nf3	Average Nr	S.D Nr
500	45309	46655	45883	45949	675.4228305
400	51999	55930	56910	54946.33333	2599.072976
300	478117	498250		488183.5	14236.18083
250	814949	788549		801749	18667.61902
<b>2 HL-3 12hrs</b>					
Strain Level	Nf1	Nf2	Nf3	Average Nr	S.D Nr
500	46315	46299	44183	45599	1226.318066
400	66310	69149	69955	68471.33333	1914.661937
300	553199	523199		538199	21213.20344
250	1032950	1089735		1061342.5	40153.05857
<b>2 HL-3 24hrs</b>					
Strain Level	Nf1	Nf2	Nf3	Average Nr	S.D Nr
500	44999	46150	46020	45723	630.3625941
400	59949.5	50150	52849	54316.16667	5061.816234
300	532177	546120		539148.5	9859.18985
250	706038	716533		711285.5	40153.05857

<b>2 HL-8 0hrs</b>					
Strain Level	Nf1	Nf2	Nf3	Average Nr	S.D Nr
500	20399	23250	22699	22116	1512.272132
400	38790	37510	42199	39499.66667	2423.716224
300	328449	301550		314999.5	19020.46531
250	661799	623150		642474.5	27328.96999
<b>2 HL-8 8hrs</b>					
Strain Level	Nf1	Nf2	Nf3	Average Nr	S.D Nr
500	26099	25105	21393	24199	2480.370134
400	44899	48050	49849.5	47599.5	2505.808303
300	33102	342155		187628.5	218533.472
250	660548	692130		676339	22331.84636
<b>2 HL-8 12hrs</b>					
Strain Level	Nf1	Nf2	Nf3	Average Nr	S.D Nr
500	25539	24925	25586	25350	368.8102493
400	56850	55349	56735	56311.33333	835.3863378

300	379120	341549		360334.5	26566.70888
250	1032959	989735		1011347	30563.98351
<b>2 HL-8 24hrs</b>					
<b>Strain Level</b>	<b>Nf1</b>	<b>Nf2</b>	<b>Nf3</b>	<b>Average Nr</b>	<b>S.D Nr</b>
500	25355	26099	26543	25999	600.2799347
400	48749	49050	52149	49982.66667	1882.126546
300	309815	311895		310855	1470.782105
250	703260	680357		691808.5	16194.86661

## Appendix (B) –Specimen Preparation and Testing



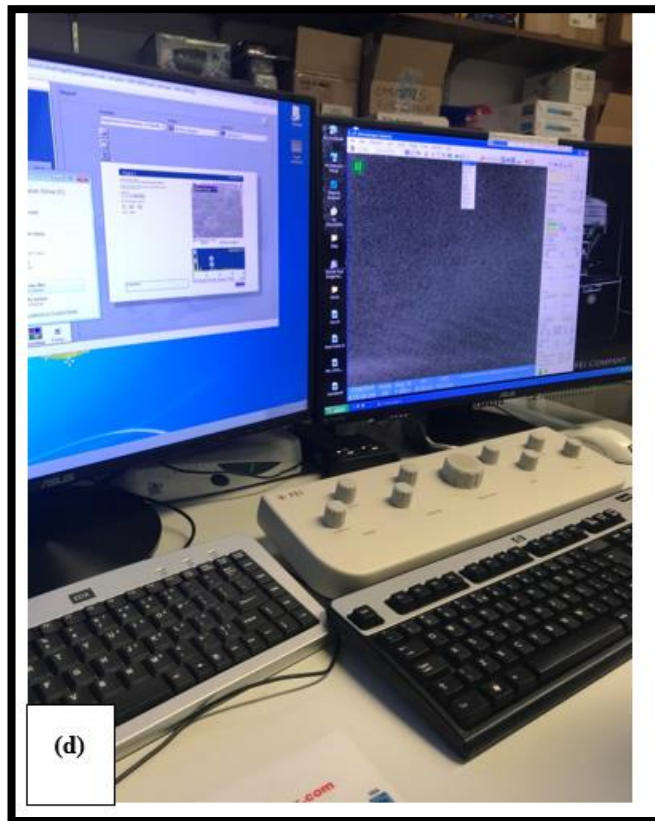
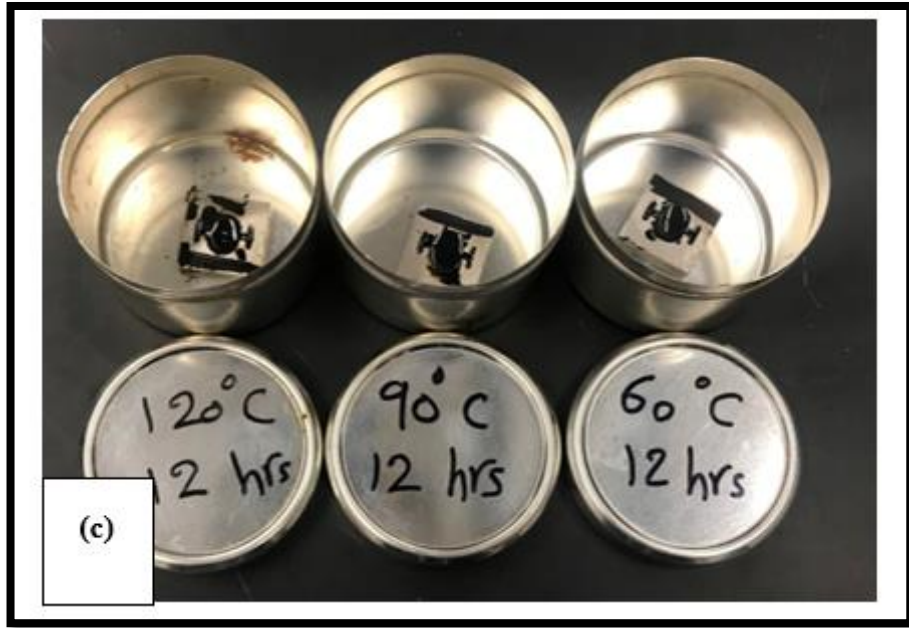




Figure 1: (a) ESEM sample mould design (b) flatten the binder sample on the heat plate (c) blending zones samples on the containers (d) observation of the asphalt binder under ESEM (e) image processing



Figure 2: Dynamic modulus test samples after testing









**Figure 3: (a) Rutting samples under HWTD (b) & (c) rutting samples after testing**